Biomedical Materials for Multi-functional Applications

Amit Mahajan · Sandeep Devgan · Redouane Zitoune *Editors*

Additive Manufacturing of Bio-implants

Design and Synthesis

Springer

Biomedical Materials for Multi-functional Applications

Series Editors

Arnab Chanda, Indian Institute of Technology Delhi, Centre for Biomedical Engineering, New Delhi, Delhi, India

Sarabjeet Sidhu, Sardar Beant Singh State University, Department of Mechanical Engineering, Gurdaspur, Punjab, India

The series 'Biomedical Materials for Multi-functional Applications' is intended for the audience with an interest in biomaterials for various applications, including bio-implants, bio-instrumentation, biomechanics, and tissue engineering. The book titles under this series will bring different areas of biomedical engineering, bioengineering, materials science, mechanical engineering, and biosciences under one umbrella of biomedical materials. The books in this series will provide deep insights into the state-of-art of biomedical materials and deal with diverse and interdisciplinary aspects of biomaterials, ranging from basic science to host responses, as well as real-time applications. Some of the topics include but are not limited to: functional materials, smart materials, biomimetic materials, polymers, composites, ceramics, metals, alloys, and nanomaterials. This series will provide the most recent advances in biomedical materials, including design, synthesis, processing, and characterization. This series will accept both authored and edited volumes, including monographs, textbooks, reference works, and handbooks. This series aims to publish new advances in biomedical materials that have been made in the fabrication and development of biomaterials for different applications and the advancement of principles, theories, and designs. Each book title in the series will give a comprehensive overview of pioneering topics, and the readers will gain new knowledge and insights about the topic. As a collection, the series on 'Biomedical Materials for Multi-functional Applications' is anticipated to benefit a wide audience in academia, the research community, and industry.

Amit Mahajan · Sandeep Devgan ·
Redouane Zitoune
Editors

Additive Manufacturing of Bio-implants

Design and Synthesis

Springer

Editors
Amit Mahajan
Department of Mechanical Engineering
Khalsa College of Engineering
and Technology
Amritsar, Punjab, India

Sandeep Devgan
Department of Mechanical Engineering
Khalsa College of Engineering
and Technology
Amritsar, Punjab, India

Redouane Zitoune
Institut Clément Ader
Toulouse University
Toulouse, France

ISSN 2731-9695 ISSN 2731-9709 (electronic)
Biomedical Materials for Multi-functional Applications
ISBN 978-981-99-6904-3 ISBN 978-981-99-6972-2 (eBook)
https://doi.org/10.1007/978-981-99-6972-2

This Springer imprint is published by the registered company Springer Nature Singapore Pte Ltd.
The registered company address is: 152 Beach Road, #21-01/04 Gateway East, Singapore 189721, Singapore

Paper in this product is recyclable.

Preface

Today, metallic biomaterials fabricating industries are facing intricacy in manufacturing bio-implants that have long-term applications in the patient body. Manufacturing processes play a significant role in fabricating and developing different biomedical devices. Additive manufacturing (AM) or 3D printing is one of the key techniques of novel medical devices, which can process complicated or customized structures to match the properties of human tissues. AM allows for the fabrication of devices with optimal architectures, complicated morphologies, surface integrity, and regulated porosity and chemical composition. Various AM methods can now consistently fabricate dense products for a variety of materials, comprising steels, titanium alloys, Co-Cr alloys, metal-based composites, and nanocomposites. This book elucidated the chronology of various techniques that are categorized under additive manufacturing. Moreover, the futuristic techniques or advancements in this area are also described. The available literature focused on the microstructure and various properties of 3D-printed alloys. However, the research on the wear characteristics, corrosion resistance, and biocompatibility of 3D printed technology for biomedical applications is limited. This book comprises the helicopter view of different surface analysis trends of additive manufactured alloys.

Chapter 1 focused on the state of the art of AM processes in both aeronautical and biomedical applications. The link between process parameters and both the macroscopic and microscopic properties of printed parts was studied, with suggestions on how this may be improved to allow for the manufacture of high-resolution, high-fidelity, and defect-free parts. Particular attention was paid to the integrity of printed parts when subjected to common loading, such as tensile, bending, and microhardness testing. This chapter also examined the potential of AM techniques for repairing damaged parts, which is a growing concern in industries where repair is more economical than integral part replacement. Chapter 2 provided the concepts of combining nanotechnology with additive manufacturing for generating novel methodologies in materials manufacturing by improving mechanical, electrical, biological, and bulk properties. It also incorporated carbon nanotubes (CNTs) in various AM techniques, a possible futuristic material in biomedical domain that is known for its versatile characteristics of high biocompatibility and bio-mimetic

properties in host structures. Chapter 3 studied the formation of the bioactive HA powder and further deposited the layer of HA powder on AISI 304L stainless steel substrate using thermal spray high-velocity oxy-fuel (HVOF) additive manufacturing process.

Chapter 4 explicated information about the surface modification technique to enhance the mechanical engineering as well as biomedical engineering applications of titanium and its alloys. Chapter 5 discussed the applications of 3D-printing in various sectors such as medical, epidemic disease accessories, dental implants, agriculture, and aerospace. Chapter 6 focused on the instrumentation and monitoring of additive manufacturing (AM) processes for biomedical applications. The defects generated during AM processes and their links with process parameters were studied, with suggestions to minimize or eliminate these defects. Chapter 7 provided a concise overview of the tribological performance of additive-manufactured biomedical implants. The impact of different additively manufactured techniques on the tribological characteristics of various biomaterials was elucidated.

Chapter 8 discussed the role and future scope of the overall equipment effectiveness (OEE) technique to enhance the functionality of additive manufacturing processes in bio-medical industries. Chapter 9 provided a detailed, critical, and analytical review of previous studies and research in the field of metals and alloys used as implant materials and investigated the corrosion aspects of additively manufactured metallic biomaterials. Chapter 10 elaborated on the aspect of design, material, and fabrication processes to manufacture customized Functionally Graded Material (FGM)-based implants. Chapter 11 developed and evaluated a novel design for a hip implant that offers ease of installation and replacement, with the potential to minimize interfacial micro-motion, alleviate stress shielding, and enhance the dynamic stability of total hip replacements (THR).

This book is a valuable resource for additive manufacturing (AM) and biomaterials researchers, engineers, and clinicians, guiding them toward developing optimized implants with superior biological, mechanical, electrochemical, and tribological characteristics.

Amritsar, Punjab, India — Amit Mahajan
Amritsar, Punjab, India — Sandeep Devgan
Toulouse, France — Redouane Zitoune

Contents

1 Challenges in Additive Manufacturing: Influence of Process Parameters on Induced Physical Properties of Printed Parts 1
N. Dhoonooah, K. Moussaoui, F. Monies, W. Rubio, and R. Zitoune

2 Additive Manufacturing Incorporated Carbon Nanotubes (CNTs); Advances in Biomedical Domain 33
Sandeep Devgan, Amit Mahajan, and Vinod Mahajan

3 Formation, Testing, and Deposition of Bioactive Material Using Thermal Spray Additive Manufacturing Technique 45
Talwinder Singh and Davinder Singh

4 Controlled Oxide Deposition Improves Mechanical and Biomedical Applications of Titanium Alloy 59
Anil Kumar, Sunil Sinhmar, Suresh Kumar, and Rishabh Sharma

5 Instrumentation and Monitoring of Additive Manufacturing Processes for the Biomedical Applications 73
L. de Peindray d'Ambelle, K. Moussaoui, and C. Mabru

6 A Concise Study on Tribological Properties of Additive Manufactured Biomaterials 107
Jasjeevan Singh, Amit Mahajan, Atul Agnihotri, and Ruchi Handa

7 Role and Scope of OEE to Improve Additive Manufacturing Processes in Biomedical Industries 115
Sandeep Singh, Davinder Singh, Mahesh Gupta, Bhupinder Singh Chauhan, and Jasjeevan Singh

8 Corrosion Performance of Additively Manufactured Metallic Biomaterials: A Review 127
Davinder Singh, Talwinder Singh, and Sandeep Singh

9 Emerging Functionally Graded Materials for Bio-implant Applications—Design and Manufacturing 137
Rakesh Kumar and Anupam Agrawal

10 Biomechanical Evaluation of Load Transfer and Stability in a Corrugated Hip Stem: A Comparative Analysis 147
Vivek Gupta, Gurpreet Singh, and Arnab Chanda

11 Applications of 3D Printing in Medical, Engineering, Agricultural, and Other Sectors 159
Shaik Himam Saheb

About the Editors

Dr. Amit Mahajan is Associate Professor at Khalsa College of Engineering and Technology, Amritsar, India. His research interests include additive manufacturing, surface modification of biomaterials, and electrical discharge machining. In his Ph.D., he profitably fabricated the nano-structured bio-favorable coatings on metallic biomaterials using powder mixed electrical discharge machining technique. His research aimed to design the carbon nanotubes (CNTs) and μ-hydroxyapatite (μHAp) mixed coatings on β-type titanium alloy. He investigated the biological responses in terms of hydrophobicity and hydrophilicity tribological properties, corrosion inertness, bioactivity, etc. Currently, he works on the fabrication of alloys with proper fraction composition of carbon nanotubes (CNTs) and μ-hydroxyapatite (μHAp) via additive manufacturing. He has contributed 23 research papers and chapters to leading international journals, books, and conferences. He also serves as Reviewer for several national and international journals of repute.

Dr. Sandeep Devgan is Associate Professor at Khalsa College of Engineering and Technology, Amritsar, India. His research interests include CNTs-based nanotechnology, surface modification of biomaterials, and powder-mixed electrical discharge machining. In his Ph.D., he profitably fabricated the nano-structured bio-favorable coatings on the metallic biomaterials using powder mixed electrical discharge machining technique. His research was aimed to design the carbon nanotubes (CNTs) and μ-hydroxyapatite (μHAp) mixed coatings on β-type titanium alloy. He investigated the biological responses in terms of hydrophobicity and hydrophilicity tribological properties, corrosion inertness, bioactivity, etc. Currently, he works on alloy fabrication with the proper fraction composition of carbon nanotubes (CNTs) and μ-hydroxyapatite (μHAp) via additive manufacturing. He has contributed 22 research papers and chapters to leading international journals, books, and conferences.

Dr. Redouane Zitoune is Full Professor in Mechanical Engineering at Clement Ader Institute (ICA UMR 5312) of Paul Sabatier University (Toulouse, France) and heads the composite research group since 2020. His research activities focus

on the manufacturing and machining of aerospace materials. His current research interests include damage analysis during the manufacturing of composite materials. He is also interested in the thermal analysis of composite structures using numerical and experimental approaches with different techniques of instrumentation, such as optical fibers, infrared cameras, etc. He has published more than 160 technical papers in national and international journals and conferences. In the area of machining of composite materials, he has organized the first national conference and served as Guest Editor of several referenced international journals and co-editor of three books.

Chapter 1
Challenges in Additive Manufacturing: Influence of Process Parameters on Induced Physical Properties of Printed Parts

N. Dhoonooah, K. Moussaoui, F. Monies, W. Rubio, and R. Zitoune

1 Introduction

Additive manufacturing (AM) refers to the technologies used for manufacturing 3D objects through the layered addition of build material. It is contrasted with subtractive manufacturing, in which objects are formed by removing material from an initial block to produce the final shape. The AM technique of 3D printing was first used to develop prototypes in the 1980s, but these trialled objects were usually not functional. At the time, the process was referred to as rapid prototyping since it allowed for reduced-scale models of the final product to be obtained quickly, without the typical set-up process and costs incurred in creating life-size prototypes. As the process improved over the next two decades, it grew to encompass rapid tooling, used for creating moulds for building final products, and by the early 2000s, to create the fully functional final form of the products themselves [1].

AM is advantageous in that it allows the production of complex geometries and internal features which would be difficult to manufacture conventionally. Contrarily to subtractive manufacturing, it also allows human operators and physical tools to reach the interior of a part and other areas that are hard to access, for adding or modifying features in specific locations. AM is already employed extensively for shaping high-performance metals and alloys commonly used in the aerospace and medical industries, and increasingly so for producing near-net shapes in applications where complexity and customisation are key. According to the American Professional Association Report, global revenue from AM for dental applications is indeed forecasted to rise by $9.7 billion (a 35% annual increase) by 2027. In the medical

N. Dhoonooah · K. Moussaoui · F. Monies · W. Rubio · R. Zitoune (✉)
Institut Clément Ader (ICA), UMR-CNRS 5312, "INSA, UPS, Mines Albi, ISAE", Université de Toulouse, 133 C Avenue de Rangueil, 31077 Toulouse, France
e-mail: Redouane.zitoune@iut-tlse3.fr

A. Mahajan et al. (eds.), *Additive Manufacturing of Bio-implants*, Biomedical Materials for Multi-functional Applications, https://doi.org/10.1007/978-981-99-6972-2_1

industry, the use of 3D printing rises daily, where approximately 11% of the total revenue is accounted for by AM components used in medical devices or implants. This rise is being driven mainly by patients' requirements for customised medical parts [2].

In this article, we will first explore what makes biocompatible metals and alloys so popular in the industry, and especially how additive manufacturing is beneficial in producing customised bioimplants. We will touch briefly on the application of AM for repairing implants that may have sustained damage during handling and transportation, prior to insertion into the human body, before focussing elaborately on the challenges of selecting optimal process parameters and operating conditions to achieve high-quality and high-performance printed parts. Further, we will study parametric influence on the external morphology of deposited beads, on the formed microstructure, and on macrostructure and potential defects. Finally, we will summarise the content and outline possible avenues for further research.

2 Uses of AM in the Biomedical Sector

Biocompatible metals and alloys are being increasingly chosen as the build material for porous orthopaedic implants because of medical practitioners' attention to their higher intrinsic mechanical strength and corrosion resistance. These properties make them suitable for patient-specific implants that speed up recovery even while reducing the need for physical amputation [3]. Porous biomaterials have three distinct advantages over conventional ones:

(i) They have a range of controllability, which increases their usefulness from a design perspective. Their mechanical properties are highly influenced by the microstructure of the printed material, so that a designer could easily tailor the mechanical properties of these biomaterials to the desired level of performance by simply altering the orientation of the microstructure.
(ii) Different microstructures may be formed within the same texture of porous material, or through combining solid materials with porous materials, giving rise to the possibility of manufacturing parts with mixed material compositions. As each individual microstructure lends different mechanical properties to the overall part, particular regions in the implant may be primed for reducing stress shielding [4].
(iii) They allow the manufacturing of patient-specific implants based on specific physical and biological requirements.

Ideally, biomaterials should be biocompatible, easy to print, non-toxic in biological environments, and able to morphologically mimic living tissue. The choice of build material for AM bioimplants depends primarily on the physical utility and properties desired in the printed surgical tools, prosthetic limbs, tissue scaffolds, etc. Polymers are the most widely used material in the medical sector, with a usage

rate as high as 86%. For applications which prioritise strength, durability and flexibility, thermoplastics like acrylonitrile butadiene styrene (ABS) and nylon [5] are commonly used. Metals and alloys are primarily used for fabricating high-strength parts such as orthopaedic implants, plates and screws. Ceramics are suitable for bio-active orthopaedic implants, while composites are used in porous orthopaedic implants to which their mechanical properties are better suited.

For printing polymers, commonly used AM techniques include Fused Deposition Modelling (FDM), three-dimensional printing (3DP), stereolithography (STL or SLA) and Selective Laser Sintering (SLS). In FDM, the cross-sectional geometry of the desired part is laid out layer by layer, by extruding the building material in filament form through a temperature-controlled nozzle. Commonly used build materials include ABS, polycarbonate, biodegradable PLA or PLGA, as well as low-melting-point metals and alloys of tin, lead and bismuth. In 3DP, the powder-based feedstock is thinly laid out layer by layer, and an inkjet printing head binds the loose powder particles together using liquid adhesive [6]. Build materials include polymers, ceramics, sand and metal powders such as stainless steel. Stereolithography uses an ultraviolet (UV) laser focussed on a vat of liquid photosensitive polymer to cure the material, with one cross section being traced at a time, and is generally used for bioprinting scaffolds for cell culture and developing both soft and hard tissues and organs. Finally, SLS combines the selective laser technique of SLA and the layering of powder material layering from 3DP, and is generally used for manufacturing metallic implants, dental, cranial, and orthopaedic parts, and temporary and degradable rigid implants.

For metallic materials, common techniques are Selective Laser Sintering (SLS), Selective Laser Melting (SLM), Direct Metal Laser Sintering (DMLS), Electron Beam Melting (EBM) and Laser Metal Deposition (LMD). EBM has, for instance, been used to manufacture implants for skeletal and long bone repair, as well as prosthetic rehabilitation and vertebral replacement [7]. AM metallic components usually have more adaptable mechanical strength; can be more geometrically versatile; produced faster than conventionally manufactured ones, due to minimum human effort in the manufacturing process and a reduced design cycle time. SLS, SLM, DMLS and EBM all fall under the Powder Bed Fusion (PBF) umbrella, illustrated in Fig. 1(left), but differ from one another according to the heat source used and type of material joined.

Selective laser sintering uses a high-power laser, such as a carbon dioxide laser, to fuse small, powdered particles of plastic such as nylon and polyetherketoneketone (PEKK), metal, ceramic or glass into a mass with a desired 3D shape. The laser selectively fuses, or sinters, powdered material by scanning cross sections generated from a 3D CAD file onto the surface of a powder bed. After each scan is complete, the powder bed is then lowered through a one-layer thickness and a new layer of material applied on top. The process is repeated until the part is fully formed. Since the density of the final part relies on peak laser power rather than pulse duration, the SLS machine typically uses a pulsed laser. The filler material is preheated in the powder bed itself somewhat below its melting point, making it easier for the laser to bridge a smaller temperature gap to the actual meting point. However, selective

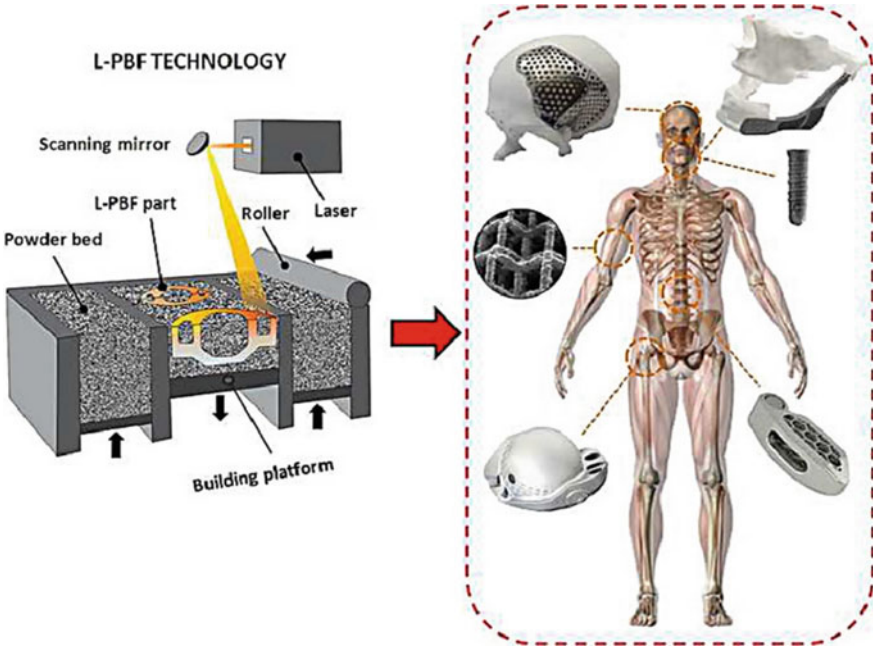

Fig. 1 A schematic set-up of the L-PBF additive manufacturing technique (left) and the different areas of the human body in which metallic bioimplants are commonly used (right) [8]

laser melting is comparable to SLS since it also uses a laser as the heat source, but the filler powder is fully melted rather than sintered. It is commonly used for metallic powders of aluminium alloys, titanium and its alloys, and stainless steel. SLM produces physical metal parts from an initial 3D CAD model. The 3D data is initially sent to the AM machine in an STL file, and this then gets converted to a 3D physical object as a laser heat source collectively scans and fuses metal powder onto a substrate, producing a layered part. Objects manufactured using SLM demonstrate good dimensional accuracy and formed microstructure, as well as excellent mechanical properties [9]. The technique also allows significant reductions in investment cost and lead time in the production of hard metal dies. However, studies on SLM have shown that it produces metallic parts with high porosity, in turn lowering the density and mechanical performance of the printed objects. SLM thus remains limited in the context of industrial applications [9].

Precise, high-resolution parts with complex geometries that may not be easily manufactured conventionally can be additively manufactured using Direct Metal Laser Sintering. It is similar in operation to SLM and employs full material melting despite the term'sintering' being used. In this process, a printed part is formed layer by layer using a laser which aims at specific points in space in a powder bed, guided by a digital CAD file. Once a layer has been printed, the machine automatically spreads more powder over the formed part and repeats the process. Parts printed using

DMLS are generally accurate and have high-quality surface finishes along with near-wrought mechanical properties. The technique is ideal for low-volume parts that are otherwise difficult or impossible to manufacture conventionally because of hollow spaces, undercuts, challenging angles, and other complex features.

As a process, electron beam melting is comparable to SLM, but the laser heat source is replaced by an electron gun. Since an electron beam is employed, the build chamber includes a vacuum instead of an inert atmosphere, though a small amount of inert gas, usually helium, is retained to allow better process control. The part to be manufactured may be modelled using CAD software, obtained by 3D scanning or downloaded as a model. The 3D model is then "sliced" digitally according to the desired successive physical layers of deposited material, and this information sent directly to the 3D printer, where manufacturing starts. The powdered metal filler is loaded into the tank of the machine and deposited in thin layers that are preheated before being fused by the electron beam. These steps are repeated until the part is fully printed.

Laser metal deposition is a directed energy deposition process. The heat source used is a laser beam which melts the metal substrate surface even as filler material is deposited into the melt pool formed, and fuses with the substrate. When incident on the substrate, the laser heat source melts a thin layer of base material in a controlled manner, and this ensures a sound metallurgical bond between the substrate and filler material, which can be powdered or in wire form. LMD is typically used to produce and repair high-value parts and components, extending the durability of claddings and coatings, and the operational life cycle of parts in general. It is also beneficial in that highly complex parts can be repaired with automated methods, and the low heat input from the laser beam keeps the heat-affected zone (HAZ) relatively small and the strength of the base material relatively unchanged from its initial value. Also, LMD is widely used for various applications in the offshore, oil and gas, aerospace, power generation, automotive and utilities industries.

3 Addressing Manufacturing Defects Using AM

Metallic bioimplants are usually high value and made from expensive elemental metals and alloys. They are required to have both a high-quality finish and mechanical performance to be viable for use inside the human body. Manufacturing such implants additively thus requires a detailed and comprehensive method, particularly to reduce the additional costs incurred in rectifying manufacturing errors in the part. These errors and other defects developed during manufacturing are however not inevitable, and AM implants can sustain further damages during handling and transportation from the factory. While aeronautical metallic components having sustained damage from prolonged operation may be repaired using AM during their life cycle, this does not apply to bioimplants after they have been inserted into a human body. In the case of bioimplants, techniques such as directed energy deposition (DED) can instead

be used for adding functions and features to existing printed components; modifying bioimplants to make them functionally graded, and repairing minor damages in implants sustained during handling and transportation as mentioned above, prior to them being inserted into the body. Functional gradient materials (FGMs) are able to carry out multiple functions, efficiently mimic the hierarchical and gradient structure of naturally occurring systems such as human bone tissue, and showcase desired mechanical and biological response by producing various gradations [10]. In repair, DED acts as a hybrid secondary AM technique since it does not build the initial component itself. An integral repair procedure is generally conducted through five stages, from identifying and classifying damage in a component to obtaining the fully restored component, through surface preparation, material deposition and post-processing of the repaired substrate.

Surface preparation refers to the various processes which can be used to treat the surface of a material prior to carrying out any surface-related application, such as applying a coating, using adhesives, and performing a repair, among others. They can be conducted either chemically or mechanically. In AM, adequately preparing the substrate surface is crucial to ensuring a good degree of fusion between the substrate and the deposited metallic powder and reducing the occurrence of both porosity-related defects and residual stresses. Machining is particularly useful for preparing metallic substrates prior to repair since the metal may be cut to a desired final shape and size using controlled material removal. Machining alloys like Ti6Al4V and Inconel 718 can however prove challenging, due to the need for high-performance cutting which increases mechanical stability, process reliability and tool life. For the DED technique, existing literature has shown that V-shaped grooves machined down to the defect(s) in a damaged part significantly improve its mechanical performance post repair.

Upon completion of a repair procedure, post-repair treatments may be applied to the sample to improve its rendering, both in terms of visual appearance and thermo-mechanical properties. These treatments can be either mechanical and heat based in nature, the former including machining, polishing and shot peening, and the latter solution annealing and precipitation/age hardening, among others. Finally, physical validation is crucial to ensuring that a repaired part is fit for purpose. High-quality microstructure and lack of defects in a printed part lead to higher confidence in the performance and integrity of the part, as well as adequate lifetime, so that it will not have to be repaired again or replaced due to failure in the near future. Common quality control and validation techniques for metallic components include microstructural characterisation, Vickers microhardness measurement, tensile testing and non-destructive testing (NDT) methods.

4 Influence of Process Parameters on the External Morphology of Deposited Beads

The quality of an AM part is characterised by several quantifiable physical metrics at various scales. These include the physical conditions (melt-pool modes and aspect ratios), defects (relative density, porosity and distortion tolerance), mechanical properties (surface roughness, and tensile and fatigue properties), microstructural properties (grain phases, size, aspect ratio, boundary angle and misorientation) and manufacturing performance (time, energy, cost and efficiency). Achieving homogeneity and good surface quality in a finished part depends not only on the as-received properties of the powdered feedstock, manufacturing process and AM equipment used, but more importantly the different process parameters employed. These parameters can be controlled to produce the desired results, but they remain limited by the capability and customisability of the printing machine.

In PBF, for instance, AM part quality is mostly influenced by the laser power (P), scanning velocity (v), hatch spacing (h) and layer thickness (t)—these four parameters are usually characterised by the parametric combination of volumetric energy density, VED [11]. Other combinations of process parameters that have been considered in existing literature include linear energy density and surface energy density [12]. For the Laser Additive Manufacturing-DED (LAM-DED) technique, changes in laser power and beam diameter have been observed to significantly influence laser–matter interactions. A change in laser power notably determines whether a melt pool will form in the conduction or keyhole mode at the surface of the substrate. Laser–matter interaction is further influenced by the chemical-, thermal-, mechanical-, optical- and surface-related properties of the substrate. In both PBF and DED, parameters determine the thermal input to the material being printed, directly influencing the dimensions of the melt pool, characteristics of the solidification cycle and thermal history of the final product. Thermal history includes melt-pool temperature, thermal gradient and cyclical cooling and re-heating rates, and in turn influences the final microstructure: the size, morphology and texture of the grains, the type, size and spatial distribution of defects, and the occurrence of residual stresses. All these define the overall microstructural evolution, mechanical response and eventual defects arising in the printed material [13].

It has been observed that usually laser power is the parameter which most significantly influences metal-based AM, followed by laser scan speed [14, 15]. An increase in laser power imparts more energy to the substrate, resulting in the formation of larger melt pools [16]. If the increase in thermal energy is too significant, this can result in a change from a conductive regime to a keyholing one. This fundamental change in melt-pool physics usually results in gas porosity near the bottom of the melt pool. Higher laser speed may also lead to unstable melt conditions, resulting in a geometrically inconsistent weld-track. Variations in process parameters can be interpreted with respect to a linear energy density parameter such as power/speed, where a higher ratio indicates more energy being input for melting the feedstock and/or substrate material. However, it needs to be noted that parametric changes may also

indicate a transition in melt-pool physics away from the conductive mode. Controlling beam parameters such as laser defocus [17] and/or beam diameter [18] can also be used to reduce overall build time, while tuning shield gas parameters is crucial to removing all by-products while preventing disruption of the powder bed [19, 20]. Generally, other methods such as ultrasound, the direct introduction of nanoparticles for inoculation [21] and the introduction of carbon nanotubes could be used for grain refinement and reinforcement [22–24].

Currently, no de-facto parameter exists to universally characterise the AM process, but those listed are sufficient to describe melt-pool dimensions, porosity and microstructure. Lack of fusion results from a too low laser power and too high scanning speed, leading to an incomplete print. However, applying an unnecessarily high amount of laser power to the feedstock can lead to keyholing in PBF: this is to be avoided since the collapse of the keyhole introduces significant porosity in the printed part [25–27]. Jadhav et al. [28] observed that keyholing may be favourable only for highly conductive metals and alloys such as copper, since they have the capacity to conduct heat away at a fast rate prior to the keyhole collapsing, thereby reducing the occurrence of pores. Corbin et al. [29] studied the effect of DED process parameters such as laser power, scanning speed, working distance, substrate temperature, track order and normalised enthalpy, on the external morphology of laser-deposited Inconel 718 powder onto a substrate of the same material. They showed that scanning speed had a significant effect on bead width and height, while laser power only influenced bead width. Working distance affected the height and angle of repose of the deposited bead, varying the height by up to 270%. The influence of the working distance was also driven by the beam spot size and powder distribution, indicating that the values of bead height and angle of repose are maximised when the focus of the powder stream is coincident with the deposition surface [29]. The relationship between track height and working distance was also seen to be a critical factor in ensuring the stability of the deposition process. Further, as shown in Fig. 2, preheating the substrate prior to deposition significantly increased both the bead width and height. The increase in substrate temperature is indicated by the increasing values of laser power, and the changes in bead morphology can be justified through a better adhesion between the substrate and deposited material, as well as the formation of larger melt pools at the surface of the substrate since less laser energy goes to melting an already hot substrate to create the melt pool, as opposed to an initially cool, untreated substrate surface [30]. In this view, Sreekanth et al. [30] preconised against using too low powder feed rates as higher laser energy is then available for melting the substrate instead of the feedstock, yielding higher levels of dilution and eventually leading to keyholing.

In their study on the deposition of single tracks of Inconel 718 powder on wrought substrate of the same material, Sreekanth et al. identified the same direct link between increased scanning speed and bead width and height, as summarised in Fig. 3. They further showed that the occurrence of porosity-related defects decreased with increased laser power and that the bead width increased with increased laser power: the latter is justified by the formation of larger melt pools at the surface of the increasingly hot substrate. For porosity due to carrier gases trapped within deposited beads,

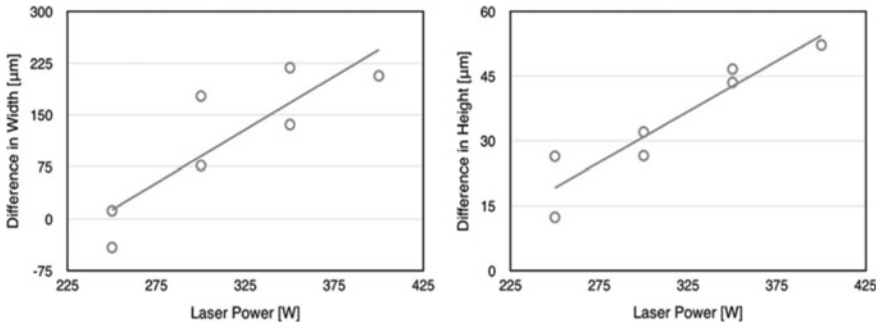

Fig. 2 Differences in width and height between room temperature and preheated deposits when varying laser power [29]

the higher laser energy likely increases the solubility of these gases and reduces the size of spherical defects hence formed. As shown by Kobryn et al. [31] and Vilaro et al. [32], porosity-related defects due to a lack of fusion originate from inadequate levels of dilution of the melt pool into the substrate or into neighbouring beads, resulting in sharp voids that are detrimental to the mechanical performance of the deposited sample. By observing the visual appearance of the deposited bead, Sreekanth et al. also highlighted their distinct appearance compared to that of the wrought substrate. This has been found common to several studies about powder deposition, where the final deposited sample is made to undergo thermal and other post-processing treatments to improve its aesthetic and performance aspects to match those of the original wrought substrate.

Another parameter influencing the mechanical properties, anisotropy, formed microstructure, degree of porosity and distribution of residual stresses of a fabricated part is the deposition strategy [33]. To evaluate the influence of pathways and overlaps on final geometry, density and microstructure for DED-manufactured parts, Ribeiro et al. [34] deposited commercial AISI 316L stainless steel in the shape of cubes of edge 16 mm on Ø25mm stock, with a laser spot of 0.8 mm. Based on parametric data from previous tests, the scanning speed was set at 2000 mm/min, with a powder feed rate of 5 g/min and laser power of 600W, all factors remaining constant throughout the deposition process. Under these conditions, the first deposited layer measured 0.8 mm in width and 0.3 mm in height [34]. A constant Z-increment of 0.3 mm was hence applied. A total of four different deposition strategies were considered, as shown in Fig. 4. The trajectory of the laser was made to rotate through 67° for the zigzag path, and through 90° for the chessboard, while no rotation was carried out for the contour [34].

It was seen that for the various strategies, the slowdown points of the kinematically operated laser coincide with the extremities of the layers repeatedly, so that these receive more heat and are kept at higher temperatures for longer durations [34]. This repetitive heating process causes the extremities to melt more than once and

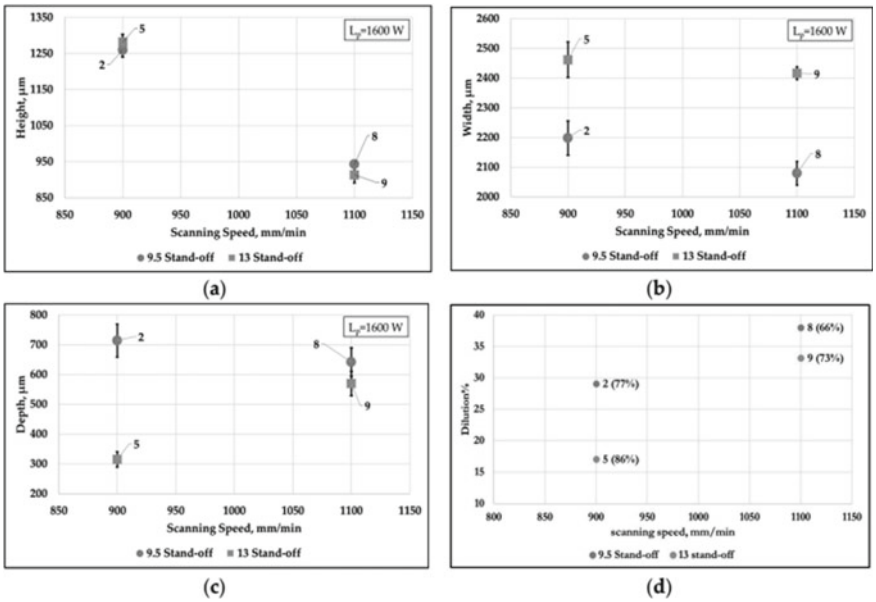

Fig. 3 Influence of scanning speeds of 900 mm/min and 1100 mm/min on **a** height, **b** width, **c** depth, **d** % dilution of deposits at laser stand-off distances of 9.5 mm and 13 mm at a constant laser power of 1600 W [30]

hence solidify into lower layer thicknesses, forming shorter walls in the positive Z-direction. Overall, the contour strategy (D) was reported to have the best performance, followed by the zigzag (B), chessboard (C) and linear (A) paths. In terms of physical properties, the linear, zigzag and chessboard strategies resulted in workpieces with a narrow range of microhardness between 218 and 228 HV. The contour strategy produced the deposit with the lowest average value of microhardness at 209 HV, closest to that of annealed 316L stainless steel [35], and with the most uniform thermal distribution.

Existing literature has also shown that the value of overlap between two adjacent beads is highly dependent on the bead width. By using a numerical optimisation algorithm, Zhang et al. [36] found the optimal overlap for a bead of height 0.46 mm and width 2 mm to be 31% while Chen et al. [37] determined the optimal overlap to be 20% for beads with widths between 6 and 12 mm. Instead of a universal value being recommended for the overlap, it needs to be optimised through experimental trial and error with consideration for the geometric dimensions of the deposited beads in any given study.

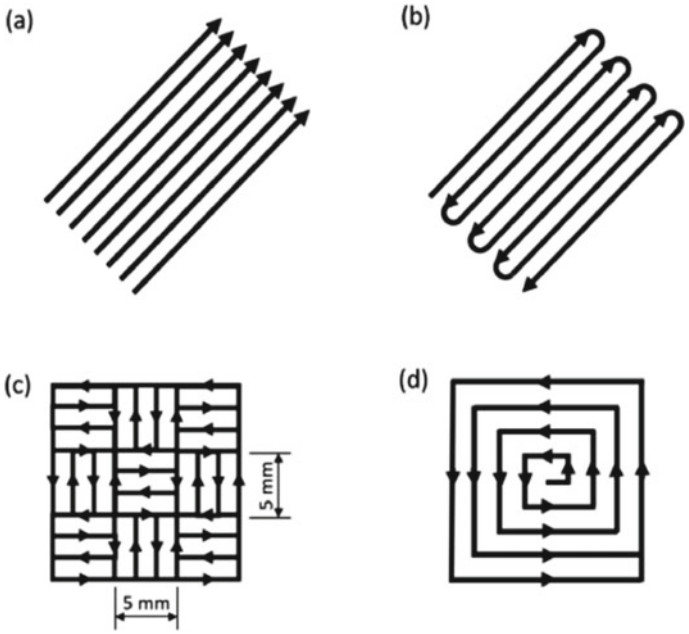

Fig. 4 Deposition strategies showing **a** uni-directional or linear, **b** bi-directional or zigzag, **c** chessboard and **d** contour, or spiral, paths [34]

5 Influence of Process Parameters on the Formed Microstructure

In terms of workpiece material, laser power intensity and interaction time, laser–matter interactions in AM techniques such as PBF and DED are similar to those in laser welding. Lasers exist in several types, and are characterised according to their wavelengths, power intensities, beam profiles, gain mediums, interaction times and applications in manufacturing processes. According to Majumdar et al. [38], the combined parameters of wavelength, repetition rate, interaction time, peak power intensity and beam profile determine how the laser interacts with the free electrons present in the workpiece. Laser absorption into the metallic workpiece is determined by the interaction of the laser beam with the free electrons in the metal, by the movement of electrons within the lattice structure and by defects in the workpiece. Electron transfer converts the energy of the laser into thermal energy in the workpiece, resulting in a temperature increase and eventually causing a melting process to occur. When photon energies from the laser beam are not sufficiently high for ejecting electrons from the workpiece material, dislocations and grain boundaries in the workpiece lattice instead cause the excited electrons to scatter, resulting in overall heating. Heating due to laser irradiation within the workpiece material is

dependent on the laser power and thermal diffusivity of the material, where the irradiated material can reach temperatures sufficient for melting and vaporisation to occur [38].

Other than laser power density, additional key parameters influencing the melt-pool flow and defects in deposited beads include laser scanning speed, and the composition and flow rate of the inert shielding gas [39]. The scanning speed contributes to the interaction time of the laser with the workpiece material, thus influencing the overall laser power intensity. Understanding the influence of the laser power density and interaction time on the deposition process is thus key to understanding the laser–matter interaction when using a laser beam for fusing metallic powder in AM. The HAZ in a material deposition process refers to the non-melted area of metal that has undergone changes in material properties as a result of being exposed to high temperatures in a process of welding, high-heat cutting or deposition. It lies between the weld and the base (unaffected) parent metal in welding, and between the deposited bead and substrate in processes such as DED. Figure 5 shows the gradient in temperature along the HAZ, from the zone of direct impact of the laser onto the substrate, to the unaffected base material in which no changes occur to the initial microstructure.

The HAZ can vary in severity and size depending on the properties of the material involved in the process, the intensity of the laser beams and the deposition technique used. The thermal process occurring in DED generally reaches temperatures up to,

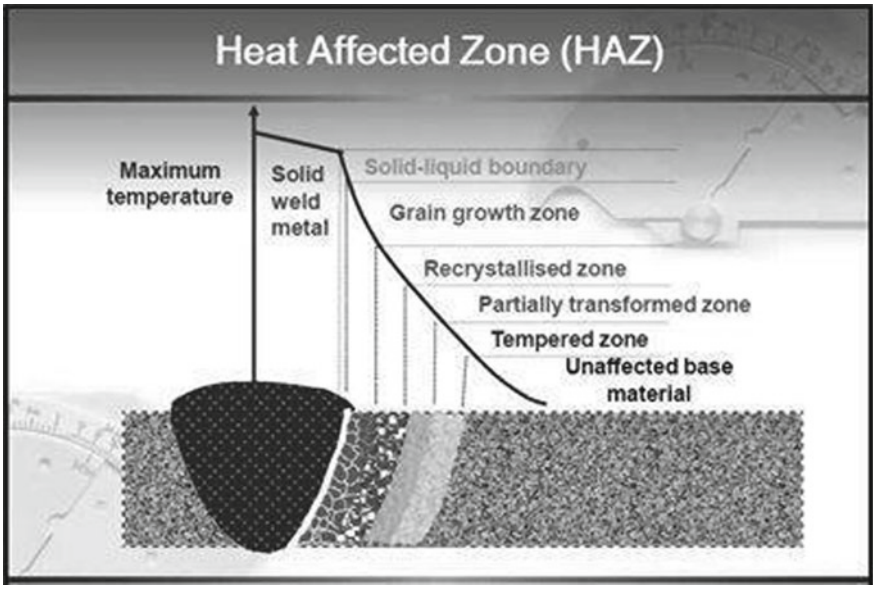

Fig. 5 Diagram showing the different thermally affected zones, along a gradient from the zone of maximum temperature to the unaffected base material [40]

and often exceeding, the fusion temperature of the deposited material. The repetitive heating and cooling cycles undergone by the substrate as successive layers are deposited and thus cause alterations to its initial microstructure. The size of the HAZ is influenced by the level of thermal diffusivity and conductivity, density and specific heat of the substrate, as well as the amount of thermal energy being imparted to it. Materials with a high thermal diffusivity have higher rates of heat transfer, so that they cool down more quickly and the width of the HAZ is reduced. For materials with a lower coefficient, the heat is however retained, resulting in a wider HAZ. The extent of the HAZ is thus seen to be dependent on the amount of heat applied to the substrate, the duration of exposure to this heat and the intrinsic material properties of the substrate itself. For materials exposed to higher amounts of thermal energies over a longer period, the HAZ tends to be larger. Weld-track geometry further influences the dimensions of the HAZ as it affects the properties of the heat sink, where a larger heat sink generally increases the rate of cooling.

As mentioned above, heating and cooling cycles set up during material deposition, as well as the melt pool, have a direct influence on the formed microstructure of the printed part. Process parameters are integral to this, since they not only determine melt-pool dimensions, but also the resulting microstructure. Rapid heating and cooling cycles are characteristics of the AM process, with cooling rates as high as 105–107 $K{\cdot}s^{-1}$ and correspondingly high-temperature gradients of 106−107 $K{\cdot}m^{-1}$ having been reported for the PBF process [41]. Due to the rapid solidification, microstructures formed are usually a mix of equiaxed or epitaxial crystals at the periphery and dendritic parallel to the direction of scanning [42]. Laser power and scanning velocity have been identified as having a direct influence on grain morphology: in 17-PH stainless steel, they directly determine the austenitic grain size [43] and, when finely tuned, can result in the production of <011> grains specifically, simultaneously improving the ductility and strength of steel and balancing the trade-off that usually occurs between the two parameters [44]. A lamellar microstructure consisting of <100> and <110> grains may also be obtained through the sole control of process parameters [45].

The microstructure of printed parts may be further tailored using specific beam shapes. Roehling et al. [46], for instance, demonstrated that an elliptical laser beam can be used to improve the mechanical properties of printed parts. Since the solidification process in AM is highly directional, crystallisation usually occurs in a predominant direction, resulting in the final part exhibiting anisotropic properties [47]. Overlap between the melt pools of beads deposited side by side leads to remelting, creating new microstructural textures and features that are usually not possible with conventional manufacturing [48], such as spiralling microstructures [49], lamellar grains in 316L stainless steel [45] and duplex microstructures in Ti6Al4V [50]. The microstructure of metal AM parts may be directly varied by adjusting process parameters, as indicated by the various patterns in Fig. 6, and the unique microstructures achievable with AM make these alloys comparable in strength, or stronger, than their conventionally manufactured cast or wrought counterparts [51]. The rapid heating and cooling cycles set up in the AM process however generate high residual stresses in the printed parts, leading to eventual warpage and cracking, and the prevalence of

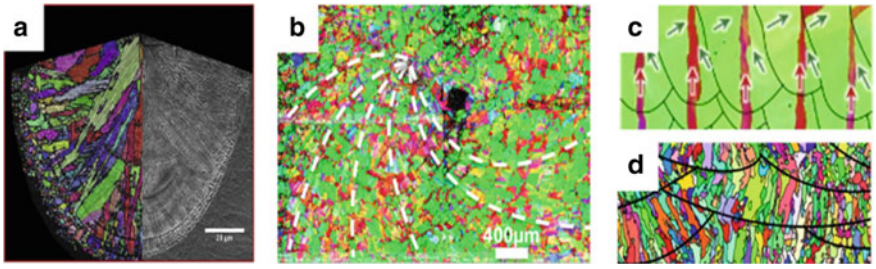

Fig. 6 Microstructures and mechanical properties in AM; (**a**) Microstructure of a melt pool, equiaxed at the periphery and dendritic along the solidification direction; (**b**) Spiral microstructure pattern observed due to 67-degree layer rotation scanning strategy; (**c**) Lamellar grains comprised of alternating <100> and <110> grains in stainless steel 316 L by altering laser power and scanning speed; (**d**) Preferred nucleation of < 110 > grains in stainless steel 316 L [51]

pores in metallic AM objects degrades their performance under fatigue as compared to that of conventionally manufactured ones [52, 53].

The resulting microstructure of additively manufactured alloys such as Ti6Al4V further depends on the technique used, since each is based on different sets of process parameters and handling of the build material. Selective laser sintering (SLS) is used mainly for producing highly dense components such as biocompatible polymers for use in engineering scaffolds for growing porous tissue [54, 55]. Manufacturing biomedical implants with a porous structure which mimics the mechanical properties of biological bone is especially relevant to orthopaedic biomedical applications, since porosity and stiffness can be tuned in the printed part to obtain the exact desired characteristics for simulating human tissue. However, since SLS mainly uses polymer powders as the build material, very limited information is available on the use of Ti6Al4V powder. Significant differences in temperature between the sintered material and surrounding loose powder set up a thermal diffusion gradient, resulting in incomplete melting of the powder and it subsequently attaching to the printed struts. The loose powder can be melted by the laser beam to attach it to each layer boundary; for inclined struts, the loose powder may be fused with the previous sintered layer of material [21]. In practice, several particles of metal below the current layer are found to be completely or partially melted and attached to the lower layer of material, lending it higher surface roughness than the upper surfaces.

A study by Cheng et al. [56] on Ti6Al4V manufactured using the SLS technique showed the improvement in performance of porous implants as compared to solid ones. They investigated the capacity of 3D implants with micro- or nano-rough surfaces and trabecular-bone-inspired porosity for improving the ingrowth of vertical bone, and showed that, by increasing the porosity of the additively manufactured Ti6Al4V, the compressive moduli of the builds could be decreased to mimic the natural modulus of human bone. Porous implants also demonstrated significantly superior pull-out strength values as compared to solid ones. Cheng et al. concluded that ingrowth of new bone into the pores of the implant was highly correlated with the mechanical strength of the boundary. The pull-out force values demonstrated better

osseointegration for porous SLS-manufactured Ti6Al4V implants as compared to solid ones, and it was seen that both types of implants had nanoscale and microscale surfaces, increasing the osteogenic differentiation of osseointegration in vivo and mesenchymal stem cells in vitro [57, 58]. The superior mechanical strength and bone-to-implant contact observed in porous implants was therefore a direct result of the improved surface area due to porosity, instead of variations in surface processing only [21].

The Direct Metal Laser Sintering (DMLS) technique is currently capable of producing nearly fully dense specimens with a density approximating 99.7% [59, 60]. As reported extensively in existing literature, high-density titanium alloys manufactured by DMLS exhibit mechanical properties nearly identical to conventionally manufactured alloys [21, 61]. Hyzy et al. [58, 62] also suggested that DMLS is the optimal technique for fabricating Ti6Al4V, while Konecna et al. [63] showed that the resistance of DMLS-manufactured Ti6Al4V alloys to long fatigue crack growth is comparable to that of conventionally manufactured ones. In addition, Ahmed et al. [64] observed that process parameters such as laser scanning speed and laser power significantly influenced the formed microstructure and mechanical properties of a sintered Ti6Al4V specimen.

Xu et al. [65] studied the effects of post-annealing treatment on the microstructure and mechanical properties of sintered Ti6Al4V alloys at different temperatures of 700 °C, 750 °C, and 799 °C for a total soaking time of 4 h. They observed that the annealing temperature influenced the microstructure of the sintered alloy: the DMLS specimens had an acicular martensitic microstructure different from that of the commercial Grade 5 alloy. The application of hot isostatic pressure (HIP) was thus suggested to further improve the properties of the fabricated specimen. Konečná et al. [63] investigated the effects of build direction and layered microstructure by conducting fatigue testing on sintered Ti6Al4V specimens along three different directions. The printed specimens were heat treated using precipitation hardening to improve their static strength and reduce any residual stresses. The microstructure thus characterised revealed columnar elongated former β grains growing parallel to the build direction. Thin needles of α stage in β lattice were also noticed inside these grains, as well as an initial metastable α' martensitic phase, considered to be normal in an "as organised" microstructure with no heat treatment but which later changed to a combination of $\alpha + \beta$ phases post heat treatment. The thickness of the α needles was found to be approximately 0.5 μm, a figure slightly higher than that of the as-built specimen.

A study by Bača et al. [66] on the microstructure of Ti6Al4V produced through successive stress relief cycles showed the presence of micro-shrinkage from lower values of laser power and temperature. The initiation of the fatigue crack was however seen on the surface inverse to the notch. From several studies conducted on the topic, it was estimated that the optimal process parameters for delivering an isotropic fatigue life material are a thickness layer of 50 μm, laser power of 400W and heat treatment carried out at 720 °C.

Porous Ti6Al4V implants manufactured by Selective Laser Melting (SLM) were found to be suitable for the purpose of growing cells in vitro. Structures such as

mesh scaffolds, analogue porous bone models and other porous bones have been extensively studied [67–71], while some researchers have even attempted attaching carrier agents to the metallic powders to produce honeycomb-like pores with specific pore sequences [72]. Generally, manufacturing metallic implants is not a straightforward task since it involves developing complex porous metal structures [73]. By controlling process parameters in a precise manner, however, these structures can be readily manufactured using the SLM technique. Along with being cost-effective, this technique also allows for significant savings in manufacturing time and for the customisation of various configurations, no matter how challenging. Zhang et al. [74] studied the effect of scan line spacing on SLM-produced Ti6Al4V specimens by using thin wall struts of approximately 200, 300, 400, 500, 600 and 700 μm in size for each specimen. They concluded that implants require a scan line distance larger than 500 μm to form interconnected pores for practical applications, while lower spot sizes can be used to control thin-wall width for implants. It was also observed that porosity increased linearly with increasing scan line distance. It is generally understood that implants require highly porous yet organised structures [75], and this study proved that the porous structure of implants can be enhanced by manipulating scan line distances and that the degree of porosity can be tuned to match patient-specific requirements. The implants have further been shown to improve biological fixation to achieve durability and stability in vivo. Scan line spacing can however have the potentially harmful consequence of pore allocation being strongly dependent on directional solidification and the formation of rough surface pores. Typically, Ti6Al4V specimens manufactured by SLM using the as-received alloy powder show a mixture of α and β phases in their formed microstructure, as well as an enhanced needle-shaped β phase. Poondla et al. [76] and Sun et al. [77] analysed SLM-produced specimens by heating them and subsequently cooling them at different rates, before carrying out a particle morphology analysis. They observed the different particle morphologies to have similar microstructures, with the initial microstructure of the specimens lying in the martensitic phase. Vrancken et al. [78] obtained similar experimental results, where they observed the vanadium (V) atoms in the solid β phase to not have sufficient time to diffuse from the unit cells during rapid cooling rates exceeding 103 K/s, and thus transform to the α phase. The β phase arising during the SLM process through the conversion of martensite is thus a diffusion-less transformation [79], where no stable bonding or accidental breach of the atom occurs through the boundary. The martensitic phase is hence believed to overcome the atomic order, chemical composition and crystalline defects of the parent specimen.

Selective laser-melted Ti6Al4V is typically ductile, but it can still experience brittle failure from the deformation of concentrated local stress and temperature increases resulting from different cooling shear bands. Adiabatic shear band (ASB) formation is also possible, especially in the case of titanium metal alloys [80]. Previous studies have shown that failure can indeed occur due to additional thermal softening which promotes the development of ASB, and that pores can potentially act as an initiation location for the same. Porous titanium alloy specimens were successfully manufactured using SLM, by Mullen et al. [81, 82] who also studied

the geometric influence of the unit cell on the mechanical properties of the printed specimen and showed that the technique can produce porous material with arbitrary degrees of porosity and adequate compressive strength. This was confirmed by Stamp et al. [83], Douglas T. et al. [84] and Warnke et al. [85], who manufactured porous alloys for biomedical applications particularly. Yadroitsev et al. [86] varied the process parameter of scanning strategy to fabricate Ti6Al4V using SLM: their "two-zone technique" (strategy A) resulted in the highest density specimens while the second approach (strategy B) reduced the area of the HAZ and remelting number of the final microstructure [87].

Heat treatment is usually employed for modifying the microstructure and/or reducing residual stresses following the fabrication process. Benedetti et al. [88] studied the effect of such post-sintering treatments on the fatigue and biological response of SLM-produced Ti6Al4V specimens and observed that the α' phase can change into α + β phase without any grain growth after the treatment has been applied. Further, other post-processing treatments such as shot peening and HIP resulted in the formation of smoother, more uniform surfaces with impact dimples (for the shot-peened material) and without (for the HIPed material). Ti6Al4V specimens manufactured using the Laser Engineered Net Shaping (LENS) technique usually demonstrate higher critical tensile strength, elongation and yield strength than conventionally manufactured or annealed specimens [21]. Bandopadhyay et al. [89] investigated the compressive behaviour and microstructural properties of LENS-produced Ti6Al4V by using two different values of laser power to melt the metallic feedstock in a deposition process for producing porous specimens. They also studied the influence of variations in process parameters such as laser scan speed and powder feed rate on the resulting porosity in printed material [89].

The bulk density of LENS-produced specimens generally relies on the process parameters employed, and previous analyses have shown a surface of open porosity, with the bulk density varying from 67 to 85%. The interconnectivity of the pores however has been shown to vary along different directions in the printed material, with higher pore connectivity along the build direction than perpendicular to it. Both as-received and LENS-treated Ti6Al4V powder exhibited a combination of microstructures consisting of both α and β specimens, but the latter was also seen to comprise the needle-formed β phase, revealing a significant degree of the β phase at high temperatures. Sandgren et al. [90] reported a different mechanism for confining the development of small fatigue cracks in LENS-produced Ti6Al4V, with a formed microstructure containing large columnar β grains about 1–20 mm in length and 0.2–4.0 mm wide, perpendicular to the substrate. Reported fatigue crack growth (FCG) data was obtained from 2 and 3D tomography renovations while fracture length measurements were obtained from scanning electron microscopy (SEM). The tensile load facture surface was determined by distinguishing it from the fatigue fracture surface, and crack propagation observed to occur within one of the columnar β grains. Zhai et al. [91] analysed the propagation behaviour of long and small cracks in LENS-produced Ti6Al4V and assessed long fatigue crack growth in tensioned specimens using the conformity method to observe how the crack propagates. A surface flaw tension experiment was elaborated for small FCG, and the crack growth

pattern captured using the direct current potential drop (DCPD) technique. Finally, FCG data for small cracks in conventional mill annealed Ti6Al4V indicated the acceleration and retardation of crack growth rates due to the presence of certain microstructural features.

6 Influence of Process Parameters on Macrostructure and the Occurrence of Defects

The main objective of the manufacturing process is to create a functional defect-free part that exhibits superior physical and mechanical properties [51]. This is of particular importance in processing metallic materials for engineering applications, where micro-defects such as pores generally act as initiation sites for cracks and fatigue, leading to an eventual degradation of quality in the final printed part. A lack of mastery of the capabilities of the AM process and understanding of surface feature quality in AM metallic parts, however, persist [92]. Rough surfaces in printed metallic parts are indeed detrimental to their performance under fatigue, and surface irregularities play a key role in the failure mechanism resulting from this fatigue. This can be mitigated by a better understanding of surface roughness and how it may be controlled to prevent failure. The surface quality of additively manufactured parts is influenced by several factors such as the "staircase effect", which results from layered material build-up during the manufacturing process, and hence in high surface roughness [93]. It also varies with the set of process parameters, such as laser power and laser speed, used for printing the part [94]. Process parameters are typically optimised according to the arithmetic mean of measured surface roughness (Ra) values [92, 95] or through qualitative observations. As-built surfaces typically show a surface of fully melted material beneath a layer of powdered particles stuck to this surface. To develop a feedback loop for optimising the manufacturing process, measurements of surface quality are no-contact and taken from a height above the printed part. Mean values of surface roughness are then calculated [96], but these are skewed by a superficial increase in height from the presence of non-melted powder particles on the printed surface [97]. These protrusions have no influence on the part performance under fatigue since they carry little stress [98], but the presence of surface notches leads to stress concentration, and in this case, Ra values are not dependable for predicting material properties or behaviour [99]. Non-destructive evaluation methods are typically used for characterising performance under fatigue with respect to surface features.

For any AM technique, it also remains fundamentally important to understand the mechanism of formation of defects and identify the process parameters giving rise to these. Techniques which use local concentrated sources of thermal energy to produce metallic parts, such as PBF, EBM, DED and WAAM, generally give rise to defects classified according to their degree of severity, namely, (i) pores and voids and (ii) cracks, delamination and/or distortions. Pores and voids are the main defects

found in AM parts with no significant distortion, delamination or cracks otherwise present. Contrastingly, cracks, delamination and distortion (which can result from pore formation) have a more severe effect on the properties of printed parts since they may reduce usability, disrupt the printing process and even physically harm the printing machine itself, as distorted or delaminated parts collide with the recoater blade or drum in PBF or the deposition nozzle in DED. Most machines are generally equipped with fail-safe mechanisms to halt the printing process in the instance of a collision being detected, but minor distortions and cracks can override this since they cause no significant collision that can be detected. The printed part will however still be unusable and can be inspected for defects only after it has been retrieved from the manufacturing chamber. If significant distortion occurs during the printing process, this may also halt the machine and render the previously deposited layers unusable, thereby causing a waste of time, effort and material. Selecting the right process parameters thus allows for defect mitigation and the production of parts with superior physical and mechanical properties.

Pores and voids can be broadly classified into the categories of lack-of-fusion defects, gas porosities and keyhole porosities, all of which result from different sets of process parameters. Porosity is a defect that commonly occurs in metal AM parts, negatively affecting their mechanical properties. Porosity-related defects in parts manufactured by powder-feed DED may be of two types: powder induced and process induced [100]. Powder-induced pores result from the entrapment of the carrier gas inside the feedstock during powder atomisation and are generally spherical in shape. These spherical pores can translate directly to as-fabricated parts. Process-induced pores, on the other hand, occur when the applied thermal energy is insufficient for complete melting of the feedstock or when spatter ejection occurs. These pores are typically non-spherical in shape and occur in a variety of sizes, ranging from the sub-microscopic to the macroscopic. As highlighted by Sames et al. [101], most studies report porosity as being directly influenced by process methodology, so that process parameters need to be accurately tuned to avoid the risk of pore formation. The physical differences in these types of pores are illustrated in Fig. 7.

The occurrence of porosity or voids in a deposited material effectively reduces material density and can be seen at the surface and/or within the bulk of the fabricated part. Most studies on optimising part quality in DED indeed centre on reducing porosity and achieving near-theoretical density. Several factors influence the formation and evolution of pores within a part, such as inherent porosity in the powdered feedstock, gas entrapment during the process (typically visible in the form of spherical pores) and a lack of fusion between the substrate and deposited layer or between successive layers themselves (visible as non-spherical pores) [103]. Issues related to a range of process parameters can also give rise to porosity-related defects in the material. For instance, insufficient laser power being supplied during the deposition process results in a lack of fusion between the substrate and feedstock. Regions with insufficient fusion are characterised by non-melted powder particles visible inside or around the pore. Another type of process-induced porosity, known as shrinkage porosity (or "hot tearing"), arises from the incomplete flow of metal into the melt pool during the solidification process. Further, spatter ejection may also lead to regions of

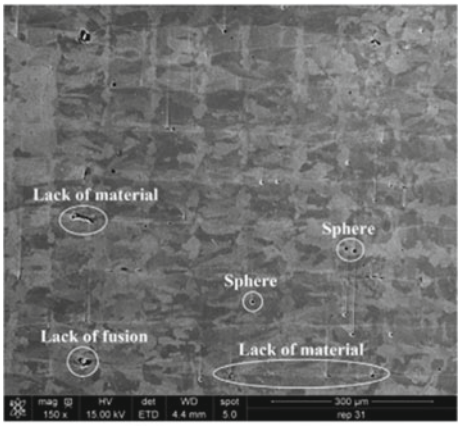

(a) Specimen 31, plane XY

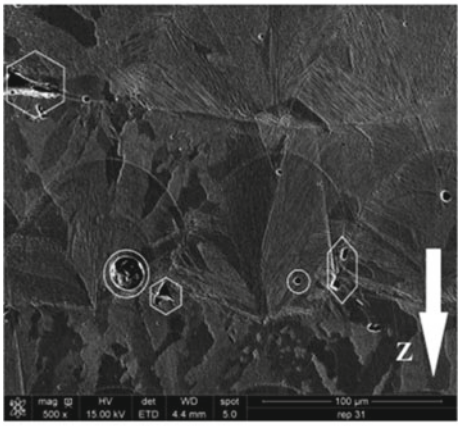

(b) Specimen 31, plane XZ

Fig. 7 SEM micrographs showing different types of defects in SLM-ed Inconel 718, with volumetric energy density, VED = 31.75 J/mm^3. Defects in the circles are of the spherical, gas-entrapment type while the ones in hexagons indicate lack of fusion between the substrate and deposited material or between successive material layers [102]

porosity due to the application of excessive thermal energy. This occurs in contrast to pores arising from a lack of fusion where insufficient energy is applied. In PBF, process-induced porosity may occur during the mechanism of powder consolidation from a loosely packed powder bed into a fully dense part [104]. The powder distributed includes particles that are larger than the layer thickness so that, upon melting, these consolidate into a layer of the required height.

Porosity-related defects can be further categorised according to whether they occur between deposited material layers (***interlayer*** porosity which occurs due to a lack of fusion) or within layers (***intralayer*** porosity which may lead to keyholing). The concept of global energy density (GED) for laser-based DED processes was introduced to establish the relationship between these two types of porosity, as defined according to Eq. 1 [105, 106]:

$$GED = \frac{P}{vd} \tag{1}$$

where P is the laser power, ν is the scanning speed and d is the laser spot size.

GED can be readily correlated with dilution. Lower values of GED lead to a lower degree of dilution, indicating a higher tendency to defects due to a lack of fusion, whereas higher values of GED lead to a higher degree of dilution, indicating a higher tendency for the keyholing phenomenon to occur [106]. Wolff et al. highlighted that interlayer and intralayer porosity-related defects occur in regions of low and high values of GED, respectively [105]. Dass et al. further reported that the likelihood of lack-of-fusion defects occurring increases with decreasing GED in the region of low GED, while the likelihood of keyholing occurring decreases with increasing GED in the region of high GED [106]. The track overlap ratio has also been shown to affect the degree of porosity in parts fabricated by the LAM-DED process [106]. For LAM-DED, this ratio typically represents 25% of the width of the deposited bead [106].

When fusion process parameters are optimised, the process-induced porosity can be reduced to very low levels in all of DED, LM and EBM, resulting in AM parts that are over 99% dense [32, 107, 108]. While the differences in how process-induced porosity arises have not been fully studied, several studies have been carried out on the influence of process parameters (notably laser power and scanning speed) on powder- and process-induced porosity [31]. In a comparison study between the processes of electron beam melting (EBM) and selective laser melting (SLM) for depositing Ti6Al4V powder, Zhao et al. [109] observed differences in both the distribution and characteristics of pores. Most pores formed in the SLM process were located at the interface between deposited beads, showing a close correlation between pore distribution and the deposition strategy. The input beam energy for EBM is also much higher than for SLM, so that the former process benefits from lower porosity: the spherical pores detected by Zhao et al. were powder induced rather than process induced. In processes with a laser beam input, such as SLM, however, the formation of flat- or irregular-shaped pores was attributed to incomplete homologous melting and solidification, especially for the smallest deposited part [109].

A study by Kumar et al. [110] on the influence of laser power and scan speed on porosity in laser powder bed fusion-processed Inconel 718 showed that the physical characteristics of the melt pool are critical regarding porosity fraction and pore shape. These both vary with the size and shape of the melt pool, in turn determined by the deposition process parameters. This was also observed by Criales et al. [111] in their study on L-PBF process parameters and scan strategy for Inconel 625. Kumar et al. observed the melt-pool width to be a critical parameter in optimising the hatch distance, which is important to the process as it determines the remelting and solidification of previously solidified beads during subsequent laser passes, and poses a risk of void formation, increase in surface roughness and complicated evolution of the microstructure [110]. Furthermore, significant variations in the width and depth of the melt pool can lead to uneven melting of the metal powder. For a given laser beam diameter and hatch distance, some powder particles partially fuse in the region where the hatch distance exceeds the melt-pool dimensions, leading to physical defects [110]. These significantly impact the build quality and determine the level of post-processing required for AM parts.

In their study, Kumar et al. found increasing scanning speed to improve the process efficiency; however, this increase was limited by pore formation at a given threshold of laser power. Low scanning speeds could reduce the pore formation but delay completion of the part deposition process. To optimise build quality and/or time taken to complete deposition, especially in industrial contexts, the parameters under investigation therefore need to be varied carefully. The study also showed that increasing the scan speed led to a linear increase in porosity fraction. However, increasing the laser power resulted in a rapid reduction of this porosity fraction. A trade-off is thus needed to assess acceptable levels of porosity against increasing efficiency and increasing cost. Using a single correlated parameter such as energy density could not be used to characterise both trends for the build quality. To achieve optimised porosity levels of <1% and <2%, Kumar et al. hence chose to propose individual windows for the process parameters of energy density, scan speed and laser power.

Studies on porosity have suggested that the degree of porosity in printed parts itself may be of less importance than the morphology of the pores, and their mechanism of formation, in determining the mechanical properties of the final product. For instance, Gong et al. [112] showed that 1% of keyhole porosities had very little influence on the tensile strength of AM parts, while the same degree of lack-of-fusion porosities significantly degraded their mechanical properties. Under static loading conditions, the size of small pores, below a certain critical level, may be harmless to the performance of the overall part (dependent on the material under consideration) [113], but morphology is more significant: by classifying voids according to principal curvature analysis, Kasperovich et al. [114] observed that sharp irregularities in pores can act as stress concentrators. Snow et al. [115] also drew attention to the formation of pores and voids being partly stochastic since the complete systematic control of process conditions such as power fluctuations, particle packing and scatter remains intractable. The presence of pores in printed material therefore does not influence part quality by itself, as opposed to the geometry and mechanism of formation of the pores. Since pores and voids are highly likely to occur during the AM process, it may be both impractical and unnecessary to eliminate them completely, but some level and type of porosity could be allowed, depending on the application of the AM part, and even controlled through an appropriate selection of process parameters.

Another type of defect that is commonly observed in AM is cracking. Cracks that propagate through deposited layers or between them are usually formed during the solidification of the melt pool, especially in the case of high or uneven cooling rates. This leads to non-uniform material shrinkage and states of residual stress (within compositionally singular or different materials). When the material is loaded, these cracks can propagate or even initiate new cracks. The occurrence of cracks can significantly reduce overall strength and fatigue life of printed parts, the mitigation of which is imperative through careful process planning and parameter control.

Process parameters also have a direct influence on the residual stresses set up in AM parts from the rapid cyclical heating and cooling that occurs during printing [116, 117], and which may induce cracks, delamination and distortions. Through extensive experimental study, Bartlett and al. [118] concluded that residual stresses may be minimised by using the lowest possible effective energy input. Along with

tuning process parameters, substrate or base plate preheating may also be used as a solution for mitigating the magnitude of residual stresses and their impact on the quality of the final product [51]. Preheating may moreover reduce the mechanical performance of printed parts, due to the formation of larger grain sizes at lower cooling rates. Preheating temperatures also have to be finely tuned according to the thermodynamic system of the alloy under consideration: if they exceed a certain threshold, the formation of undesirable microstructures may have an adverse effect on the mechanical properties of the printed material [119]. Additionally, preheating consumes a higher amount of energy during the AM process and thermal control of the base plate needs to be carefully designed to ensure even and homogeneous heating. It is therefore a safer and more straightforward option to manage residual stresses through an appropriate selection of process parameters, which can be varied to not only minimise the occurrence of defects but also enhance the final quality of printed material. Pressure in the manufacturing chamber for instance may be adjusted to determine the morphology of the melt pool [120] and stability of any keyhole arising during the process [121]. Ikehata et al. [122] demonstrated that different gaseous atmospheres and concentrations may be calibrated for refining the grain in AM parts, indicating that the shielding gas used to prevent oxidation during printing may also act as a process parameter. In the PBF process, nominal laser power delivered to the feedstock can also be reduced by the shielding gas used [123], while the type of gas used and flow velocities influence the quality of printing. Shielding gas velocities can disrupt the packing of particles in the powder bed and give rise to porosity [123, 124]. Further, the shielding gas can directly affect the characteristics of the vapour plume [123, 125, 126] as the impingement angle of the plume disrupts the powder bed and the shape of the plume relative to the direction of flow of the shielding gas affects oxidation and reduction characteristics [127]. The altered characteristics of the oxidation process would then in turn affect the melt-pool dynamics and part quality due to the modified oxygen levels. The vapour plume formed under different process conditions also leads to differences in spatter, which has been seen to cause defects in AM parts.

It is important to note that most optimisation processes in AM are based on the assumption of the parameters having a constant value. This is not always true since any printing process includes a level of uncertainty for which analysis methods can be applied. Some parameters have however been studied in detail, such as the effective layer thickness which varies throughout the printing process and reaches a steady state [53, 128, 129] different from the nominal powder thickness set by the practician at the start. This may occur due to powder packing density and material consolidation during each deposition process [129] and shows that process windows should be established for considering these factors during optimisation, as demonstrated by Ahn et al. [130]. Optimised parameters may indeed vary between the initial and steady-state stages of the printing process and parameters should only be considered to be "constant" when a quasi-steady state has been reached in the process.

Furthermore, process parameter optimisation is not uniform across all properties of interest and applications. Gong et al. [14], for instance, demonstrated that different sets of parameters are required for maximising each of tensile strength,

hardness and fatigue resistance in Ti6Al4V. The AM practitioner should therefore base the selection of process parameters on the manufacturing objectives and application requirements. It is commonly assumed that minimising surface roughness in AM parts is essential to achieving a better fatigue response, for instance, but this is applicable rather to aerospace and automotive applications, where structural efficiency and integrity are key to the performance of the printed part [131, 132]. In the production of medical implants, however, a higher surface roughness is preferred for osteogenesis, where mechanical properties are not maximised but instead specifically tailored to the original bone material [133]. For orthodontic applications, the production of customised brackets requires minimal distortion and porosity in the material [134], proving that parametric optimisation is always application specific. The optimisation of process parameters is also directly linked to part quality, since they influence the physics of the manufacturing process: an inadequate parametric selection will result in poorly fabricated parts along with wasted time, materials and energy. While parameters have been traditionally optimised for high part densification, certain newer applications may require them to be tailored for a desired output not related to the highest achievable strength or ductility of the printed part. Setting clear and definite application objectives is thus central to selecting the right process parameters.

7 Conclusion

In this chapter, we have reviewed the influence of process parameters on induced physical properties of parts printed using various AM techniques. We have focussed particularly on metallic bioimplants since these are generally high value, and manufacturing them additively lends to customisation, for which there is rising demand from patients. Due to the costs incurred, the margin of error during fabrication needs to be kept low as physical defects and poor mechanical performance can prove even more expensive to rectify in the finished product. It is important to select a controlled set of process parameters and operating conditions which ensure a high-quality finish and robust performance of the part, especially for sustained operation in the inner environment of the human body. While parametric optimisation is not fully mastered yet, it has been studied by a number of researchers as outlined in this chapter.

Studies on the influence of first-order process parameters on the external morphology of deposited metal powder beads have shown that the scanning speed has a significant effect on bead width and height, while laser power only influences bead width—increasing power results in larger bead widths and a reduced occurrence of porosity-related defects. Additionally, preheating the substrate prior to deposition significantly increases both bead width and height. Using too low powder feed rates has however been preconised against, as higher laser energy is then available for melting the substrate instead of the feedstock, yielding higher levels of dilution and eventually leading to keyholing. Insufficient laser power being supplied during the deposition process results in a lack of fusion between the substrate and feedstock,

giving rise to porosity. Regions with insufficient fusion are characterised by non-melted powder particles visible inside or around the pore, while shrinkage porosity arises from the incomplete flow of metal into the melt pool during the solidification process. Low scanning speeds have notably been shown to reduce pore formation, but they delay completion of the deposition process. In industrial contexts, a trade-off between reducing defects and achieving process efficiency is thus essential to the manufacturing process.

The evaluation of different deposition strategies has shown that the contour strategy results in the best part performance, followed by zigzag, chessboard and linear paths. In terms of physical properties, the linear, zigzag and chessboard paths can result in workpieces with a narrow range of microhardness, while contours result in deposits with low average microhardness, but the most uniform thermal distribution. Different AM techniques employ different process parameters and handling of the build material, and this also influences the formed microstructure of printed parts; this is especially true for printed Ti6Al4V alloys. Microstructure has also been found to be directly influenced by the thermal history of the final part, since it directly determines the size, morphology and texture of the grains, the type, size and spatial distribution of defects, and the occurrence of residual stresses.

Finally, in view of this evaluation, we suggest further research into optimising material deposition with respect to first-order parameters, particularly scanning speed and powder feed rate, as this remains limited in existing literature. We further propose deeper study into the feasibility of using DED for bioimplant manufacture since it appears to be an established, widely used AM technique, and does not result in significant thermal distortion in the base metal.

References

1. Linke R (2017) Additive manufacturing, explained [online]. Available at: https://mitsloan.mit.edu/ideas-made-to-matter/additive-manufacturing-explained. Accessed 22 September 2022
2. Javaid M, Haleem A (2018) Additive manufacturing applications in medical cases: a literature-based review. Alexandria J Med 54:411–422
3. Vignesh M, Ranjith Kumar G, Sathishkumar M, Manikandan M, Rajyalakshmi G, Ramanujam R, Arivazhagan N (2021) Development of biomedical implants through additive manufacturing: a review. J. Materi Eng Perform 30:4735–4744. https://doi.org/10.1007/s11665-021-05578-7
4. Hack H et al (2017) Mechanical properties of additive manufactured nickel alloy 625. Addit Manuf 14:105–115
5. Dominguez R, Ku-Herrera JJ, Hernandez-Perez A (2017) An assessment of the effect of printing orientation, density, and filler pattern on the compressive performance of 3D printed ABS structures by fuse deposition. Int J Adv Manuf Technol 2017:1–11
6. Dao D (2014) Precision engineering & prototyping. Lecture Notes. Rapid Prototyping & Reverse Engineering, ENG3313, School of Engineering, Griffith University, Gold Coast
7. Kanishka K, Acherjee B (2023) A systematic review of additive manufacturing-based remanufacturing techniques for component repair and restoration. J Manuf Process 89:220–283

8. Nouri A, Rohani Shirvan A, Li Y, Wen C (2021) Additive manufacturing of metallic and polymeric load-bearing biomaterials using laser powder bed fusion: a review. J Mater Sci Technol 94:196–215
9. Chittewar SL, Patil NG (2021) Surface integrity of conventional and additively manufactured nickel superalloys: a review. Mater Today Proc 44:701–708
10. Shi H, Zhou P, Li J, Liu C, Wang L (2021) Functional gradient metallic biomaterials: techniques, current scenery, and future prospects in the biomedical field. Front Bioeng Biotechnol 8:616845
11. Gu DD, Meiners W, Wissenbach K, Poprawe R (2012) Laser additive manufacturing of metallic components: materials, processes, and mechanisms. Int Mater Rev 57:133–164
12. Sun S, Brandt M, Easton M (2017) Powder bed fusion processes: an overview. Laser addit manuf 2017:55–77
13. Shamsaei N, Yadollahi A, Bian L, Thompson SM (2015) An overview of direct laser deposition for additive manufacturing; Part II: mechanical behavior, process parameter optimization and control. Addit Manuf 8:12–35
14. Gu H, Gong H, Pal D et al (2013) Influences of energy density on porosity and microstructure of selective laser melted 174PH stainless steel. In: 2013 solid freeform fabrication symposium, vol 474
15. Liu Y, Liu C, Liu W et al (2019) Optimization of parameters in laser powder deposition AlSi10Mg alloy using Taguchi method. Opt Laser Techn 111:470–480
16. Gockel J, Sheridan L, Koerper B, Whip B (2019) The influence of additive manufacturing processing parameters on surface roughness and fatigue life. Int J Fatigue 124:380–388
17. Metelkova J, Kinds Y, Kempen K et al (2018) On the influence of laser defocusing in selective laser melting of 316L. Addit Manuf 23:16169
18. Sow M, De Terris T, Castelnau O et al (2020) Influence of beam diameter on Laser Powder Bed Fusion (LPBF) process. Addit Manuf 36:101532
19. Ladewig A, Schlick G, Fisser M, Schulze V, Glatzel U (2016) Influence of the shielding gas flow on the removal of process byproducts in the selective laser melting process. Addit Manuf 10:1–9
20. Anwar AB, Pham QC (2018) Study of the spatter distribution on the powder bed during selective laser melting. Addit Manuf 22:86–97
21. Harun WSW, Manam NS, Kamariah MSIN, Sharif S, Zulkifly AH, Ahmad I, Miura H (2018) A review of powdered additive manufacturing techniques for Ti-6al-4v biomedical applications. Powder Technol 331:74–97
22. Basariya MR, Srivastava V, Mukhopadhyay N (2014) Microstructural characteristics and mechanical properties of carbon nanotube reinforced aluminum alloy composites produced by ball milling. Mater Des 64:542–549
23. Wang P, Zhang B, Tan CC et al (2016) Microstructural characteristics and mechanical properties of carbon nanotube reinforced Inconel 625 parts fabricated by selective laser melting. Mater Sci Techn 112:290–299
24. Wang L-z, Chen T, Wang S (2017) Microstructural characteristics and mechanical properties of carbon nanotube reinforced AlSi10Mg composites fabricated by selective laser melting. Optik 143:173–179
25. King WE, Barth HD, Castillo VM et al (2014) Observation of keyholemode laser melting in laser powderbed fusion additive manufacturing. J Mat Proc Techn 214:2915–2925
26. Bayat M, Thanki A, Mohanty S et al (2019) Keyholeinduced porosities in Laserbased Powder Bed Fusion (LPBF) of Ti6Al4V: highfidelity modelling and experimental validation. Add Manuf 30:100835
27. Cunningham R, Zhao C, Parab N et al (2019) Keyhole threshold and morphology in laser melting revealed by ultrahighspeed xray imaging. Science 363:849–852
28. Jadhav SD, Goossens LR, Kinds Y, Van Hooreweder B, Vanmeensel K (2021) Laserbased powder bed fusion additive manufacturing of pure copper. Addit Manuf 42:101990
29. Corbin DJ, Nassar AR, Reutzel EW, Beese AM, Kistler NA (2017) Effect of directed energy deposition processing parameters on laser deposited Inconel® 718: external morphology. J Laser Appl 29:022001

30. Sreekanth S, Ghassemali E, Hurtig K, Joshi S, Andersson J (2020) Effect of direct energy deposition process parameters on single-track deposits of alloy 718. Metals 10:96. https://doi.org/10.3390/met10010096
31. Kobryn PA, Moore EH, Semiatin SL (2000) Effect of laser power and traverse speed on microstructure, porosity, and build height in laser-deposited Ti-6Al-4V. Scr Mater 43:299–305
32. Vilaro T, Colin C, Bartout JD (2011) As-fabricated and heat-treated microstructures of the Ti-6Al-4V alloy processed by selective laser melting. Metall. Mater Trans A Phys Metall Mater Sci 42:3190–3199
33. Ahn D-G (2021) Directed energy deposition (DED) process: state of the art. Int J Precis Eng Manuf Green Tech 8:703–742
34. Ribeiro KSB, Mariani FE, Coelho RT (2020) A study of different deposition strategies in direct energy deposition (DED) processes. Procedia Manuf 48:663–670
35. ASM International Handbook Committee, 1990. Metals Handbook. 10th ed. vol. 1. Novelty: ASM International
36. Zhang K, Wang S, Liu W, Shang X (2014) Characterization of stainless-steel parts by laser metal deposition shaping. Mater Des 55:104–119. https://doi.org/10.1016/j.matdes.2013.09.006
37. Chen T, Wu W, Li W, Liu D (2019) Laser cladding of nanoparticle TiC ceramic powder: effects of process parameters on the quality characteristics of the coatings and its prediction model. Opt Laser Technol 116:345–355
38. Majumdar JD, Manna I (2003) Laser processing of materials. Sadhana 28(3–4):495–562
39. Lancaster JF (1984) The physics of welding. Phys Technol 15(2):73
40. TWI Ltd (2023) What is the Heat Affected Zone (HAZ)? TWI. Available at: https://www.twi-global.com/technical-knowledge/faqs/what-is-the-heat-affected-zone. Accessed May 17, 2023
41. DebRoy T, Wei H, Zuback J et al (2018) Additive manufacturing of metallic components–process, structure and properties. Progr Mat Sci 92:112–224
42. Piglione A, Dovgyy B, Liu C et al (2018) Printability and microstructure of the CoCrFeMnNi highentropy alloy fabricated by laser powder bed fusion. Materi Lett 224:22–25
43. Nguyen DS, Park HS, Lee CM (2020) Optimization of selective laser melting process parameters for Ti6Al4V alloy manufacturing using deep learning. J Manuf Proc 55:230–235
44. Sun Z, Tan X, Tor SB, Chua CK (2018) Simultaneously enhanced strength and ductility for 3Dprinted stainless steel 316L by selective laser melting. NPG Asia Mater 10:127–136
45. Sun S-H, Ishimoto T, Hagihara K et al (2019) Excellent mechanical and corrosion properties of austenitic stainless steel with a unique crystallographic lamellar microstructure via selective laser melting. Script Materi 159:89–93
46. Roehling TT, Shi R, Khairallah SA et al (2020) Controlling grain nucleation and morphology by laser beam shaping in metal additive manu facturing. Mater Des 195:109071
47. Kok Y, Tan XP, Wang P et al (2018) Anisotropy and heterogeneity of microstructure and mechanical properties in metal additive manufacturing: a critical review. Mater Des 139:565–586
48. Dilip J, Zhang S, Teng C et al (2017) Influence of processing parameters on the evolution of melt pool, porosity, and microstructures in Ti6Al4V alloy parts fabricated by selective laser melting. Progr Addit Manuf 2:157–167
49. Pham MS, Dovgyy B, Hooper PA, Gourlay CM, Piglione A (2020) The role of sidebranching in microstructure development in laser powderbed fusion. Nat Comm 11:1–12
50. Bustillos J, Kim J, Moridi A (2021) Exploiting lack of fusion defects for microstructural engineering in additive manufacturing. Addit Manuf 48:102399
51. Chia HY, Wu J, Wang X, Yan W (2022) Process parameter optimization of metal additive manufacturing: a review and outlook. J Mater Inf 2:16
52. Brandl E, Heckenberger U, Holzinger V, Buchbinder D (2012) Additive manufactured AlSi10Mg samples using Selective Laser Melting (SLM): Microstructure, high cycle fatigue, and fracture behavior. Mater Des 34:159–169

53. Spierings AB, Starr TL, Wegener K (2013) Fatigue performance of additive manufactured metallic parts. Rap Prot J
54. Kirboga S, Öner M (2013) Application of experimental design for the precipitation of calcium carbonate in the presence of biopolymer. Powder Technol 249:95–104
55. Van den Eynde M, Verbelen L, Van Puyvelde P (2015) Assessing polymer powder flow for the application of laser sintering. Powder Technol 286:151–155
56. Cheng A et al (2017) Laser sintered porous Ti–6Al–4V implants stimulate vertical bone growth. Ann Biomed Eng 45:1–11
57. Cheng A et al (2016) Laser sintered constructs with bio-inspired porosity and surface micro/nano roughness enhance mesenchymal stem cell differentiation and matrix mineralization in vitro. Tissue Int 99:625–637
58. Hyzy S et al (2016) Novel hydrophilic nanostructured microtexture on direct metal laser sintered Ti-6Al-4V surfaces enhances osteoblast response in vitro and osseointegration in a rabbit model. J Biomed Mater Res A 104:2086–2098
59. Ahmed M et al (2017) The effect of thermo-mechanical processing and ageing time on microstructure and mechanical properties of powder metallurgy near β titanium alloys. J Alloys Compd 714:610–618
60. Greitemeier D et al (2017) Fatigue performance of additive manufactured TiAl6V4 using electron and laser beam melting. Int J Fatigue 94:211–217
61. Manfredi D et al (2013) Direct Metal Laser Sintering: an additive manufacturing technology ready to produce lightweight structural parts for robotic applications, La Metall. Ital 1:15–24
62. Harun W, Safian S, Idris M (2009) Evaluation of ABS patterns produced from FDM for investment casting process. Comput Method Exp Mater Characterisation IV 64:319–328
63. Konečná R et al. (2017) High cycle fatigue life of Ti6Al4V alloy produced by direct metal laser sintering, Solid State Phenom 258:522–525 (Ahmed et al., 2016)
64. Ahmed SH et al (2016) Effect of process parameters on hardness, temperature profile and solidification of different layers processed by direct metal laser sintering (DMLS). AIP conference proceedings. AIP Publishing
65. Xu Y et al (2017) Effect of annealing treatments on the microstructure, mechanical properties and corrosion behavior of direct metal laser sintered Ti-6Al-4V. J Mater Eng Perform 26:2572–2582
66. Bača A, Konečná R, Nicoletto G (2017) Influence of the direct metal laser sintering process on the fatigue behavior of the Ti6Al4V alloy. Mater Sci Forum 891:317–321
67. Wauthle R et al (2015) Effects of build orientation and heat treatment on the microstructure and mechanical properties of selective laser melted Ti6Al4V lattice structures. Addit Manuf 5:77–84
68. Wauthle R et al (2015) Revival of pure titanium for dynamically loaded porous implants using additive manufacturing. Mater Sci Eng C 54:94–100
69. Van Hooreweder B et al (2017) Improving the fatigue performance of porous metallic biomaterials produced by selective laser melting. Acta Biomater 47:193–202
70. Van Hooreweder B, Kruth J-P (2017) Advanced fatigue analysis of metal lattice structures produced by selective laser melting, CIRP Ann. Manuf Technol 66:221–224
71. Van Hooreweder B et al (2012) Analysis of fracture toughness and crack propagation of Ti6Al4V produced by selective laser melting. Adv Eng Mater 14:92–97
72. Shen Y, Gu D, Wu P (2008) Development of porous 316L stainless steel with controllable microcellular features using selective laser melting. Mater Sci Technol 24:1501–1505
73. Lindemann CFW, Jahnke U (2017) 11—Modelling of laser additive manufactured product lifecycle costs A2—Brandt. Laser Additive Manufacturing, Woodhead Publishing, Cambridge, Milan, pp 281–316
74. Zhang S et al (2014) Effects of scan line spacing on pore characteristics and mechanical properties of porous Ti6Al4V implants fabricated by selective laser melting. Mater Des 63:185–193
75. Van Bael S et al (2012) The effect of pore geometry on the in vitro biological behavior of human periosteum-derived cells seeded on selective laser-melted Ti6Al4V bone scaffolds. Acta Biomater 8:2824–2834

76. Poondla N et al (2009) A study of the microstructure and hardness of two titanium alloys: commercially pure and Ti–6Al–4V. J Alloys Compd 486:162–167
77. Sun S-D et al (2010) Hot deformation behavior and microstructure evolution of TC4 titanium alloy. Trans Nonferrous Metals Soc China 20:2181–2184
78. Vrancken B et al (2012) Heat treatment of Ti6Al4V produced by selective laser melting: microstructure and mechanical properties. J Alloys Compd 541:177–185
79. Sun J, Yang Y, Wang D (2013) Mechanical properties of a Ti6Al4V porous structure produced by selective laser melting. Mater Des 49:545–552
80. Liao S-C, Duffy J (1998) Adiabatic shear bands in a Ti-6Al-4V titanium alloy. J Mech Phys Solids 46:2201–2231
81. Mullen L et al (2010) Selective laser melting: a unit cell approach for the manufacture of porous, titanium, bone in-growth constructs, suitable for orthopedic applications. II. Randomized structures. J Biomed Mater Res B Appl Biomater 92:178–188
82. Mullen L et al (2009) Selective laser melting: a regular unit cell approach for the manufacture of porous, titanium, bone in-growth constructs, suitable for orthopedic applications. J Biomed Mater Res B Appl Biomater 89:325–334
83. Stamp R et al (2009) The development of a scanning strategy for the manufacture of porous biomaterials by selective laser melting. J Mater Sci Mater Med 20:1839–1848
84. Douglas T et al (2009) Rapid prototyping: porous titanium alloy scaffolds produced by selective laser melting (SLM) for bone tissue engineering. Tissue Eng A 15:07–08
85. Warnke PH et al (2008) Rapid prototyping: porous titanium alloy scaffolds produced by selective laser melting for bone tissue engineering, Tissue Eng. Part C Methods 15:115–124
86. Yadroitsev I, Krakhmalev P, Yadroitsava I (2014) Selective laser melting of Ti6Al4V alloy for biomedical applications: temperature monitoring and microstructural evolution. J Alloys Compd 583:404–409
87. Yadroitsev I, Bertrand P, Smurov I (2007) Parametric analysis of the selective laser melting process. Appl Surf Sci 253(19):8064–8069
88. Benedetti M et al (2017) The effect of post-sintering treatments on the fatigue and biological behavior of Ti-6Al-4V ELI parts made by selective laser melting. J Mech Behav Biomed Mater 71:295–306
89. Bandyopadhyay A et al (2010) Influence of porosity on mechanical properties and in vivo response of Ti6Al4V implants. Acta Biomater 6:1640–1648
90. Sandgren HR et al (2016) Characterization of fatigue crack growth behavior in LENS fabricated Ti-6Al-4V using high-energy synchrotron x-ray microtomography. Addit Manuf 12(Part A):132–141
91. Zhai Y, Galarraga H, Lados DA (2016) Microstructure, static properties, and fatigue crack growth mechanisms in Ti-6Al-4V fabricated by additive manufacturing: LENS and EBM. Eng Fail Anal 69:3–14
92. Townsend A, Senin N, Blunt L, Leach RK, Taylor J (2016) Surface texture metrology for metal additive manufacturing: a review. Precis Eng 46:34–47
93. Barari A, Kishawy HA, Kaji F, Elbestawi MA (2016) On the surface quality of additive manufactured parts. Int J Adv Manuf Technol
94. Fox JC, Moylan SP, Lane BM (2016) Effect of process parameters on the surface roughness of overhanging structures in laser powder bed fusion additive manufacturing. 3rd CIRP conference on surface integrity
95. Triantaphyllou A, Giusca CL, Macaulay GD, Hoebel M, Leach RK, Tomita B, Milne KA (2015) Surface texture measurement for additive manufacturing. Surf Topogr Metrol Prop 3(2)
96. Grimm T, Wiora G, Witt G (2015) Characterization of typical surface effects in additive manufacturing with confocal microscopy. Surf Topogr Metrol Prop 3(1)
97. Whip B (2018) The effect of processing parameters on surface roughness influencing performance in additively manufactured alloy 718. Wright State University
98. Kantzos C, Cunningham RW, Tari V, Rollett AD (2018) Characterization of metal additive manufacturing surfaces using synchrotron X-ray CT and micromechanical modeling. Comput Mech 2018:575–580

99. Arola D, Ramulu M (1999) An examination of the effects from surface texture on the strength of fiber reinforced plastics. J Compos Mater 33(2):102–123
100. Sames WJ, Medina F, Peter WH, Babu SS, Dehoff RR (2014) Effect of process control and powder quality on inconel 718 produced using electron beam melting. In: Superalloy 718 and Derivatives, Pittsburgh, PA
101. Sames WJ, List FA, Pannala S, Dehoff RR, Babu SS (2016) The metallurgy and processing science of metal additive manufacturing. Int Mater Rev 61:315–360
102. Moussaoui K, Rubio W, Mousseigne M, Sultan T, Rezai F (2018) Effects of Selective Laser Melting additive manufacturing parameters of Inconel 718 on porosity, microstructure and mechanical properties. Mater Sci Eng, A 735:182–190
103. Gualtieri T, Bandyopadhyay A (2018) Additive manufacturing of compositionally gradient metal-ceramic structures: Stainless steel to vanadium carbide. Mater Des 139:419–428
104. Korner C, Bauereiss A, Attar E (2013) Fundamental consolidation mechanisms during selective beam melting of powders. Modelling Simul Mater Sci Eng 21:18
105. Wolff SJ (2018) Laser-matter interactions in directed energy deposition [PhD thesis] Northwestern University. https://doi.org/10.21985/n2-vfnr-8542
106. Dass A, Moridi A (2019) State of the art in directed energy deposition: from additive manufacturing to materials design. Coatings 9:418. https://doi.org/10.3390/coatings9070418
107. Frazier W (2014) Metal additive manufacturing: a review. J Mater Eng Performance, 1–12
108. Svensson M (2009) Ti6Al4V manufactured with electron beam melting (EBM): mechanical and chemical properties. In: Aeromat 2009, Dayton, OH
109. Zhao X, Li S, Zhang M, Liu Y, Sercombe TB, Wang S, Hao Y, Yang R, Murr LE (2016) Comparison of the microstructures and mechanical properties of Ti–6Al–4V fabricated by selective laser melting and electron beam melting. Mater Des 95:21–31
110. Kumar P, Farah J, Akram J, Teng C, Ginn J, Misra M (2019) Influence of laser processing parameters on porosity in Inconel 718 during additive manufacturing. Int J Adv Manuf Technol 103:1497–1507
111. Criales LE, Arisoy YM, Lane B et al (2017) Laser powder bed fusion of nickel alloy 625: experimental investigations of effects of process parameters on melt pool size and shape with spatter analysis. Int J Mach Tools Manuf 121:22–36
112. Gong H, Rafi K, Gu H et al (2015) Influence of defects on mechanical properties of Ti–6Al–4V components produced by selective laser melting and electron beam melting. Mater Des 86:545–554
113. Du Plessis A, Yadroitsava I, Yadroitsev I (2020) Effects of defects on mechanical properties in metal additive manufacturing: a review focusing on Xray tomography insights. Mater Des 187:108385
114. Kasperovich G, Haubrich J, Gussone J, Requena G (2016) Correlation between porosity and processing parameters in TiAl6V4 produced by selective laser melting. Mater Des 105:160–170
115. Snow Z, Nassar A, Reutzel EW (2020) Review of the formation and impact of flaws in powder bed fusion additive manufacturing. Addit Manuf 2020:101457
116. Li C, Liu Z, Fang X, Guo Y (2018) Residual stress in metal additive manufacturing. Proced Cirp 71:348–353
117. Mercelis P, Kruth JP (2006) Residual stresses in selective laser sintering and selective laser melting. Rap Prot J
118. Bartlett JL, Li X (2019) An overview of residual stresses in metal powder bed fusion. Addit Manuf 27:131–149
119. Ali H, Ma L, Ghadbeigi H, Mumtaz K (2017) Insitu residual stress reduction, martensitic decomposition and mechanical properties enhancement through high temperature powder bed preheating of selective laser melted Ti6Al4V. Mater Sci Engin A 695:211–20
120. Calta NP, Martin AA, Hammons JA et al (2020) Pressure dependence of the lasermetal interaction under laser powder bed fusion conditions probed by in situ Xray imaging. Addit Manuf 32:101084

121. Wang L, Zhang Y, Chia HY, Yan W (2022) Mechanism of keyhole pore formation in metal additive manufacturing. npj Comput Mater 8:111
122. Ikehata H, Mayweg D, Jägle E (2021) Grain refinement of Fe–Ti alloys fabricated by laser powder bed fusion. Mater Des 204:109665
123. Shen H, Rometsch P, Wu X, Huang A (2020) Influence of gas flow speed on laser plume attenuation and powder bed particle pickup in laser powder bed fusion. JoM 72:1039–1051
124. Weaver J, Schlenoff A, Deisenroth D, Moylan S (2021) inert gas flow speed measurements in laser powder bed fusion additive manufacturing, advanced manufacturing series (NIST AMS), National Institute of Standards and Technology, Gaithersburg, MD
125. Caballero A, Suder W, Chen X, Pardal G, Williams S (2020) Effect of shielding conditions on bead profile and melting behaviour in laser powder bed fusion additive manufacturing. Addit Manuf 34:101342
126. Reijonen J, Revuelta A, Riipinen T, Ruusuvuori K, Puukko P (2020) On the effect of shielding gas flow on porosity and melt pool geometry in laser powder bed fusion additive manufacturing. Addit Manuf 32:101030
127. Eo DR, Chung SG, Jeon JM, Cho JW (2021) Melt pool oxidation and reduction in powder bed fusion. Addit Manuf 41:101982
128. Bidare P, Maier RRJ, Beck RJ, Shephard JD, Moore AJ (2017) An openarchitecture metal powder bed fusion system for insitu process measurements. Addit Manuf 16:177–185
129. Jansen D, Hanemann T, Radek M et al (2021) Development of actual powder layer height depending on nominal layer thicknesses and selection of laser parameters. J Mater Proc Techn 298:117305
130. Ahn IH (2019) Determination of a process window with consideration of effective layer thickness in SLM process. Int J Adv Manuf Techn 105:4181–4191
131. BlakeyMilner B, Gradl P, Snedden et al (2021) Metal additive manufacturing in aerospace: a review. Mater Des 209:110008
132. Vasco JC (2021) Additive manufacturing for the automotive industry. In: Addit Manuf. Elsevier, pp 505–30
133. Elsayed M, Ghazy M, Youssef Y, Essa K (2019) Optimization of SLM process parameters for Ti6Al4V medical implants. Rapid Prot J
134. Yang Y, Lu Jb, Luo ZY, Wang D (2012) Accuracy and density optimization in directly fabricating customized orthodontic production by selective laser melting. Rap Prot J

Chapter 2
Additive Manufacturing Incorporated Carbon Nanotubes (CNTs); Advances in Biomedical Domain

Sandeep Devgan, Amit Mahajan, and Vinod Mahajan

1 Introduction

Additive manufacturing (AM) can fabricate complex 3D components through a layer-by-layer process by incorporating a variety of powders and wires of multiple materials [1]. Additive manufacturing opens up opportunities for the manufacturing of biological, optical, fluidic, electrical and thermal configurations for various micro-elements of complex scaffolds, sensors, solar panels, robotic motors, electronics and mechanical devices, aerospace fields, automotive parts, etc. [2]. Unlike traditional subtractive manufacturing methods that involve removing material from a larger block, additive manufacturing builds objects by adding material layer upon layer. This layer-by-layer approach allows for intricate and complex geometries that would be challenging or impossible to achieve with other manufacturing techniques [3]. Nonetheless, additive manufacturing continues to advance and evolve, with ongoing research and development focused on improving speed, scalability, materials compatibility, and overall manufacturing capabilities [4]. The principle of additive manufacturing offers several advantages over traditional manufacturing methods. It allows for greater design flexibility, faster prototyping, reduced material waste, and the ability to create complex geometries that may be difficult or impossible to produce using conventional techniques [5]. Additionally, additive manufacturing enables customization and on-demand production, which can lead to cost savings, shorter lead times, and more sustainable manufacturing practices [6].

S. Devgan (✉) · A. Mahajan · V. Mahajan
Department of Mechanical Engineering, Khalsa College of Engineering and Technology, Amritsar 143001, India
e-mail: devgan.sandeep186@gmail.com

A. Mahajan et al. (eds.), *Additive Manufacturing of Bio-implants*, Biomedical Materials for Multi-functional Applications, https://doi.org/10.1007/978-981-99-6972-2_2

2 Additive Manufacturing (AM) and Its Unique Characteristics

Additive manufacturing acts as a revolutionary technology in manufacturing industries that has transformed the way we design, prototype, and manufacture objects and has encompassed various unique characteristics as shown in Table 1.

Table 1 Additive manufacturing (AM) and its unique characteristics

S. no	Features	Characteristics description
1	Design freedom	Exhibits unmatched design freedom, enabling the fabrication of wide range of customized and optimized components, which are difficult or impossible to create using traditional manufacturing methods [7]
2	Customization and personalization	Offers the feasibility to create highly customized products that are matched to specific needs. For instance, in the medical and dentistry industries, where patient-specific implants, prostheses, and orthotics with precise fit are fabricated through additive manufacturing are the best model of customization in process [8]
3	Material versatility	Compatible with a wide range of materials, including plastics, metals, ceramics, and composites. This versatility allows for the production of objects with diverse mechanical, thermal, or electrical properties, opening up opportunities for innovative applications [9]
4	Sustainability	Contribute to sustainability efforts by reducing material waste, energy consumption, and carbon emissions. It enables the production of lightweight structures, optimized designs, and the use of recycled or biodegradable materials [10]
5	Rapid prototyping	Ability to rapidly produce prototypes that accelerates the product development cycle, allowing for faster iterations and design modifications [11]
6	Cost savings	Facilitate cost-cutting approach by eliminating the need for tooling and molds. Additive manufacturing also minimizes material waste as it only uses the essential amount of material for fabrication [11]

3 Nanomaterial-Integrated Additive Manufacturing

A unique concept, i.e., integration of nanomaterials with additive manufacturing techniques holds great potential to enhance the performance and expand the range of applications for 3D printed objects [12]. Ongoing research efforts in this field are paving the way for the development of advanced functional structures and materials with improved properties and tailored functionalities. Numerous studies have explored the integration of nanomaterials into various additive manufacturing techniques, yielding promising results [13, 14]. Various types of nanomaterials used with their key advancements and applications are shown in Table 2.

Table 2 Various types of nanomaterials used with their key advancements and applications

S. no	Types	Various nanomaterials used	Properties influence	Applications
1	Nanocomposites for enhanced mechanical properties	Carbon nanotubes, titanium nanotubes, graphene, nanoceramics	Tensile strength, impact resistance, wear resistance and stiffness	Aerospace fields, automotive parts, orthopedic applications
2	Conductive nanomaterials for electronics	Nanomaterials with high electrical conductivity such as silver nanoparticles and carbon nanotubes, copper fibers	Electrical conductivity, resistivity, dielectric strength, etc	Sensors, conductive traces, electrodes, wearable devices flexible electronics components sensors, solar panels, robotic motors
3	Nanoceramics for improved thermal properties	Ceramic nanoparticles, such as aluminum oxide and boron nitride	Thermal conductivity, thermal expansion, heat resistance, heat capacity, etc	Fluidic devices, Heat sinks, electronic packaging, coils, and thermal management systems
4	Biocompatible nanomaterials for medical domain	Biodegradable nanoparticles, nanohydrogels, and various non-toxic nanocomposites like hydroxyapatite	Biocompatibility, cytotoxicity, cell adhesions, hydrophobic/ hydrophilic properties	Bio-implants, drug delivery systems, tissue engineering scaffolds, and pores structures for tissue regenerations
5	Functional nanomaterials for specialized applications	Magnetic nanoparticles like ferrite nanoparticles or iron oxide nanoparticles, mimetic structures like nano-spheres, nono-rods, chemically inert materials, etc	Permeability and various electronic properties, bio-mimetic properties, bio-inertness, etc	Electrical motor elements, magnetic sensors and actuators, catalysts, nano-structured scaffolds, etc

In recent decades, nanomaterials compatible with biological systems have been explored for 3D printing medical implants, drug delivery systems, and tissue engineering scaffolds. Examples include biodegradable nanoparticles, nanohydrogels, and nanocomposites with enhanced biocompatibility and controlled release properties [15]. Therefore, the nano-scale manufacturing of biomaterials began with the promising of a new domain of nano-cellular responses at the molecular level [16]. The studies were begun with the idea that the nano-scaled manufacturing enhances the biological properties, i.e., cellular functioning along with cell adhesion properties and bulk properties, i.e., mechanical characteristics along with strength, toughness, etc. [9].

3.1 Carbon Nanotubes (CNTs)

During past few decades, in the realm of materials science, Iijima's study on carbon nanotubes (CNTs) from 1991 [17] was revolutionary in material manufacturing domain and promptly investigators from other fields began to pay attention to this unique substance. However, in twenty-first century, Carbon Nanotubes (CNTs) are widely used as ideal reinforcement material or synthesizing of complex components in biomedical domain due to their superior bulk properties, i.e., high tensile strength (100 GPa), high weight-to-strength ratio, Young's modulus (1 TPa), low density (1.7–2.0 g/cm^3), high toughness, exceptional corrosion resistance properties, favorable biocompatibility, and excellent thermal and electrical properties [18, 19]. Various reports on CNT's reinforcement show enhanced bulk properties, accompanied by bio-favorable characteristics. Like, interfacial bonding of additive manufactured polymer/CNT nanocomposites in terms of ultimate tensile stress and fracture stress was studied by Sandoval et al. [20]. The study concluded that a 0.05% (w/v) of CNT addition elevated the ultimate tensile stress and fracture stress of the nanocomposites to 17% and 37%, respectively. Ushiba et al. [21] successfully fabricate the 3D micro/nano-structural single-walled carbon nanotube (SWCNT)/polymer nanocomposites into arbitrary structures with enhanced mechanical and electrical properties. Moreover, Gonçalves et al. [22] showed that a 3D printed nanocomposite hydroxyapatite (HA)/CNTs/PCL scaffold structure has sufficient compressive strength, appropriate porosity, pore size and electrical conductivity, as well as bioactivity and biocompatibility, making it an appropriate choice for utilization in bone regenerative medicine. These studies demonstrated that CNT-reinforced additive manufacturing showed great enhancements in mechanical, biological, electrochemical, and tribological properties of novel fabricated materials and became a next-generation material that is broadly incorporated in biomedical industries.

4 CNTs Incorporated Various AM Techniques

Additive manufacturing, also known as 3D printing, encompasses several different techniques and processes for creating three-dimensional objects. It offers numerous techniques and has found applications across various industries, for instance, powder-bed 3D printing, directed energy deposition (DED), material extrusion, vat photopolymerization, binder jetting, material jetting, and sheet lamination as revealed in Fig. 1.

A vital technique of AM, i.e., 3D inkjet printing, is a low-temperature, low-pressure process in which printing material is extruded through a small nozzle within a print head and layer-by-layer deposition of liquid materials or solid suspensions. The 3D inkjet printing is also known as droplet-based 3D printing, in which the liquid materials or inks are deposited onto a build platform through tiny nozzles in a controlled manner. This method is accessible to various materials like polymers and a wide range of conductive nanoparticles [23].

However, in 3D inkjet technique, the formation of CNT printable ink is the most challenging section which needs significant consideration of various factors such as ink stability, material quality and degree of dispersion and purity of CNT. However, the non-polar feature of CNTs restricts the dispersion of them in water and other polar solvents [25]. Various studies addressed the potentials of 3D inkjet technique of AM for the fabrication of complex shapes. For instance, Wang et al. [26] utilized inkjet printing to fabricate conductive patterns of multi-walled carbon

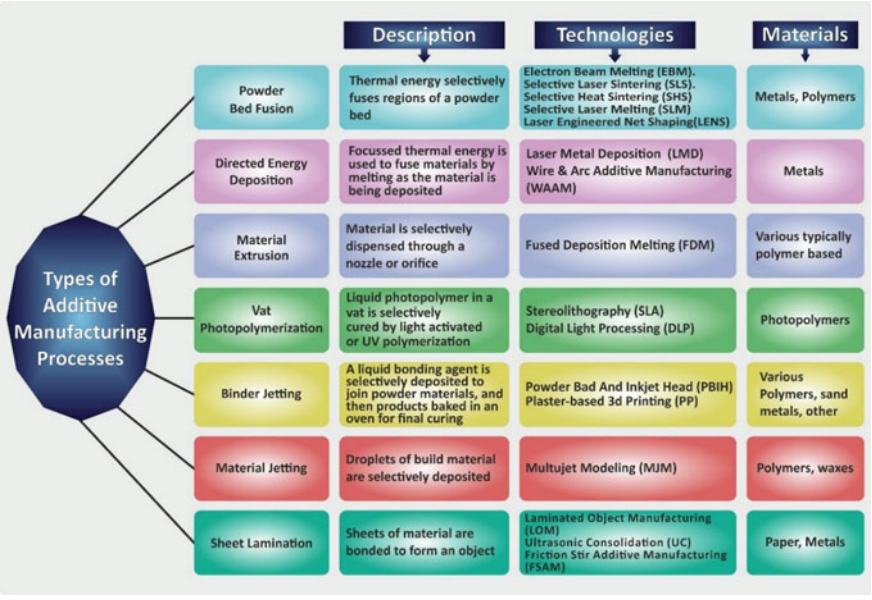

Fig. 1 Various techniques of additive manufacturing [24]

nanotubes (MWCNTs) and Ag nanoparticles. Both the powders are dispersed in water in the presence of dodecyl benzenesulfonate (SDBS) and acceptable stability of patterns was achieved after 50 cycles. However, high retention ratio of 96.9% of its initial capacitance after 3000 cycles was obtained when asymmetric super-capacitors (ASCs) with saturated MWCNT negative electrodes were prepared by addition of nano-manganese dioxide (MnO_2) into the ink. Chou et al. [27] fabricate the porous Fe–Mn substrate with inkjet 3D printing and done investigation on mechanical, electrical, and biological properties. The yield strength, ultimate strength, and Young's modulus of 3D printed iron alloy were significantly closer to that of human bone. In addition, the alloy showed a significantly higher value of the cell viability or cytotoxicity that contributes to the biocompatibility of the alloy. Kang et al. [28] successfully fabricated the all-inkjet-3D printed flexible nano-bio-devices with amphiphilic biomaterial and an M13 phage by incorporating single-walled carbon nanotubes (SWCNT). Inkjet-printed nano-structured electrodes of SWCNT and M13 phage show favorable hydrostability and better electrochemical characteristics (Fig. 2).

Similarly, the direct-write assembly (DW) is an extrusion-based multi-material direct printing system which utilized positive pressure to extrude liquid materials through a small nozzle- or droplet-based DW ejects onto a workpiece [29]. Although Skylar-scott et al. [30] fabricate high-resolution freestanding structure like helical springs using 85% Ag nano-particle ink for direct-write assembly (DW) 3D printing.

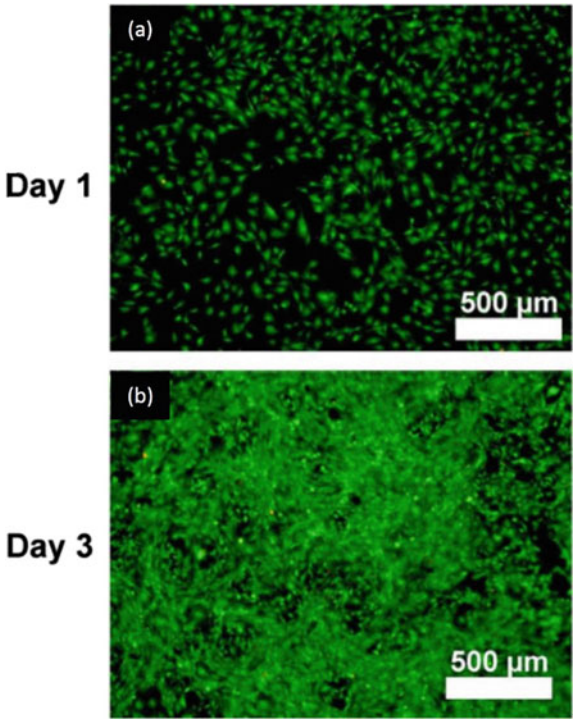

Fig. 2 Fluorescent images from the live/dead assay of live (green) and dead (red) MC3T3 cells attached after 1 and 3 days' culture on 3D printed Fe–30Mn [28]

The observation was laid to manage the location of nozzle and the laser head to avoid the upstream heat transmission and achieved the favorable results. Ou et al. [31] utilized direct-write (DW) 3D printing incorporating aerosol jet focusing through generating aerosol drips by exciting the ink with an ultrasonic atomizer. They fabricated the poly(3,4-ethylenedioxythiophene) polystyrene sulfonate structures on flexible polyimide substrates for biomedical applications. The utilization of well-dispersed high-S Sb_2Te_3 nanoflakes and high-σ multi-walled carbon nanotubes (MWCNTs) lead to enhanced inter-particle connectivity and the thermoelectric performance of polystyrene sulfonate configurations. They concluded that aerosol jet utilization in direct-write assembly enhances the capabilities of process offering the adaptability to print inks constituted of a wide range of materials, like metallic nanoparticles, carbon nanotubes, and biological materials, with a wide span of viscosities.

Another type of additive manufacturing is fused deposition modeling (FDM) in which 3D fused filament fabrication (FFF) is done via material extrusion. In this process, material is selectively dispensed trough a nozzle or orifice and constructs parts via layer by layer through depositing molten substance in a predetermined path [31]. Herein, Wu and Liao [32] successfully fabricated the 3D printing filaments generated from maleic acid grafted PHA (PHA-g-MA) and acid oxidized multi-walled carbon nanotubes (MWCNTs) via fused deposition modeling (FDM). They concluded that by the accumulation of 1 wt% of MWCNTs-COOH, the tensile strength and modulus of PHA-g-MA were significantly increased to 32 MPa and 467 MPa, respectively. Prashantha and Roger [33] successfully had done fused deposition modeling (FDM) on PLA/graphene nanocomposites containing 10 wt% graphene and confirmed the improvement in the thermal and mechanical properties. Fused deposition modeled alloy exhibited uniform distribution of graphene in the PLA matrix with the enhancement in the modulus and strength. Moreover, the additive manufacturing through fused deposition modeling (FDM) has been increasing in fabrication of the biocompatible composite scaffolds with better control of pore size and distribution [34]. Kim et al. [35] studied the in vivo examination on fused deposition 3D printed (FDM) scaffolds by implantation into rabbit femoral bone. The scaffolds consist of biocompatible (D,L-lactide:glycolide) (DL-PLGA) and β-tricalcium phosphate and hydroxyapatite (HA) composites and exhibited sympathetic morphology and biocompatibility and favorable bone regeneration properties. Wu et al. [36] formed a poly(vinyl alcohol)/hydroxyapatite nanocomposites via fused deposition modeling FDM process with high-dimensional accuracy. The nanocomposite scaffolds exhibited higher compressive strength and improved biocompatibility.

Likewise, powder-bed 3D printing is also an additive manufacturing (AM) technique which utilized laser as heat source for the fusion powder particles and commonly known as powder-bed fusion (PBF) technology. Various metals like stainless steel, aluminum, and cobalt, and different polymers like nylon, glass-filled nylon, polypropylene, etc. can be deposited with this process [37]. Likewise, Zhou et al. [38] utilized the powder-bed 3D printing technique and the unique hydrophilic and metal

compatible nanostructure of CNTs leads to develop fine and well-distributed carbon-rich titanium nanocomposites without altering the morphology of powder particles and flowability. H. Shahali et al. [39] fabricated Ti-6Al-4 V porous structures and scaffolds via powder-bed 3D printing technique. They concluded that the pore size and Young's modulus achieved by the powder-bed 3D printing technique was very significant to bone ingrowth (porosity range of 80–95% with Young's modulus of 0.12–1.25 GPa). Moreover, Khimich et al. [40] utilized the powder-bed 3D printing technique to fabricate Ti-Nb alloy. The nano-Ti-Nb alloy powders with grain size of 90 nm were produced by mechanical alloying and the fabricated alloy exhibited the volume fraction of isolated porosity is 2 vol. % and the total porosity is 20 vol. %. MG63 cell line proliferation was done for cell viability analysis of the fabricated porous samples. The cytotoxicity test affirmed that porous Ti-Nb sample surfaces exhibit favorable cell viability.

A unique technique, i.e., micro-stereolithography (MSL) works on the vat photopolymerization technique in which each layer is shaped from fluidic photopolymer resin which re-crystallized with the exposure of ultraviolet rays. Micro-stereolithography (MSL) technique is majorly utilized in the manufacturing of sensors, and other structural objects in microsystems [41]. Farahani et al. [42] investigated the biomaterial domain of micro-stereolithography (MSL) technique by utilizing the functionalization of purified single-walled carbon nanotubes (SWCNTs) in 3D printing process. The morphological, mechanical, and electrical properties of 3D printed nanocomposites were investigated through the preparation of biofunctionalized SWCNTs (BF-SWCNTs) in epoxy resin with solution of dichloromethane. The results concluded that the tensile strength and the modulus of the nanocomposites increased by 76% and 93%, respectively, by the addition of only 1 wt% of biofunctionalized SWCNTs.

An extended version of micro-stereolithography (MSL) is dynamic optical projection stereolithography (DOPS) which utilized a digital-mirror device (DMD), named as dynamic optical projection stereolithography (DOPS) in the fabrication process [43]. Likewise, Chivate, A. and Zhou [44] proposed the modified Schlieren-based observation mechanism for the fabrication of micro-lenses in biomedical domain. The physical experimental results showed the effectiveness of the proposed examination method which exploited confocal magnifying optics to generate a virtual monitor at the camera's focal surface axis. For instance, Miri et al. [45] presented the applications of dynamic optical projection stereolithography (DOPS) in 3D bioprinting of vascular tissue constructs. They concluded that this technique offers functional bioinks which induce angiogenesis and capillary formation within constructs and output structure exhibits suitable vascularization resulting in enhanced tissue regeneration.

Similarly, selective laser sintering (SLS) technique utilized laser powder-bed fusion technique commonly used to sinter powdered material (typically nylon or polyamide) for binding the material for solidification [46]. For example, Li et al. [47] utilized selective laser sintering (SLS) technique by incorporating self-made multi-walled carbon nanotube-wrapped flexible thermoplastic polyurethane (TPU) powder. The MWCNT-wrapped TPU powder was composed of dispersion of MWCNTs in ethanol through ultrasonication and further stirred mechanically to obtain dried

MWCNT-wrapped TPU powder. Machining resulted in the decrease in mechanical strength to some amount after successful completion of 1000 bending cycles. Zhang et al. [48] proposed selective laser sintering (SLS) technique incorporating carbon nanotubes (CNTs) for the fabrication of magnesium-based pore structures for a wide range of applications like biomedical and other industrial domains. They concluded that addition of high laser absorptivity materials (such as carbon nanotubes (CNTs), graphene) can significantly enhance the absorption rate of the Mg alloy powder to the laser. Wu et al. [49] fabricated CNTs/AZ31B composites by selective laser sintering (SLS), and they concluded that the laser absorption was increased by 7.9% by incorporating 1.5 wt% CNTs into AZ31B alloy.

Furthermore, solvent-cast 3D printing (SC-3DP) is also an additive manufacturing technology which utilized volatile solvent binding system. In volatile solvent binding system, the ink having powders of metals or any other materials, mutually with a binder system (containing polymer, volatile solvent, and any other additive), is extruded through a small orifice and sintered to intended configuration [50]. Chizari et al. [51] fabricate stent structure by utilizing mixed solution of CNTs and PLA as printing ink via solvent-cast 3D printing technology. The mixture was prepared by dispersion of ball-milled MWCNTs into the dichloromethane solution and direct dissolving PLA in dichloromethane. They concluded that 30 wt% CNT concentration is the optimal values for printability, mechanical properties, and conductivity of the fabricated stent shapes.

A new concept of two-photon polymerization (TPP) fabricates the solid 3d printed configuration from photoactivable material by non-linear two-photon absorption process. In two-photon absorption process, the transparent photo-material can absorb concurrently two photons in a very small area named as "voxel" which generates focalization cone. Correspondingly, in the voxel, the liquid monomer becomes a solid polymer by chemical reaction [52]. Ushiba et al. [21] utilized two-photon polymerization (TPP) 3D printing technology to fabricate 3D single-walled carbon nanotube (SWCNT)/polymer nanomaterial substrates and attain very small spatial resolution of 200 nm in lateral dimensions. The photo-initiator and photo-sensitizer were mixed via stirring after the dispersion of SWCNTs into an acrylate monomer through sonication. They achieved the suitable nanocomposite structures having equal distribution of SWCNTs with enhanced mechanical properties. Similarly, Sanjuan-Alberte et al. [53] utilized two-photon polymerization (TPP) 3D printing technique with the aim of generating the compatible soft interfaces between biological and electrical structures. In this regard, they develop the substrates by the dispersion of multi-walled carbon nanotubes (MWCNTs) with hydrogels through the formulation of gelatine methacrylate (GelMa)-based inks for two-photon polymerization (TPP). The cell viability analysis affirmed the favorable growth of support human-induced pluripotent stem cell-derived cardiomyocyte (hPSC-CMs) feasibility. Moreover, the MWCNTs acted as conductive nanofillers which improve electrochemical properties.

Hence, there is a requirement of the biomedical domain to manufacture such construct which fulfill the all aspects of ideal biomedical devices, whereas carbon nanotube (CNT)-incorporated AM is unique solution for this purpose and encourages the manufacturing community for next-generation bio-products.

5 Conclusion

This article revealed the versatility of additive manufacturing through their various techniques by integrating nanotechnology especially carbon nanotubes (CNTs). It presents the potentials of carbon nanotube (CNT)-incorporated additive manufacturing along with the enormous capabilities to obtain bio-favorable substrates with desirable surface morphological properties. Although various outcomes of AM process are addressed and concluded that carbon nanotube (CNT)-incorporated additive manufacturing exhibited precise manufacturing and better surface properties in comparison to the several existing techniques. Despite the versatility of additive manufacturing (AM), opportunities arise related to the scaling up the fabrication of nanomaterial-enhanced 3D printed objects. In conclusion, As the technology continues to advance, there is a need of multidisciplinary efforts to eliminate the constraints related to integration of additive manufacturing (AM) and nano-biotechnology fields for the development of new generation bio-products.

References

1. Ngo TD, Kashani A, Imbalzano G, Nguyen KT, Hui D (2018) Additive manufacturing (3D printing): a review of materials, methods, applications and challenges. Compos B Eng 143:172–196
2. Nazir A, Gokcekaya O, Billah KMM, Ertugrul O, Jiang J, Sun J, Hussain S (2023) Multi-material additive manufacturing: a systematic review of design, properties, applications, challenges, and 3D printing of materials and cellular metamaterials. Mater Design, 111661
3. Yang Y, Song X, Li X, Chen Z, Zhou C, Zhou Q, Chen Y (2018) Recent progress in biomimetic additive manufacturing technology: from materials to functional structures. Adv Mater 30(36):1706539
4. Behera D, Chizari S, Shaw LA, Porter M, Hensleigh R, Xu Z, Cullinan MA (2021) Current challenges and potential directions towards precision microscale additive manufacturing–Part II: laser-based curing, heating, and trapping processes. Precis Eng 68:301–318
5. Qian X, Ostwal M, Asatekin A, Geise GM, Smith ZP, Phillip WA, McCutcheon JR (2022) A critical review and commentary on recent progress of additive manufacturing and its impact on membrane technology. J Membr Sci 645:120041
6. Liu G, Zhang X, Chen X, He Y, Cheng L, Huo M, ... Lu J (2021) Additive manufacturing of structural materials. Mater Sci Eng R Reports145:100596
7. Yang S, Zhao YF (2015) Additive manufacturing-enabled design theory and methodology: a critical review. Int J Adv Manuf Technol 80:327–342
8. Castro e Costa E, Duarte JP, Bartolo P (2017) A review of additive manufacturing for ceramic production. Rapid Prototyping J 23(5):954-963
9. Singh S, Ramakrishna S, Singh R (2017) Material issues in additive manufacturing: a review. J Manuf Process 25:185–200
10. Mani M, Lyons KW, Gupta SK (2014) Sustainability characterization for additive manufacturing. J Res Nat Inst Stand Technol 119:419
11. Najmon JC, Raeisi S, Tovar A (2019) Review of additive manufacturing technologies and applications in the aerospace industry. Additive manufacturing for the aerospace industry, 7–31
12. Koumoulos EP, Gkartzou E, Charitidis CA (2017) Additive (nano) manufacturing perspectives: the use of nanofillers and tailored materials. Manuf Rev 4:12

13. Kumar A (2018) Methods and materials for smart manufacturing: additive manufacturing, internet of things, flexible sensors and soft robotics. Manuf Lett 15:122–125
14. Ramachandran MG, Rajeswari N (2022) Influence of nano silica on mechanical and tribological properties of additive manufactured PLA bio nanocomposite. Silicon, 1–7
15. González-Henríquez CM, Sarabia-Vallejos MA, Rodriguez-Hernandez J (2019) Polymers for additive manufacturing and 4D-printing: materials, methodologies, and biomedical applications. Prog Polym Sci 94:57–116
16. Singh J, Singh G, Pandey PM (2021) Additive manufacturing of functionalized nanomaterials for the modern health care industry. In: Additive manufacturing with functionalized nanomaterials, pp 55–85. Elsevier
17. Baddour CE, Briens C (2005) Carbon nanotube synthesis: a review. Int J Chem Reactor Eng, 3(1)
18. de Menezes BRC, Rodrigues KF, da Silva Fonseca BC, Ribas RG, do Amaral Montanheiro TL, Thim GP (2019) Recent advances in the use of carbon nanotubes as smart biomaterials. J Mater Chem B 7(9):1343–1360
19. Devgan S, Mahajan A, Sidhu SS (2021) Multi-walled carbon nanotubes in powder mixed electrical discharge machining: an experimental study, state of the art and feasibility prospect. Appl Phys A 127(11):806
20. Sandoval JH, Soto KF, Murr LE, Wicker RB (2007) Nanotailoring photocrosslinkable epoxy resins with multi-walled carbon nanotubes for stereolithography layered manufacturing. J Mater Sci 42:156–165
21. Ushiba S, Shoji S, Masui K, Kuray P, Kono J, Kawata S (2013) 3D microfabrication of single-wall carbon nanotube/polymer composites by two-photon polymerization lithography. Carbon 59:283–288
22. Goncalves EM, Oliveira FJ, Silva RF, Neto MA, Fernandes MH, Amaral M, ... & Vila M (2016) Three-dimensional printed PCL-hydroxyapatite scaffolds filled with CNT s for bone cell growth stimulation. J Biomed Mater Res Part B Appl Biomater 104(6):1210–1219
23. Chua CK, Leong KF (2014) 3D Printing and additive manufacturing: Principles and applications (with companion media pack)-of rapid prototyping. World Scientific Publishing Company
24. Mahajan A, Singh G, Devgan S (2023) Additive manufacturing of metallic biomaterials: a concise review. Arch Civil Mech Eng 23(3):1–15
25. Aleeva Y, Pignataro B (2014) Recent advances in upscalable wet methods and ink formulations for printed electronics. J Mater Chem C 2(32):6436–6453
26. Wang S, Liu N, Tao J, Yang C, Liu W, Shi Y, ... Gao Y (2015). Inkjet printing of conductive patterns and supercapacitors using a multi-walled carbon nanotube/Ag nanoparticle based ink. J Mater Chem A 3(5):2407–2413
27. Chou DT, Wells D, Hong D, Lee B, Kuhn H, Kumta PN (2013) Novel processing of iron–manganese alloy-based biomaterials by inkjet 3-D printing. Acta Biomater 9(10):8593–8603
28. Kang TH, Lee SW, Hwang K, Shim W, Lee KY, Lim JA, ... Yi H (2020) All-inkjet-printed flexible nanobio-devices with efficient electrochemical coupling using amphiphilic biomaterials. ACS Appl Mater Interfaces 12(21):24231–24241
29. Aabith S, Caulfield R, Akhlaghi O, Papadopoulou A, Homer-Vanniasinkam S, Tiwari MK (2022) 3D direct-write printing of water soluble micromoulds for high-resolution rapid prototyping. Addit Manuf 58:103019
30. Skylar-Scott MA, Gunasekaran S, Lewis JA (2016) Laser-assisted direct ink writing of planar and 3D metal architectures. Proc Natl Acad Sci 113(22):6137–6142
31. Kristiawan RB, Imaduddin F, Ariawan D, Ubaidillah, Arifin Z (2021) A review on the fused deposition modeling (FDM) 3D printing: filament processing, materials, and printing parameters. Open Eng 11(1):639–649
32. Wu CS, Liao HT (2017) Interface design of environmentally friendly carbon nanotube-filled polyester composites: Fabrication, characterisation, functionality and application. Express Polymer Lett 11(3)

33. Prashantha K, Roger F (2017) Multifunctional properties of 3D printed poly (lactic acid)/graphene nanocomposites by fused deposition modeling. J Macromolecular Sci Part A 54(1):24–29
34. Korpela J, Kokkari A, Korhonen H, Malin M, Närhi T, Seppälä J (2013) Biodegradable and bioactive porous scaffold structures prepared using fused deposition modeling. J Biomed Mater Res B Appl Biomater 101(4):610–619
35. Kim J, McBride S, Tellis B, Alvarez-Urena P, Song YH, Dean DD, ... & Hollinger JO (2012) Rapid-prototyped PLGA/β-TCP/hydroxyapatite nanocomposite scaffolds in a rabbit femoral defect model. Biofabrication4(2):025003
36. Wu J, Chen N, Bai F, Wang Q (2018) Preparation of poly (vinyl alcohol)/poly (lactic acid)/hydroxyapatite bioactive nanocomposites for fused deposition modeling. Polym Compos 39:E508–E518
37. Glasschroeder J, Prager E, Zaeh MF (2015) Powder-bed-based 3D-printing of function integrated parts. Rapid Prototyping J 21(2):207–215
38. Zhou W, Sasaki S, Kawasaki A (2014) Effective control of nanodefects in multiwalled carbon nanotubes by acid treatment. Carbon 78:121–129
39. Shahali H, Jaggessar A, Yarlagadda PK (2017) Recent advances in manufacturing and surface modification of titanium orthopaedic applications. Procedia Eng 174:1067–1076
40. Khimich MA, Prosolov KA, Mishurova T, Evsevleev S, Monforte X, Teuschl AH, ... & Sharkeev YP (2021) Advances in laser additive manufacturing of Ti-Nb alloys: from nanostructured powders to bulk objects. Nanomaterials 11(5):1159
41. Leigh SJ, Purssell CP, Bowen J, Hutchins DA, Covington JA, Billson DR (2011) A miniature flow sensor fabricated by micro-stereolithography employing a magnetite/acrylic nanocomposite resin. Sens Actuat A 168(1):66–71
42. Farahani RD, Dalir H, Le Borgne V, Gautier LA, El Khakani MA, Lévesque M, Therriault D (2012) Reinforcing epoxy nanocomposites with functionalized carbon nanotubes via biotin–streptavidin interactions. Compos Sci Technol 72(12):1387–1395
43. Sun C, Fang N, Wu DM, Zhang X (2005) Projection micro-stereolithography using digital micro-mirror dynamic mask. Sens Actuat A 121(1):113–120
44. Chivate A, Zhou C (2023) Enhanced Schlieren system for in situ observation of dynamic light-resin interactions in projection-based Stereolithography process. J Manuf Sci Eng 145(8):081005
45. Miri AK, Khalilpour A, Cecen B, Maharjan S, Shin SR, Khademhosseini A (2019) Multiscale bioprinting of vascularized models. Biomaterials 198:204–216
46. Gueche YA, Sanchez-Ballester NM, Cailleaux S, Bataille B, Soulairol I (2021) Selective laser sintering (SLS), a new chapter in the production of solid oral forms (SOFs) by 3D printing. Pharmaceutics 13(8):1212
47. Li Z, Wang Z, Gan X, Fu D, Fei G, Xia H (2017) Selective laser sintering 3D printing: a way to construct 3d electrically conductive segregated network in polymer matrix. Macromol Mater Eng 302(11):1700211
48. Zhang WN, Wang LZ, Feng ZX, Chen YM (2020) Research progress on selective laser melting (SLM) of magnesium alloys: a review. Optik 207:163842
49. Wu J, Wang L (2018) Selective laser melting manufactured CNTs/AZ31B composites: heat transfer and vaporized porosity evolution. J Mater Res 33(18):2752–2762
50. Guo SZ, Gosselin F, Guerin N, Lanouette AM, Heuzey MC, Therriault D (2013) Solvent-cast three-dimensional printing of multifunctional microsystems. Small 9(24):4118–4122
51. Chizari K, Daoud MA, Ravindran AR, Therriault D (2016) 3D printing of highly conductive nanocomposites for the functional optimization of liquid sensors. Small 12(44):6076–6082
52. Lin Y, Xu J (2018) Microstructures fabricated by two-photon polymerization and their remote manipulation techniques: toward 3D printing of Micromachines. Adv Opt Mater 6(8):1701359
53. Sanjuan-Alberte P, Vaithilingam J, Moore JC, Wildman RD, Tuck CJ, Alexander MR, ... & Rawson FJ (2021) Development of conductive gelatine-methacrylate inks for two-photon polymerisation. Polymers 13(7):1038

Chapter 3
Formation, Testing, and Deposition of Bioactive Material Using Thermal Spray Additive Manufacturing Technique

Talwinder Singh and Davinder Singh

1 Introduction

Hydroxyapatite (HA): Ca_{10} $(PO_4)_6$ $(OH)_2$ is a hydrated calcium phosphate mineral gaining wide attention owing to its good biocompatibility and chemical similarity with human bones [1, 2]. HA supports bone regeneration and repair when employed as medical implant in dental and orthopedic applications [3]. However, poor mechanical properties of hydroxyapatite such as low impact resistance, brittleness, and less tensile strength restrict its use in load-bearing applications such as hip and knee replacements [4, 5]. Therefore, HA is preferred as a bio-coating material applied on a tougher metallic substrate [6]. HA-coated implants possess superior bioactivity properties along with enhanced strength and thus boost healing process of the implant [7].

Among all existing advanced additive manufacturing techniques, the thermal spray under high-velocity oxy-fuel (HVOF) additive manufacturing is one of the most admired powder deposition approach for many industries such as aerospace, automobile, power generation, chemical, and biomedical [8–10]. In high-velocity oxygen-fuel (HVOF) process, fuel (natural gas, hydrogen, acetylene, propane, kerosene, propylene, etc.) and oxygen are mixed together and delivered to the combustion chamber for combustion. The resultant high-pressure hot gases exit the nozzle with supersonic speed. The injected powder melts partially in the gas stream, propels, and gets deposited over substrate with high bond strength and low porosity [11–13]. Hasan and Stokes [4] observed HVOF additive technique results in superior HA deposition with maximum purity and crystallinity values of 99.84% and 93.81, respectively, as compared to plasma spray method. In addition, deposited material

T. Singh (✉) · D. Singh
Department of Mechanical Engineering, Punjabi University, Patiala, Punjab, India
e-mail: tp_tiet@yahoo.co.in

A. Mahajan et al. (eds.), *Additive Manufacturing of Bio-implants*, Biomedical Materials for Multi-functional Applications, https://doi.org/10.1007/978-981-99-6972-2_3

under HVOF spraying is less prone to oxidation, decomposition of particles, and phase change when compared with arc spraying and plasma spraying technique [14, 15]. Likewise, Ham et al. [16] found coated samples under HVOF thermal spray results in improved elongation owing to nonexistence of crack propagation in the deposited layer when compared with Cr-plated samples. Furthermore, high-velocity oxy-fuel additive technique provides significantly dense coating with a low level of porosity (mostly $< 1\%$) [17]. Li et al. [18] also witnessed higher bond strength (31 MPa) of HA-coated samples under HVOF sprayed method compared to plasma spray technique (14 MPa). Henao et al. [19] investigated bioactive behavior of HA/TiO_2 deposition on a Ti-6Al-4V alloy using HVOF thermal sprayed method under in vitro conditions and noticed apatite layer (bone) formation on top surface of the coating which was not present on uncoated Ti-6Al-4V alloy and thereby suggests HVOF additive manufacturing a step forward in the growth of bioactive coatings for medical implants. Mardali et al. [20] compared corrosion behavior and microstructure of HA deposited on magnesium-based substrates—AZ61—using HVOF and flame spraying. Findings revealed HVOF results in more stable phases, higher corrosion resistance, and less roughness when compared with flame sprayed coatings.

Based on the literature review, in the present experimental study, high-velocity oxy-fuel (HVOF) thermal spray additive manufacturing technique has been selected in order to deposit developed bioactive powder on stainless steel AISI 304 L substrate for medical implant applications. Central composite rotatable design (CCRD) and desirability optimization approach have been employed to attain optimum HVOF additive manufacturing parameters that result in maximum microhardness number (VHN: Vickers hardness number). The research methodology for the present study is given in Fig. 1.

2 Materials and Methods

2.1 Forming Bioactive Powder

In the current experimental study, bioactive hydroxyapatite (HA) powder has been formed from natural apatite substance (i.e., chicken eggshell) through heat treatment method. The collected eggshells were boiled for 1 h in distilled water and then oven dried at 500 °C for 30 min. to minimize the moisture content. To make bioactive powder, the dried eggshells were first crushed in grinder and then mechanically ball milled using cast iron spherical balls having diameter = 4.8 mm and weight = 390 gm with drum rotation = 30 r.p.m. (Fig. 2) to get required powder size range of 30–50 microns suitable for deposition on metallic substrate under high-velocity oxy-fuel (HVOF) thermal spray additive manufacturing technique [21, 22].

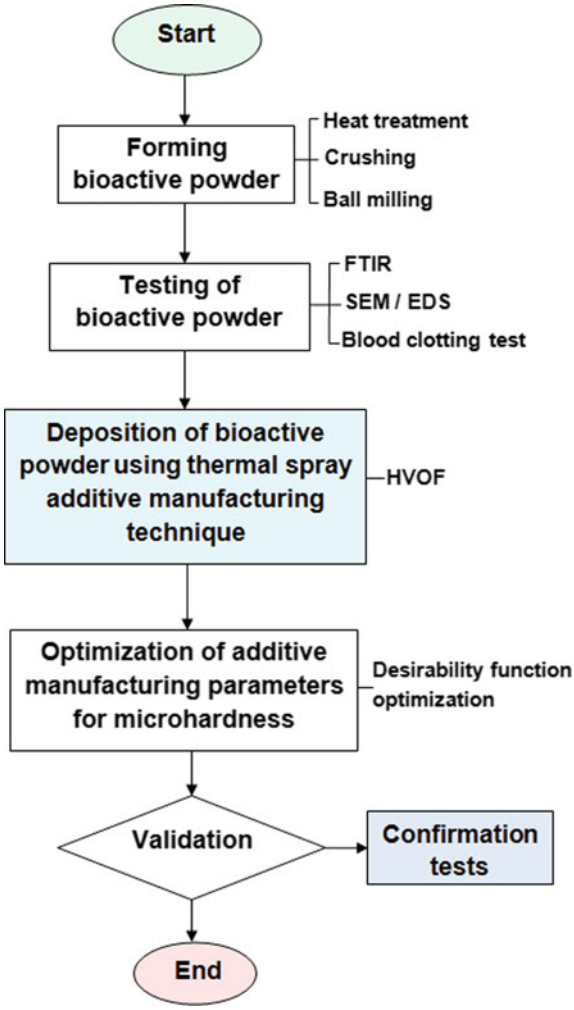

Fig. 1 Research methodology

2.2 Testing of Bioactive Powder

Before deposition of developed bioactive powder on substrate, the following tests were conducted to confirm the traces of HA compound and to access the biocompatibility of the powder with human blood.

2.2.1 FTIR (Fourier Transform Infrared Spectroscopy)

Figure 3 illustrates FTIR spectrum of the developed bioactive powder. Results revealed presence of hydroxyl group (OH^-) at peak band of 3414.31 cm^{-1} attributed

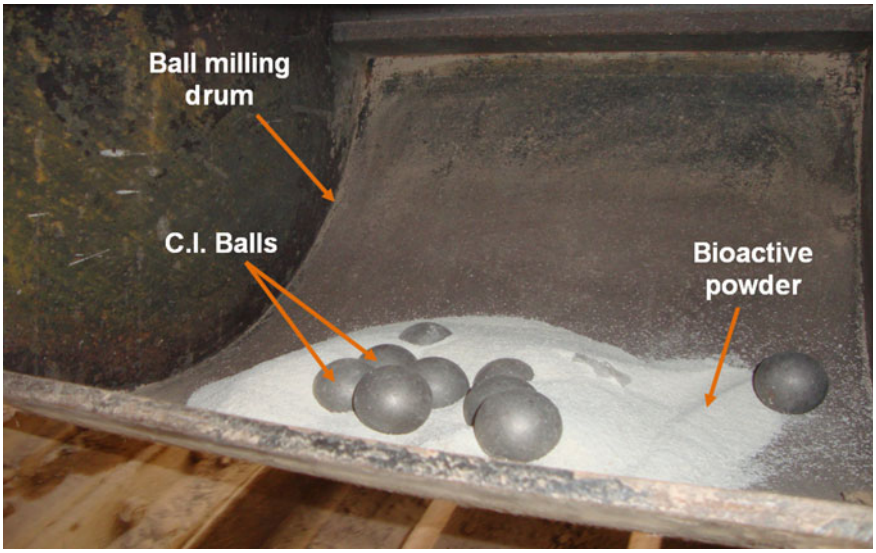

Fig. 2 Ball milling process

to hydroxyapatite compound in the developed powder. Similarly, phosphate (PO_4^{3-}) group peak characteristics are witnessed at location of 875.73 cm^{-1} and 711.16 cm^{-1}. The existence of peak bands at 1797.88 cm^{-1} and 1417.89 cm^{-1} are corresponding to carbonate (CO_3^{2-}) groups present in the developed bioactive powder configuration. It has been concluded from the FTIR analysis that the compound peaks present in the analyzed hydroxyapatite (HA) powder from chicken eggshell are identical to the commercial hydroxyapatite structure [23].

2.2.2 SEM–EDS Characterization

Figure 4 shows characterization of the developed bioactive powder through SEM (scanning electron microscopy) and EDS (energy dispersive spectroscopy). Results verify eggshell powder comprises large amount of calcium (Ca = 44.48 %) along with phosphorus (P = 19.27 %) as revealed from EDS analysis corresponding to spectrum 1 (Fig. 4), and therefore makes it suitable material for boosting bone growth when utilized in medical implants.

2.2.3 Blood Clotting Test

Blood clotting is essential to stop bleeding after an injury to a blood vessel. This clotting builds a shielding layer over the injured blood vessel, and thus allows it to heal. To perform blood clotting test (Fig. 5), blood sample was taken in capillary

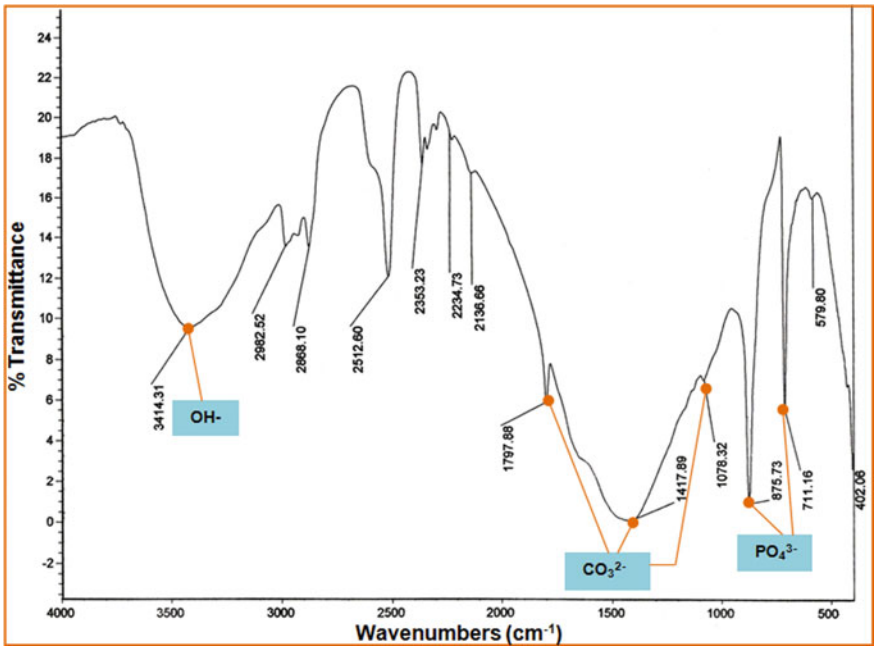

Fig. 3 FTIR spectrum of developed bioactive powder

tube and transferred on test slide for microscopic examination. Figure 5d shows fibrinogen protein present in normal blood sample at 40X magnification that involved in the forming of blood clots and the clotting time of normal blood was observed as 74.0 s. Figure 5e depicts image of blood mixed with developed bioactive powder and the clotting time in this case was reduced significantly to 36.46 seconds. Finally, blend the normal blood with anticoagulant solution (i.e., sodium citrate 3.8% (w/v) and the developed bioactive powder as seen in Fig. 5f. The purpose of adding anticoagulant solution is to prevent coagulation of blood but in contrary to that, the formation of blood clot was seen in 38.42 s just because to high compatibility of developed bioactive powder (from eggshell) with human blood and thus it can be considered as a bioactive material for implant applications and a viable substitute for costlier commercial HA powder.

2.3 Deposition of Bioactive Material

2.3.1 Preparation of Base Metal Substrate

Stainless steel AISI 304L was selected as base metal substrate because of notable mechanical properties such as high corrosion resistance, excellent tensile strength,

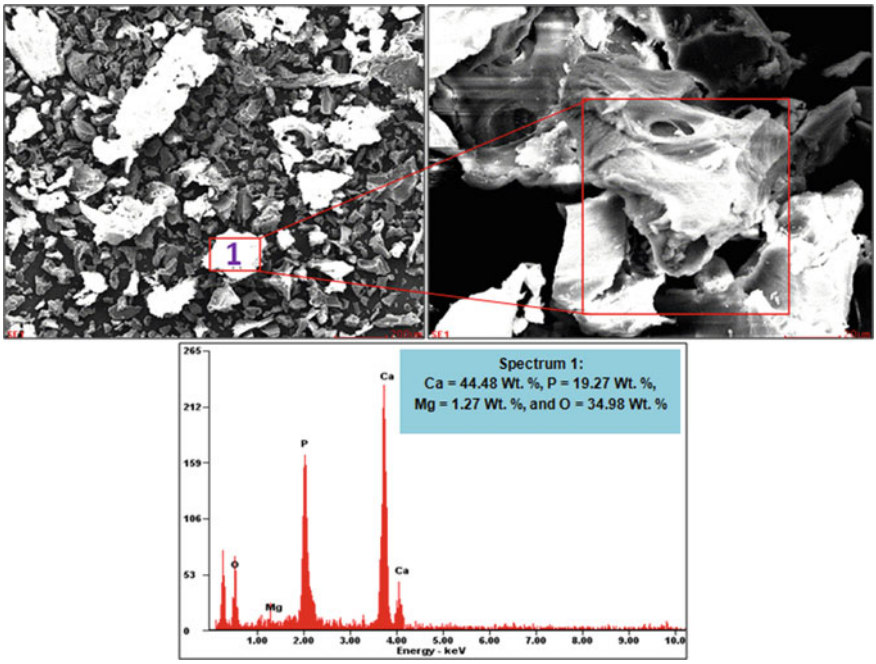

Fig. 4 SEM–EDS characterization of developed bioactive powder

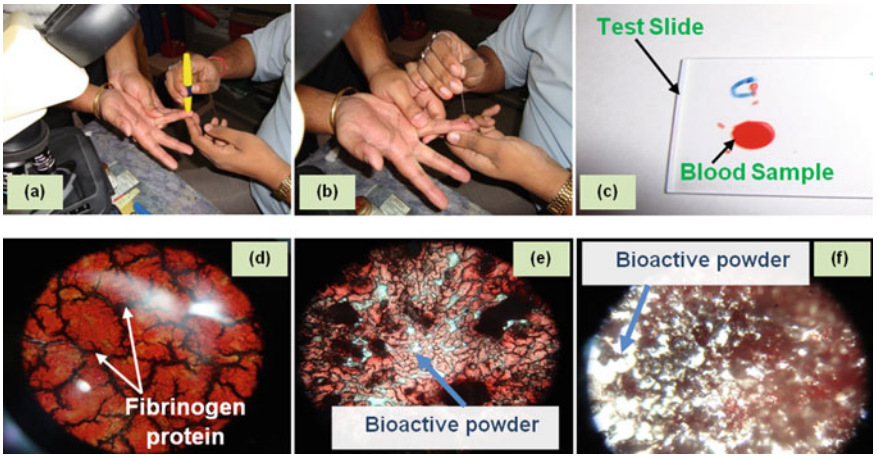

Fig. 5 Blood clotting test procedure: **a**, **b** Blood sample collection, **c** Test slide, **d** Normal blood at 40X magnification, **e** Blood mixed with developed bioactive powder, **f** Blood mixed with anticoagulant and bioactive powder

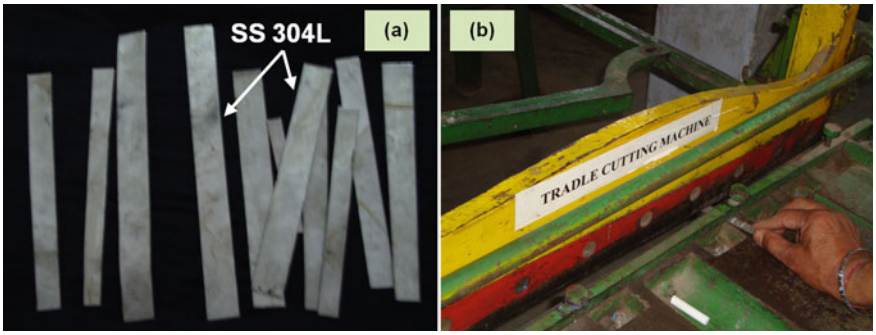

Fig. 6 Preparation of base metal substrate

Table 1 Elemental composition of stainless steel AISI 304L

Element	C	Cr	Mn	Si	P	S	Ni	Fe
Weight %	0.08	18.0–20.0	2.00	1.00	0.045	0.03	8.0–10.5	Balance

and is widely employed material in medical device industry, orthopedic and dental medical implants, etc. [24]. Available base material substrate (1.5 mm thickness) was cut into the required rectangular sample size of 20 mm × 30 mm using treadle cutting machine as shown in Fig. 6. The elemental composition of stainless steel AISI 304L is given in Table 1.

2.3.2 Thermal Spray Additive Manufacturing Technique

Layer of bioactive powder has been deposited on AISI 304L stainless steel substrate under thermal spray HVOF (high-velocity oxy-fuel) additive manufacturing process at Metallizing Equipment Co. Pvt. Ltd. (MEC), Jodhpur (India). Figure 7a depicts the principle of HVOF thermal spray technique in which acetylene (fuel gas) and oxygen mixture is delivered to the combustion chamber for combustion. The hot gases produced in the combustion chamber having pressure nearly 1 MPa exit the nozzle at supersonic speed. The injected powder propelled (up to 800 m/s) by high-velocity gas stream; melts partially and deposits upon the surface of base metal substrate. The fuel-oxygen hoses, powder feeder line, and coolant supply lines are attached to the HVOF gun as shown in Fig. 7b.

2.3.3 Central Composite Rotatable Design of Experiment (CCRD)

Figure 7c shows additive layered samples obtained under different thermal spray HVOF parameters. In the present investigation, four variables ($y = 4$) or input HVOF parameters were selected as standoff distance (SOD), acetylene supply rate (ASR),

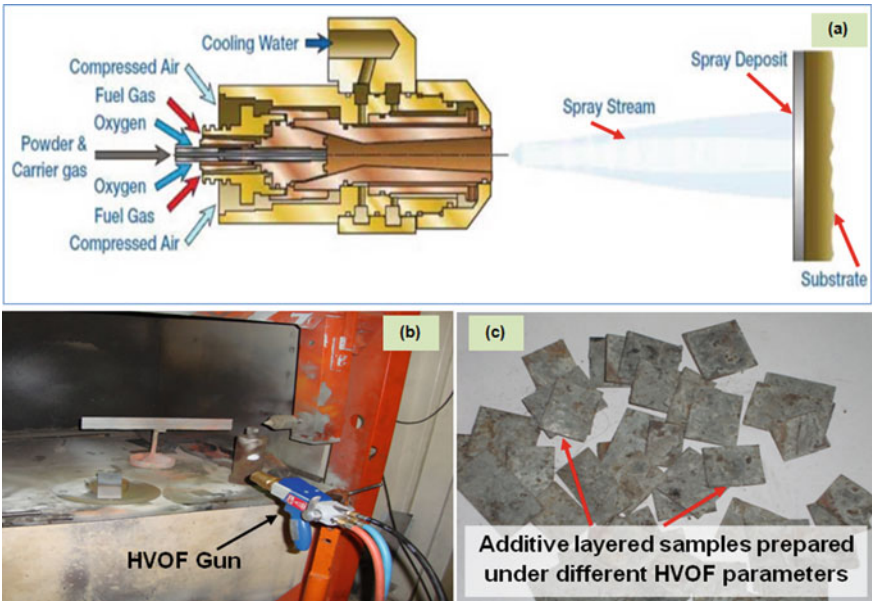

Fig. 7 Experimental setup: **a** Principle of HVOF, **b** HVOF gun, **c** Additive layered samples prepared under different HVOF parameters

oxygen supply rate (OSR), and powder feed rate (PFR). The output variable or response factor was microhardness number (VHN: Vickers hardness number). Experimental plan was designed using design expert software 7.0 under central composite rotatable design (CCRD) approach where each input HVOF parameter was varied over five levels as shown in Table 2. Central composite design (CCD) plan comprises 16 experiments (± 1 level, 2^y; $y = 4$), 8 runs ($\pm\alpha$ level; $2y = 8$), and 2 experiments at center (0 level) in order to examine HVOF gun repeatability. The value of alpha has been finalized as 2 ($\alpha = 16^{1/4}$) to augment experimental design as CCRD. Totally 26 experiments were conducted at 5 levels and microhardness values (Vickers hardness number (VHN)) were calculated using MVH-II digital microhardness tester under applied load = 200 grams for time = 20 sec for each sample. Table 3 gives CCRD design layout and obtained results for microhardness number (VHN).

Table 2 Thermal spray HVOF parameter levels

HVOF parameters	5-levels				
	−α (lowest axial)	−1 (low)	0 (center)	+1 (high)	+α (highest axial)
Standoff distance (inch.)	2	4	8	12	16
Acetylene supply rate (m^3/min.)	40	50	60	70	80
Oxygen supply rate (m^3/min.)	30	40	50	60	70
Powder feed rate (gm/min.)	10	15	45	75	105

3 Results and Discussion

3.1 Effect of Input HVOF Parameters on Microhardness (VHN)

Figure 8 illustrates 3D surface plots to examine the effect of input thermal spray HVOF parameters on microhardness (VHN). The value of microhardness increases significantly with an increase in standoff distance (SOD) from 4 inch to 12 inch as noticed from Fig. 8a. However, with change in powder feed rate (PFR) from 15 to 75 gm/min., the microhardness increases slightly. The highest value of microhardness (VHN) has been observed corresponding to SOD = 12 inch with PFR = 75 gm/min. Figure 8b depicts the effect of oxygen supply rate (OSR) and acetylene supply rate (ASR) on microhardness. With change in OSR from 40 m^3/min. to 60 m^3/min., the microhardness remains almost constant. But the value of microhardness increases rapidly with increase in fuel (acetylene) supply rate. The maximum value of microhardness (VHN) has been found at a combination of OSR = 60 m^3/min. and ASR = 70 m^3/min. Other studies [25, 26] also witnessed similar findings under thermal spray HVOF material deposition technique.

3.2 Optimization of HVOF Parameters and Validation

Desirability function optimization technique was applied to attain optimum setting of input HVOF parameters that result in maximum microhardness value. This method is preferred by many industries to get optimum manufacturing process parameters for different responses simultaneously [27]. The desirability scale range, i.e., 0 to 1 signifies absolutely unwanted value (0) to completely satisfactory value (1) of the suggested optimal solutions. Table 4 shows different constraints considered during optimization process and Fig. 9 (optimization ramp plots) gives optimum HVOF parameters as standoff distance (SOD) = 12 inch., acetylene supply rate (ASR) =

Table 3 CCRD design layout and results obtained for microhardness number (VHN)

Run no	Standoff distance (inch.)	Acetylene supply rate (m^3/min.)	Oxygen supply rate (m^3/min.)	Powder feed rate (gm/min.)	Microhardness (VHN)
1	8	60	70	45	310
2	4	50	40	75	302
3	4	50	60	75	280
4	12	50	60	15	480
5	8	40	50	45	270
6	4	50	40	15	218
7	12	50	40	75	410
8	2	60	50	45	370
9	4	70	60	15	250
10	8	60	50	45	370
11	8	60	50	10	290
12	4	70	40	75	340
13	12	70	60	15	597
14	12	70	40	15	590
15	12	50	60	75	520
16	8	60	50	45	350
17	4	70	60	75	515
18	8	80	50	45	410
19	12	70	40	75	460
20	4	70	40	15	245
21	4	50	60	15	335
22	12	50	40	15	236
23	8	60	50	105	390
24	12	70	60	75	460
25	8	60	30	45	350
26	16	60	50	45	300

70 m^3/min., oxygen supply rate (OSR) = 60 m^3/min., and powder feed rate (PFR) = 74.87 gm/min. that results in highest microhardness number, VHN = 504.998 at desirability level of 0.757. Confirmation tests (repeated thrice) were also conducted at the obtained optimum HVOF parameters under same experimental setup conditions. Results (Table 5) show percentage error among predicted and observed value of microhardness (VHN) is much lower, i.e., 3.06 %, and thus validates the experimental outcomes.

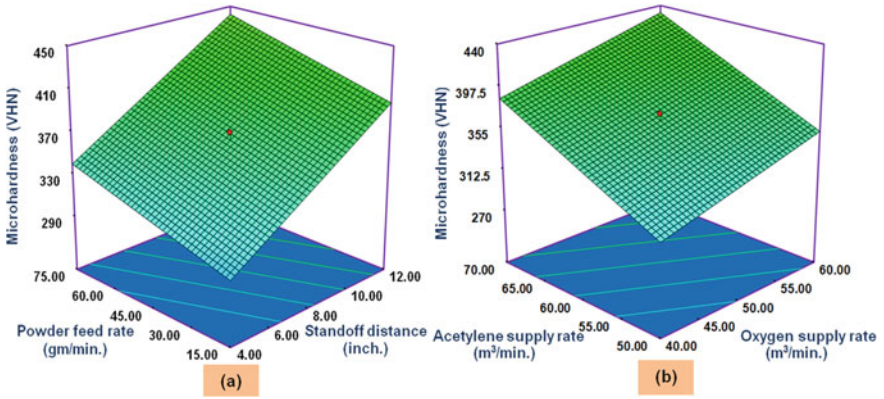

Fig. 8 Effect of HVOF parameters on microhardness (VHN)

Table 4 Constraints applied during optimization process

Constraints	Goal	Lower limit	Upper limit
Standoff distance (inch.)	Within limit	4	12
Acetylene supply rate (m^3/min.)	Within limit	50	70
Oxygen supply rate (m^3/min.)	Within limit	40	60
Powder feed rate (gm/min.)	Within limit	15	75
Microhardness (VHN)	Maximize	218	597

4 Conclusions

In the current experimental research, bioactive powder has been developed, tested, and deposited on AISI 304L stainless steel substrate using thermal spray high-velocity oxy-fuel (HVOF) additive manufacturing technique. Desirability function optimization has been applied to attain optimum setting of input HVOF parameters that result in maximum microhardness (VHN) value. The following conclusions are drawn from the present study:

(1) FTIR spectra of the developed bioactive powder reveal presence of hydroxyl group (OH^-) at peak band of 3414.31 cm^{-1}; phosphate group (PO_4^{3-}) at 875.73 cm^{-1}, 711.16 cm^{-1}; and carbonate group (CO_3^{2-}) at 1797.88 cm^{-1}, 1417.89 cm^{-1}, respectively, which confirms existence of hydroxyapatite compound in the developed powder.

(2) SEM–EDS characterization highlights presence of large amount of calcium (Ca = 44.48%) along with phosphorus (P = 19.27%) in the developed bioactive powder and therefore makes it suitable material for boosting bone growth when utilized in medical implants.

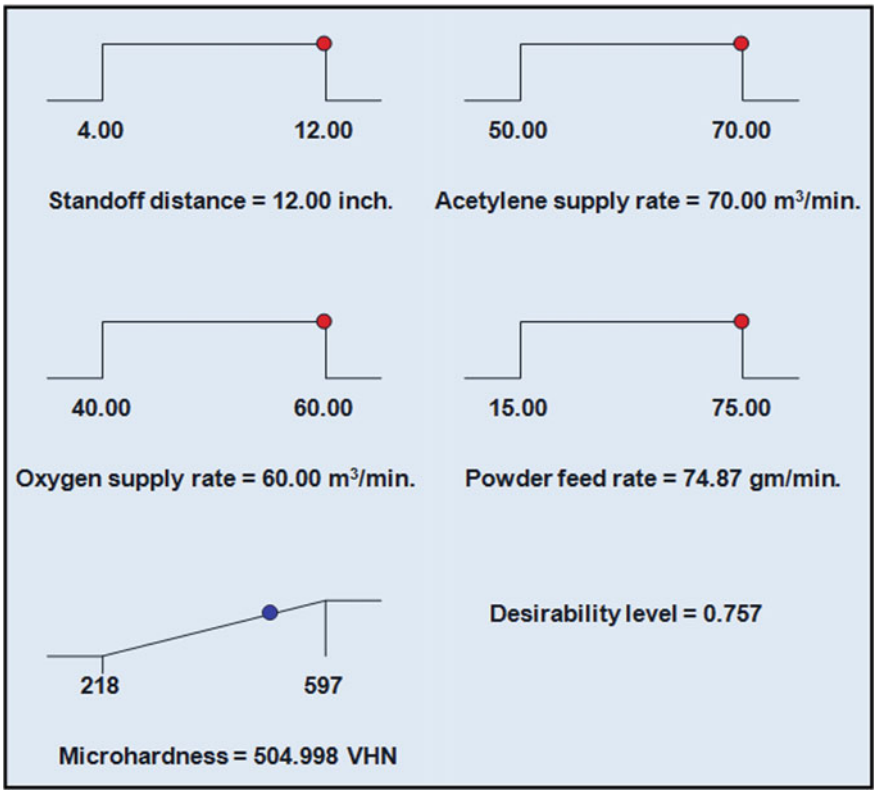

Fig. 9 Optimization ramp plots

Table 5 Confirmation test results

	Results obtained at optimum HVOF parameters: standoff distance (SOD) = 12 inch., acetylene supply rate (ASR) = 70 m^3/min., oxygen supply rate (OSR) = 60 m^3/min., and powder feed rate (PFR) = 74.87 gm/min		
	Predicted value	Experimental observed value	Error (%)
Microhardness (VHN)	504.998	490	3.06

(3) Blood clotting test shows blending of developed bioactive powder with blood results in significant reduction of clotting time (= 36.46 s) compared to normal blood clotting time (= 74.0 s).
(4) 3D surface plots reveal standoff distance and acetylene supply rate as dominating factors affecting microhardness compared to powder flow rate and oxygen supply rate HVOF parameters.

(5) Desirability function optimization recommends optimum thermal spray HVOF additive manufacturing parameters as standoff distance (SOD) = 12 inch., acetylene supply rate (ASR) = 70 m^3/min., oxygen supply rate (OSR) = 60 m^3/min., and powder feed rate (PFR) = 74.87 gm/min. that results in highest microhardness number, VHN = 504.998 at desirability level of 0.757.
(6) Confirmation tests show percentage error among predicted and observed values of microhardness (VHN) is much lower (3.06%), and thus validates the experimental outcomes.

References

1. Park J, Um S-H, Seo Y, Lee J, Kim Y-C, Ok M-R, Hwang S-W, Sun J-Y, Han H-S, Jeon H (2023) Improving hydroxyapatite coating ability on biodegradable metal through laser-induced hydrothermal coating in liquid precursor: application in orthopedic implants. Bioactive Mater 25:796–806. https://doi.org/10.1016/j.bioactmat.2022.06.020
2. Singh J, Singh JP, Kumar S, Gill HS (2023) Short review on hydroxyapatite powder coating for SS 316L. J Electroch Sci Eng 13(1):25–39. https://doi.org/10.5599/jese.1611
3. Hasan MF, Wang J, Berndt CC (2013) Effect of power and stand-off distance on plasma sprayed hydroxyapatite coatings. Mater Manuf Process 28(12):1279–1285. https://doi.org/10.1080/10426914.2013.811730
4. Hasan S, Stokes J (2011) Design of experiment analysis of the sulzer metco DJ high velocity oxy-fuel coating of hydroxyapatite for orthopedic applications. J Therm Spray Technol 20:186–194. https://doi.org/10.1007/s11666-010-9566-0
5. Mittal M, Nath SK, Prakash S (2013) Improvement in mechanical properties of plasma sprayed hydroxyapatite coatings by Al_2O_3 reinforcement. Mater Sci Eng C 33(5):2838–2845. https://doi.org/10.1016/j.msec.2013.03.005
6. Levingstone TJ (2008) Ceramics for medical applications. Dublin City University, Ireland
7. Singh G, Sharma S, Mittal M, Singh G, Singh J, Changhe L, Khan AM, Dwivedi SP, Mushtaq RT, Singh S (2022) Impact of post-heat-treatment on the surface-roughness, residual stresses, and micromorphology characteristics of plasma-sprayed pure hydroxyapatite and 7%-Aloxite reinforced hydroxyapatite coatings deposited on titanium alloy-based biomedical implants. J Market Res 18:1358–1380. https://doi.org/10.1016/j.jmrt.2022.03.065
8. Stokes J, Looney L (2004) Residual stress in HVOF thermally sprayed thick deposits. Surf Coat Technol 177–178:18–23. https://doi.org/10.1016/j.surfcoat.2003.06.003
9. Vats A, Kumar A, Patnaik A, Meena ML (2021) Influence of deposition parameters on tribological performance of HVOF coating: a review. IOP Conf Series Mater Sci Eng 1017:012015. https://doi.org/10.1088/1757-899X/1017/1/012015
10. Praveen AS, Sarangan J, Suresh S, Channabasappa BH (2016) Optimization and erosion wear response of NiCrSiB/WC–Co HVOF coating using Taguchi method. Ceramics Int Part B 42(1):1094–1104. https://doi.org/10.1016/j.ceramint.2015.09.036
11. Praxair Surface Technologies, a Linde Company (2019) Retrieved April 24, 2023, from https://www.praxairsurfacetechnologies.com/en/materials-and-equipment/coating-equipment/thermal-spray-coating-systems/high-velocity-oxygen-fuel-hvof
12. Metallizing Equipment Company Private Limited (2023) Retrieved April 24, 2023, from https://www.mecpl.com/products/coating-equipments/hvof-spray.
13. Prasanna ND, Siddaraju C, Shetty G, Ramesh MR, Reddy M (2018) Studies on the role of HVOF coatings to combat erosion in turbine alloys. Mater Today Proc Part 3, 5(1):3130–3136. https://doi.org/10.1016/j.matpr.2018.01.119

14. Yu J, Liu X, Yu Y, Li H, Liu P, Huang K, Sun R (2022) Research and application of high-velocity oxygen fuel coatings. Coatings 12(6):828. https://doi.org/10.3390/coatings12060828
15. Oksa M, Turunen E, Suhonen T, Varis T, Hannula S-P (2011) Optimization and characterization of high velocity oxy-fuel sprayed coatings: techniques, materials, and applications. Coatings 1(1):17–52. https://doi.org/10.3390/coatings1010017
16. Ham G-S, Kreethi R, Kim H-J, Yoon S-H, Lee K-A (2021) Effects of different HVOF thermal sprayed cermet coatings on tensile and fatigue properties of AISI 1045 steel. J Market Res 15:6647–6658. https://doi.org/10.1016/j.jmrt.2021.11.102
17. Anusha K, Routara BC, Guha S (2023) A review on high-velocity oxy-fuel (HVOF) coating technique. J Ins Eng (India) Series D, https://doi.org/10.1007/s40033-022-00434-x
18. Li H, Khor KA, Cheang P (2000) Effect of the powders' melting state on the properties of HVOF sprayed hydroxyapatite coatings. Mater Sci Eng A 293(1–2):71–80. https://doi.org/10.1016/S0921-5093(00)01245-4
19. Henao J, Sotelo-Mazon O, Giraldo-Betancur AL, Hincapie-Bedoya J, Espinosa-Arbelaez DG, Poblano-Salas C, Cuevas-Arteaga C, Corona-Castuera J, Martinez-Gomez L (2020) Study of HVOF-sprayed hydroxyapatite/titania graded coatings under in-vitro conditions. J Market Res 9(6):14002–14016. https://doi.org/10.1016/j.jmrt.2020.10.005
20. Mardali M, SalimiJazi HR, Karimzadeh F, Luthringer B, Blawert C, Labbaf S (2019) Comparative study on microstructure & corrosion behavior of nanostructured hydroxyapatite coatings deposited by high velocity oxygen fuel and flame spraying on AZ61 magnesium based substrates. Appl Surf Sci 465:614–624. https://doi.org/10.1016/j.apsusc.2018.09.127
21. TWI limited (2023) Retrieved April 28, 2023, from https://www.twi-global.com/technical-knowledge/faqs/faq-what-types-of-metal-powder-are-used-with-hvof-spraying
22. Watanabe M, Owada A, Kuroda S, Gotoh Y (2006) Effect of WC size on interface fracture toughness of WC–Co HVOF sprayed coatings. Surf Coat Technol 201(3–4):619–627. https://doi.org/10.1016/j.surfcoat.2005.12.019
23. Ungureanu DN, Avram D, Angelescu N, Catangiu A, Anghelina FV, Despa V (2018) Comparative study of bioceramic powders synthesis based on calcium and phosphates. Scient Bull Valahia Univ Mater Mech 16(14):13–16. https://doi.org/10.1515/bsmm-2018-0002
24. Baila D, Tonoiu S (2019) Thin films deposition on 304L stainless steel using e-gun technology for medical applications. IOP Conf Ser Mater Sci Eng 591:012001. https://doi.org/10.1088/1757-899X/591/1/012001
25. Rajendran PR, Duraisamy T, Chidambaram Seshadri R, Mohankumar A, Ranganathan S, Balach&ran G, Murugan K, Renjith L (2022) Optimisation of HVOF spray process parameters to achieve minimum porosity and maximum hardness in WC-10Ni-5Cr coatings. Coatings 12(3):339.https://doi.org/10.3390/coatings12030339
26. Kumar GSP, Kumar MH, Thomas S, Yegnesh HM, Bharadwaj S, Hebbar GS (2021) Studies on parametric optimization of HVOF-sprayed Cr_2O_3 coatings on Al6061 alloy. Trans Indian Inst Met 74:2013–2025. https://doi.org/10.1007/s12666-021-02295-6
27. Myers RH, Montgomery DC, Anderson-Cook CM (2016) Response surface methodology: process and product optimization using designed experiments, 4th edn. Wiley, New York

Chapter 4
Controlled Oxide Deposition Improves Mechanical and Biomedical Applications of Titanium Alloy

Anil Kumar, Sunil Sinhmar, Suresh Kumar, and Rishabh Sharma

1 Introduction

Titanium (Ti) is the ninth most abundant element among all other elements available on the earth's crust with an atomic number of 22. Titanium has a metallic luster with silvery appearance, low density and high strength [1]. Valuable properties of titanium like excellent corrosion resistance and a high strength to weight ratio make it popular in various engineering applications where resistance to corrosion is crucial. Titanium alloys are a combination of titanium with other elements, typically aluminum, vanadium, iron and molybdenum. These alloys exhibit enhanced properties compared to pure titanium, such as improved strength, hardness and heat resistance [2–4]. Grade 5 is the most widely used titanium alloy consisting of 90% titanium, 6% aluminum and 4% vanadium. It offers an excellent balance of strength, low weight and corrosion resistance making it suitable for aerospace, marine, medical implants and chemical processing industries. Titanium grade 2 alloys contains 99.2% pure titanium making it more ductile and formable than grade 5. It is commonly used in applications where formability and corrosion resistance are essential such as chemical processing equipment medical implants and marine components [5–8]. Titanium is widely used as a biomaterial in various medical and dental applications due to its excellent biocompatibility and medical properties. Here are some key points about titanium as a biomaterial:

A. Kumar (✉) · S. Kumar · R. Sharma
Department of Mechanical Engineering, BRCM College of Engineering and Technology, Bahal, Bhiwani, India
e-mail: mr.anilsuthar@rediffmail.com

S. Sinhmar
Materials Science and Engineering, National Post-Doctoral Fellow, IIT Kanpur, Kanpur, India

A. Mahajan et al. (eds.), *Additive Manufacturing of Bio-implants*, Biomedical Materials for Multi-functional Applications, https://doi.org/10.1007/978-981-99-6972-2_4

- Biocompatibility: Titanium exhibits excellent biocompatibility, meaning it is well tolerated by the human body. When implanted, titanium does not elicit significant immune responses or toxic reactions. This makes it suitable for long-term applications within the body.
- Corrosion resistance: Titanium has a naturally occurring oxide layer on its surface, which provides excellent corrosion resistance. This oxide layer protects the metal from degradation when exposed to bodily fluids preventing the release of harmful ions or corrosion byproducts.
- Strength and durability: Titanium has a high strength to weight ratio making it strong and durable. It can withstand mechanical strength in load bearing applications such as orthopedic implants without fracturing or deforming easily.
- Osseointegration: Titanium has the ability to integrate with living bone, a process known as osseointegration. The surface of titanium implants can be modified to enhance this property, facilitating the direct bonding of bone to the implant surface. This promotes the stability and longevity of the implant.
- Versatility: Titanium can be fabricated into various forms such as screws, rods and dental implants. It can also be used in combination with other materials such as polymers or ceramics to enhance specific properties or tailor its behavior for specific applications.
- Imaging compatibility: Titanium is radiolucent meaning it does not interfere significantly with imaging techniques such as X- rays or magnetic imaging (MRI). This allows for easier post-implant evaluation and monitoring.
- Allergic potential: Although rare some individuals may exhibit hypersensitivity or allergic reactions to titanium implants. However, titanium is generally considered to have low allergic potential compared to other metals.

Due to these characteristics, titanium is used in a wide range of medical applications, including orthopedic implants such as hip and knee replacements, dental implants, surgical instruments, cardiovascular device, external fixation devices, etc. Extensive researches and developments have been conducted to optimize the use of titanium as a biomaterial and it continues to be a material of choice in many biomedical applications [9–17]. While titanium is widely used as a biomaterial due to its excellent biocompatibility and osseointegration nature but it also has some considerable limitations. Poor wear resistance, lack of bioactivity, limitations in complex shape and design, etc. are some points that diminish the biomedical applications of non-treated titanium. Sometimes infection and tissue spoilage problems are observed with untreated titanium implants [18]. Thus, to reduce the effect of these limitations, various surface treatment methods are adopted to improve the biocompatibility of titanium alloys like anodizing, thermal oxidation, plasma oxidation, etc. [19–21]. Anodic oxidation also refers to anodizing or electrochemical oxidation in which a thin layer (10 μm) of oxide film deposits on the surface of titanium alloy [22]. Titanium is used as an anode in electrolytic cells where a potential difference of 10 volts is applied resulting in the formation of a thin and porous titanium oxide layer. The surface roughness and topography created through the anodizing enhance osseointegration and promote cell adhesion [23]. Anodized titanium alloy promotes the

formation of a homogeneous and stable oxide layer (TiO_2) on the titanium substrate. TiO_2 acts as a protective barrier between the implant and the surrounding biological environment [24]. The oxide layer prevents direct contact between the implant material and bodily fluids, reducing the release of metal ions and potential adverse reactions. A uniformly deposited oxide layer reduces the susceptibility of the material to corrosion in the harsh physiological environment. Improved corrosion resistance maintains the structural integrity of the implants and prevents the release of metallic debris that could induce inflammatory responses or tissue damage [25]. Nanoporous oxide film deposited within a 0.5% HF solution at 10 volts promotes a favorable environment for bone cell attachment and cell proliferation [26]. Anodizing parameters such as voltage and electrolyte composition can be adjusted to control the surface roughness and topography of the anodized titanium alloys. Surface roughness plays a crucial role in cell adhesion, migration and proliferation. By modifying the surface roughness, anodizing can optimize the interactions between the implant and cells leading to improved biocompatibility[27]. The surface roughness level is proportional to the increasing thickness of the oxide film, initially surface roughness increases at a very slow rate but increases rapidly when anodic voltage exceeds 50 volts. However, the surface roughness increases linearly from 25 nm at 5 volts up to 100 nm at 70 volts and then accelerates to 150 nm at 80 volts [28]. The EDS analysis explicates that the presence of calcium, oxide, phosphorus and sulfur [29] within TiO_2 supports cell proliferation. Palladium treated [30] and thermally oxidized titanium [31] within the HCl solution enhance the anti-corrosive as well as wear strength of the metal substrate. Traditional antibiotics are not sufficient to control bacterial infection of medical devices [32] because a thin biofilm deposition occurs around the surface thus nano-structured treated surfaces are highly recommended for medical devices [33] and implants [34].

2 Materials and Methods

2.1 Pretreatment

A thin sheet of titanium grade 5, provided by the supplier (Om Steel Industries, Pune, India), in dimensions 200 × 300 × 0.2 mm is used as a specimen in the presented research work. The specimen was very dirty, greasy and stained; thus, it needs pretreatment before anodization. Initially, a sample of 10 mm in diameter was cut from the sheet in the form of a disc for the execution of the experimental analysis. The specimen was mechanically polished in a scheduled manner by using emery paper of grits 320, 400, 600, 1000, 1200 and 1500 followed by silicon carbide polishing. To remove the foreign materials and stain marks retained by mechanical polishing, the specimen was agitated in a mixture of 5% HF, 10% NH_4F and 10% HNO_3 for 5 min at 25 °C temperature. After this, the specimen was placed in an acetone bath for 2 min and then air dried at room temperature.

2.2 Anodic Oxidation

A set of experiments was conducted to achieve a thin adhered film with a homogeneous nano-structured surface. For this, anodic oxidation of the titanium alloy specimen was performed within 0.5 M H_2SO_4 along with varying concentrations of HF solution. The specimen was connected to the negative terminal (anode) of an external D.C. power source (Keithley, 2220 series) whereas a platinum bar of diameter 10 mm was placed as a counter electrode (cathode). The schematic is depicted in Fig. 1. Both, electrodes remained stationary at a gap of 25 mm and a uniform current density of 10A/dm^2 was applied for 10 min at Ti terminal. Detailed process parameters are given in Table 1. The heat generated within the electrochemical cell was dissipated by a mechanical stirrer, and the solution temperature was maintained at 25 °C. Finally, the anodized sample was carefully removed from the solution, washed in distilled water and air dried. A comparative analysis of anodized as well as non-anodized samples was carried out to differentiate remarkable property changes caused by anodization.

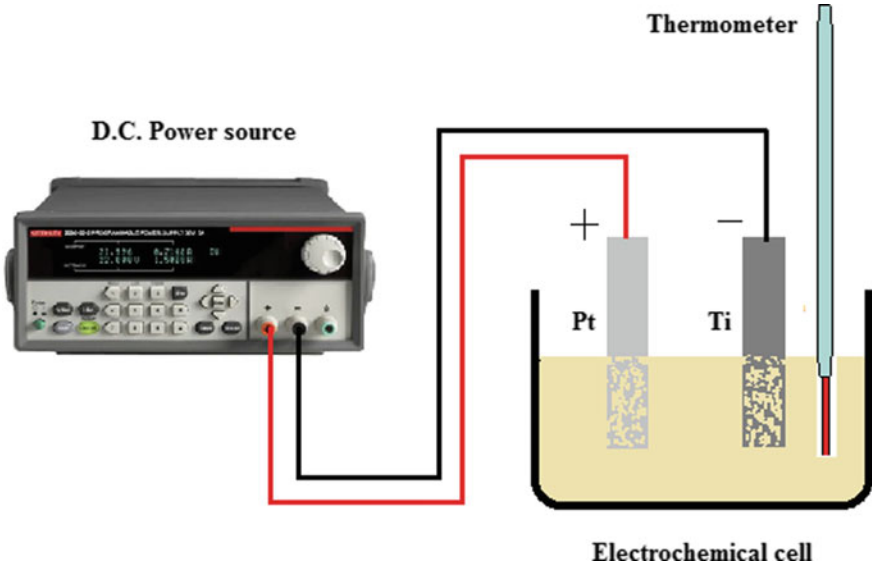

Fig. 1 Schematic diagram of the setup utilized to execute anodic oxidation of titanium alloy

Table 1 Anodizing process parameters

Counter electrode	99.2% pure platinum rod (10 mm diameter)
H_2SO_4 concentration	0.5 M
HF concentration	5%, 10%, 15% and 20% by volume
Anodic current density	1 A/dm^2
Solution temperature	278 K
Agitation	Mechanical stirrer

3 Characterization

The surface morphology, homogeneity and topography of anodized nanosurfaces were evaluated by Scanning Electron Microscope (SEM, EVO 18 Carl Zeiss). An anodized sample was mounted on a stainless steel specimen holder (Kurt Hollocher), to allow the conductivity of a high-speed electron beam the sample was sputtered with a thin layer of gold film without charging the sample. Highly magnified images in the range of 1000X to 20000X were captured to represent clear nano-textured surface morphology. An X-Ray Diffractometer (XRD, Bruker D8 advanced) equipped with CuK_α radiation source was utilized to exhibit the phase analysis of the anodized surface. The QV 1000 micro-hardness tester (Vicker's type) was utilized to determine the surface hardness of the anodized surface. A small load range of 25gf to 100gf was applied by a diamond shaped indenter, which supports auto loading. The applied successive load range was sufficient to mark an indent within the oxide film and was not allowed to penetrate beneath the oxide layer. Five indents were marked for a 10-s time span and then averaged to determine the surface hardness of the oxidized surface.

Osteoblast cell line (KBH5448) was provided by KRISHGEN Bio Systems, Mumbai (India). The cells were cultured in DMEM (Dulbecco's Modified Eagle Medium) with l-glutamine, supplemented with 10% FBS (Fetal Bovine Serum) and 1% antibiotic solution. The anodized samples were sterilized in acetone and air dried. The sterilized samples were placed in well plates and cultured in an incubator at a temperature of 37 °C with 5% CO_2 and an increased humidity level of 95%. The cells were cultured for at least 24 h. When approximately 90% of cells reached the confluent monolayer stage, the cultured solution was removed. The investigated cells were washed with Phosphate Buffered Saline (PBS) and sterilized in an acetone bath for 10 min and air dried. The cells were cultivated on the plate surface, with 0.25% trypsin–EDTA. The harvested cells were investigated by a Fuchs Rosenthal Hematological Camera.

4 Results and Discussion

4.1 Aesthetical Appearance of the Anodized Sample

It has been observed that the anodic oxidation of the titanium alloy results in colorful patterns at different anodic voltage levels, as shown in Fig. 2. The oxide deposition commences immediately after the completion of the electric circuit, and a colorful surface appears within a few minutes, whereas incremental change in the potential difference supports rapid deposition of an oxide layer of dark shade. The change in color of the oxide film is only an interference of light phenomenon; thus, it is voltage-dependent directly. It has been observed that voltage is a leading parameter for anodization because oxide deposition rate is directly proportional to applied voltage. Initially, a thin film of 200 nm thickness was deposited at 10 V and the thickness continuously increased with the increase in voltage, but after 50 V' oxide deposition rate slowed down and became dull after 90 V. Fragile and intermittent oxide film was observed at 90 V which doesn't have any valuable application.

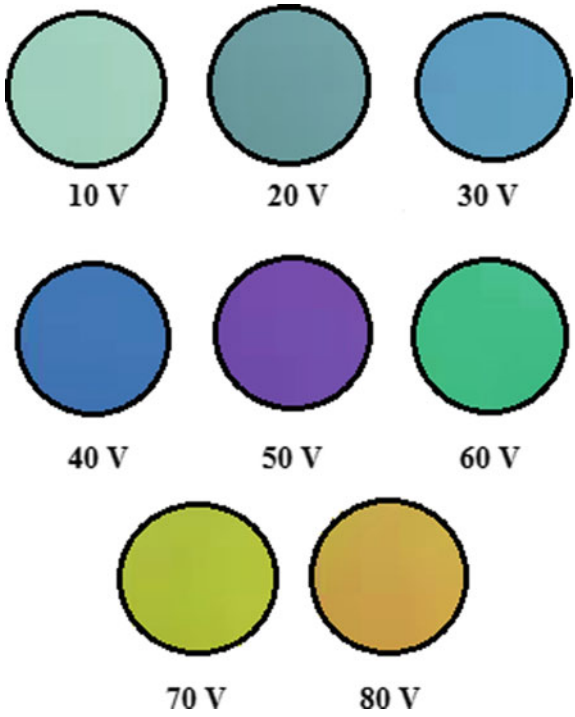

Fig. 2 Aesthetical appearance of the anodized titanium alloy at various anodic voltages

4.2 Surface Morphology and Phase Examination

Micrographs depicted in Fig. 3 revealed the surface morphology of the non-anodized specimen in image (A), polished Ti specimen (B) and anodized Ti alloy within a consistent value of H_2SO_4 at 0.5 M whereas 5%, 10%, 15% and 20% HF from (C), (D), (E) and (F), respectively. Comparative analysis of images (A) and (B) explicates that electrochemical polishing furnishes a uniform surface finish of extreme level; thus, pretreatment is very essential before anodization of titanium if nanoporous structure is the preeminent requirement. Homogeneous nanoporous structure appeared at lower concentrations of HF (upto 10%) whereas pore diameter, homogeneity and porosity were disturbed at higher concentration of HF. A fine and homogeneous porous structure has been obtained at an anodic voltage of 40 V within an electrolytic concentration of 0.5 M H_2SO_4 and 10% HF. A qualitative phase analysis was conducted through XRD at a constant angle of incidence, say 2ϴ. Phase analysis of an anodized sample is represented in a graphical manner in Fig. 4 at various concentration levels of HF (5%, 10%, 15%, 20% and 25%) whereas 0.5 M H_2SO_4 remains constant. Dominant phase conversion from anatase to rutile appeared at 5% and 10% HF concentrations. Amorphous to crystal transformation or simply anatase to rutile conversion was interrupted by increasing HF concentration; refer to Table 2.

4.3 Surface Hardness Evaluation

A diamond-shaped indenter was used to mark an impression on the sample's surface, with the estimated value at a specific load range being observed from a digital display. Five observations were conducted for a specific load and then averaged to determine the value of surface hardness. The actual data observed from Vicker's micro hardness tester are depicted in Table 3, and the same observed data are plotted in a bar diagram as shown in Fig. 5.

Anodized surface offers high surface hardness as compared to non-anodized surface and offers a strong resisting force to mark a scratch through externally applied load. A tough and hard surface becomes more durable, with almost six to seven times the hardness achieved by the anodic oxidation process.

4.4 Biocompatible Behavior

The biocompatible behavior of the sample KBH5448 is represented in Fig. 6. It has been observed that the most important factor influencing the growth of the cells is culture time. In the case of a non-anodized sample, no serious cell development has been observed. Whereas in case of anodized sample, severe cell growth has

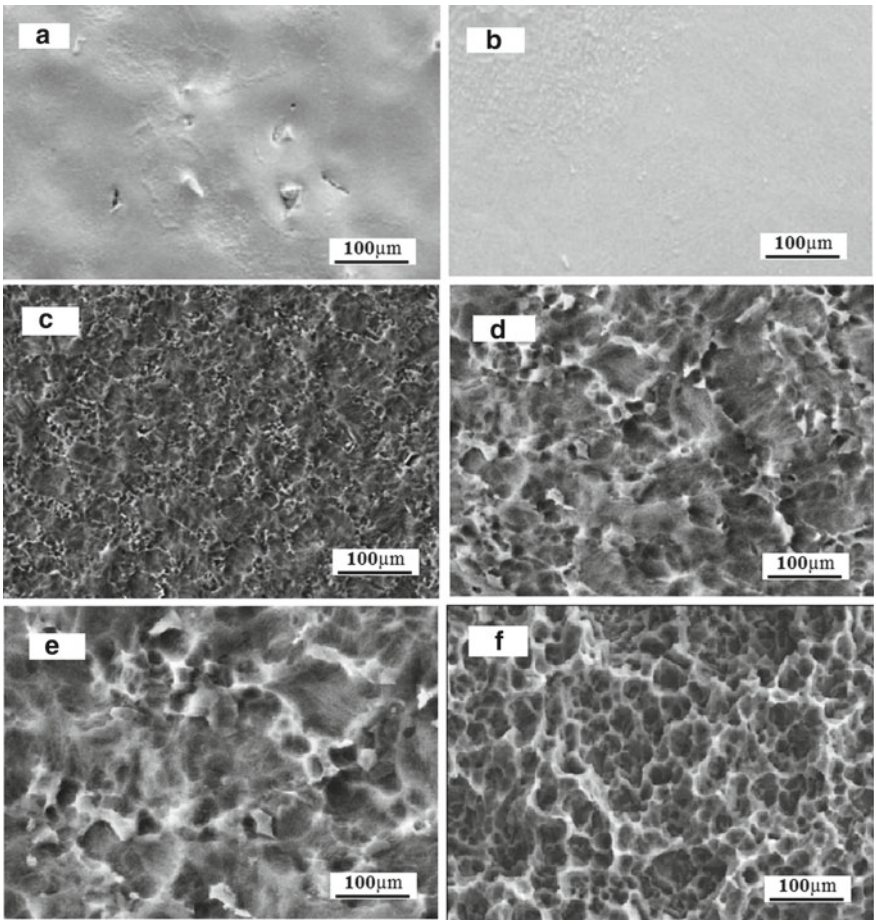

Fig. 3 SEM images of unpolished Ti alloy (**a**), uniform surface finishing observed after electropolishing (**b**), anodized Ti specimen within 0.5 M H_2SO_4 and 5% HF (**c**), 10% HF (**d**), 15% HF (**e**) and 20% HF (**e**) at optimum voltage of 40 V for each case

occurred. Figure 6 represents a Ti6Al4V sample that was anodized at 40 V within a 0.5 M H_2SO_4 electrolyte with 10% HF solution and cultured for 24 h. A nanoporous surface supports vigorous cell growth and more elongated filopodia; refer Fig. 6c, d. Highly magnified SEM images of the sample's surface exhibit that the filopodia grabbed strongly with the nanoporous titanium oxide surface; this is clearly visible in Fig. 6e, F.

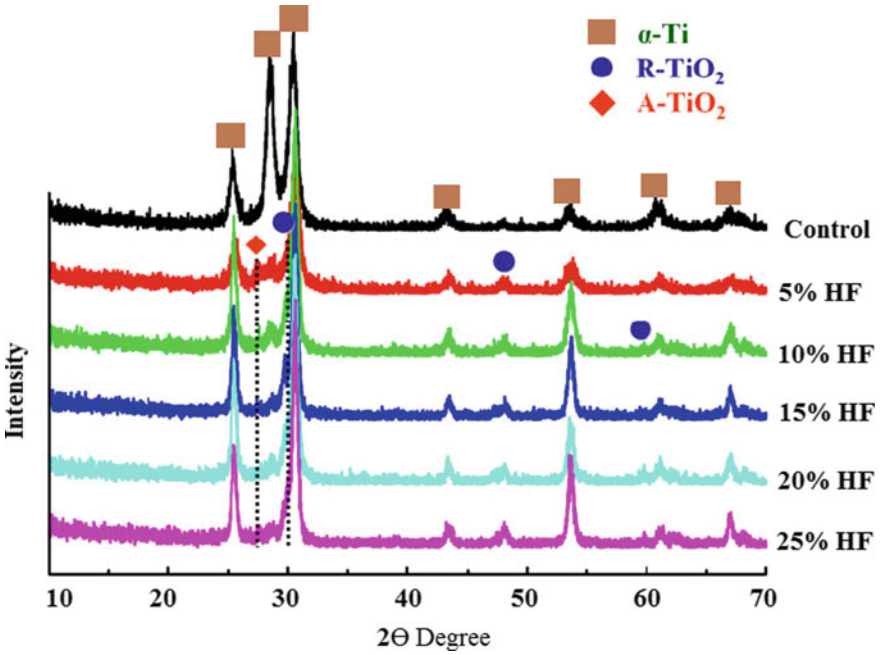

Fig. 4 Quantitative phase analysis of the anodized Ti alloy at varying concentration levels of HF (say; 5%, 10%, 15%, 20% and 25% HF)

Table 2 XRD analysis

Sample material	%age of HF within 0.5 M of H_2SO_4				
	5% HF	10% HF	15% HF	20% HF	>20% HF
Ti6AL4V	Rutile	Rutile	Anatase	Anatase	α-Ti

5 Conclusions

1. To achieve a homogeneous nanoporous oxide surface over titanium alloy, it is essential to be pretreated before anodization because a highly finished surface improves pore homogeneity as well as uniform deposition of oxide film.
2. Voltage and current density are observed as optimum process parameters for anodization and must be controlled to enhance aesthetic and morphological qualities of the metal substrate. The composition of HF within the sulfuric acid electrolyte facilitates the adhesion of oxide film with high porosity.
3. Among other oxidation processes, anodization is a very cheap and fast process to improve the architectural appearance of the metal surface especially for titanium or its alloys. Furthermore, surface hardness can also be improved almost five to

Table 3 Data collected from microhardness tester (Vicker's type) for the evaluation of surface hardness within specific load range of 25, 50, 75, 100 gf, for anodized as well as non-anodized sample

Load (gf)	25	50	75	100
For anodized sample				
Observed value of surface hardness (HV)	418, 420, 418, 412, 432	406, 420, 416, 419, 419	420, 420, 412, 418, 420	416, 411, 400, 449, 419
Averaged value of surface hardness (HV)	420	416	418	419
For non-anodized sample				
Observed value of surface hardness (HV)	75, 70, 72, 84, 84	77, 77, 75, 78. 68	70, 76, 75, 78, 91	74, 71, 73, 85, 82
Averaged value of surface hardness (HV)	77	75	78	77

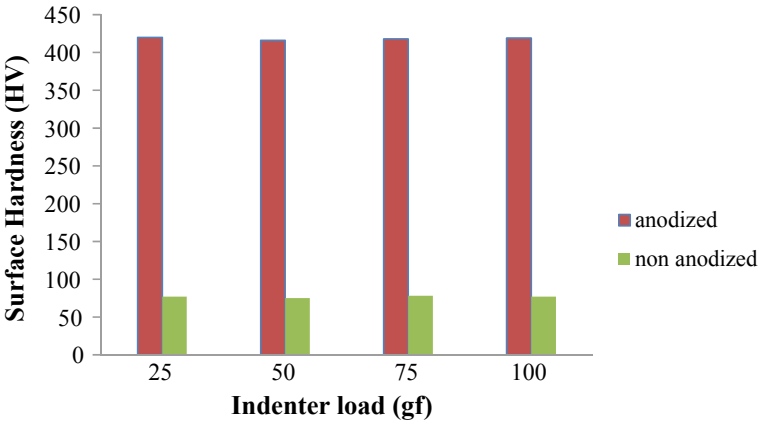

Fig. 5 Evaluation of surface hardness for anodized and non-anodized samples for a load range of 25gf–100gf

six times as compared to non-anodized Ti, which improves engineering as well as biomedical applications of the Ti alloy.

4. Nanoporous titanium oxide improves biocompatibility and supports new cell formation whereas increasing culture time increases new cell formation vigorously. Porous surface supports cell proliferation and filopodia adhere strongly to nano-textured surface. Thus, it has been concluded that a biomaterial must be treated sincerely before implantation because nanoporous oxide film offers high bone cell attachment, cell proliferation and osseointegration properties.

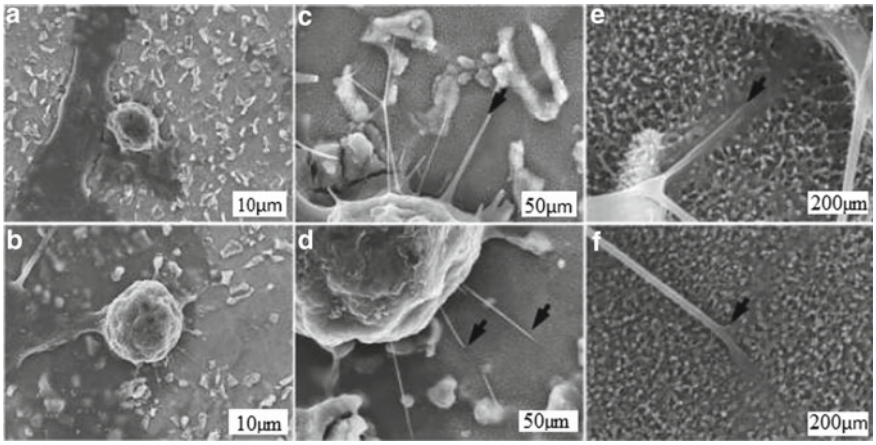

Fig. 6 SEM micrographs of anodized Ti6Al4V cultured for 24 h support new cell formation as in (A and B), highly magnified views of the newly formed cells (C and D) and strong adhered filopodia with nano-textured surface (E and F)

Acknowledgements The first author, Dr. Anil Kumar, is working as an Associate Professor in the Department of Mechanical Engineering, BRCM College of Engineering and Technology, Bahal (Bhiwani), India. He has more than 10 years of teaching and research experience. His specialization is nanocomposites and surface modification techniques of alloys to enhance their engineering applications. Second author, Dr. Sunil Sinhmar, is working as National Post Doctoral Fellow at IIT Kanpur and his expertise is in manufacturing and material science. The presented research work has already performed by authors during their Ph.D. The authors are also grateful to the Institute Instrumentation Centre, IIT Roorkee, India, for their supportive and favorable assistance to perform the characterization work.

References

1. Benedek C, Veresné Bálint M (2022) Characteristics and uses of propolis. Elelmiszervizsgalati Kozlemenyek 68(3):4028–4035
2. de Viteri VS, Fuentes E (2013) Titanium and titanium alloys as biomaterials. Tribology—fundamentals and advancements
3. Wally ZJ et al. (2015) Porous titanium for dental implant applications, pp 1902–1920
4. Webster TJ, Yao C (2016) Anodization: a promising nano modification technique of titanium-based implants for orthopedic applications. Surgical Tools Medical Devices, Second Edition, pp 55–80
5. Balasundaram T, Raja K (2016) Growth and characterization of titanium nanotubes anode for solar cell application by electrochemical anodization method. Int J Adv Engg Tech/Vol. VII/Issue II 359:363
6. Dubey RS (2013) Synthesis and characterization of titania nanotube arrays by electrochemical method for dye sensitized solar cells. Scholars Res Library Arch Appl Sci Res 5(5):28–32
7. Hack RHRGK (2020) Mechanical properties. Encyclopedia of earth sciences series

8. Chao Liang H, zhong Li X (2009) Effects of structure of anodic TiO_2 nanotube arrays on photocatalytic activity for the degradation of 2,3-dichlorophenol in aqueous solution. J Hazard Mate 162(2–3):1415–1422
9. Elias CN, Lima JHC, Valiev R, Meyers MA (2008) Biomedical applications of titanium and its alloys, 1–4
10. Eschbach L (2013) RMS foundation 2544 Bettlach titanium alloys : application as bone implants implant testing and failure analysis titanium : history titanium : application as bone implants RMS foundation 2544 Bettlach commercial pure titanium ISO 5832–2 CP titanium is cla, pp. 1–15
11. Hammouda IM, El-wassefy NA, Marzook HA, Habib ANEA, El-awady GY (2014) Micro-photographic analysis of titanium anodization to assess bio-activation 3(1):7–17
12. Lin C, Yu Y, Chen S, Liou Y (2010) Anodic growth of highly ordered titanium oxide nanotube arrays : effects of critical anodization factors on their photocatalytic activity 4(5):373–378
13. Kumar A, Kushwaha MK (2019) Nanoporous oxide surface obtained on titanium (Grade 5) alloy to analyze surface hardness and anti-wear character 8:211–222
14. Kumar A (2020) Evaluation of mechanical properties of titanium alloy after thermal oxidation process. Trans Indian Inst Metals
15. Kumar A (2002) Anodization of titanium alloy (Grade 5) to obtain nanoporous surface using sulfuric acid electrolyte, no. Grade 5
16. Kumar A (2020) Nano-porous oxide deposition on titanium alloy (grade-5) to enhance its biocompatibility along with tribological and mechanical analysis. Int J Mater Eng 11(2):91–104
17. Science E, June T, Lin C, Lai Y, Zhuang H, Lin C (2016) Some critical structure factors of titanium oxide manotube array in its photocatalytic activity some critical structure factors of titanium oxide nanotube array in its photocatalytic activity, pp 3–9
18. İzmir M, Ercan B (2019) Anodization of titanium alloys for orthopedic applications. Front Chem Sci Eng 13(1):28–45
19. Qi Y, Shang Y, Sui L (2018) State of Osseointegrated titanium implant surfaces in topographical aspect. J Nanosci Nanotechnol 18(12):8016–8028
20. Rosa LES (2020) Analysis of the hardness and tribological properties of grade 2 titanium using the thermal oxidation process at different temperatures. Mater Lett, p 128679
21. Swiatkowska I, Martin N, Hart AJ (2019) Journal of trace elements in medicine and biology blood titanium level as a biomarker of orthopaedic implant wear. J Trace Elem Med Biol 53(February):120–128
22. Traid HD, Vera ML, Ares AE, Litter MI (2015) Porous titanium dioxide coatings obtained by anodic oxidation for photocatalytic applications. Procedia Mater Sci 9:619–626
23. Aniołek K, Kupka M, Barylski A, Dercz G (2015) Mechanical and tribological properties of oxide layers obtained on titanium in the thermal oxidation process. Appl Surf Sci 357:1419–1426
24. Kirmanidou Y et al (2016) New Ti-alloys and surface modifications to improve the mechanical properties and the biological response to orthopedic and dental implants : a review, vol 2016
25. Orsini G, Assenza B, Scarano A, Piattelli M, Piattelli A (2000) Surface analysis of machined versus sandblasted and acid-etched titanium implants. Int J Oral Maxillofacial Implants 15(6):779–84
26. Jayaraman M, Meyer U, Bühner M, Joos U, Wiesmann HP (2004) Influence of titanium surfaces on attachment of osteoblast-like cells in vitro. Biomaterials 25(4):625–631
27. Wu L, Wen C, Zhang G, Liu J, Ma K (2017) Influence of anodizing time on morphology, structure and tribological properties of composite anodic films on titanium alloy. Vacuum 140:176–184
28. Zu C (1999) Surface characterization of implant materials c . p . Ti , Ti–6Al–7Nb and Ti–6Al–4V with different pretreatments, 35–46
29. Zhang R et al (2016) Fabrication of micro/nano-textured titanium alloy implant surface and its influence on hydroxyapatite coatings. J Wuhan Univ Technol Mater Sci Edn 31(2):440–445
30. Bloyce A, Qi PY, Dong H, Bell T (1998) Surface modification of titanium alloys for combined improvements in corrosion and wear resistance. Surf Coat Technol 107(2–3):125–132

31. Dong H, Bell T (2000) Enhanced wear resistance of titanium surfaces by a new thermal oxidation treatment. Wear 238(2):131–137
32. Ercan B, Taylor E, Alpaslan E, Webster TJ (2011) Diameter of titanium nanotubes influences anti-bacterial efficacy. Nanotechnology 22(29)
33. Hatem A et al (2018) Tribocorrosion behavior of low friction TiSiCN nanocomposite coatings deposited on titanium alloy for biomedical applications. Surf Coat Technol 347(February):1–12
34. Huang B-H et al (2021) Surface properties and biocompatibility of anodized titanium with a potential pretreatment for biomedical applications. Metals 11(7):1090

Chapter 5
Instrumentation and Monitoring of Additive Manufacturing Processes for the Biomedical Applications

L. de Peindray d'Ambelle, K. Moussaoui, and C. Mabru

1 Introduction

In the recent years, the demand for patient-specific biomedical products increased because of global population aging, obesity, and the increase in road traffic accidents. Therefore, there is a substantial need to manufacture such devices quite rapidly to reduce the risk of repeated procedures and/or surgery operation time. Additionally, recent context such as the world pandemic of COVID has raised the question of how to provide medical products in large quantities and short time [1, 2]. Additive manufacturing (AM) has been a suitable candidate as a manufacturing process in the biomedical field. This technique has many advantages such as rapid prototyping, design customization, complex-shape parts construction, and reduced waste production [1–6]. Moreover, since the parts build up from a Computer-Aided Design (CAD), AM can be used to produce patient-specific devices and anatomical structures [1, 3, 5, 6]. That is why AM is nowadays under development in biomedicine, enabling to build of parts difficult to achieve with conventional techniques [3, 4]. Patient-specific structures reduce the surgery operation time, and the fabrication of highly porous scaffolds or implants is more and more developed in the industry. More recently, a study by Rehman et al. [2] demonstrated how the rapidity and cost-effectiveness of AM could significantly help to meet shortages in medical devices during a worldwide pandemic like COVID-19.

Several types of AM techniques already exist and are implemented at an industrial scale. According to the application and the material to be printed, one process can be preferred over another. There have been comparisons established between metal AM processes for biomedical applications and the commonly used processes are Laser-Powder Bed Fusion LPBF (also called Selective Laser Melting SLM), Electron Beam

L. de Peindray d'Ambelle · K. Moussaoui (✉) · C. Mabru
UMR-CNRS 5312, Institut Clément Ader (ICA), 3 Rue Caroline Aigle, 31400 Toulouse, France
e-mail: kamel.moussaoui@isae-supaero.fr

A. Mahajan et al. (eds.), *Additive Manufacturing of Bio-implants*, Biomedical Materials for Multi-functional Applications, https://doi.org/10.1007/978-981-99-6972-2_5

Melting (EBM), and Binder Jetting (BJ) [2, 7, 8]. The strengths and limitations of these processes are summed up in Table 1. LPBF and EBM are the two main AM processes used in the biomedical field, especially for implant fabrication.

In the biomedical field, the raw material for AM depends on the application. Each application requires specific characteristics to be met thanks to the process and material chosen. AM of metallic parts is the most common in the field of biomedicine, even if other applications like the fabrication of natural tissues, bones and blood vessels require for instance hydrogels, bio-glasses, bioceramics [6]. The most used AM metals in biomedicine are Ti-, Zn- and Co-based alloys, steel, and Mn-based alloys [8, 10, 11]. Titanium under its pure form or Ti-based alloys, more often Ti-6Al-4V, $Ti_{15}Nb_4Ta_4Zr$, or Ti-24Nb-4Zr-8Sn demonstrate an excellent corrosion resistance as well as tensile stress, fracture toughness, and fatigue stress [12–20]. The possibility to manufacture porous Ti-based components ensures a fast bone tissue ingrowth [21, 22]. Additionally, the long-term toxicity of those alloys is minimal, but it is possible that some osseointegration and biocompatibility limitations can occur. Still, Ti-based alloys are part of the most biocompatible metals. Since this metal and this alloy are highly reactive with atmospheric gasses, Ti components require surface treatment involving the use of ceramics [23].

Co–Cr-based alloys are also widely used because of their corrosion resistance, high mechanical properties, and wear resistance [24–30]. The most common are Co–Cr–Mo and Co–Ni-Cr–Mo. These alloys have better properties for biomedical applications than stainless steels but are costlier. Nevertheless, Co–Cr alloys have a higher elastic modulus than a compact bone, which can lead to stress-shielding and reduced osseointegration. Besides, there is still a risk of cobalt release in the body which is toxic [10]. Stainless steels are low cost and demonstrate good mechanical resistance, biocompatibility [31–33]. However, their lower corrosion resistance could

Table 1 Comparison of metal AM processes for biomedical applications [1, 2, 9]

Process	Strengths	Limitations
LPBF	• Good geometrical accuracy and resolution • Good mechanical properties • Nearly full dense part • Low surface roughness • Variety of printable alloys • Controlled porosity	• Costly because of the infrastructure needed
EBM	• Low residual stresses • High mechanical strength • Nearly full dense part • Controlled porosity • No post-process heat treatment needed	• Difficulties for high-dimensional parts • Rough surface • Lower resolution • Explosive risk
BJ	• Involving low temperatures and pressures • No post-processing • Low cost	• Low resolution • Lower strength

lead to the release of undesired metallic ions, like nickel and chromium, and harmful reactions in the patient's body [10]. This effect can be prevented by using Ni-free steels or steels with low Ni-contents like 316L [33]. The latter has better properties for biomedical properties such as an enhanced strength, plasticity, corrosion and wear resistance, and biocompatibility. Other alloys such as Mg-based alloys are also utilized as biomaterial [10, 34]. These materials usually are suitable for their suitable mechanical properties and biodegradability. However, Mg alloys for clinical applications generally have insufficient corrosion and wear resistance when placed in the body environment. The release of Mg hydroxide that is converted rapidly to Mg chlorides could be harmful to the patient [35].

There are several types of applications of metal AM in the biomedical field. Implants manufactured by additive techniques and installed in a patient's body can be permanent or not when they are biodegradable. Metal AM can be also used to fabricate surgical tools or other medical devices. Some examples of applications for AM in biomedicine are described in the following section. Implants are meant to replace defective or missing tissues and bones in a human body. AM is developing in the fabrication of permanent implants like joints [36], bones [16, 18], and dental implants [9, 37]. Some examples of biomedical applications with AM parts are shown in Fig. 1.

Besides, the freedom of design offered by AM techniques enables the production of surgical tools and medical instruments with better ergonomics and better

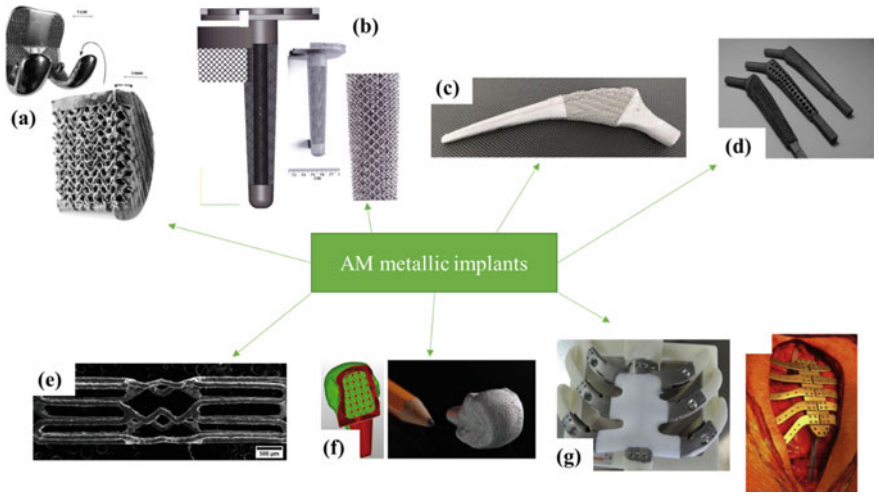

Fig. 1 Examples of metallic AM parts for biomedical implants. **a** Co-29Cr-6Mo femoral implant with mesh structure fabricated by EBM [36]. **b** Ti-6Al-4V tibial knee stem with mesh structure fabricated by EBM [36]. **c** Hip stem with mesh structure fabricated by SLM [3]. **d** Ti-6Al-4V hip stems with mesh structures and different porosity rates fabricated by EBM [13]. **e** Co-Cr-based alloy cardiovascular stent fabricated by SLM [26]. **f** Finger implant fabricated by SLM [38]. **g** Titanium sternal implants fabricated by AM [15]

customization than conventional manufacturing methods. Moreover, the cost-effectiveness and rapidity of such processes give the possibility to produce a high number of tools and instruments, which is advantageous in developing countries. Metallic surgical tools made by AM are mainly made with 316L stainless steel, Ti-based alloys, and Co-Cr-based alloys [7]. Examples of metallic AM surgical tools and medical instruments are steerable grasping tools [39], electrodes [40], or instruments for hip and knee replacements [41]. The parts fabricated by AM for biomedical applications should respect a series of criteria regarding their properties and characteristics. They are very specific to the field of application and the use of the part. An implant, scaffold, or screw to be inserted in a human's body will not have the same "exigences" as a surgical tool. These different properties will be gathered and summer up according to the applications. An implant is used to mimic the functionality of a tissue or bone. Therefore, some of its characteristics must be similar or identical to the original part of the body that it has replaced.

1.1 Biocompatibility

Since it is introduced in the body, the implant should be made of a biomaterial and be biocompatible. Success of the implant introduction depends on the reaction of the human body, which is not only the host response to the biomaterial but also the degradation of this material in the body environment [42]. According to this response, the implant will be considered as bioactive, meaning that it enables an efficient osseointegration or biotolerant. If the material is not biocompatible, some issues can occur such as thrombosis (causing blood coagulation) tissue encapsulation, allergies, or intoxication [11, 43].

1.2 Mechanical Properties

The human bone, divided into an outer and inner region, has an elastic modulus of 20 and 0.5 GPa, respectively. In general, this elastic modulus depends on the type of bone and the direction of measurement while testing [43–45]. The outer bone density is about 2 $g.cm^{-3}$, and this also varies according to the type of bone, its geometry and its porosity [14, 46, 47]. For metallic implants made of Ti-based or Co–Cr-based alloys, the elastic moduli are higher than the human bone and for instance, a Ti implant has a density around 4 $g.cm^{-3}$, which is twice the bone's density. Therefore, a metallic implant's stiffness could cause a "stress-shielding" effect in the patient's body which is a response to the high mechanical stress applied by the implant. This phenomenon hinders the implant's longevity because of bone resorption and implant loosening [43]. In contrary, in a healthy patient's body, the bone remodels in response to the mechanical stress applied [48, 49]. Furthermore, the implant should also have high compressive, shear and tensile strength to avoid fracture occurrence. The fatigue

strength of the material is also an important factor as brittle fractures can occur under cycle loading of the implant [1, 6].

1.3 Porosity

The implant stability in the body depends on its fixation with surrounding tissues. The human bone consists of an outer cortical dense bone, which has a high technical strength. The porosity of the cortical bone in less than 10 vol% whereas the inner trabecular bone has a porosity rate about 50–90%. This interconnected pore system is essential to ensure cell penetration, bone tissue ingrowth, vascularization, and nutrient delivering. AM is suitable to fabricate parts with a desired rate of porosity and ensure the implant's osseointegration and fixation [14, 22]. It is possible to differentiate two types of porosity in a structure, closed-cell, and open-cell. The closed-cell structure consists of pores enclosed by a thin metallic membrane and is generally present in metallic foams. These pores have various sizes, locations, and shapes in the structure. Whereas in an open-cell structure, the pores are interconnected. The porosity is necessary for bone tissue ingrowth and fixation of the implants but affects drastically the fatigue strength of the part. It has been shown that for Co–Cr and Ti-6Al-4V porous coated alloys on solid core structures, the fatigue resistance decreased significantly [50, 51]. It is also possible to ensure mechanical properties and decrease the part's weight thanks to cellular structures and scaffolds [19, 22, 52–54]. The advantage of cellular structures and scaffolds is the control of the voids and strut's locations, sizes, and shapes [55]. The optimal pore size depends on the proteins and enzymes to infiltrate or attach to the AM part but also the original body part to be regenerated [56]. The scaffold's characteristics determine afterwards the mechanical properties of the implant and should match the properties of the original part of the body to mitigate the stress-shielding effect [57].

1.4 Surface Finish

In addition, AM parts should have a specific surface property such as surface wettability, roughness, and texture. These properties particularly affect the wetting of the implant by fluids like blood, the adhesion of osteoblasts on the implant's surface, the adsorption of proteins. The roughness and texture have an influence on cell attachment on the implant surface [17, 27, 47].

1.5 Corrosion and Wear Resistance

The corrosion and wear resistance are two important characteristics for a metallic implant. When placed in the human body, surrounded by body fluids, the biomaterial is confronted to corrosion. Different types of corrosion like crevice corrosion, pitting corrosion, galvanic corrosion, or electrochemical corrosion can occur and lead to the release of metallic ions by the implant in the body [43, 47, 58]. This phenomenon can be the cause of intoxication and allergies, for instance with the release of nickel ions from stainless steels alloys [11, 59]. Besides, corrosion can cause modifications of the part's surface roughness hence a deterioration of the cell adhesion and bone tissue ingrowth. The following part gives an overview of the common part defects encountered in metal AM, especially for LPBF and EBM (two most used processes in biomedicine). Then, instrumentation and monitoring techniques for a better control and understanding of these metal AM processes are discussed. Finally, multi-sensor approaches, as well as their strength and limitations, are detailed. Perspectives of the instrumentation and monitoring for additive manufacturing in the biomedical applications are given.

2 Common AM Parts' Defects in the Biomedical Field and Relation to Process Parameters

The defects observed on AM metallic parts are related to process parameters. In AM techniques such as LPBF, EBM, SLS, these parameters are numerous and interrelated which complexifies the optimization of part's quality. Common defects and their link to process parameters will be described in the following section. Some solutions to mitigate defects occurrence have been explored in literature and will be summarized.

2.1 Pores

In powder-bed AM techniques, the presence of undesired and uncontrolled pores is one of the most encountered defects. Pore defects can be divided into two categories: gas pores and lack-of-fusion (LOF) pores. Pores are formed through different mechanisms related to process parameters. These defects will have an effect on the part's mechanical properties [4, 60]. Gas pores gather keyhole pores, hydrogen pores, or powder feedstock pores (Fig. 2a–c) [4, 61]. These pores have a size between 5 and 50 μm and could have various shapes but are often recognizable by their spherical shape. Gas pores are caused by an entrapment of gas in the feedstock powder particles or in the melt pool during fabrication. In general, these types of pores occur in high-energy areas and they are larger when the laser energy density increases [61–63]. The latter depends on the laser power and scanning speed: keyhole pores tend to appear

more when the laser power is high combined with a low scanning speed (Fig. 2e, f) [64, 65]. Hydrogen pore formation is reduced thanks to lower laser power and higher cooling rates (shorter time between melting and solidification) (Fig. 2h) [66]. Finally, the powder feedstock pores are more numerous when the raw powder contains more porosities because of gas atomization (Fig. 2g) [67]. To achieve a stable melting pool and prevent the formation of keyhole and hydrogen pores, one way is to lower the excessive energy density by controlling the laser power and scanning speed [61, 66].

LOF pores (Fig. 2d) are present between consecutive tracks, consecutive layers, or between the part and the substrate. They are usually irregularly shaped and reach sizes from 50 µm to several millimeters [61, 68]. LOF pores occur if the bonding with the previous track was incomplete or there is spattering (also called balling). This phenomenon prevents the powder bed from being spread uniformly and discontinuities appear on the surface on the tracks [68–72]. The LOF can be caused by an insufficient laser energy density, for instance due to a Gaussian laser distribution where the sides have a lower energy. In addition, the incomplete melting can come

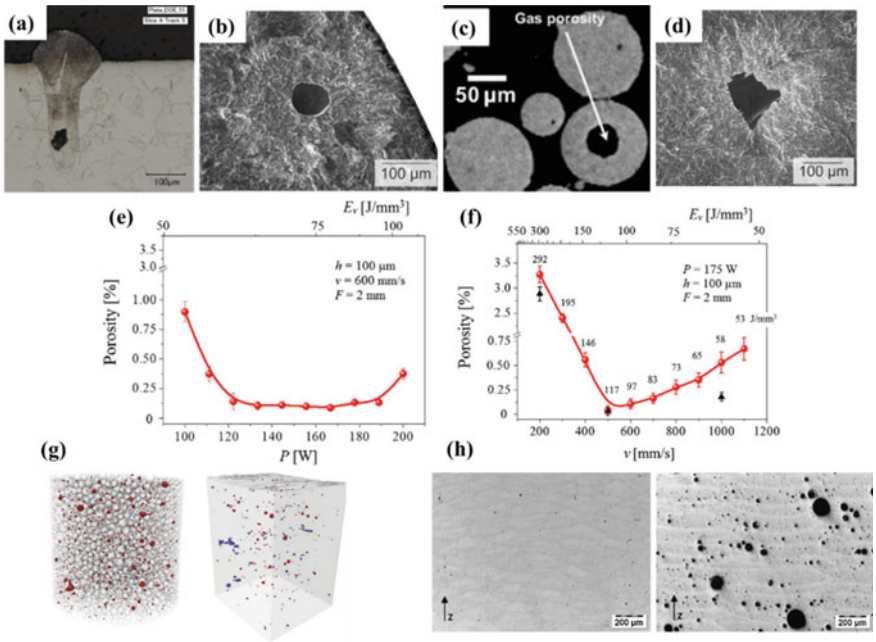

Fig. 2 **a** Metallographic cross-section showing a keyhole pore in a 316L track made by LPBF [75]. **b** Fractography of a Ti-6Al-4V EBM specimen showing a gas pore [76]. **c** SE-SEM micrograph of a gas pore within a feedstock powder particle (Ni-based superalloy) [77]. **d** Fractography of a Ti-6Al-4V SLM specimen showing a LOF pore [76]. **e** Influence of laser power on the total porosity for SLM of Ti-6Al-4V [63]. **f** Influence of scanning speed on the total porosity for SLM of Ti-6Al-4V [63]. **g** µSXCT measurements showing porosities in the Ti-6Al-4V feedstock material (left) and in the EBM as-built part [67]. **h** Increase of the hydrogen pore density when increasing the scanning speed with the laser beam diameter. LPBF of AlSi10Mg samples [66]

from the combination of low power and high scanning speed [65]. Hatch spacing between tracks of a layer could also affect the LOF pores formation: when the hatch spacing increases the LOF occurrence tends to increase [73]. As for the balling effect, it has been shown that it occurs when the melt pool is unstable because of high laser power and high scanning speed [61]. Instead of a Gaussian laser beam, [74] studied a Bessel beam for the LPBF process and obtained a porosity rate 7 times lower than with the Gaussian beam (for the same processing parameters).

Porosity defects affect the final mechanical properties, especially tensile/compressive strengths, and fatigue performances of the AM metallic parts. The tensile properties mainly depend on the microstructure and the phases of the material. Mechanical properties such as tensile/compressive strengths are rarely affected by small gas pores but can be significantly affected by LOF pores [61]. Gong et al. [78] showed the impact of pore defects on the tensile behavior of LPBF parts. For gas pores volume <1% caused by a high energy density, the tensile properties were not affected but the effect appeared for a porosity >5 vol%. Tensile strength is hindered by LOF defects because these large irregularities cause stress concentrations that affect the mechanical properties. Pore defects also affect the fatigue resistance of the printed material, and it was shown for instance by Gong et al. [78] for LPBF parts. The fatigue performances were reduced because of the LOF defects that created brittle fracture in the material. Leuders et al. [79] also demonstrated the detrimental effect of pores in LPBF parts fabricated with Ti-6Al-4V on their fatigue resistance. The mean fatigue life of these samples ranged from 27 000 to 290 000 cycles. As a comparison, the authors treated their AM parts via Hot Isostatic Pressing (HIP) and obtained a mean fatigue life of 2×10^6 cycles.

2.2 Cracks

In metallic AM, two types of crack defects can occur: hot cracking (also called hot tearing or liquation cracking) and cold cracking (also called solid-state cracking or solidification cracking). The occurrence of cracks in the material strongly depends on the presence of internal defects such as pores (Fig. 3a, c) [80] but also are influenced by process parameters (Fig. 3b). Cracks within the AM parts hinder the mechanical properties. Hot cracking occurs in the zone surrounding the melt pool, which is called the partially melted zone. The latter consists in partially melted grains (S) and an intergranular liquid (L). The fracture of hot cracking does not show a dendritic structure because of the presence of the liquid phase. The hot cracking susceptibility in the partially melted zone is affected by the material grain structure, the hot ductility and contraction of the metal used. Cold cracking occurs in the fusion zone (or Heat Affected Zone HAZ), i.e. the completely solidified zone during the terminal stage of solidification. The fracture surface of a cold crack reveals a dendritic structure. The dendrites, at the end of solidification, are separated by a liquid film that persists at lower temperatures and weakens the material, making it susceptible to cracking if

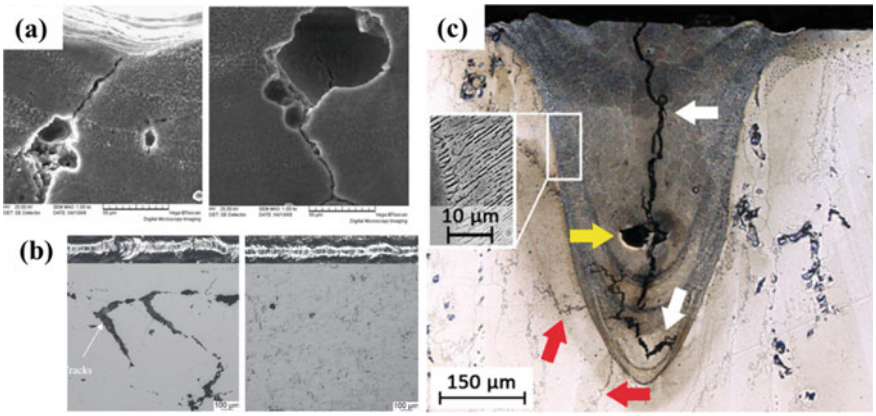

Fig. 3 **a** Cold cracking induced with a pore [80]. **b** Optical microscopy of single tracks and cross-sections produced with laser power of 120 W (110 W on the right image) and scanning speed of 0.2 m.s^{-1} (0.4 m.s^{-1} on the right image) [84]. **c** Cross-section of a LPBF-ed aluminum alloy single track showing cold cracking with white arrows, hot cracking with red arrows and keyhole pore with yellow arrow [85]

there are tensile stresses. Cold cracking is affected by the solidification range of the metal, its composition, ductility, contraction among others [61, 81–83].

Cracking occurrence is strongly related to process parameters such as the heat input during metal AM. For the LPBF process, scanning speed and laser power influence the energy density applied in the melt pool, and high energy density has been proven to yield to cracks. An increase of the laser power leads to the change of the melting mode by going from a conduction mode of the heat to a keyhole mode (Fig. 3c) [84, 85]. Additionally, the manipulation of the lasering mode (for instance quasi continuous instead of continuous wave) can be used to reduce the cooling rate and prevent the formation of brittle phases, which promote crack initiation [86]. In the case of fabrication of titanium aluminide alloy parts with EBM, [87] showed that a high energy input combined with a reheating process avoids the formation of cracks. This effect is due to a higher sensibility of the material to cold cracking than hot cracking and it would mean that materials prone to cold cracking must be manufactured with a higher heat input than materials prone to hot cracking [82]. The hot cracking occurrence tends to increase with a high scanning speed [88, 89]. Nie et al. [89] showed that very low scanning speeds (≈80 mm/s) could prevent the crack formation in SLM Al-4.24Cu-1.97 Mg–0.56Mn parts. Other parameters such as the hatch spacing can have an influence on cracking. For aluminum alloys printed by LPBF, it has been shown that a smaller hatch spacing enables the remelting of the crack and its elimination thanks to a higher overlapping ratio of the melt pool [88].

2.3 Surface Roughness

In metal AM, surface defects might occur, and the final surface roughness is an important factor to control, especially for biomedicine applications [90]. Surface roughness of AM parts can be evaluated and is related to process parameters but also feedstock material properties. An insufficient surface roughness could hinder the cell adherence, fixation, and tissue ingrowth on the implant. In contrary, too rough surfaces and the presence of large surface defects could deteriorate the mechanical properties of the parts [10]. In AM, the surface roughness is caused by the staircase effect, partially molten powder particles and balling effect [91] (Fig. 4c). An efficient way to overcome the staircase effect is to lower the layer thickness as shown Fig. 4a. It leads to an increase in the resolution of the part, but it is detrimental to manufacturing time. To improve surface finish, fine powders are also preferred. However, fine powder tends to agglomerate which affects the flowability, an essential factor for the spreading of the powder bed in AM [92, 93]. In terms of parameters, a sufficient energy input and combining lower scan speed with higher laser power should mitigate surface roughness [61, 94]. As an example, the effect of laser power and scanning speed on the part's roughness has been studied by Moussaoui et al. [95] (Fig. 4b).

For as-built parts (i.e. not machined or blasted), the surface roughness is important, and it is a cause of the deterioration of fatigue properties [98]. To reduce the detrimental effect of roughness and surface defects on the part's mechanical properties, the metallic AM parts often are machined, sand-blasted, or polished to modify their surface roughness according to the application [4, 98–100].

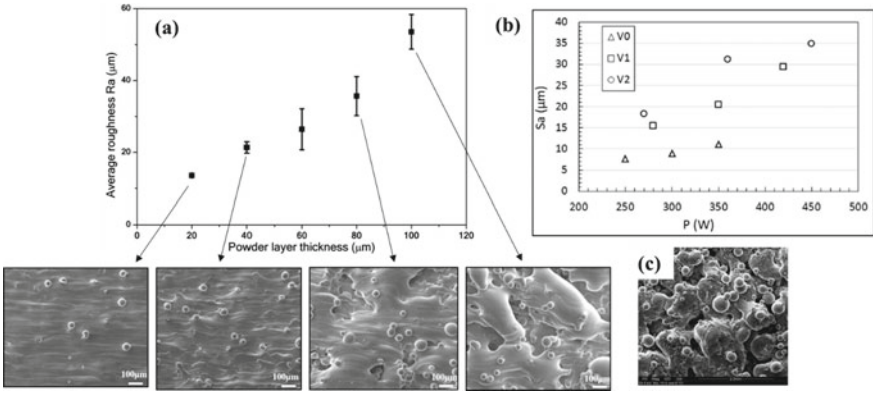

Fig. 4 **a** Average surface roughness as a function of layer thickness for LPBF-ed Ti-6Al-4V samples. SEM micrographs of top surface structure [96]. **b** Effect of laser power and scanning speed on surface roughness of LPBF-ed Inconel 718 sample [95]. **c** SEM image showing balling effect on the surface of SLS-ed 316 SS samples [97]

2.4 Residual Stresses

Residual stresses represent important part defects in metal AM. In laser-based AM processes, residual stresses are mainly formed because of high cooling rates and large thermal gradients. They have an impact on the mechanical properties, crack occurrence and deformation [61, 82, 100]. In a similar way to cracking, two mechanisms have been identified for residual stress formation in LPBF. One is caused by thermal gradients due to the rapid heating of the surface and slow heat conduction throughout the part. Consequently, the deposited layer solidifies but is constrained by the underlying layers, which creates elastic compressive strains. The second mechanism takes place during the cooling of the layer, when it shrinks because of thermal contraction. This shrinkage is restricted because of underlying cold layers, and this leads to tensile stresses [101]. The residual stress occurrence will then depend on the heating and cooling mechanisms. These mechanisms are influenced by process parameters such as the energy input, deposition strategy, and layer thickness [102].

2.5 Geometrical Defects

Geometrical defects in metal AM parts are dimensional and geometrical deviations of the part compared to its CAD model. These deviations are mainly due to distortions (Fig. 5a, b) and delamination (Fig. 5c) caused by residual stresses. Delamination is a cracking due to the layer-by-layer manufacturing. Because of steep thermal gradients, the residual stresses created between layers can be higher than the bonding between layers and this leads to delamination [82]. The geometrical defects could be induced by unsuitable laser spot size or by the nature, thickness, and preheating of the substrate [103]. Indeed, Fu et al. [104] obtained smaller distortion on LPBF parts thanks to a fine laser beam because of its significant in-situ stress relief annealing. Besides, the choice of the substrate is important since a thick substrate will lead to more distortion. It has also been showed that preheating the base plate is an efficient way to effectively reduce the part's distortions [105]. In addition, process parameters including the laser power, scanning speed, layer thickness, and scanning strategy influence the residual stresses and thus the distortions (Fig. 5d) [102, 106, 107].

2.6 Microstructure and Anisotropic Mechanical Properties

AM metallic parts have textured columnar grain structures (Fig. 6), which leads to anisotropic mechanical properties. Thus, controlling the microstructure is a challenge for such processes, especially to fabricate high-quality parts for biomedicine. This microstructure is typical for AM process because of the layer-by-layer construction and heating of the part. When the part solidifies, the grains grow parallel to the

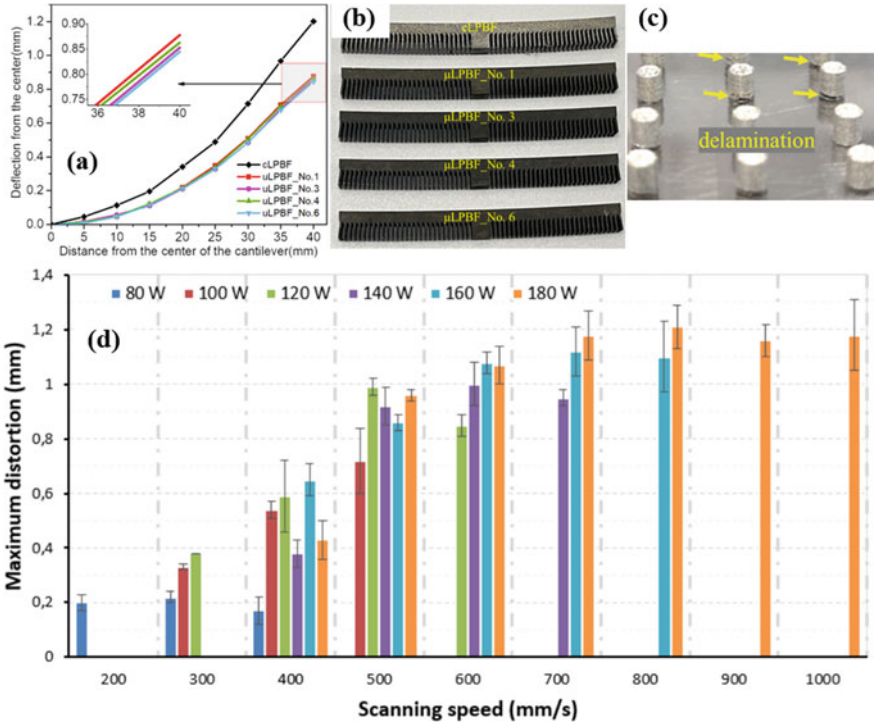

Fig. 5 **a** Deflection of LPBF-ed 316 L cantilever samples. Comparison between conventional and micro-LPBF (cLPBF and µLPBF) processes [104]. **b** Corresponding distorted samples [104]. **c** Delamination of NiTi samples fabricated by µLPBF [103]. **d** Effects of laser power and scanning speed on the maximum deflection of maraging steel 300 samples made by LPBF [102]

maximal thermal gradient direction, which is generally oriented downward from the melt pool to the bottom surface. Therefore, the remelted grains of previous layers grow epitaxially along the build direction (BD) and become large columnar grains. Moreover, some crystallographic growth directions are preferred like the <100> direction along BD for face-centered cubic (FCC) metals because it is the least close packed. The crystallographic structures are strongly dependent of the melt pool dynamics and shape. The melt pool shape and dynamics are determined by process parameters, especially the key parameters, i.e. laser power, scanning speed, and scanning strategy [61, 95].

The typical microstructure of metal AM parts affects the mechanical properties, which are anisotropic. This anisotropy is observable when testing the fatigue life of the material or its tensile strength. Differences exist between samples extracted parallel and perpendicular to the BD. Tensile mechanical properties are often better along the direction perpendicular to the BD than along the direction parallel to the BD. This is caused by the columnar microstructure oriented along the BD, Amato et al. [111] showed that there are more grain boundaries perpendicular to the BD than

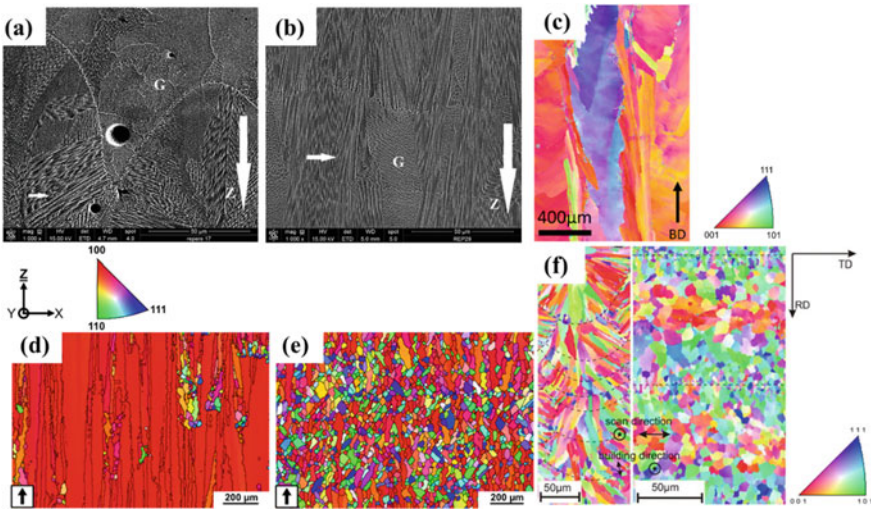

Fig. 6 **a** SEM micrograph of LPBF-ed Inconel 718 sample showing columnar cellular microstructure with VED[1] = 31.75 J.mm^{-3} [95]. **b** SEM micrograph of LPBF-ed Inconel 718 sample showing columnar cellular microstructure with VED = 61.2 J.mm^{-3} [95]. **c** EBSD images of LPBF-ed 316 L samples along building direction [108]. **d** EBSD images of EBM-ed Inconel 718 samples showing columnar grains [109]. **e** EBSD images of EBM-ed Inconel 718 samples showing equiaxed grains [109]. **f** EBSD images of AlSi10Mg samples fabricated by LPBF. The melt pool borders are indicated by dotted black lines [110]

parallel to the BD. The anisotropy of mechanical properties can also be explained by the defect orientation (e.g. LOF defects) in the material. Vilaro et al. [112] correlated the presence of defects in the parallel direction to a lower elongation to fracture than samples in perpendicular direction. This anisotropy also concerns the fatigue properties of the parts where fatigue strength is higher in the perpendicular direction than in the parallel one [113, 114].

In a nutshell, metal AM is a suitable process for patient-specific biomedical devices such as implants. In this field of application, the parts manufactured should respect demanding characteristics such as biocompatibility, porosity, and mechanical properties. Nevertheless, AM processes being usually very complex to master perfectly because of the numerous interrelated parameters and the strong influence of these parameters on part's properties. Common defects such as undesired pores, cracks, roughness, or anisotropic mechanical properties occur with non-optimal parameters and process instabilities. These issues prevent the parts manufactured by metal AM from being used and implanted in the patient's body. Thus, there is a serious need for a better control of the process during manufacturing. Instrumentation enables to trace and monitor the parameters and physics impacting the part's characteristics. Through these observations, it is possible to correlate the physical

[1] In this study «VED» stands for Volumetric Energy Density, which is defined as the ratio between laser power and the scanning speed x the hatch distance x the layer thickness [95].

phenomena and the material's properties to better understand the process. This understanding is a key to manufacture defect-free high-quality parts meeting with the needs of the biomedical application.

3 Needs for Process Instrumentation and Monitoring

Instrumentation and monitoring of the metal AM processes are needed to better understand and control process physics and avoid the occurrence of defects. Instrumentation is a non-destructive experimental approach consisting of placing sensors in-situ (in the AM machine) to observe quantities in real time. The quantity to be detected by a sensor can be either an input (laser power, scanning speed…) or an output (melt pool geometry and temperature, distortion…). This instrumentation is used to trace a quantity during fabrication or detect the occurrence of a defect or an instability of the process. In metal AM processes, instrumentation and monitoring systems have been tested and are reported in literature. According to the physical quantity to be monitored, the suitable sensor and measuring technique vary. Moreover, a sensor is chosen because of other criteria such as its price, its dimensions, its weight, and its technical characteristics. Once the sensor is selected, it must be calibrated and placed in the fabrication environment either in contact or at a specific distance from the object. There are several limitations to the placement of a sensor in an AM machine: the space available to place the sensor, the constraints for the wiring between the sensor and treatment system, the presence of a laser and reflected laser beams, the high temperatures involved in some processes, the dust and smoke. Consequently, the positioning and protection of a sensor are critical to ensure a good observation and/or measurement without being affected by the process. Commonly, in-situ instrumentation uses thermal, optical, or acoustical techniques to observe and measure different quantities on the part or on the process variables. These techniques are also used to detect defects such as pores, residual stresses…According to what is going to be observed and/or measured by the sensor, the scale differs. Indeed, an observation/measure could be made at a microscopic (small representative volume), mesoscopic (track or group of tracks), or macroscopic scale (layers or entire part) [115].

3.1 Temperature Measurements

Thermal techniques including thermography and pyrometry have been largely explored in literature for in-situ monitoring of metal AM such as LPBF. These techniques are contactless, non-intrusive, and non-destructive and can be used to measure surface temperatures or the temperature of the melt pool. Another thermal technique also used, usually to calibrate other sensors, is the use of thermocouples. They measure locally the temperature, in contact with the object. These methods are

however still constrained to the placement of the sensors in the fabrication area, the complexity of calibration, and the challenges concerning data management.

3.1.1 Thermography

Thermography evaluates the thermal radiation emitted by the object. It is based on Planck's law giving the relationship between the spectral emissive power per area emitted by a black body,[2] the wavelength of observation and the body's temperature. The measure is generally done for a specific spectral range given independently from the temperature range used. Planck's law [116] is given by Eq. (1):

$$L_\lambda(\lambda, T) = \frac{2hc^2}{\lambda^5} \frac{1}{\exp\left(\frac{hc}{k_b \lambda T}\right) - 1} \tag{1}$$

With L_λ the spectral radiance of the black body, h the Planck constant, c the speed of light in the studied medium, and k_b the Boltzmann constant. From this equation, the radiance temperature can be deducted and is given by Eq. (2):

$$T = C_2 ln^{-1}(1 + \left(\frac{C_1}{L_\lambda(T)}\right)) \tag{2}$$

With $C_1 = \frac{2hc^2}{\lambda^5}$ and $C_2 = \frac{2h}{k_b \lambda}$.

In fact, there is proportionality between a black body and a real body which is the emissivity ε. The latter depends on the material, the temperature, the wavelength but also on the surface of the material (polished, oxidized, rough…) and the emission angle. In general, real objects emit a flux inferior to the black bodies' flux. The following relation consequently exists:

$$L_{\lambda, real\ object}(\lambda) = \varepsilon(\lambda, T).L_{\lambda, black\ body}(\lambda, T) \tag{3}$$

For this reason, it is essential to calibrate a contactless thermal sensor to take the emissive properties of the heated body into account. It will be shown that emissivity is the most common limitation in such thermal techniques. Thermography can be used to monitor the characteristics of the melt pool in metal AM such as LPBF and EBM. Determining the melt pool size and temperature is possible with thermography when choosing the right spectral range and position for the sensor. Price et al. [117] used an NIR camera (MCS640 Luma Sense, spectral range from 780 to 1080 nm) placed at the front side of an EBM machine to detect temperatures in the range of 600–3000 °C with a maximum frame rate of 60 Hz. The fixed value of 0.3 for the emissivity was chosen. Besides, two lenses were tested with different distances from the target. The camera

[2] A black body is an ideal body, which absorbs the integrality of incident radiations and emits a radiation, which is equivalent to the one given by Planck's law.

measured the temperature at each step of the process (powder spreading, preheating, contour melting and hatch melting). These observations enabled to determine melt pool dimensions and temperature profile across the melt pool center.

One of the challenges of this study was the determination of the emissivity of Ti powders at high temperature since it has been assumed and thus led to only approximative temperature results. Krauss et al. [118] focused on the monitoring of the HAZ (i.e. solidified area close to the melt pool with temperature above 1255 °C). For the LPBF processing of Inconel 718 parts, thermal imaging with a LWIR (Microbolometer detector Infractec Variocam, spectral range 8–14 μm, resolution 640 × 480 pixels) camera was used. The camera was mounted outside the building chamber and inclined by a 45° angle from the build plate. This system enabled to acquire only a small section of the total building area. The evaluation of the circularity and aspect ratio of the HAZ could help detecting deviations and drifts in the scanning unit. Bayle et Doubenskaia [119] used a FLIR (Phoenix RDAS, spectral range 3–5 μm, resolution 320 × 256 pixels) camera in a LPBF process to monitor the HAZ temperature. The camera was installed in the LPBF furnace. This system enabled to have an estimation of the stability of the melting process via visual inspection. Indeed, the authors could obtain information about phenomena occurring during process such as droplet formation and removal in the laser-powder interaction zone.

Measurement of surface temperature via thermography for in-process monitoring in LPBF and EBM has also been studied. Rodriguez et al. [120] installed a FLIR camera (FLIR SC645, FLIR Systems Inc., resolution 640 × 480 pixels) with a temperature range up to 2000 °C into an EBM machine. The camera was positioned above the build chamber, behind a ZnSe viewing window (Fig. 7a). The IR images were captured after the melting step to measure surface temperature profiles of each layer. The authors developed a procedure for the emissivity measurement of Ti-6Al-4V and a thermal model to determine the factors influencing the view of the machine's thermal enclosure for the IR camera. The temperature was calculated from the powder bed's emitted radiations and some discontinuities caused by over-melting could be observed.

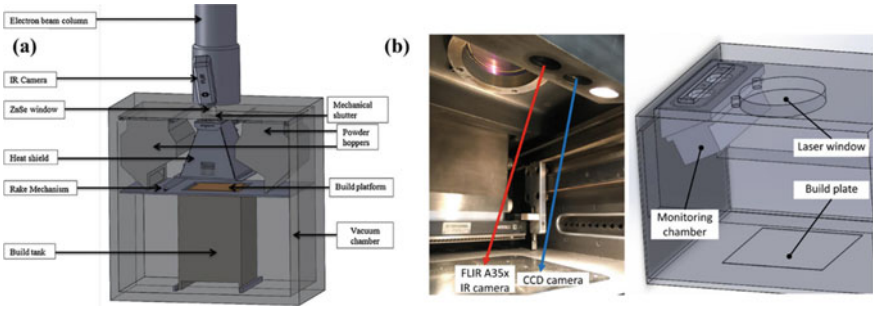

Fig. 7 **a** Experimental thermography setup for the EBM process adapted from [120]. **b** Experimental thermography setup for the LPBF process adapted from [122]

Wegner et Witt [121] implemented an IR imaging system to measure the distribution of surface temperature and the temperature of the molten material during the SLS process. MWIR cameras (InfraTec Jade III, resolution 320 × 240 pixels, spectral range 3–5 μm) with a maximum temporal resolution of 700 Hz were installed in two different ways above the building area. The first camera to measure the temperature distribution on the surface replaced the xy-scanner head with an angle of 5° to the building surface. The second setup was placed next to the scanner head with an observation angle of 23° and could measure the melt pool temperature while the laser is working. The authors carried out experiments on the radiant heaters' temperature and studied the influence factors on the homogeneity of the surface's temperature. Williams et al. [122] also used a FLIR (A35) IR camera (resolution 320 × 256 pixels) located in an aluminum box and viewing through a germanium window in the LPBF process (Fig. 7b). The camera is positioned with an angle of 66° from the build plate and images are recorded at a rate of 60 Hz during the whole process. The surface temperature is measured during the build process part way through on layer. These measurements enabled to correlate layer temperature with final part's microstructure and defect occurrence.

One application of thermography as an in-process monitoring technique is the detection of defects during manufacturing. Dinwiddie et al. [123] placed a FLIR MWIR camera (SC8200) in front of the EBM machine's window equipped with a shutter. When this shutter is open, metallization occurs and the transmission through the window is reduced, which complexifies the calibration of the IR system. Moreover, the position of the camera reduces the spatial measurement area and hinders the focus from front to back. Because this shutter prevents the operators from measuring properly with their IR system, they decided to replace it by a film and explored another solution with a protective mirror. Thanks to their setup, the authors could measure the width of the electron beam and detect an over-melting phenomenon during the preheating phase. Eventually, the continuous IR camera monitoring enabled to detect porosity caused by insufficient energy input and unmolten powder. With their setup composed of a LWIR camera, Krauss et al. [118] could detect artificial flaws and pores by measuring the temporal evolution and spatial distribution of the total irradiance during the making of a new layer. Thanks to the thermography imaging and the linear profile of the spatial irradiance after exposure and during solidification, flaws with diameter >100 μm could be detected. Lastly, thermography was used by Schwerdtfeger et al. [124] during EBM to measure build height and detect flaws during construction. They positioned a FLIR camera (A320, resolution 320 × 240 pixels) alongside the electron beam gun with an angle of 15° to the powder bed and protected by a ZnSe window.

3.1.2 Pyrometry

A pyrometer is composed by a lens connected to electronics via an optic fiber. It converts a radiation into an electric signal and indicates, without contact with the object, its temperature in a specific spectral range. Like other thermal methods,

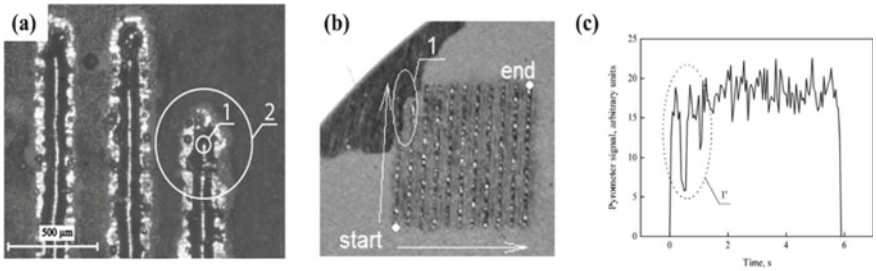

Fig. 8 **a** Laser spot size 1 and pyrometer view field for remelted track in LPBF. **b** Powder layer with an irregularity of powder thickness in the two first tracks. **c** Evolution of the pyrometer with a zoom on the irregularity area. Adapted from [125]

the measure made by a pyrometer depends on the material's emissivity and varies with its temperature and surface. A classical pyrometer indicates the temperature thanks to the measure of a radiation in a spectral range which allows to get the emissivity value. Multi-wavelength pyrometers make the ratio between two energies at two different wavelengths considering that the emissivity varies thinly between both. Pavlov et al. [125] mounted a two-wavelength pyrometer (InGaAs photodiodes, wavelengths 1.26 µm and 1.4 µm, bandwidth of 100 nm) coaxially to the laser beam of a LPBF machine. The surface temperature was monitored in a temperature range of 900–2600 °C. In this study, the diameter of the view field of the pyrometer is 560 µm while the laser spot diameter is 70 µm (Fig. 8a). With this setup, the authors studied three cases: (1) time variance of the pyrometer during multiple tracks scanning; (2) effect of the layer thickness on the pyrometer's signal; and (3) effect of hatch spacing. They found that the signal acquired by the pyrometer is sensitive to process parameters and could be used as an online quality control during manufacturing (Fig. 8b, c).

Furomoto et al. [126] studied the consolidation of metal during LPBF thanks to a two-wavelength pyrometer (InAs and InSb detectors) combined with a high-speed camera. The pyrometer was equipped with a germanium optical filter with a 1 mm thickness to cut wavelengths <1600 nm. The temperature range for this pyrometer was 400–2200 °C. The surface temperature during consolidation was measured and the detection was immediate when the laser beam reached the pyrometer's laser spot. The temperature measured by the pyrometer shows a tendency as a function of the energy density. This system could follow the surface temperature during consolidation but without the view of the melt pool behavior, real-time interpretation of the data was not possible. Bayle et Doubenskaia [119] combined their IR camera measurements with the measurements from a coaxial pyrometer (spectral range 1.001–1.573 µm) with a temperature range of 1100–3500 °K. The measurements from the pyrometer allowed to observe the influence of heat accumulation on temperature distribution and they can be used to ensure the process stability.

3.1.3 Thermocouples

Thermocouples measure locally the temperature of an object they are in contact to. When two materials of different thermoelectrical properties are in contact, there is a potential difference that appears at the junction, and it is proportional to the temperature. It is then possible to determine the junction's temperature. As said previously, thermocouples are easy to position and cost-efficient. They are often used to calibrate other thermal sensors such as pyrometers and IR cameras. In the work of Rodriguez et al. [120], thermocouples were used as validation tools to compare the IR camera's measures to the temperature measurement of the thermocouples. The EBM-ed parts were fabricated on the thermocouple while acquiring IR images which allowed to verify the solid emissivity of the material. Williams et al. [122] also used thermocouples to calibrate a thermal imaging device for the monitoring of LPBF. Shishkovsky et al. [127] inserted different types of thermocouples into the powder bed for the SLS process to measure the temperature distribution near the laser-sintering zone. The thermocouples located on the periphery of sintering did not show high absolute values. The thermocouples signal strongly depends on their localization in the powder bed. This method could help the authors to understand the behavior of specific materials during SLS and they wanted to use thermocouples as indicators of the process for the fabrication of Functionally Graded Materials (FGM).

3.1.4 Imaging with CCD Cameras

CCD (Charge-Coupled Device) sensors in high-speed cameras consist in a thin silicon layer divided into pixels (each pixel is a semi-conductor). When this layer is exposed to light, an electrical charge is converted into a numerical image. After exposure, each pixel cell is amplified one by one until the entire matrix is converted. The advantage of CCD sensor is its high sensitivity and the fact that it does not require a specific lighting source and does not respond to specific radiations. Thus, this type of sensor is largely used in processes involving a laser source such as LPBF. Yadroitsev et al. [128] processed the signal from a CCD sensor (resolution 782 $\times$ 582 pixels) positioned coaxially to the laser in LPBF to measure the temperature distribution in the melt pool. The software used was developed in DIPI laboratory (ENISE, France). The brightness temperatures were measured at the wavelength of 0.8 μm and for 1873 K, the maximum error was about $\pm$25 K. The brightness temperature could be obtained along the laser scanning direction and the true temperature of the melt poll was confronted to the irradiation time and laser power. This method enabled to correlate the maximum melt pool temperature to scanning parameters and the part's microstructure.

In this section, temperature measurement instrumentation for metal AM has been described. The focus was on LPBF and EBM processes, which are the common processes used in the biomedical field. There are several techniques and sensors for temperature measurement. They are broadly studied in laboratory scale to observe in real-time surface temperatures, melt pool temperature and can give access to other

information such as defect occurrence. However, thermography is still confronted to the emissivity issue, which prevent the results from being precise. Emissivity differs with several parameters and during the process, and most of the studies do not take that into account. In coaxial systems, spectral aberrations can hinder the results as well as dust and debris produced during AM. Another challenge is also the real time and fast data processing and image treatment.

3.2 Geometrical Measurements and Visual Inspection

Geometrical measurements during metal AM consist in determining geometrical features at different scales such as the geometry and dimensions of the melt pool, the layer, or the entire part. Other sensors based on imaging will be used as visual inspection tool to check on the process stability and detect defects or errors during manufacturing.

3.2.1 Imaging with CCD Cameras

Yadroitsev et al. [128] used the installed CCD sensor (resolution 782 × 582 pixels) to measure the width of the melt pool by capturing view of the tracks. These data were correlated to temperature changes versus parameters. Kleszczynski et al. [129] used a monochrome CCD camera (Kodak 29 megapixel, resolution 6576 × 4384 pixels) for visual detection and error analysis during LPBF process. The camera was positioned in front of the fabrication area window with an angle from the build plate. Perspective distortion was corrected by a tilt and shift lens. The CCD camera helped to detect process errors such as balling, insufficient powder supply, support connection, or support. With these errors, the process could be demolished and must be stopped. Besides, this visual inspection tool can help to detect errors affecting the part's quality like recoater damage, poor compound, dimensional inaccuracy. This system enables an observation of the powder bed while processing and could be used to better control the geometrical accuracy of the parts.

3.2.2 Imaging with CMOS Cameras

CMOS sensors (Complementary Metal Oxide Semiconductor) convert the charges of each pixel into a voltage which is transmitted as a numerical signal. On CMOS sensors, each pixel is an amplifier that makes them faster than CCD with better contrast. For a visual inspection of the powder deposition in the LPBF process, Craeghs et al. [130] installed a CMOS camera coupled with a photodiode. The radiation emitted by the melt pool is transmitted to a beam splitter through a F-θ field mirror and semi-mirror to the photodiode and CMOS sensor. The latter collects the melt pool characteristics such as its area, length, and width. The implemented system

was tested for the detection of wear and local damage of the coater blade, monitoring of defects such as balling and overheating and process errors. To obtain the images of the melt pool with this setup, Field Programmable Gate Array (FPGA) chips were used for very fast and real-time image processing. The gathered information about defects and melt pool characteristics during processing can be used to control the process quality.

To get spatial information of the melt pool, Mazzoleni et al. [131] chose a compact industrial CMOS camera (Ximea xiQ—USB3 Vision Camera, MQ013xG-ON model) that was placed coaxially to the laser in LPBF via a dichroic mirror (reflective between 400 and 1000 nm). It was equipped with a short-pass filter at 1000 nm, a bandpass filter in the visible range at 650 nm, and a long-pass filter in the NIR range between 850 and 1000 nm. This sensor had a sufficient temporal and spatial resolution to observe the melt pool dynamics and spatter ejections. The challenge encountered was the NIR band reaching the sensor. Craeghs et al. continued their research on that topic [132]. In addition, Abdelrahman et al. detected fusion defects of the powder bed with optical imaging thanks to a 36.3-megapixel CMOS camera (Nikon D800E, resolution 7360 $\times$ 4612 pixels) placed inside the LPBF machine. Six images are captured in five different locations after layer exposure and after powder recoating, one image is captured using flashes. The CMOS camera was used to detect post-powder-recoat and post-laser-scan anomalies. After post-processing of the images, the 3D indexing method was utilized and proved the efficiency of this visual system.

3.2.3 X-ray Imaging

Zhao et al. [133] used high-speed X-ray imaging and diffraction techniques during LPBF to have information on melt pool size and shape, powder ejection, solidification, and phase transformation. A short-period (1.8 cm) pseudo pink beam is generated by an undulator with a first harmonic energy of 24.4 keV. The X-rays penetrate the sample from the side and the detectors are placed about 300 mm downstream from the sample. This technique enables to follow the powder bed fusion processes by X-ray dynamic imaging. The spatial and temporal resolution of this method is unprecedented giving an observation of critical phenomena. This could help understanding defect formation and help the process optimization. Leung et al. [134] also used in-situ X-ray imaging of LPBF to capture thermophysical phenomena. They obtained radiographs during the process, and they could observe the melt pool morphology and defect occurrence such as spattering, formation of denuded zones. Similar study has been realized by Calta et al. and Uhlman et al. [135, 136].

3.3 Other Quantities

Aside from the temperature, geometrical features, and visual aspects, other quantities can be measured and observed during LPBF and EBM. The following studies are specific cases either focusing on an original quantity or involving techniques that are still sparse in literature.

3.3.1 Acoustic Signatures

Acoustic emission sensors have been utilized recently in AM because they show similar trend than with conventional metal components. The frequency response has been proven to be a strong indicator of the weld quality being correlated to defect formation [137] or crack propagation [138]. This method is increasingly becoming important for non-destructive in-situ observation of metal AM since it is worth of investigation regarding the geometrical complexity of LPBF-ed parts [139, 140].

3.3.2 Residual Stresses

As developed in the first part of this chapter, residual stresses are common defects favorizing failures and hindering mechanical properties of AM parts. Investigations on the detection of residual stresses in process have been done in literature and gave consistent results. Van Belle et al. [141] mounted a strain gauge rosette under the build plate and monitored the variation of the gauge during processing. The residual stress corresponding to elastic bending was extracted from these measurements. This method enabled to estimate the maximum residual stress on the last molten layer and still needs to be compared to numerical simulation. Furthermore, Shiomi et al. [142] used the same technique in SLS to observe strain changes in the build plate. They could analyze the residual stresses evolution during fabrication.

3.3.3 Defects' Detection

To detect defects such as pores during fabrication, radiography has already been tested in metal AM. The radiation energy passing through the material allows to form an image where the areas where the defects are located are missing [143]. Moreover, eddy current testing can detect surface and subsurface defects thanks to a local change of the electrical conductivity [139]. Schwerz et al. [72] used a CMOS sensor during LPBF to study spattering and its relationship with internal defects. In this part, needs for instrumentation and monitoring in metal AM processes have been exposed. A literature review of existing techniques for physical quantity observation via process instrumentation has been done. Temperature measurements and visual inspection studies are prominent for the LPBF and EBM processing since there is a

significant constraint of the sensor positioning in/near the fabrication area. Moreover, the instrumentation explored in the previous section generally focuses on one physical quantity to be correlated to part's quality and/or process parameters. The complexity of metal AM comes from the numerous and interrelated parameters, which are all related to process signatures and induced part's properties. Thus, monitoring of a single quantity leads to important limitations to understand and further control the process. A novel field of interest has been the multi-physics or multi-scale, multi-sensor approaches for the instrumentation and monitoring of metal AM. This new method is sparse in literature but allows a deeper understanding of the processes.

4 Multi-sensor Approach for AM Process Monitoring

Chivel [144] combined a CCD camera with a pyrometer in LPBF to observe the sintering/melting behavior of the layers and the melting of a 3D object. The temperature of the irradiation zone was measured with the high-speed CCD sensor and the maximal color temperature with the pyrometer. This two-sensor system allowed the author to correlate the overheating phenomenon with the loss of stability of the molten layer. Additionally, the melt pool penetration into loose powder mechanisms has been identified. Islam et al. [145] have also used a combined system in LPBF consisting of a pyrometer (TCS Laser-Technik) with a CMOS camera with a diode laser illumination. The pyrometer laser spot was larger than the process laser spot. To protect the sensors, a shielding glass was utilized and led to errors in the measurements that had to be considered. With this method, the authors could obtain temperature profiles and image analyses with different parameters. The combination of the two sensors enabled the detection of balling effect for specific temperatures and process inputs. Hirvimäki et al. [146] combined a CCD spectrometer (Ocean Optics HR2000+) with a pyrometer (TCS Thyssen Laser-Technik, spectral ranges 1200–1400 nm and 1400–1700 nm) and an active illumination system (Cavilux HF with Baumer camera and dichroic window) in LPBF. The spectrometer was used to study the effect of process parameters on the radiation. The pyrometer was used to measure the temperature distribution with changing parameters. The active illumination system gave visual information according to the process parameters. Each of these three methods presented advantages and drawbacks given in Table 2.

For laser cladding, Liu et al. [147] implemented a multi-sensor instrumentation composed of a high-speed CCD camera, a pyrometer, and an IR camera (FLIR Thermovision A40). The pyrometer was used to measure the brightness temperature of the melt pool and the IR camera measured the melt pool size, temperature distribution, and the cooling rate with different process parameters. This system enabled the study of mass and heat transfers during processing. Lane et al. [148] chose to combine a thermal camera with a high-speed visible camera and a photodiode for the LPBF process. Images from the photodetector and the camera were simultaneously merged to better understand the melt pool behavior. The authors noted a strong relationship between the photodetector signal and the location and motion of the melt

Table 2 Advantages and drawbacks of the tested sensors [146]

Sensor	Advantages	Drawbacks
CCD spectrometer	• Spectral range from 200 to 600 nm • Emission intensity for the whole range at the same time • Good resolution (about 0.035 nm) • Can be used to find single emissivity peaks	• Sensitivity to disturbance • Fairly slow integration time • Lots of data
Pyrometer	• Short integration time (about 2.5 ms) • High temperature (about 1500 °C) • Not significantly affected by lighting conditions	• Generally, too large equipment • Only measures the temperature
Active illumination system	• Can detect defects such as cracks, shrinkage, bending… • Can obtain more information about the melt pool	• Lots of data • Expensive • Difficult to place

pool according to the scan strategy. Nevertheless, they concluded that a filtering or processing of the signal spot detector's signal would need the spatial coordinates of the laser spot to differentiate the periodic behavior of the scan strategy from the occurrence of a defect.

In addition to the several instrumentation and monitoring methods tested for LPBF and EBM processes, it is necessary to mention methods implemented for other metal AM processes, even if they are rarely or not used in the biomedical field. Direct Energy Deposition divided into Wire-Arc Additive Manufacturing (WAAM) and Laser Metal Deposition (LMD) are often instrumented for the same reasons as LPBF and EBM, but the placement of sensors in the fabrication area in DED is usually easier. Indeed, for WAAM and LMD, building chambers are bigger and since they are not powder-bed processes, characteristics of the built part can be observed directly during fabrication. Like LPBF and EBM, thermal and geometrical quantities are the most observed. Thermal quantities in DED can be measured by pyrometry [149–152]; by thermocouples [153, 154]; with photodiodes [155]; by thermal imaging [156–161]. For the observation of geometrical quantities in the DED process, high-speed cameras have been used [159, 162–171] as well as profilometers [172–175]; displacement sensors [176] but also thermal sensors [155]. A particularity of DED processes is the ability to follow some of the built part's properties in-process and during manufacturing. Distortions [153, 177, 178], surface characteristics [155], defects occurrence [179–181] can also be measured. Furthermore, multi-sensing systems are consequently more easily installed in DED machines. Xu et al. [182] created a multi-sensor instrumentation for the WAAM process. They combined an IR sensor, oxygen content sensor, an arc current and arc voltage sensor, a gas flow sensor, a feed speed sensor, and a laser profilometer. This system enables the heat

monitoring, the bead geometry control, and the environmental monitoring. Chabot [172] implemented a multi-sensor instrumentation for the WAAM process for a global multi-physics monitoring.

5 Conclusions and Perspectives

This chapter introduced the instrumentation and monitoring for additive manufacturing processes in the biomedical applications. In the recent years, the demand for patient-specific implants and surgical tools has increased and novel more efficient manufacturing is emerging. AM is a suitable and interesting manufacturing technique in biomedicine for its rapidity and its freedom of design. Depending on the application, several materials are additively manufactured such as polymers, ceramics, or metals. The focus of this study has been made on metal AM and especially LPBF and EBM, which are the most used processes in biomedical applications. The metal implants fabricated by AM must meet with specific and demanding criteria concerning their structural and mechanical properties. Nonetheless, the complexity of metal AM, involving numerous interrelated parameters all related to process physics and part's properties, prevents this method from being used intensively at an industrial scale. Common defects such as pores, cracks, distortions, and surface roughness are detrimental for the fabricated implants. To better understand the process characteristics and physics, instrumentation and monitoring have been studied. Instrumentation consists in installing sensors in the building area to observe and/or measure during the process the inputs (process parameters), physical quantities or outputs (part's characteristics). There are several sensors to be used to study a specific quantity during a metal AM process. The measure can be done at different scales from the scale of the melt pool to the scale of the powder bed. Efficient and relevant instrumentation has been developed to follow thermal quantities or for visual inspection of LPBF and EBM. Other promising new methods are emerging such as acoustic emission sensing or in-situ X-ray imaging. The positioning of a sensor involves its placement in the fabrication environment, its calibration, the signal acquisition, and post-processing. Limitations at each step of this installation have been highlighted in literature. Since the elements are correlated to each other in metal AM processes, a single sensor instrumentation rapidly appears to be limited for a good and consistent exploitation of the monitoring. Thus, multi-sensor instrumentations are recently experimented to have a deeper understanding of the processes. Instrumentation and monitoring have the perspective of implementing a closed-loop control system into the AM machine making it possible to control and adjust the process parameters to control the deposition in real time. In addition, data from monitoring can be used to feed process simulation models. Simulation and experimental results can be compared to further investigate the process variables and predict the defect occurrence and instabilities. This field of research aims to correct in real time the eventual failures to save time, expense, and material by avoiding intensive part machining, post-treatment or avoiding the fabrication of a new component.

References

1. Liu Y, Wang W, Zhang L-C (2017) Additive manufacturing techniques and their biomedical applications. Family Med Commun Hlth 5:286–98
2. Rehman M, Yanen W, Mushtaq RT, Ishfaq K, Zahoor S, Ahmed A, et al (2023) Additive manufacturing for biomedical applications: a review on classification, energy consumption, and its appreciable role since COVID-19 pandemic. Prog Addit Manuf [Internet]. 2022 [cited 2023 May 17]; Available from: https://doi.org/10.1007/s40964-022-00373-9
3. Bozkurt Y, Karayel E (2021) 3D printing technology; methods, biomedical applications, future opportunities and trends. J Market Res 14:1430–1450
4. Du C, Zhao Y, Jiang J, Wang Q, Wang H, Li N et al (2023) Pore defects in laser powder bed fusion: formation mechanism, control method, and perspectives. J Alloy Compd 944:169215
5. Moridi A (2020) Biomedical applications of metal additive manufacturing: current state-of-the-art and future perspective. AJBSR 7:6–10
6. Tom T, Sreenilayam SP, Brabazon D, Jose JP, Joseph B, Madanan K et al (2022) Additive manufacturing in the biomedical field-recent research developments. Results Eng 16:100661
7. Culmone C, Smit G, Breedveld P (2019) Additive manufacturing of medical instruments: a state-of-the-art review. Addit Manuf 27:461–473
8. Velásquez-García LF, Kornbluth Y (2021) Biomedical applications of metal 3D printing. Annu Rev Biomed Eng 23:307–338
9. Dawood A, Marti BM, Sauret-Jackson V, Darwood A (2015) 3D printing in dentistry. Br Dent J 219:521–529
10. Chua K, Khan I, Malhotra R, Zhu D (2021) Additive manufacturing and 3D printing of metallic biomaterials. Eng Regeneration 2:288–299
11. Prasad K, Bazaka O, Chua M, Rochford M, Fedrick L, Spoor J et al (2017) Metallic biomaterials: current challenges and opportunities. Materials 10:884
12. Aranda JL, Jiménez MF, Rodríguez M, Varela G (2015) Tridimensional titanium-printed custom-made prosthesis for sternocostal reconstruction. Eur J Cardiothorac Surg 48:e92–e94
13. Harrysson OLA, Cansizoglu O, Marcellin-Little DJ, Cormier DR, West HA (2008) Direct metal fabrication of titanium implants with tailored materials and mechanical properties using electron beam melting technology. Mater Sci Eng C 28:366–373
14. Heinl P, Müller L, Körner C, Singer RF, Müller FA (2008) Cellular Ti–6Al–4V structures with interconnected macro porosity for bone implants fabricated by selective electron beam melting. Acta Biomater 4:1536–1544
15. Kamel MK, Cheng A, Vaughan B, Stiles B, Altorki N, Spector JA et al (2020) Sternal reconstruction using customized 3D-printed titanium implants. Ann Thorac Surg 109:e411–e414
16. Kittichokechai P, Sirichatchai K, Puncreobutr C, Lohwongwatana B, Saonanon P (2022) A novel patient-specific titanium mesh implant design for reconstruction of complex orbital fracture. Plast Reconstr Surg Glob Open 10:e4081
17. Ponader S, Vairaktaris E, Heinl P, Wilmowsky C v., Rottmair A, Körner C, et al (2008) Effects of topographical surface modifications of electron beam melted Ti-6Al-4V titanium on human fetal osteoblasts. J Biomed Mater Res Part A 84A:1111–9
18. Rotaru H, Schumacher R, Kim S-G, Dinu C (2015) Selective laser melted titanium implants: a new technique for the reconstruction of extensive zygomatic complex defects. Maxillofacial Plastic Reconstructive Surgery 37:1
19. Van der Stok J, Van der Jagt OP, Amin Yavari S, De Haas MFP, Waarsing JH, Jahr H et al (2013) Selective laser melting-produced porous titanium scaffolds regenerate bone in critical size cortical bone defects. J Orthop Res 31:792–799
20. Zhang LC, Klemm D, Eckert J, Hao YL, Sercombe TB (2011) Manufacture by selective laser melting and mechanical behavior of a biomedical Ti–24Nb–4Zr–8Sn alloy. Scripta Mater 65:21–24
21. Li X-K, Yuan C-F, Wang J-L, Zhang Y-Q, Zhang Z-Y, Guo Z (2013) The treatment effect of porous titanium alloy rod on the early stage Talar osteonecrosis of sheep. PLoS ONE 8:e58459

22. Wu S-H, Li Y, Zhang Y-Q, Li X-K, Yuan C-F, Hao Y-L et al (2013) Porous titanium-6 aluminum-4 vanadium cage has better Osseointegration and less Micromotion than a polyether-ether-ketone cage in sheep vertebral fusion. Artif Organs 37:E191-201
23. Jakubowicz J (2020) Special issue: Ti-based biomaterials: synthesis, properties and applications. Materials 13:1696
24. Arjunan A, Robinson J, Baroutaji A, Tuñón-Molina A, Martí M, Serrano-Aroca Á (2021) 3D printed cobalt-chromium-molybdenum porous Superalloy with superior antiviral activity. Int J Mol Sci 22:12721
25. Barazanchi A, Li KC, Al-Amleh B, Lyons K, Waddell JN (2020) Mechanical properties of laser-sintered 3D-printed cobalt chromium and soft-milled cobalt chromium. Prosthesis 2:313–320
26. Finazzi V, Demir AG, Biffi CA, Migliavacca F, Petrini L, Previtali B (2020) Design and functional testing of a novel balloon-expandable cardiovascular stent in CoCr alloy produced by selective laser melting. J Manuf Process 55:161–173
27. Ganbold B, Heo S-J, Koak J-Y, Kim S-K, Cho J (2019) Human stem cell responses and surface characteristics of 3D printing Co–Cr dental material. Materials 12:3419
28. Kazantseva NV, Ezhov IV, Davydov DI, Merkushev AG (2019) Analysis of structure and mechanical properties of Co–Cr–Mo alloy obtained by 3D printing. Phys Metals Metallogr. 120:1172–1179
29. Limmahakhun S, Oloyede A, Sitthiseripratip K, Xiao Y, Yan C (2017) Stiffness and strength tailoring of cobalt chromium graded cellular structures for stress-shielding reduction. Mater Des 114:633–641
30. Shah FA, Omar O, Suska F, Snis A, Matic A, Emanuelsson L et al (2016) Long-term osseointegration of 3D printed CoCr constructs with an interconnected open-pore architecture prepared by electron beam melting. Acta Biomater 36:296–309
31. Karamian E, Kalantar Motamedi MR, Khandan A, Soltani P, Maghsoudi S (2014) An in vitro evaluation of novel NHA/zircon plasma coating on 316L stainless steel dental implant. Progress Nat Sci Mater Int 24:150–156
32. Kong D, Ni X, Dong C, Lei X, Zhang L, Man C et al (2018) Bio-functional and anti-corrosive 3D printing 316L stainless steel fabricated by selective laser melting. Mater Des 152:88–101
33. Yang K, Ren Y (2010) Nickel-free austenitic stainless steels for medical applications. Sci Technol Adv Mater 11:014105
34. Hort N, Huang Y, Fechner D, Störmer M, Blawert C, Witte F et al (2010) Magnesium alloys as implant materials—principles of property design for Mg–RE alloys. Acta Biomater 6:1714–1725
35. Kamrani S, Fleck C (2019) Biodegradable magnesium alloys as temporary orthopaedic implants: a review. Biometals 32:185–193
36. Murr LE, Amato KN, Li SJ, Tian YX, Cheng XY, Gaytan SM et al (2011) Microstructure and mechanical properties of open-cellular biomaterials prototypes for total knee replacement implants fabricated by electron beam melting. J Mech Behav Biomed Mater 4:1396–1411
37. Mobbs RJ, Coughlan M, Thompson R, Sutterlin CE, Phan K (2017) The utility of 3D printing for surgical planning and patient-specific implant design for complex spinal pathologies: case report. J Neurosurg Spine 26:513–518
38. Merkt S, Kleyer A, Hueber AJ (2014) The additive manufacture of patient-tailored finger implants. Laser Tech J 11:54–56
39. Sakes A, Hovland K, Smit G, Geraedts J, Breedveld P (2018) Design of a novel three-dimensional-printed two degrees-of-freedom steerable electrosurgical grasper for minimally invasive surgery. J Med Dev [Internet]. 2018 [cited 2023 May 24];12. Available from.https://doi.org/10.1115/1.4038561
40. Sun Z, Vladimirov G, Nikolaev E, Velásquez-García LF (2018) Exploration of metal 3-D printing technologies for the microfabrication of freeform, finely featured, Mesoscaled structures. J Microelectromech Syst 27:1171–1185
41. Nahata S, Ozdoganlar OB (2019) Feasibility of metal additive manufacturing for fabricating custom surgical instrumentation for hip and knee implants. Procedia Manufacturing 34:772–779

42. Williams DF (2008) On the mechanisms of biocompatibility. Biomaterials 29:2941–2953
43. Geetha M, Singh AK, Asokamani R, Gogia AK (2009) Ti based biomaterials, the ultimate choice for orthopaedic implants—a review. Prog Mater Sci 54:397–425
44. Katz JL (1980) Anisotropy of Young's modulus of bone. Nature 283:106–107
45. Martin RB (1991) Determinants of the mechanical properties of bones. J Biomech 24:79–88
46. Gibson LJ (1985) The mechanical behaviour of cancellous bone. J Biomech 18:317–328
47. Saini M (2015) Implant biomaterials: a comprehensive review. WJCC. 3:52
48. Ryan G, Pandit A, Apatsidis DP (2006) Fabrication methods of porous metals for use in orthopaedic applications. Biomaterials 27:2651–2670
49. Sumner DR, Turner TM, Igloria R, Urban RM, Galante JO (1998) Functional adaptation and ingrowth of bone vary as a function of hip implant stiffness. J Biomech 31:909–917
50. Kohn DH, Ducheyne P (1990) A parametric study of the factors affecting the fatigue strength of porous coated Ti-6A1-4V implant alloy. J Biomed Mater Res 24:1483–1501
51. Yue S, Pilliar RM, Weatherly GC (1984) The fatigue strength of porous-coated Ti–6% Al–4% V implant alloy. J Biomed Mater Res 18:1043–1058
52. Arabnejad S, Johnston B, Tanzer M, Pasini D (2017) Fully porous 3D printed titanium femoral stem to reduce stress-shielding following total hip arthroplasty. J Orthop Res 35:1774–1783
53. Liu Y, Li S, Hou W, Wang S, Hao Y, Yang R et al (2016) Electron beam melted beta-type Ti–24Nb–4Zr–8Sn porous structures with high strength-to-modulus ratio. J Mater Sci Technol 32:505–508
54. Li Y, Zhou J, Pavanram P, Leeflang MA, Fockaert LI, Pouran B et al (2018) Additively manufactured biodegradable porous magnesium. Acta Biomater 67:378–392
55. Xiao X, Wang W, Liu D, Zhang H, Gao P, Geng L et al (2015) The promotion of angiogenesis induced by three-dimensional porous beta-tricalcium phosphate scaffold with different interconnection sizes via activation of PI3K/Akt pathways. Sci Rep 5:9409
56. Bružauskaitė I, Bironaitė D, Bagdonas E, Bernotienė E (2016) Scaffolds and cells for tissue regeneration: different scaffold pore sizes—different cell effects. Cytotechnology 68:355–369
57. Parthasarathy J, Starly B, Raman S (2011) A design for the additive manufacture of functionally graded porous structures with tailored mechanical properties for biomedical applications. J Manuf Process 13:160–170
58. Amarnath G, Muddugangadhar B, Tripathi S, Dikshit S, Ms D (2011) Biomaterials for dental implants: an overview. Int J Oral Implantology Clin Res 2:13–24
59. Putra NE, Leeflang MA, Minneboo M, Taheri P, Fratila-Apachitei LE, Mol JMC et al (2021) Extrusion-based 3D printed biodegradable porous iron. Acta Biomater 121:741–756
60. Hojjatzadeh SMH, Parab ND, Guo Q, Qu M, Xiong L, Zhao C et al (2020) Direct observation of pore formation mechanisms during LPBF additive manufacturing process and high energy density laser welding. Int J Mach Tools Manuf 153:103555
61. Fu J, Li H, Song X, Fu MW (2022) Multi-scale defects in powder-based additively manufactured metals and alloys. J Mater Sci Technol 122:165–199
62. Galy C, Le Guen E, Lacoste E, Arvieu C (2018) Main defects observed in aluminum alloy parts produced by SLM: from causes to consequences. Addit Manuf 22:165–175
63. Kasperovich G, Haubrich J, Gussone J, Requena G (2016) Correlation between porosity and processing parameters in TiAl6V4 produced by selective laser melting. Mater Des 105:160–170
64. Cunningham R, Zhao C, Parab N, Kantzos C, Pauza J, Fezzaa K et al (2019) Keyhole threshold and morphology in laser melting revealed by ultrahigh-speed x-ray imaging. Science 363:849–852
65. McCann R, Obeidi MA, Hughes C, McCarthy É, Egan DS, Vijayaraghavan RK et al (2021) In-situ sensing, process monitoring and machine control in laser powder bed fusion: a review. Addit Manuf 45:102058
66. Weingarten C, Buchbinder D, Pirch N, Meiners W, Wissenbach K, Poprawe R (2015) Formation and reduction of hydrogen porosity during selective laser melting of AlSi10Mg. J Mater Process Technol 221:112–120

67. Cunningham R, Nicolas A, Madsen J, Fodran E, Anagnostou E, Sangid MD et al (2017) Analyzing the effects of powder and post-processing on porosity and properties of electron beam melted Ti-6Al-4V. Mater Res Lett 5:516–525
68. Laleh M, Hughes AE, Yang S, Wang J, Li J, Glenn AM et al (2021) A critical insight into lack-of-fusion pore structures in additively manufactured stainless steel. Addit Manuf 38:101762
69. Gu D, Hagedorn Y-C, Meiners W, Meng G, Batista RJS, Wissenbach K et al (2012) Densification behavior, microstructure evolution, and wear performance of selective laser melting processed commercially pure titanium. Acta Mater 60:3849–3860
70. Louvis E, Fox P, Sutcliffe CJ (2011) Selective laser melting of aluminium components. J Mater Process Technol 211:275–284
71. Qu M, Guo Q, Escano LI, Nabaa A, Hojjatzadeh SMH, Young ZA et al (2022) Controlling process instability for defect lean metal additive manufacturing. Nat Commun 13:1079
72. Schwerz C, Raza A, Lei X, Nyborg L, Hryha E, Wirdelius H (2021) In-situ detection of redeposited spatter and its influence on the formation of internal flaws in laser powder bed fusion. Addit Manuf 47:102370
73. Cao L (2020) Mesoscopic-scale simulation of pore evolution during laser powder bed fusion process. Comput Mater Sci 179:109686
74. Tumkur TU, Voisin T, Shi R, Depond PJ, Roehling TT, Wu S, et al (2021) Nondiffractive beam shaping for enhanced optothermal control in metal additive manufacturing. Sci Adv 7:eabg9358
75. King WE, Barth HD, Castillo VM, Gallegos GF, Gibbs JW, Hahn DE et al (2014) Observation of keyhole-mode laser melting in laser powder-bed fusion additive manufacturing. J Mater Process Technol 214:2915–2925
76. Günther J, Krewerth D, Lippmann T, Leuders S, Tröster T, Weidner A et al (2017) Fatigue life of additively manufactured Ti–6Al–4V in the very high cycle fatigue regime. Int J Fatigue 94:236–245
77. Chauvet E, Kontis P, Jägle EA, Gault B, Raabe D, Tassin C et al (2018) Hot cracking mechanism affecting a non-weldable Ni-based superalloy produced by selective electron Beam Melting. Acta Mater 142:82–94
78. Gong H, Rafi K, Gu H, Janaki Ram GD, Starr T, Stucker B (2015) Influence of defects on mechanical properties of Ti–6Al–4V components produced by selective laser melting and electron beam melting. Mater Des 86:545–554
79. Leuders S, Thöne M, Riemer A, Niendorf T, Tröster T, Richard HA et al (2013) On the mechanical behaviour of titanium alloy TiAl6V4 manufactured by selective laser melting: Fatigue resistance and crack growth performance. Int J Fatigue 48:300–307
80. Min D, Shen J, Lai S, Chen J, Xu N, Liu H (2011) Effects of heat input on the low power Nd:YAG pulse laser conduction weldability of magnesium alloy AZ61. Opt Lasers Eng 49:89–96
81. Kou S (2003) Solidification and liquation cracking issues in welding
82. Oliveira JP, Santos TG, Miranda RM (2020) Revisiting fundamental welding concepts to improve additive manufacturing: from theory to practice. Prog Mater Sci 107:100590
83. Robinson JL, Scott MH (1997) Liquation cracking during the welding of austenitic stainless steels and nickel alloys. Philos Trans Royal Soc London Ser A Math Phys Sci 295:105–117
84. Song B, Dong S, Zhang B, Liao H, Coddet C (2012) Effects of processing parameters on microstructure and mechanical property of selective laser melted Ti6Al4V. Mater Des 35:120–125
85. Stopyra W, Gruber K, Smolina I, Kurzynowski T, Kuźnicka B (2020) Laser powder bed fusion of AA7075 alloy: Influence of process parameters on porosity and hot cracking. Addit Manuf 35:101270
86. Xiao H, Li S, Han X, Mazumder J, Song L (2017) Laves phase control of Inconel 718 alloy using quasi-continuous-wave laser additive manufacturing. Mater Des 122:330–339
87. Tang HP, Yang GY, Jia WP, He WW, Lu SL, Qian M (2015) Additive manufacturing of a high niobium-containing titanium aluminide alloy by selective electron beam melting. Mater Sci Eng A 636:103–107

88. Hu Z, Nie X, Qi Y, Zhang H, Zhu H (2021) Cracking criterion for high strength Al–Cu alloys fabricated by selective laser melting. Addit Manuf 37:101709
89. Nie X, Zhang H, Zhu H, Hu Z, Ke L, Zeng X (2018) Effect of Zr content on formability, microstructure and mechanical properties of selective laser melted Zr modified Al-4.24Cu-1.97Mg-0.56Mn alloys. J Alloys Compounds 764:977–86
90. Yu M, Wan Y, Ren B, Wang H, Zhang X, Qiu C et al (2020) 3D printed Ti–6Al–4V implant with a micro/nanostructured surface and its cellular responses. ACS Omega 5:31738–31743
91. Mumtaz K, Hopkinson N (2009) Top surface and side roughness of Inconel 625 parts processed using selective laser melting. Rapid Prototyping J 15:96–103
92. Kiani P, Scipioni Bertoli U, Dupuy AD, Ma K, Schoenung JM (2020) A statistical analysis of powder Flowability in metal additive manufacturing. Adv Eng Mater 22:2000022
93. Spierings AB, Voegtlin M, Bauer T, Wegener K (2016) Powder flowability characterisation methodology for powder-bed-based metal additive manufacturing. Prog Addit Manuf 1:9–20
94. DebRoy T, Wei HL, Zuback JS, Mukherjee T, Elmer JW, Milewski JO et al (2018) Additive manufacturing of metallic components—process, structure and properties. Prog Mater Sci 92:112–224
95. Moussaoui K, Rubio W, Mousseigne M, Sultan T, Rezai F (2018) Effects of Selective Laser Melting additive manufacturing parameters of Inconel 718 on porosity, microstructure and mechanical properties. Mater Sci Eng A 735:182–190
96. Qiu C, Panwisawas C, Ward M, Basoalto HC, Brooks JW, Attallah MM (2015) On the role of melt flow into the surface structure and porosity development during selective laser melting. Acta Mater 96:72–79
97. Gu D, Shen Y (2009) Balling phenomena in direct laser sintering of stainless steel powder: Metallurgical mechanisms and control methods. Mater Des 30:2903–2910
98. Moon S, Ma R, Attardo R, Tomonto C, Nordin M, Wheelock P et al (2021) Impact of surface and pore characteristics on fatigue life of laser powder bed fusion Ti–6Al–4V alloy described by neural network models. Sci Rep 11:20424
99. Greitemeier D, Palm F, Syassen F, Melz T (2017) Fatigue performance of additive manufactured TiAl6V4 using electron and laser beam melting. Int J Fatigue 94:211–217
100. Shipley H, McDonnell D, Culleton M, Coull R, Lupoi R, O'Donnell G et al (2018) Optimisation of process parameters to address fundamental challenges during selective laser melting of Ti-6Al-4V: a review. Int J Mach Tools Manuf 128:1–20
101. Mercelis P, Kruth J (2006) Residual stresses in selective laser sintering and selective laser melting. Rapid Prototyping J 12:254–265
102. Mugwagwa L, Yadroitsev I, Matope S (2019) Effect of process parameters on residual stresses, distortions, and porosity in selective laser melting of maraging steel 300. Metals 9:1042
103. Fu J, Hu Z, Song X, Zhai W, Long Y, Li H et al (2020) Micro selective laser melting of NiTi shape memory alloy: defects, microstructures and thermal/mechanical properties. Opt Laser Technol 131:106374
104. Fu J, Qu S, Ding J, Song X, Fu MW (2021) Comparison of the microstructure, mechanical properties and distortion of stainless steel 316 L fabricated by micro and conventional laser powder bed fusion. Addit Manuf 44:102067
105. Corbin DJ, Nassar AR, Reutzel EW, Beese AM, Michaleris P (2018) Effect of substrate thickness and preheating on the distortion of laser deposited Ti–6Al–4V. J Manuf Sci Eng [Internet]. 2018 [cited 2023 Jun 9];140. Available from: https://doi.org/10.1115/1.4038890
106. Mugwagwa L, Dimitrov D, Matope S, Yadroitsev I (2018) Influence of process parameters on residual stress related distortions in selective laser melting. Procedia Manuf 21:92–99
107. Salem M, Le Roux S, Hor A, Dour G (2020) A new insight on the analysis of residual stresses related distortions in selective laser melting of Ti-6Al-4V using the improved bridge curvature method. Addit Manuf 36:101586
108. Montero-Sistiaga ML, Godino-Martinez M, Boschmans K, Kruth J-P, Van Humbeeck J, Vanmeensel K (2018) Microstructure evolution of 316L produced by HP-SLM (high power selective laser melting). Addit Manuf 23:402–410

109. Helmer H, Bauereiß A, Singer RF, Körner C (2016) Grain structure evolution in Inconel 718 during selective electron beam melting. Mater Sci Eng A 668:180–187
110. Thijs L, Kempen K, Kruth J-P, Van Humbeeck J (2013) Fine-structured aluminium products with controllable texture by selective laser melting of pre-alloyed AlSi10Mg powder. Acta Mater 61:1809–1819
111. Amato KN, Gaytan SM, Murr LE, Martinez E, Shindo PW, Hernandez J et al (2012) Microstructures and mechanical behavior of Inconel 718 fabricated by selective laser melting. Acta Mater 60:2229–2239
112. Vilaro T, Colin C, Bartout JD (2011) As-fabricated and heat-treated microstructures of the Ti-6Al-4V alloy processed by selective laser melting. Metall Mater Trans A 42:3190–3199
113. Nicoletto G (2017) Anisotropic high cycle fatigue behavior of Ti–6Al–4V obtained by powder bed laser fusion. Int J Fatigue 94:255–262
114. Qin Z, Kang N, El Mansori M, Wang Z, Wang H, Lin X et al (2022) Anisotropic high cycle fatigue property of Sc and Zr-modified Al–Mg alloy fabricated by laser powder bed fusion. Addit Manuf 49:102514
115. Mani M, Lane B, Donmez A, Feng S, Moylan S, Fesperman R (2015). Measurement science needs for real-time control of additive manufacturing powder bed fusion processes [Internet]. National Institute of Standards and Technology; 2015 Feb p. NIST IR 8036. Report No.: NIST IR 8036. Available from: https://nvlpubs.nist.gov/nistpubs/ir/2015/NIST.IR.8036.pdf
116. Valiorgue F, Brosse A, Naisson P, Rech J, Hamdi H, Bergheau JM (2013) Emissivity calibration for temperatures measurement using thermography in the context of machining. Appl Therm Eng 58:321–326
117. Price S, Cooper K, Chou K (2023) Evaluations of temperature measurements by near-infrared thermography in powder-based electron-beam additive manufacturing. University of Texas at Austin; 2012 [cited 2023 Jun 12]. Available from: https://repositories.lib.utexas.edu/handle/2152/88450
118. Krauss H, Eschey C, Zaeh MF (2012) Thermography for monitoring the selective laser melting process. University of Texas at Austin; 2012 [cited 2023 Jun 9]. Available from: https://repositories.lib.utexas.edu/handle/2152/88469
119. Bayle F, Doubenskaia M (2008) Selective laser melting process monitoring with high speed infra-red camera and pyrometer. Fundamentals of Laser Assisted Micro- and Nanotechnologies [Internet]. SPIE; 2008 [cited 2023 Jun 12]. p. 39–46. Available from: https://doi.org/10.1117/12.786940.full
120. Rodriguez E, Mireles J, Terrazas CA, Espalin D, Perez MA, Wicker RB (2015) Approximation of absolute surface temperature measurements of powder bed fusion additive manufacturing technology using in situ infrared thermography. Addit Manuf 5:31–39
121. Wegner A, Witt G (2011) Process monitoring in laser sintering using thermal imaging. University of Texas at Austin; 2011 [cited 2023 Jun 12]. Available from: https://repositories.lib.utexas.edu/handle/2152/88364
122. Williams RJ, Piglione A, Rønneberg T, Jones C, Pham M-S, Davies CM et al (2019) In situ thermography for laser powder bed fusion: Effects of layer temperature on porosity, microstructure and mechanical properties. Addit Manuf 30:100880
123. Dinwiddie RB, Dehoff RR, Lloyd PD, Lowe LE, Ulrich JB (2023) Thermographic in-situ process monitoring of the electron-beam melting technology used in additive manufacturing. Thermosense: Thermal Infrared Applications XXXV [Internet]. SPIE; 2013 [cited 2023 Jun 12]. p. 156–64. Available from: https://doi.org/10.1117/12.2018412.full
124. Schwerdtfeger J, Singer RF, Körner C (2012) In situ flaw detection by IR-imaging during electron beam melting. Rapid Prototyping J 18:259–263
125. Pavlov M, Doubenskaia M, Smurov I (2010) Pyrometric analysis of thermal processes in SLM technology. Phys Procedia 5:523–531
126. Furumoto T, Ueda T, Alkahari MR, Hosokawa A (2013) Investigation of laser consolidation process for metal powder by two-color pyrometer and high-speed video camera. CIRP Ann 62:223–226

127. Shishkovsky IV, Scherbakov VI, Morozov YG, Kuznetsov MV, Parkin IP (2008) Surface Laser Sintering of exothermic powder compositions. J Therm Anal Calorim 91:427–436
128. Yadroitsev I, Krakhmalev P, Yadroitsava I (2014) Selective laser melting of Ti6Al4V alloy for biomedical applications: temperature monitoring and microstructural evolution. J Alloy Compd 583:404–409
129. Kleszczynski S, zur Jacobsmühlen J, Sehrt JT, Witt G (2012) Error detection in laser beam melting systems by high resolution imaging. University of Texas at Austin; 2012 [cited 2023 Jun 12]. Available from: https://repositories.lib.utexas.edu/handle/2152/88467
130. Craeghs T, Clijsters S, Yasa E, Kruth J-P (2011) Online quality control of selective laser melting. University of Texas at Austin; 2011 [cited 2023 Jun 9]. Available from: https://repositories.lib.utexas.edu/handle/2152/88350
131. Mazzoleni L, Demir AG, Caprio L, Pacher M, Previtali B (2020) Real-time observation of melt pool in selective laser melting: spatial, temporal, and wavelength resolution criteria. IEEE Trans Instrum Meas 69:1179–1190
132. Craeghs T, Clijsters S, Kruth Jean-P, Bechmann F, Ebert Marie-C (2012) Detection of process failures in Layerwise laser melting with optical process monitoring. Physics Procedia 39:753–9
133. Zhao C, Fezzaa K, Cunningham RW, Wen H, De Carlo F, Chen L et al (2017) Real-time monitoring of laser powder bed fusion process using high-speed X-ray imaging and diffraction. Sci Rep 7:3602
134. Leung CLA, Marussi S, Atwood RC, Towrie M, Withers PJ, Lee PD (2018) In situ X-ray imaging of defect and molten pool dynamics in laser additive manufacturing. Nat Commun 9:1355
135. Calta NP, Wang J, Kiss AM, Martin AA, Depond PJ, Guss GM et al (2018) An instrument for in situ time-resolved X-ray imaging and diffraction of laser powder bed fusion additive manufacturing processes. Rev Sci Instrum 89:055101
136. Uhlmann E, Krohmer E, Schmeiser F, Schell N, Reimers W (2020) A laser powder bed fusion system for in situ x-ray diffraction with high-energy synchrotron radiation. Rev Sci Instrum 91:075104
137. Li L (2002) A comparative study of ultrasound emission characteristics in laser processing. Appl Surf Sci 186:604–610
138. Wang F, Mao H, Zhang D, Zhao X, Shen Y (2008) Online study of cracks during laser cladding process based on acoustic emission technique and finite element analysis. Appl Surf Sci 255:3267–3275
139. Muktadir M, Hasan MN, Alam M (2023) Additive manufacturing and acoustic Emission: a brief review. J Additive Manuf Technol 632 p
140. Spears TG, Gold SA (2016) In-process sensing in selective laser melting (SLM) additive manufacturing. Integr Mater Manuf Innov. 5:16–40
141. Van Belle L, Vansteenkiste G, Boyer JC (2013) Investigation of residual stresses induced during the selective laser melting process. Key Eng Mater 554–557:1828–1834
142. Shiomi M, Osakada K, Nakamura K, Yamashita T, Abe F (2004) Residual stress within metallic model made by selective laser melting process. CIRP Ann 53:195–198
143. Lopez A, Bacelar R, Pires I, Santos TG, Sousa JP, Quintino L (2018) Non-destructive testing application of radiography and ultrasound for wire and arc additive manufacturing. Addit Manuf 21:298–306
144. Chivel Y (2013) Optical in-process temperature monitoring of selective laser melting. Phys Procedia 41:904–910
145. Islam M, Purtonen T, Piili H, Salminen A, Nyrhilä O (2013) Temperature profile and imaging analysis of laser additive manufacturing of stainless steel. Phys Procedia 41:835–842
146. Hirvimäki M, Manninen M, Lehti A, Happonen A, Salminen A, Nyrhilä O (2013) Evaluation of different monitoring methods of laser additive manufacturing of stainless steel. Adv Mater Res 651:812–819
147. Liu S, Farahmand P, Kovacevic R (2014) Optical monitoring of high power direct diode laser cladding. Opt Laser Technol 64:363–376

148. Lane B, Whitenton E, Moylan S (2023) Multiple sensor detection of process phenomena in laser powder bed fusion. Thermosense: Thermal Infrared Applications XXXVIII [Internet]. SPIE; 2016 [cited 2023 Jun 12]. p. 20–8. Available from: https://doi.org/10.1117/12.2224390.full
149. Maisonneuve J (2023) Fabrication directe de pièces aéronautiques en TA6V et IN718 : projection et fusion sélective par laser [Internet] [These de doctorat]. Paris, ENMP; 2008 [cited 2023 Mar 15]. Available from: https://www.theses.fr/2008ENMP0006
150. Medrano A, Folkes J, Segal J, Pashby I (2023) Fibre laser metal deposition with wire: parameters study and temperature monitoring system. XVII International Symposium on Gas Flow, Chemical Lasers, and High-Power Lasers [Internet]. SPIE; 2009 [cited 2023 Apr 3]. p. 539–45. Available from: https://doi.org/10.1117/12.816831.full
151. Song L, Bagavath-Singh V, Dutta B, Mazumder J (2012) Control of melt pool temperature and deposition height during direct metal deposition process. Int J Adv Manuf Technol 58:247–256
152. Wu B, Pan Z, Ding D, Cuiuri D, Li H, Fei Z (2018) The effects of forced interpass cooling on the material properties of wire arc additively manufactured Ti6Al4V alloy. J Mater Process Technol 258:97–105
153. Denlinger ER, Heigel JC, Michaleris P, Palmer TA (2015) Effect of inter-layer dwell time on distortion and residual stress in additive manufacturing of titanium and nickel alloys. J Mater Process Technol 215:123–131
154. Griffith ML, Schlienger ME, Harwell LD, Oliver MS, Baldwin MD, Ensz MT et al (1999) Understanding thermal behavior in the LENS process. Mater Des 20:107–113
155. Salehi DS, Sensing and control of Nd:YAG laser cladding process
156. Altenburg SJ, Straße A, Gumenyuk A, Maierhofer C (2022) In-situ monitoring of a laser metal deposition (LMD) process: comparison of MWIR, SWIR and high-speed NIR thermography. Quant InfraRed Thermogr J 19:97–114
157. Emamian A, Farshidianfar MH, Khajepour A (2017) Thermal monitoring of microstructure and carbide morphology in direct metal deposition of Fe-Ti-C metal matrix composites. J Alloy Compd 710:20–28
158. Farshidianfar MH, Khajepour A, Gerlich A (2016) Real-time control of microstructure in laser additive manufacturing. Int J Adv Manuf Technol 82:1173–1186
159. Gharbi M, Etats de surface de pièces métalliques obtenues en Fabrication Directe par Projection Laser (FDPL): compréhension physique et voies d'amélioration
160. Gibson BT, Bandari YK, Richardson BS, Roschli AC, Post BK, Borish MC, et al (2019) Melt pool monitoring for control and data analytics in large-scale metal additive manufacturing. University of Texas at Austin; 2019 [cited 2022 Nov 28]. Available from: https://repositories.lib.utexas.edu/handle/2152/90450
161. Hu D, Kovacevic R (2003) Sensing, modeling and control for laser-based additive manufacturing. Int J Mach Tools Manuf 43:51–60
162. Akbari M, Kovacevic R (2019) Closed loop control of melt pool width in robotized laser powder–directed energy deposition process. Int J Adv Manuf Technol 104:2887–2898
163. Ding Y, Warton J, Kovacevic R (2016) Development of sensing and control system for robotized laser-based direct metal addition system. Addit Manuf 10:24–35
164. Donadello S, Motta M, Demir AG, Previtali B (2019) Monitoring of laser metal deposition height by means of coaxial laser triangulation. Opt Lasers Eng 112:136–144
165. Fathi A, Khajepour A, Toyserkani E, Durali M (2007) Clad height control in laser solid freeform fabrication using a feedforward PID controller. Int J Adv Manuf Technol 35:280–292
166. François J (2022) Apport à la compréhension et à la simulation numérique du procédé Laser Metal Deposition—poudre
167. Hofman JT, Pathiraj B, van Dijk J, de Lange DF, Meijer J (2012) A camera based feedback control strategy for the laser cladding process. J Mater Process Technol 212:2455–2462
168. Mezari R (2014) Instrumentation, identification and control of laser direct metal deposition for additive manufacturing [Internet] [phdthesis]. Ecole nationale supérieure d'arts et métiers—ENSAM; 2014 [cited 2023 Jan 19]. Available from: https://pastel.archives-ouvertes.fr/tel-01477707

169. Moralejo S, Penaranda X, Nieto S, Barrios A, Arrizubieta I, Tabernero I et al (2017) A feedforward controller for tuning laser cladding melt pool geometry in real time. Int J Adv Manuf Technol 89:821–831
170. Xiong J, Zhang G, Qiu Z, Li Y (2013) Vision-sensing and bead width control of a single-bead multi-layer part: material and energy savings in GMAW-based rapid manufacturing. J Clean Prod 41:82–88
171. Xiong J, Zhang G (2014) Adaptive control of deposited height in GMAW-based layer additive manufacturing. J Mater Process Technol 214:962–968
172. Chabot A (2023) Multiphysics monitoring methodology for DED processes : development with an experimental approach [Internet] [phdthesis]. École centrale de Nantes; 2020 [cited 2023 Feb 3]. Available from: https://theses.hal.science/tel-03164132
173. Garmendia I, Leunda J, Pujana J, Lamikiz A (2018) In-process height control during laser metal deposition based on structured light 3D scanning. Procedia CIRP 68:375–380
174. Heralić A, Christiansson A-K, Ottosson M, Lennartson B (2010) Increased stability in laser metal wire deposition through feedback from optical measurements. Opt Lasers Eng 48:478–485
175. Heralić A, Christiansson A-K, Lennartson B (2012) Height control of laser metal-wire deposition based on iterative learning control and 3D scanning. Opt Lasers Eng 50:1230–1241
176. Tang L, Landers RG (2011) Layer-to-layer height control for laser metal deposition process. J Manuf Sci Eng [Internet]. 2011 [cited 2022 Dec 2];133. Available from: https://doi.org/10.1115/1.4003691
177. Biegler M, Graf B, Rethmeier M (2018) In-situ distortions in LMD additive manufacturing walls can be measured with digital image correlation and predicted using numerical simulations. Addit Manuf 20:101–110
178. Heigel JC, Michaleris P, Palmer TA (2015) In situ monitoring and characterization of distortion during laser cladding of Inconel® 625. J Mater Process Technol 220:135–145
179. van Bohemen SMC, Hermans MJM, den Ouden G (2001) Monitoring of martensite formation during welding by means of acoustic emission. J Phys D: Appl Phys 34:3312
180. Gaja H, Liou F (2017) Defects monitoring of laser metal deposition using acoustic emission sensor. Int J Adv Manuf Technol 90:561–574
181. Ma Y, Hu Z, Tang Y, Ma S, Chu Y, Li X et al (2020) Laser opto-ultrasonic dual detection for simultaneous compositional, structural, and stress analyses for wire + arc additive manufacturing. Addit Manuf 31:100956
182. Xu F, Madhaven N, Dhokia V, McAndrew AR, Colegrove PA, Williams S et al, Multi-sensor system for wire-fed additive manufacture of titanium alloys, 9

Chapter 6
A Concise Study on Tribological Properties of Additive Manufactured Biomaterials

Jasjeevan Singh, Amit Mahajan, Atul Agnihotri, and Ruchi Handa

1 Introduction

The process of creating an object one layer at a time is known as AM. It is the inverse of subtractive manufacturing, which involves cutting away at a solid block of material till the finished product has been produced entirely. Technically, additive manufacturing can refer to any process that creates a product by building it up, such as molding, but it most commonly refers to 3D printing. Campbell et al. [1] define AM as the development of parts through layer-by-layer builds [1]. Guo and Leu [2] found that AM-based processes have been widely used in the biomedical, aerospace, and automotive industries since their inception [2]. In recent years, AM has evolved quickly. Major industrial companies that are looking for ways to improve their products have embraced it. The ability to produce near-instant parts and fully custom designs that are not possible with other manufacturing techniques has increased investment and research in additive engineering. AM is used to create lighter, stronger parts and systems in a much more efficient manner. It has applications in a variety of industries, including Jewelry production, dental and orthopedic implants, tool repair, health care, etc. AM is also used to redesign and re-manufacture various surgical instruments. Figure 1 depicts the various materials and body part implants that can be created using additive manufacturing [3].

J. Singh (✉)
IKG Punjab Technical University, Kapurthala, Punjab 144603, India
e-mail: jasjeevansingh175@gmail.com

J. Singh · A. Mahajan · A. Agnihotri · R. Handa
Department of Mechanical Engineering, Khalsa College of Engineering and Technology, Amritsar 143001, India

A. Mahajan et al. (eds.), *Additive Manufacturing of Bio-implants*, Biomedical Materials for Multi-functional Applications, https://doi.org/10.1007/978-981-99-6972-2_6

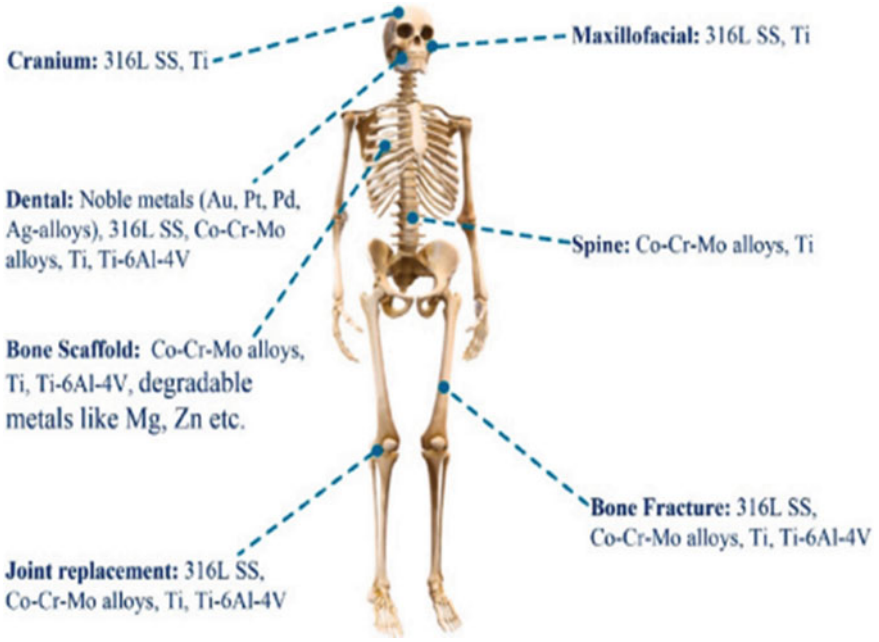

Fig. 1 Common metal implants [3]

2 Tribology in Joint Replacement of Humans

Many biomedical applications rely on tribological properties such as wear, friction, and lubrication. It is critical to choose implant materials with low friction properties, especially for parts of medical implants that are exposed to aggressive wear and abrasion against human tissues. The potential for tribology facets and applications in the biomedical field for the improvement of human health is expanding and attracting the attention of researchers. Biomaterials are materials that can treat, evaluate, or replace a tissue or organ in the body. Metals, glass, ceramics, and polymers are among the biomaterials that are widely used in biomedical applications. Human prosthesis implants such as the hip, elbow, ankle, shoulder, wrist, fingers, and knee are just a few of the key applications for these biomaterials.

Synovial joints are the most common type of joint found in our bodies. They are the ball and socket joint, the pivot joint, the condyloid joint, the hinge joints the planar joint, and the saddle joint. These joints allow a person to perform a wide range of movements while using the least amount of energy. The presence of an articular cavity filled with synovial fluid performs a lubricating function. As a result, friction and wear at the articular surfaces are reduced significantly, which is critical for the joint's long-term health. An orthopedic implant is a medical device that is used to replace a bone, joint, or cartilage that has been damaged or deformed. For example, a patient may require an implant because of a congenital disability, the loss of a limb,

or the breaking of a leg. The implant aids in bone fixation and may be used to replace articulating surfaces in various joints throughout the body. A patient may have pain in joints and bones that need to be repaired, and the implant is used to strengthen or completely replace the joints in the damaged bones or regions. Fixtures such as screws, micro-clips, plates, and stabilizing devices are common examples of such implants [4]. They are primarily used to join or secure different sections of bones or ligaments. The tribological properties are critical to the performance and lifespan of biomedical implants. The wear resistance of implant materials is influenced by their tribological properties. Low wear rates are preferable because they reduce the release of wear debris, which can cause adverse biological responses and lead to implant failure. Excessive friction can result in implant discomfort, pain, and tissue wear. Proper lubrication, whether via synovial fluid in joint replacements or bio-lubricants in other implants, is critical for reducing friction, minimizing wear, and maintaining implant function. An implant's tribological properties can affect its biocompatibility, which refers to the implant's capacity to coexist with surrounding biological tissues without creating negative effects. The majority of commercially available fixtures are made of titanium, stainless steel, and cobalt chromium alloys [5–7].

3 Tribological Characteristics of Additively Manufactured Biomaterials

3.1 Stainless Steel

Stainless steel (SS) is a biomedical material that is widely used in the fabrication of cardiovascular stents/valves, dentistry, craniofacial surgery, orthopedic prostheses, and otorhinology applications because of reasonable cost, malleability, the convenience of fabrication as well as resistance to corrosion and fatigue. Bartolomeu et al. [8] investigated the impact of three additively manufactured methods, viz., selective laser melting, hot pressing, and traditional casting upon the morphology, mechanical properties, and tribological characteristics of an austenitic 316L stainless steel. The outcomes of their study demonstrated that SLM fabricated 316L SS had better mechanical characteristics as well as tribological features as compared to hot pressing and conventional casting 316L SS alloy. Figure 2 shows an SEM image of the core region of the wear tracks that developed when 316L SS specimens were subjected to wear tests against an alumina ball while diluting with PBS fluid using the casting, HP, and SLM methods. It shows the SLM substrate had a narrower wear track, revealing less alumina ball penetrating. Zou et al. [9] reinforced the 316L stainless steel with silicon carbide via laser powder bed fusion (LPBF) additive manufactured technique and examined the wear characteristics and strength of the alloy. According to their findings, the modified alloy demonstrated improved strength and wear characteristics of the alloy. Yazici et al. [10] considered the selective laser melting (SLM) and plasma nitriding techniques to provide titanium and titanium nitride coating on

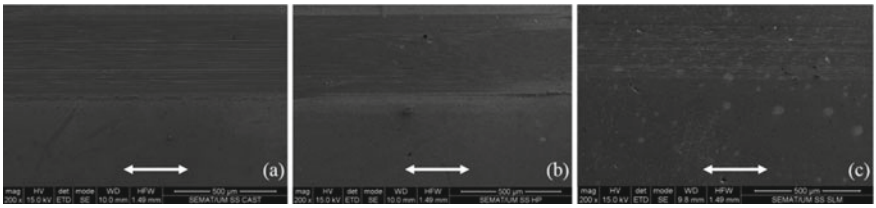

Fig. 2 SEM images of wear track: **a** Casting; **b** Hot Pressing; **c** Selective Laser Melting

316L stainless steel alloy. They claimed that modification of alloy had improved morphology, and mechanical and tribological characteristics.

3.2 Titanium and Its Alloys

Although pure Ti has good structural properties, its low mechanical properties and wear resistance limit its use. Ti alloys have poor resistance to abrasion, and the oxide film on the surface is prone to peeling off during contact friction, accelerating abrasive particle wear on the joint surface. Biomedical Ti6Al4V is a Ti alloy with a wide range of applications because of its superior biocompatibility, corrosion resistance, and mechanical properties. It is commonly used in artificial hip and knee replacements [11]. Attar et al. [12] examined the microstructure, mechanical properties, and wear parameters of laser powder bed fusion (LPBF), laser-engineered net shaping (LENS), and wire and arc additive manufacturing (WAAM) made commercially pure titanium. When compared to other AM techniques, it was shown that the titanium substrate built using LPBF had improved mechanical qualities, morphology, and wear characteristics. However, compared to conventional production methods, all of these AM substrates produced better results. SEM image of wear appearances of LPBF manufactured titanium specimen is represented in Fig. 3. Similar to this, Santos et al. [13] created the Ti–6Al–4 V alloy using the LPBF additive manufacturing method. They also used plasma electrolytic oxidation (PEO) to modify the alloy's surface, and they looked at how well the alloy substrate withstood wear. They claimed that compared to uncoated alloy substrate, AM substrate treated by PEO showed enhanced wear resistance.

3.3 Co–Cr and Its Alloys

Co–Cr–Mo alloys are the most widely used bearing materials in artificial hip and knee joints, as well as artificial intervertebral discs. Plecko et al. [14] explored the osseointegration of various metals. The findings revealed poor osseointegration, even less

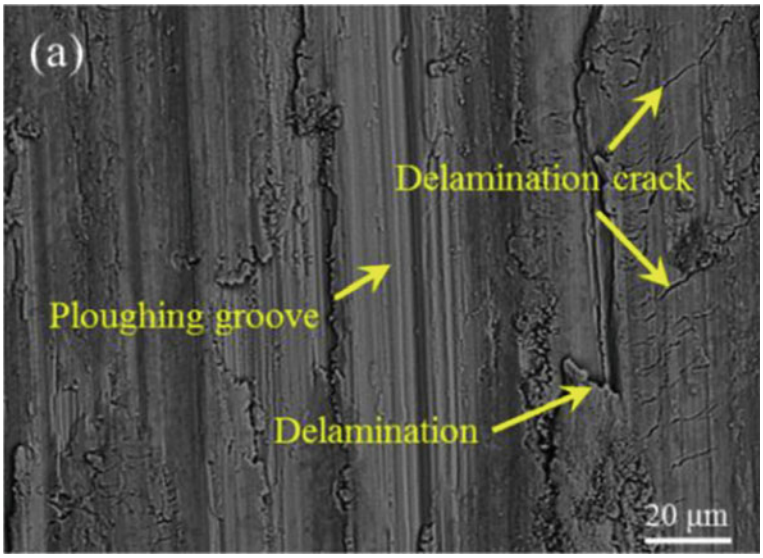

Fig. 3 SEM images of wear appearances of the titanium specimen constructed by LPBF

than that of stainless steel, introducing a new limitation for Co–Cr alloys. The findings revealed poor osseointegration, even less than that of stainless steel, introducing a new limitation for Co–Cr alloys. Figure 4 depicts a bone section's fluorescence and toluidine blue dye after the screw implant has been removed. The figure depicts lower new cells created at the interface of a Co–Cr implant (the grey color reflects old bone cells and the blue color reflects newly formed cells).

Mantrala et al. [15] investigated the electrochemical performance, tribological properties, morphology, and microhardness of the produced alloy and explored the

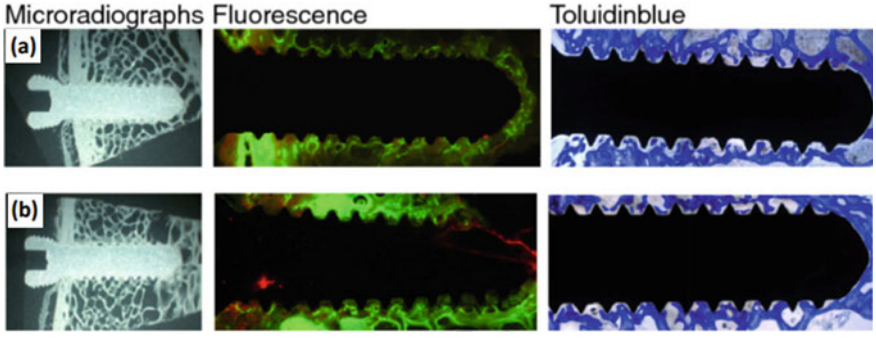

Fig. 4 Bone sections after screw implants have been removed. **a** Co–Cr alloy; **b** Stainless steel [14]

laser-engineered net shaping (LENSTM) technology for the development of Co–Cr–Mo alloy. They came to the conclusion that the substrate created with a stronger laser had better tribological and corrosion resistance responses. Amanov [16] used ultrasonic nanocrystals (UN) to modify the surface of LPBF-built Co–Cr–Mo alloy both at room temperature (AT) and at high temperature (HT). The properties of tribology and tribocorrosion on the altered surfaces were examined. When compared to untreated and treated substrates at ambient temperature, the LPBF substrate altered at high temperature demonstrated higher tribocorrosion and wear resistance properties.

3.4 Magnesium and Its Alloys

Due to their superior mechanical and thermal characteristics, biodegradable materials like magnesium (Mg) and its alloys are a compelling candidate for orthopedic and cardiovascular applications. Additive manufacturing of magnesium and its alloys has drawn tremendous attention as an approach to resolving problems with existing procedures and technologies. By using the LPBF approach, Chung et al. created the pure magnesium specimen and examined the mechanical properties of the built-up substrate. Their research revealed that the mechanical properties of the synthetic substrate were very similar to those of real human bones. The porous Mg (WE43) scaffolds were created using the LPBF technique of AM by Li et al., who also looked at the scaffolds' mechanical properties, in-vitro biodegradation rate, and biocompatibility. They discovered that the created scaffold's mechanical properties matched those of trabecular bone exactly. The AM porous WE43 Mg scaffolds showed outstanding biocompatibility and biodegradation responses.

3.5 Ceramic and Amorphous Alloy

Ceramic components or products used in medical and dental applications, primarily as implants and replacements, are known as bioceramics. Alumina, hydroxyapatite, zirconia, bioactive glass, glass ceramics, restorable calcium phosphates, and other materials are examples of bioceramics. Because of their high biocompatibility, low cytotoxicity, and high corrosion resistance, bioceramics have a high potential for use in scaffolds and bone transplants for the treatment of fractured and damaged bones [17, 18]. Further, amorphous phase alloys, also known as Bulk Metallic Glass (BMG), are currently attracting interest because of their outstanding mechanical characteristics and excellent wear and corrosion behavior. Rapid cooling and solidification of alloy melt produce an amorphous alloy, also known as metallic glass. BMGs have outstanding biological properties such as wear resistance, high strength, and corrosion resistance. As a result, Fe, Ti, and Zr-based BMGs are potential replacements for crystalline stainless steel, Zr, Ti, and alloys.

A variety of additive manufactured methods and techniques can be used to improve the friction and wear properties of metallic biomaterials. Many biomedical modification technologies have been developed or are in the process of being developed. Despite recent advances, there is still much space for growth and improvement in this field.

4 Conclusions

The current paper presents a concise review of the tribological properties of additive-manufactured bioimplants. The study concluded that additively manufactured biomaterials had improved tribological characteristics. However, some more studies are also required that investigate some other aspects such as biocompatibility and osseointegration of biomaterials. Furthermore, researches on surface modification of additive-manufactured biomaterials are limited. More in vivo research on AM biomaterials and their alloys is also necessary to recognize the clinical use of these biological assets.

References

1. Campbell I, Bourell D, Gibson I (2012) Additive manufacturing: rapid prototyping comes of age. Rapid Prototyping J 18(4):255–258
2. Guo N, Leu MC (2013) Additive manufacturing: technology, applications and research needs. Front Mech Eng 8:215–243
3. Bai L, Gong C, Chen X, Sun Y, Zhang J, Cai L, Xie SQ (2019) Additive manufacturing of customized metallic orthopedic implants: Materials, structures, and surface modifications. Metals 9(9):1004
4. Popov VL, Poliakov AM, Pakhaliuk VI (2021) Synovial joints. Tribology, regeneration, regenerative rehabilitation and arthroplasty. Lubricants 9(2):15
5. Devgan S, Mahajan A, Sidhu SS (2021) Multi-walled carbon nanotubes in powder mixed electrical discharge machining: an experimental study, state of the art and feasibility prospect. Appl Phys A 127(11):806
6. Khoo LK, Kiattavorncharoen S, Pairuchvej V, Lakkhanachatpan N, Wongsirichat N, Seriwatanachai D (2020) The affinity of human fetal osteoblast to laser-modified titanium implant fixtures. Open Dentistry J 14(1)
7. Mahajan A, Devgan S, Kalyanasundaram D (2022). Surface alteration of Cobalt-Chromium and duplex stainless steel alloys for biomedical applications: a concise review. Mater Manuf Processes, 1–11
8. Bartolomeu F, Buciumeanu M, Pinto E, Alves N, Carvalho O, Silva FS, Miranda G (2017) 316L stainless steel mechanical and tribological behavior—a comparison between LPBF, hot pressing and conventional casting. Addit Manuf 16:81–89
9. Zou Y, Tan C, Qiu Z, Ma W, Kuang M, Zeng D (2021) Additively manufactured SiC-reinforced stainless steel with excellent strength and wear resistance. Addit Manuf 41:101971
10. Yazıcı M, Kovacı H, Yetim AF, Çelik A (2018) Structural, mechanical and tribological properties of Ti and TiN coatings on 316L stainless steel. Ceram Int 44(12):14195–14201
11. Zhou J, Sun Y, Huang S, Sheng J, Li J, Agyenim-Boateng E (2019) Effect of laser peening on friction and wear behavior of medical Ti6Al4V alloy. Opt Laser Technol 109:263–269

12. Attar H, Bermingham MJ, Ehtemam-Haghighi S, Dehghan-Manshadi A, Kent D, Dargusch MS (2019) Evaluation of the mechanical and wear properties of titanium produced by three different additive manufacturing methods for biomedical application. Mater Sci Eng, A 760:339–345
13. Santos PB, de Castro VV, Baldin EK, Aguzzoli C, Longhitano GA, Jardini AL, ... de Fraga Malfatti C (2022) Wear resistance of plasma electrolytic oxidation coatings on Ti-6Al-4V eli alloy processed by additive manufacturing. Metals 12(7):1070
14. Plecko M, Sievert C, Andermatt D, Frigg R, Kronen P, Klein K, ... von Rechenberg B (2012) Osseointegration and biocompatibility of different metal implants-a comparative experimental investigation in sheep. BMC Musculoskeletal Disorders 13:1–12
15. Mantrala KM, Das M, Balla VK, Rao CS, Rao VK (2014) Laser-deposited CoCrMo alloy: microstructure, wear, and electrochemical properties. J Mater Res 29(17):2021–2027
16. Amanov A (2021) Effect of post-additive manufacturing surface modification temperature on the tribological and tribocorrosion properties of Co–Cr–Mo alloy for biomedical applications. Surf Coat Technol 421:127378
17. Dorozhkin SV (2016) Multiphasic calcium orthophosphate (CaPO4) bioceramics and their biomedical applications. Ceram Int 42(6):6529–6554
18. Rahmati B, Sarhan AA, Basirun WJ, Abas WABW (2016) Ceramic tantalum oxide thin film coating to enhance the corrosion and wear characteristics of Ti6Al4V alloy. J Alloy Compd 676:369–376

Chapter 7
Role and Scope of OEE to Improve Additive Manufacturing Processes in Biomedical Industries

Sandeep Singh, Davinder Singh, Mahesh Gupta, Bhupinder Singh Chauhan, and Jasjeevan Singh

1 Introduction

Overall Equipment Effectiveness (OEE) is a metric used to evaluate the efficiency of manufacturing processes. It considers three components: availability, performance, and quality. The implementation of OEE in additive manufacturing processes in the biomedical industries can help improve the efficiency and quality of production, leading to cost savings and improved patient outcomes [1–4]. Here are some steps to implement OEE in additive manufacturing:

- Define the scope of the analysis: Determine the machines and processes to be analyzed, as well as the specific components of OEE that will be measured. For example, if a company wants to analyze a 3D printer used to produce surgical implants, they may focus on availability (how often the machine is running), performance (how efficiently it is running), and quality (how many defective parts are produced) [4–6].

S. Singh (✉) · J. Singh
Department of Mechanical Engineering, Khalsa College of Engineering and Technology, Amritsar, Punjab, India
e-mail: er.sunny@yahoo.co.in

D. Singh
Department of Mechanical Engineering, Punjabi University, Patiala, Punjab, India

M. Gupta
Information Systems, Analytics and Operations, College of Business, University of Louisville, Louisville, Kentucky, India

B. S. Chauhan
GLA University, Mathura Road, Bharthia, Uttar Pradesh, India

A. Mahajan et al. (eds.), *Additive Manufacturing of Bio-implants*, Biomedical Materials for Multi-functional Applications, https://doi.org/10.1007/978-981-99-6972-2_7

- Collect data: In order to calculate OEE, data needs to be collected on machine uptime, speed, and quality. This can be done manually or through automation using sensors and software. Data collection should be continuous to provide real-time feedback [4].
- Analyze the data: Use the collected data to calculate OEE for the defined scope. Identify areas of low OEE and investigate root causes. This can help identify specific areas for improvement [5, 6].
- Implement improvements: Based on the analysis, make improvements to increase OEE. This may include maintenance, machine upgrades, process changes, or training for operators. It is important to track the impact of improvements on OEE [1, 7].
- Continuously monitor and adjust: Once improvements have been made, continue to monitor OEE to ensure that improvements are sustained. Adjustments may need to be made to maintain or further improve OEE [1, 7].
- By implementing OEE, companies in the biomedical industry can improve their additive manufacturing processes, leading to increased efficiency and improved quality. This can ultimately result in cost savings and better patient outcomes [2, 3].

2 Literature Review

There is a growing body of literature exploring the application of Overall Equipment Effectiveness (OEE) in Additive Manufacturing (AM) processes. OEE is a widely used metric for evaluating manufacturing efficiency and has been applied to a range of industries. In recent years, it has gained popularity in the additive manufacturing community as a way to optimize production processes and improve quality control [8]. Several studies have investigated the application of OEE in additive manufacturing for various industries, including aerospace, automotive, and biomedical. For example, a study by Hubner et al. [9] analyzed the OEE of an AM system used to produce aerospace components. The study found that OEE was affected by factors such as machine downtime and production quality. By monitoring OEE and making improvements, the authors were able to reduce production costs and improve the overall efficiency of the system. Another study applied OEE to a 3D printing process used in automotive manufacturing [10]. The authors found that OEE was impacted by factors such as material waste and equipment downtime. By addressing these issues, they were able to increase the OEE of the system by 20%. In the biomedical industry, OEE has been applied to additive manufacturing processes used to produce medical devices and implants. For example, in a study, OEE is used to enhance the processes of an Additive manufacturing (AM) system in order to produce custom orthopedic implants. The study found that OEE was impacted by factors such as machine maintenance and process optimization [2, 11]. By making improvements to the system based on OEE analysis, the authors were able to increase the efficiency of the process and reduce production costs. Overall, the literature suggests that OEE can

be a useful tool for optimizing additive manufacturing processes across a range of industries. By monitoring OEE and making improvements, companies can increase the efficiency of their production processes, reduce costs, and improve the quality of their products [11–14].

2.1 Overall Equipment Effectiveness (OEE) Paradigm

OEE is a widely recognized performance metric used to evaluate the efficiency of manufacturing processes. OEE measures three key components: availability, performance, and quality. The application of OEE has been studied in various industries, including automotive, aerospace, food processing, and pharmaceuticals. In the automotive industry, OEE has been used to evaluate the efficiency of assembly lines, stamping operations, and painting processes. A study published in the Journal of Cleaner Production applied OEE to evaluate the efficiency of an automotive paint shop. The study demonstrated that OEE provided a comprehensive assessment of the paint shop, highlighting areas for improvement and reducing downtime [15, 16]. In the aerospace industry, OEE has been applied to evaluate the efficiency of manufacturing processes for aircraft engines, landing gears, and airframes. OEE to evaluate the efficiency of a landing gear assembly line and the study showed that OEE was effective in identifying areas for improvement and reducing downtime [17, 18]. In the food processing industry, OEE has been used to evaluate the efficiency of production processes for various products, including dairy, meat, and bakery products. A study published in the Journal of Food Engineering applied OEE to evaluate the efficiency of a cheese production line. The study demonstrated that OEE provided a comprehensive assessment of the cheese production line, identifying areas for improvement and reducing downtime [19]. In the pharmaceutical industry, OEE has been applied to evaluate the efficiency of manufacturing processes for drug products. A study published in the Journal of Pharmaceutical Innovation applied OEE to evaluate the efficiency of a tablet manufacturing process. The study demonstrated that OEE provided a comprehensive assessment of the tablet manufacturing process, identifying areas for improvement and reducing downtime [20].

OEE is an effective tool to evaluate the efficiency of an AM system for producing complex metal parts. The study demonstrated that OEE was an effective tool for identifying inefficiencies in the AM process, including machine downtime, material waste, and inconsistent product quality. The study also highlighted the importance of optimizing the AM process by selecting suitable parameters, such as feedstock material, build orientation, and machine settings [21–25]. Another study stated that OEE to evaluate the efficiency of a laser powder bed fusion (LPBF) AM system for producing titanium alloy parts. The study demonstrated that OEE provided a comprehensive assessment of the LPBF process, identifying areas for improvement and reducing downtime. The study also highlighted the importance of monitoring and controlling the process parameters, such as laser power, scanning speed, and layer thickness, to optimize the AM process [26–28]. Overall, the application of OEE in AM provides a

valuable tool for manufacturers to evaluate the efficiency of their production process and identify areas for improvement. The successful implementation of OEE requires careful selection of suitable parameters, consistent monitoring of process variables, and continuous improvement efforts to optimize the AM process.

2.1.1 OEE in Biomedical Industries

In production and manufacturing industries, OEE has been used extensively to identify the efficiency and effectiveness of various production processes. This metric has been applied in the manufacturing of automotive components, electronic devices, food processing, pharmaceuticals, and other industries. The use of OEE in these industries has resulted in significant improvements in efficiency, productivity, and profitability. A study published in the International Journal of Production Economics evaluated the effectiveness of OEE in the manufacturing of automotive components. The study demonstrated that OEE provided a comprehensive assessment of the manufacturing process, highlighting areas of inefficiency, and improving the overall equipment utilization. The study also showed that the use of OEE resulted in a significant increase in productivity and profitability [23, 29–31]. In the electronics industry, OEE has been applied to evaluate the efficiency of various production processes. A study published in the International Journal of Production Research evaluated the effectiveness of OEE in the production of electronic circuit boards. The study demonstrated that OEE provided a comprehensive assessment of the production process, highlighting areas for improvement, and increasing the equipment utilization rate. The use of OEE resulted in a significant increase in productivity and profitability [32–34] (Fig. 1).

In the food processing industry, OEE has been used to evaluate the efficiency of production processes for various products, including dairy, meat, and bakery products. A study published in the Journal of Productivity and Performance Management applied OEE to evaluate the efficiency of a cheese production line. The study demonstrated that OEE provided a comprehensive assessment of the cheese production line, identifying areas for improvement and reducing downtime [35–37]. In the pharmaceutical industry, OEE has been applied to evaluate the efficiency of manufacturing processes for drug products. The study demonstrated that OEE provided a comprehensive assessment of the tablet manufacturing process, identifying areas for improvement and reducing downtime [38].

- Calculations and formulas to find/enhance OEE:

Overall Equipment Effectiveness (OEE) is a widely used performance metric to evaluate the efficiency of manufacturing processes. It measures the availability, performance, and quality of a process, and can be calculated using the following formula [1–4]:

In general,

$$\text{OEE} = \text{Availability} \times \text{Performance} \times \text{Quality}$$

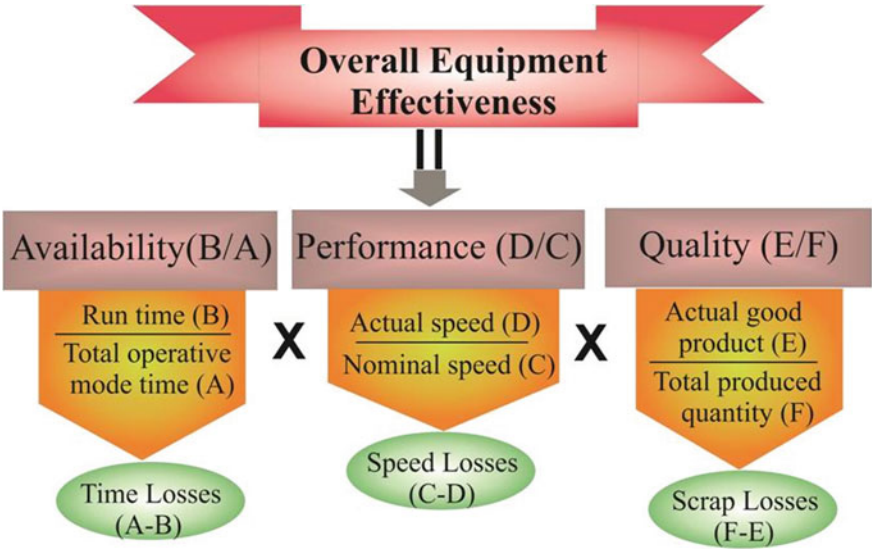

Fig. 1 Elements of overall equipment effectiveness [1]

where Availability = (Operating time–downtime)/Operating time

Performance = (Ideal cycle time × Total count)/Operating time

Quality = Good count/Total count.

The availability metric measures the percentage of time that a machine or process is available for production. It is calculated by subtracting the total downtime from the operating time and dividing by the operating time. Downtime can include unplanned stops, changeovers, maintenance, and any other non-productive time. The performance metric measures the efficiency of the process. It is calculated by multiplying the total count by the ideal cycle time and dividing by the operating time. The ideal cycle time is the time it should take to produce one unit of the product, assuming no downtime or defects. The quality metric measures the percentage of good units produced. It is calculated by dividing the number of good units produced by the total count of units produced.

There are various strategies that can be implemented to enhance OEE in additive manufacturing processes in the bio-medical industry. These include:

- Reducing setup time: By optimizing the setup process and reducing the time, it takes to prepare the machine for production, more time can be allocated for production, increasing availability.
- Improving maintenance procedures: Regular maintenance and inspection of machines can help prevent breakdowns and reduce downtime.
- Streamlining production flow: By optimizing the flow of materials and products through the manufacturing process, the overall performance can be improved.

- Implementing quality control measures: Ensuring that products meet quality standards can reduce the amount of rework required and improve overall quality.
- Investing in training: Providing employees with training and support can help improve their skills and knowledge, leading to better performance and quality.

By implementing strategies to enhance OEE, companies can improve their production processes and reduce downtime, ultimately leading to increased productivity and profitability. In conclusion, the application of OEE has been studied in various industries and has been demonstrated to be effective in evaluating the efficiency of manufacturing processes. OEE provides a comprehensive assessment of the manufacturing process, identifying areas for improvement and reducing downtime. The application of OEE in AM has gained attention as the technology has become increasingly prevalent in various industries [1]. OEE in AM refers to a comprehensive assessment of the performance of the AM process, which includes measuring the efficiency of the equipment, the quality of the output, and the availability of the equipment.

2.2 Additive Manufacturing (AM) Paradigm

Additive manufacturing (AM) has revolutionized the manufacturing industry by enabling the production of complex and customized parts with greater design freedom and reduced lead time. AM, also known as 3D printing, is a process of building a 3D object layer by layer from a digital model [39]. One of the significant advantages of AM is its ability to reduce material waste, as only the material required for the part is used. This makes AM an environmentally friendly alternative to traditional manufacturing methods such as subtractive manufacturing, which generate a significant amount of waste material [40]. AM has also enabled the production of parts with unique geometries and internal structures that are impossible to create using conventional manufacturing methods. This has led to the development of lightweight parts with superior strength-to-weight ratios, which are particularly useful in the aerospace and automotive industries [41, 42]. Furthermore, AM has enabled the production of personalized products such as medical implants, dental crowns, and hearing aids, which are customized to fit an individual's unique anatomy. However, there are also some challenges associated with AM, such as the need for high-precision and specialized equipment, the limited range of available materials, and the potential for inconsistent product quality [2, 43].

2.2.1 AM in Production and Manufacturing

AM, also known as 3D printing, is a rapidly growing field that has the potential to revolutionize the manufacturing industry. The application of AM has been studied extensively in recent years, and numerous studies have investigated its use in various industries and production processes. In the aerospace industry, AM has been used

to produce complex parts for aircraft engines, landing gears, and airframes. A study published in the Journal of Aircraft Engineering and Aerospace Technology demonstrated the potential of AM to reduce the weight of aircraft components, resulting in significant fuel savings and reduced emissions [44]. In the automotive industry, AM has been used to produce lightweight parts with complex geometries, reducing vehicle weight and improving fuel efficiency. A study published in the International Journal of Automotive Technology demonstrated the use of AM to produce automotive components with superior strength-to-weight ratios, improving vehicle performance and reducing material waste [45].

In the medical industry, AM has been used to produce customized implants, prosthetics, and surgical tools. A study demonstrated the use of AM to produce patient-specific orthopedic implants, resulting in improved surgical outcomes and reduced surgery time. In the production of consumer goods, AM has been used to produce customized products with unique designs and features [46]. Another study concluded the use of AM to produce personalized jewelry, resulting in increased customer satisfaction and improved profitability for the manufacturer. Overall, the application of AM has been studied extensively in various industries and production processes, demonstrating its potential to reduce material waste, improve product performance, and enable the production of customized products. As technology advances and more materials become available, the potential applications of AM in production and manufacturing are expected to grow, leading to further improvements in efficiency, sustainability, and product quality [46–49]. Overall, AM has transformed the biomedical industry by providing new design possibilities, reducing material waste, and enabling the production of customized and complex parts. As technology advances and more materials become available, the potential applications of AM in manufacturing are expected to grow, leading to further improvements in efficiency, sustainability, and product quality.

2.3 Findings of the Literature

AM is revolutionizing the biomedical industry by enabling the production of patient-specific implants, prostheses, and other medical devices with high precision and accuracy. However, the success of AM relies on the efficiency of the production process, which can be improved by implementing OEE as a performance metric. OEE provides a comprehensive assessment of the production process by measuring three key components: availability, performance, and quality. The application of OEE in various industries, including automotive, aerospace, food processing, and pharmaceuticals, has been extensively studied and has demonstrated significant improvements in efficiency and productivity.

The implementation of OEE in AM processes can be challenging due to the complexity of the process and the various factors that can affect the performance of the equipment. However, several studies have shown that OEE can be effectively applied to improve AM processes in the biomedical industry. The studies showed

that OEE provided a comprehensive assessment of the process, identifying areas for improvement and reducing downtime. Similarly, OEE can be applied to evaluate the efficiency of a selective laser sintering (SLS) process for producing biomedical devices. The study demonstrated that OEE was effective in identifying areas for improvement and reducing downtime [50]. Moreover, the implementation of OEE in AM processes can result in significant cost savings for the biomedical industry. OEE to evaluate the efficiency of a 3D printing process for manufacturing prostheses and it was observed that this gizmo is effective in reducing the production cost by identifying areas for improvement and reducing the downtime of the equipment [21]. The implementation of OEE in AM processes has the potential to improve the efficiency and productivity of the biomedical industry by providing a comprehensive assessment of the production process. OEE can identify areas for improvement, reduce downtime, and result in significant cost savings. However, further research is needed to develop a standardized approach for implementing OEE in AM processes. The results of this research will aid in the development of efficient and cost-effective AM processes that can revolutionize the biomedical industry.

3 Conclusion

OEE has been widely adopted in manufacturing industries as a performance metric to evaluate the efficiency of production processes. With the rapid development of AM technologies, there has been a growing interest in applying OEE to evaluate and improve AM processes, especially in the biomedical industry.

In a study, the researchers applied OEE to evaluate an AM process for producing customized dental implants. The study showed that OEE provided a comprehensive assessment of the AM process, highlighting areas for improvement and reducing the time and cost required for process optimization. The OEE metric incorporated unique characteristics to enhance AM processes, such as build time and material usage and provided a more accurate evaluation of AM efficiency. In the biomedical industry, OEE has been applied to evaluate the efficiency of AM processes for producing orthopedic implants, dental prostheses, and other medical devices. For example, a study published in the Journal of Medical Systems applied OEE to evaluate an AM process for producing cranial implants. The study showed that OEE was effective in identifying the causes of machine downtime and quality issues, and helped to improve the overall efficiency of the AM process. In conclusion, the application of OEE to AM processes in the biomedical industry has shown promising results in terms of improving efficiency, reducing costs, and improving quality. Further research is needed to develop more specialized OEE calculation methods for specific AM processes and to evaluate the impact of OEE on patient outcomes.

References

1. Singh S, Khamba JS, Singh D (2021) Analysis and directions of OEE and its integration with different strategic tools. Proc Inst Mech Eng Part E J Process Mech Eng 235(2):594–605
2. Singh S, Khamba JS, Singh D (2021) Analyzing the role of six big losses in OEE to enhance the performance: literature review and directions. Adv Indus Prod Eng Select Proc FLAME 2020:411–421
3. Singh S, Khamba JS, Singh D (2021) Interpretive structural modelling to evaluate the key barriers inhibiting successful implementation of overall equipment effectiveness. Int J Prod Qual Manag 34(3):415–444
4. Singh S, Khamba JS, Singh D (2022) Role and scope of overall equipment effectiveness implementation in Indian sugarmill industries: a justified approach. Proc Inst Mech Eng Part E J Process Mech Eng 236(2):546–555
5. Singh S, Khamba JS, Singh D (2022) Analysis of potential factors affecting execution of overall equipment effectiveness in Indian sugar mills. Proceedings of the institution of mechanical engineers, part e: journal of process mechanical engineering, 09544089221135010
6. Singh S, Khamba JS, Singh D (2023) Study of energy-efficient attributes of overall equipment effectiveness in Indian sugar mill industries through analytical hierarchy process (AHP). Int J Syst Assur Eng Manag, 1–11
7. Sandeep S, Karanbir S (2022) Scope of industrial revolution 4.0 in Indian industries. In: Электрофизические методы обработки в современной промышленности, pp 45–50
8. Kumar J, Kumar Soni V, Agnihotri G (2014) Impact of TPM implementation on Indian manufacturing industry. Int J Product Perform Manag 63(1):44–56
9. Hubner AH, Kuhn H, Wollenburg J (2016) Last mile fulfilment and distribution in omni-channel grocery retailing: a strategic planning framework. Int J Retail Distrib Manag 44(3)
10. Yang KK, Zhu JH, Wang C, Jia DS, Song LL, Zhang WH (2018) Experimental validation of 3D printed material behaviors and their influence on the structural topology design. Comput Mech 61:581–598
11. Das SK, Kumar R, Majumder MC (2020) Application of overall equipment effectiveness for additive manufacturing process optimization. J Manuf Technol Manag 31(5):1115–1131
12. da Silva LRR, Sales WF, Campos FDAR, de Sousa JAG, Davis R, Singh A, ... Borgohain B (2021). A comprehensive review on additive manufacturing of medical devices. Progress Additive Manuf 6(3):517–553
13. Karthikeyan K, Arun A, Sivakumar R, Rajaraman R (2020) An empirical analysis of overall equipment effectiveness in additive manufacturing using selective laser sintering. Int J Manuf Res 15(3):357–377
14. Naveen S, Anand S, Ramanujam R (2017) Overall Equipment Effectiveness (OEE) for 3D printing in the medical industry. Int J Adv Res Eng Technol 8(4):157–163
15. Dobra P, Jósvai J (2022) Assembly line overall equipment effectiveness (OEE) prediction from human estimation to supervised machine learning. J Manuf Mater Process 6(3):59
16. Szwedzka K, Jasiulewicz-Kaczmarek M, Szafer P (2015) The efficiency of production equipment improvement–a case study. Res Logist Prod, 5
17. Xiang ZT, Chin JF (2021) Implementing total productive maintenance in a manufacturing small or medium-sized enterprise. J Indus Eng Manag (JIEM) 14(2):152–175
18. Iranzadeh S (2019) Investigating the relationship between RPN parameters in fuzzy PFMEA and OEE in a sugar factory. J Loss Prev Process Ind 60:221–232
19. Kennedy I, Plunkett A, Haider J (2013) Implementation of lean principles in a food manufacturing company. In: Advances in sustainable and competitive manufacturing systems: 23rd international conference on flexible automation & intelligent manufacturing, pp 1579–1590. Springer International Publishing
20. Walsh J, Ranmal SR, Ernest TB, Liu F (2018) Patient acceptability, safety and access: a balancing act for selecting age-appropriate oral dosage forms for paediatric and geriatric populations. Int J Pharm 536(2):547–562

21. Mendonça PA, da Piedade Francisco R, de Souza Rabelo D (2022) OEE approach applied to additive manufacturing systems in distributed manufacturing networks. Comput Ind Eng 171:108359
22. Engelmann B, Schmitt S, Miller E, Bräutigam V, Schmitt J (2020) Advances in machine learning detecting changeover processes in cyber physical production systems. J Manuf Mater Process 4(4):108
23. Chan FTS, Lau HCW, Ip RWL, Chan HK, Kong S (2005) Implementation of total productive maintenance: a case study. Int J Prod Econ 95(1):71–94
24. Jonsson P, Lesshammar M (1999) Evaluation and improvement of manufacturing performance measurement systems-the role of OEE. Int J Oper Prod Manag
25. Tortorella G, Saurin TA, Fogliatto FS, Tlapa D, Moyano-Fuentes J, Gaiardelli P, ... Forstner FF (2022) The impact of Industry 4.0 on the relationship between TPM and maintenance performance. J Manuf Technol Manag 33(3):489–520
26. Barclift MW (2019) Cost modeling and design tools for additive manufacturing with laser powder bed fusion
27. Hoque ME, Showva NN, Ahmed M, Rashid AB, Sadique SE, El-Bialy T, Xu H (2022) Titanium and titanium alloys in dentistry: current trends, recent developments, and future prospects. Heliyon, e11300
28. Dejene ND, Lemu HG (2023) Current Status and challenges of powder bed fusion-based metal additive manufacturing: literature review. Metals 13(2):424
29. Kamble SS, Gunasekaran A, Ghadge A, Raut R (2020) A performance measurement system for industry 4.0 enabled smart manufacturing system in SMMEs-a review and empirical investigation. Int J Prod Econ 229:107853
30. Muñoz-Villamizar A, Santos J, Montoya-Torres JR, Jaca C (2018) Using OEE to evaluate the effectiveness of urban freight transportation systems: a case study. Int J Prod Econ 197:232–242
31. Abdulmalek FA, Rajgopal J (2007) Analyzing the benefits of lean manufacturing and value stream mapping via simulation: a process sector case study. Int J Prod Econ 107(1):223–236
32. Carvajal Soto JA, Tavakolizadeh F, Gyulai D (2019). An online machine learning framework for early detection of product failures in an Industry 4.0 context. Int J Comput Integr Manuf 32(4–5):452–465
33. Muchiri PN, Pintelon L, Martin H, Chemweno P (2014) Modelling maintenance effects on manufacturing equipment performance: results from simulation analysis. Int J Prod Res 52(11):3287–3302
34. Pakdil F, Leonard KM (2014) Criteria for a lean organisation: development of a lean assessment tool. Int J Prod Res 52(15):4587–4607
35. Tsarouhas P (2019) Improving operation of the croissant production line through overall equipment effectiveness (OEE) a case study. Int J Product Perform Manag 68(1):88–108
36. Tsarouhas PH (2013) Equipment performance evaluation in a production plant of traditional Italian cheese. Int J Prod Res 51(19):5897–5907
37. Tsarouhas PH (2020) Overall equipment effectiveness (OEE) evaluation for an automated ice cream production line: a case study. Int J Product Perform Manag 69(5):1009–1032
38. Stamatis DH (2017) The OEE primer: understanding overall equipment effectiveness, reliability, and maintainability. CRC Press
39. Groth CHRISTIAN, Kravitz ND, Jones PE, Graham JW, Redmond WR (2014) Three-dimensional printing technology. J Clin Orthod 48(8):475–485
40. Wirth M, Thiesse F (2014) Shapeways and the 3D printing revolution
41. Mok SW, Nizak R, Fu SC, Ho KWK, Qin L, Saris DB, ... Malda J (2016) From the printer: potential of three-dimensional printing for orthopaedic applications. J Orthopaedic Transl 6:42–49
42. Lu L, Guo P, Pan Y (2017) Magnetic-field-assisted projection stereolithography for three-dimensional printing of smart structures. J Manuf Sci Eng 139(7)
43. Ishengoma FR, Mtaho AB (2014) 3D printing: developing countries perspectives. arXiv preprint arXiv:1410.5349

44. Jansen RH, Bowman CL, Clarke S, Avanesian D, Dempsey PJ, Dyson RW (2020) NASA electrified aircraft propulsion efforts. Aircr Eng Aerosp Technol 92(5):667–673
45. Sarlioglu B, Morris CT (2015) More electric aircraft: Review, challenges, and opportunities for commercial transport aircraft. IEEE Trans Transp Electrification 1(1):54–64
46. Javaid M, Haleem A (2018) Additive manufacturing applications in orthopaedics: a review. J Clinical Orthopaedics trauma 9(3):202–206
47. Wang X, Xu S, Zhou S, Xu W, Leary M, Choong P, ... & Xie YM (2016). Topological design and additive manufacturing of porous metals for bone scaffolds and orthopaedic implants: a review. Biomaterials 83:127–141
48. Murr LE, Gaytan SM, Martinez E, Medina F, Wicker RB (2012) Next generation orthopaedic implants by additive manufacturing using electron beam melting. Int J Biomaterials
49. Mahmoud D, Elbestawi MA (2017) Lattice structures and functionally graded materials applications in additive manufacturing of orthopedic implants: a review. J Manuf Mater Process 1(2):13
50. Rajaguru K, Karthikeyan T, Vijayan V (2020) Additive manufacturing–State of art. Mater Today Proc 21:628–633

Chapter 8
Corrosion Performance of Additively Manufactured Metallic Biomaterials: A Review

Davinder Singh, Talwinder Singh, and Sandeep Singh

1 Introduction

AM allows you to build unique and complex structures. Additionally, computer-aided design and direct linking to digital scans enable direct reproducible products. However, choosing the right biomaterials and related AM procedures can be difficult, but it is a vital aspect of success. The aging population, as well as the high prevalence of cardiovascular and orthopedic illnesses, have raised the demand for biological materials [1]. In this chapter, a concise materials' selection guidance has been provided that will be beneficial for the biomedical AM discipline [2]. Following a general description of biomaterial classes (bio resistant, bio-inert, bioactive, and biodegradable), an overview of common ceramic, polymer, and metal biomaterials is discussed along with their implications, as well as their biomedical and mechanical properties. Since the topic of metal implants is rapidly growing, we devote the major portion of review to this area and present some important directions for future research. The present article delivers a summary of the topic under consideration and also consists of corrosion performance of various biomaterials, their applications, and various AM techniques and resources, so there is also the potential to deepen your knowledge of specific aspects [3].

D. Singh (✉) · T. Singh
Department of Mechanical Engineering, Punjabi University, Patiala, Punjab, India
e-mail: davinder5206@yahoo.co.in

S. Singh
Department of Mechanical Engineering, Khalsa College of Engineering and Technology, Amritsar, Punjab, India

A. Mahajan et al. (eds.), *Additive Manufacturing of Bio-implants*, Biomedical Materials for Multi-functional Applications, https://doi.org/10.1007/978-981-99-6972-2_8

2 Literature Review

Human bones have excellent mechanical and structural properties that are suitable for bearing the load of the human body. Despite these characteristics, the human body is prone to fractures caused by injury or sudden accident, fractures caused by fatigue or stress caused by repeated loading conditions, pathological fractures caused by bone infection or tumor, etc. Choosing a specific biological material to replace human bone is a very difficult task [4]. Composed of 30% by weight of matrix, 60% by weight of minerals, and 10% by weight of water, human bones often break due to trauma, pathology, erosion, and other reasons. Subsequent surgery and associated medical expenses are required. Apart from that, various health problems have been observed due to previously used non-magnesium permanent metal implants. Table 1 shows the problems encountered with non-degradable implants in the human body [5].

2.1 Magnesium Alloys

Magnesium (Mg) alloys have developed as encouraging biodegradable materials to be used in orthopedics [6], cardiac [7], respiratory [8], and urology [9]. The major benefit of Mg is that it destroys the organ completely, thus minimizing or preventing long-term complications. Another major benefit in orthopedics is that magnesium has an elastic modulus comparable to bone, by which dangerous effects of stress shielding are reduced. Three firms have so far obtained trial success and regulatory approval. Syntellix got the CE mark for the Magnezix® compression screw in 2013, after selling over 50,000 units [10]. U&i got regulatory approval from the Korean Ministry in 2015 for Resomet, an orthopedic bone screw made of an absorbable MgCa alloy [11]. Biotronik got the CE mark for Magmaris in cardiovascular health in June 2016, making it the first clinically proven bioresorbable magnesium scaffold. [12].

Because of its biocompatibility, magnesium in pure form, a biodegradable and biocompatible metallic substance, has been introduced as a viable material for biodegradable stents. The surrounding environment exposes implants to many corrosive attacks inside the human body, including amino acids in addition to blood,

Table 1 Problems related to non-biodegradable implant [5]

S. no	Problems	Causes
1	Allergic reactions	Patient's specific allergic reaction
2	Inflammatory response	Liberation of metallic ions or wear
3	Implant loosening	Inadequate bonding between bone tissue and implant
4	Bacterial infection	Subjected to further surgery

Table 2 Diversified applications of Magnesium and its alloys [15]

S. no	Field	Applications
1	General uses	Aircraft, Automotive, Armaments, Electronic, Textile, Sports, Medical, and Building industries
2	Medical	Biomedical implants such as bone, plates, screws, cardiovascular stents hip and knee joint implants, etc
3	Aircraft	Gearbox and engine components, gearbox casts, wings, fuselage skin, door, wheels, undercarriage, dashboard panels, and seat components
4	Automobile	Engine and body components, cylinder head covers, frames of seats and sunroofs, pedal brackets, driving wheels,

sodium, chlorine, proteins, blood plasma, and mucins in the case of saliva. A wide base of medical fields including various fields like dentistry, orthopedics, plastic surgery, experimental surgery, and veterinary medicine [13, 14].

Table 2 summarizes the uses of Mg in different fields. A new ternary magnesium alloy (Mg–4Li–1Ca (LC41)) adds two elements, Li and Ca, to magnesium to make it more biodegradable and lightweight for hip and knee applications. This alloy was invented by [15]. Using FEM simulations to compare commercial titanium alloys with Mg–REE alloys and by fabricating them as dynamic compression plates (DCPs) in the condition of distal fractures, the analytical results show that Mg–REE justifies the importance of alloys, due to its lightweight and biodegradability [16, 17].

2.1.1 Corrosion Performance of Mg Alloys

According to Wong et al. [18], magnesium and its alloys exhibit increased corrosion rates and H2 gas accumulation, which is irrefutable in terms of biomedical implant performance. They establish that coating a polymer film on the outer surface of a biomaterial (Mg alloy) processed with polycaprolactone and dichloromethane minimized the corrosion rate and also enhanced the mechanical properties. Kuah et al. [19] conducted a study to know how MgO inclusions affected the corrosion performance of additively produced Mg alloys. Results of this study show a significant difference in corrosion rate of binder jet printing (BJP) samples produced by using AM method in comparison with denser Mg sample that are fabricated by using casting. This is because a greater surface area in a porous structure is inadequate to account for the increased corrosion rate of the additively manufactured samples. Liu et al. [20] used the enhanced passivation effect caused by the inclusion of rare earth (RE) elements to design a high-temperature oxidation treatment to improve the corrosion resistance of WE43 alloy manufactured by additive manufacturing. After 30 days of immersion, the oxidation sample lost just 6.87% of its weight after being heated at 525 °C for 4 h. The greater passivation effect of the inclusive RE elements resulted in improved corrosion resistance due to protection from the dense oxide layer as well as the transition layer, where galvanic reactions were prevented due to the lack of precipitates. Hayashi et al. [21] examined silicate electrolyte (MAO)-based micro-arc oxidation

treatment on the surface of ZK60 magnesium alloy and discovered that it increased corrosion resistance. Gu et al. [22] examined the MAO behavior of Mg–Ca alloys, which showed significant improvement effects on corrosion resistance. It has been determined that the corrosion resistance is improved in the order of 300 V MAO < 400 V MAO < 360 V MAO. Trinidad [23] studied the corrosion patterns of commercial magnesium alloys (AZ31B, WE43, and ZM21) in phosphate-buffered saline and showed the improvement in fluoride environments. In conclusion, it can be said that corrosion rate increases with the immersion time for these three-phase alloys. For AZ31B and ZM 21 alloys, the coating thickness increases with enhanced fluoride treatment time.

2.2 Titanium Alloys

Alloys of titanium are considered favorable implants due to their small elastic modulus and ability to create pathways for bone development. AM technology is now effectively used in the manufacture of porous alloys of titanium due to the advantages of manageable and accurate manufacturing. For long-term uses in the human body, it is critical to understand the corrosion of porous titanium alloys and the underlying mechanisms [24–27]. These alloys have piqued the interest of biomedical researchers because of their great biocompatibility, high specific strength, and low elastic modulus [28, 29]. Titanium alloys show very good corrosion resistance. Nevertheless, the risk of tribo-corrosion, ion deposition, and localized corrosion in physical environments is still high in long-term use, which not only alters the surface properties of titanium alloys but also significantly increases the penetration of corrosive materials into the tissue to give because physical harm around titanium alloy implants [30]. In addition, implant failure inevitably occurs under corrosion fatigue [31], which leads to reduced implant service performance and lifespan, and even requires a second surgery.

2.2.1 Corrosion Performance of Titanium Alloys

The sample with isolated pores in the porous CP–Ti, which has a lower electrochemical potential, is more susceptible to corrosion compared to the sample with interconnected pores. To enhance the corrosion resistance of porous CP–Ti, it might be necessary to optimize the powder metallurgy techniques to ensure a more interconnected pore structure, leading to improved electrochemical behavior and better resistance to corrosion [30]. In summary, the confinement of electrolyte and the limited escape of oxygen in the isolated pores of porous CP-Ti contribute to a higher dissolution rate and reduced formation of the protective passivation film, resulting in increased corrosion susceptibility. Moreover, the porosity and pore size of porous materials are critical factors in determining their biocompatibility, making it important to optimize these characteristics for specific applications, especially in the field

of biomedicine. In conclusion, higher porosity and larger pore size are generally more favorable for bone growth and tissue integration in porous titanium alloys. Moreover, these characteristics might enhance corrosion resistance by promoting better electrolyte penetration and reducing the likelihood of localized oxygen concentration, which can lead to improved performance in certain environments [32, 33].

The study conducted by Seo and Lee [34] focused on analyzing the corrosion resistance of a heat-treated Ti–6Al–4 V alloy fabricated using additive manufacturing (AM) techniques. The researchers employed various electrochemical techniques, including potentiodynamic polarization, electrochemical impedance spectroscopy, and critical pitting temperature measurements, to evaluate the corrosion behavior of the AM Ti–6Al–4 V alloy at different stages of heat treatment. The findings of the study indicated that the corrosion resistance of the AM Ti–6Al–4 V alloy was significantly reduced compared to the untreated material. This reduction in corrosion resistance is likely attributed to the changes in the alloy's microstructure and composition resulting from the heat treatment process.

The study conducted by Ettefagh et al. [35] focused on evaluating the corrosion behavior of Ti–6Al–4 V alloy parts produced through laser-based powder bed fusion AM. The researchers aimed to investigate the effect of post-annealing heat treatment on the corrosion resistance of the AM parts by comparing them with cold-rolled commercial titanium alloy samples. The study highlights that the as-fabricated AM parts of Ti–6Al–4 V alloy exhibited significantly worse corrosion resistance compared to cold-rolled commercial titanium alloy samples due to the presence of non-equilibrium phases. However, a proper post-annealing heat treatment process at 800 °C for 2 h ameliorated the corrosion behavior. In summary, the corrosion properties of porous titanium alloys are influenced by a combination of factors, including phase structure, pore morphology, porosity, alloy composition, and surface treatments. The inherent corrosion resistance of titanium alloys, coupled with their favorable properties in biomedical applications, makes them attractive materials for various uses. To thoroughly assess the corrosion behavior of porous titanium alloys, researchers subject them to accelerated corrosion tests, which help predict their long-term performance in challenging environments [33].

2.3 Stainless Steel Alloys

Stainless steel (SS) alloys are widely used in various industrial applications due to their excellent combination of mechanical properties, corrosion resistance, and versatility. Different types of stainless steel alloys, classified based on their microstructure, include austenitic, martensitic, ferritic, and duplex (austenoferritic) stainless steels [31]. The microstructure of stainless steel is determined by its chemical composition, particularly the levels of chromium, nickel, carbon, and other alloying elements [36]. By carefully controlling the composition and content of these alloying elements, stainless steel manufacturers can tailor the properties of the alloy to meet specific application requirements [37]. Stainless steel, particularly grade 316L stainless steel,

has gained significant popularity in the medical field for various reasons, including its excellent mechanical properties, wide availability, and outstanding corrosion resistance at a reasonable cost. Due to these favorable attributes, 316L stainless steel is widely used in various medical implant devices, such as orthopedic implants (e.g., hip and knee replacements), vascular stents, bone fixation plates, dental implants, and surgical instruments [38, 39]. Indeed, the electrochemical reactions that occur inside the human body can lead to corrosion of metallic parts, including medical implants and devices. Corrosion is a critical concern in biological applications because it can have several significant implications [40]. For example, Stents made from SS 316L can release metal ions, including molybdenum (Mo), chromium (Cr), and nickel (Ni), into the surrounding tissues due to the electrochemical reactions and corrosion processes. The release of these metal ions can lead to limited immune and inflammatory responses in some individuals [41]. All of these can affect the quality of life of the transplant recipient, and failure can lead to severe pain and postoperative surgery [42].

2.3.1 Corrosion Performance of SS Alloys

In general, pores are a favorable location for corrosive attack, especially pitting. AM as a powder-based manufacturing method involves the inevitable presence of porosity in fabricated parts, which can affect mechanical properties and corrosion performance [33, 43]. Pores usually appear around unmelted powder particles or are created by gases trapped in the powder or molten pool during primary processing such as gas atomization or laser melting processes. In the context of AM parts, elemental mapping of voids involves analyzing the composition of the voids or pores present in the material [44]. Austenitic stainless steels, such as 316L and 304L, are susceptible to pitting corrosion, and the presence of unwanted inclusions, particularly manganese sulfide (MnS), can significantly influence their corrosion performance. These inclusions act as a second phase within the austenitic matrix and play a critical role in initiating and promoting pitting corrosion. By minimizing the presence of MnS inclusions or adjusting their size, the susceptibility to pitting corrosion and other localized forms of corrosion can be reduced [45, 46]. Surface roughness is a critical parameter that significantly influences the corrosion behavior of AM components. As an inherent characteristic of AM processes, the surface roughness of the printed parts can vary based on the printing method, material, and processing parameters. The presence of rough surfaces can accelerate electrochemical reactions between the component's surface and the surrounding environment, leading to both general and localized corrosion [47, 48]. Grain size is also an essential factor that can significantly affect the corrosion performance of SS, and its influence depends on the specific corrosive environment. The size of the grains in the microstructure of stainless steel can influence the stability of the passive film and the susceptibility to corrosion [49, 50]. At the same time, some studies demonstrate that while reducing the grain size to the nanoscale range can enhance some properties of stainless steel, including mechanical strength and certain types of corrosion resistance, there are also potential challenges

associated with nanocrystalline structures, particularly concerning the stability of the passive film. [51]. The effect of grain size on the corrosion performance of additively manufactured SS can indeed be a topic of controversy in the literature. The conflicting results are often attributed to the complexity of the interactions between various factors that influence corrosion behavior in AM SS materials.

3 Conclusions

This chapter reviews the additive manufacturing techniques used for printing magnesium, titanium and stainless steel. The primary emphasis is on biodegradable implants made from magnesium, as well as the challenges associated with its reactivity, high surface energy of the powder, and the rapid corrosion observed in the human body due to the alloy's high electronegativity. For magnesium implant alloys to be viable, they must possess sufficient mechanical strength, biocompatibility, and corrosion resistance, along with consistent rates of tissue healing. While these challenges initially hindered the development of biodegradable magnesium implants, the field of AM is steadily overcoming these obstacles through various approaches. Regarding titanium alloys, the chapter highlights the significance of additives in influencing their preparation and corrosion properties. The corrosion behavior of biomedical titanium alloys is complex and influenced by several factors, including alloy composition, surface properties, and pore properties. These factors must be carefully considered when designing medical metal implants to ensure optimal performance and long-term functionality. At present, the corrosion performance of titanium alloys is still poor. In addition, stainless steel components are developed with a focus on corrosion performance in a wide range of applications where high corrosion considerations are required, such as the biomedical, nuclear, and fuel cell industries. In summary, the development of metallic biomaterial implants is an area with much room for exploration and innovation.

References

1. Chen Y, Xu Z, Smith C, Sankar J (2014) Recent advances on the development of magnesium alloys for biodegradable implants. Acta Biomater 10(1):4561–4573
2. Staiger AM, Pietak J, Huadmai G, Dias (2008) Magnesium and its alloys as orthopedic biomaterials: a review. Biomaterials 27:1728–1734
3. Witte F, Hort N, Vogt C, Cohen S, Kainer KU, Willumeit R, Feyerabend F (2008) Degradable biomaterials based on magnesium corrosion. Curr Opin Solid State Mater Sci 12:63–72
4. Xin Y, Hu T, Chu PK (2011) In vitro studies of biomedical magnesium alloys in a simulated physiological environment: a review. Acta Biomater 7:1452–1459
5. Erdmann N, Bondarenko A, Hewicker-Trautwein M, Angrisani, Reifenrath J, Lucas A, Meyer-Lindenberg A (2010) Evaluation of the soft tissue biocompatibility of MgCa0.8 and surgical steel 316L in vivo: a comparative study in rabbits. Biomed Eng Online 9:63

6. Castellani C, Lindtner RA, Hausbrandt P, Tschegg E, Stanzl-Tschegg SE, Zanoni G, Beck S, Weinberg A (2011) Bone–implant interface strength and osseointegration: biodegradable magnesium alloy versus standard titanium control. Acta Biomater 7:432–440
7. Henderson SE, Verdelis K, Maiti S, Pal S, Chung WL, Chou D, Kumta PN, Almarza AJ (2014) Magnesium alloys as a biomaterial for degradable craniofacial screws. Acta Biomater 10:2323–2332
8. Waizy H, Diekmann J, Weizbauer A, Reifenrath J, Bartsch I, Neubert V, Schavan R, Windhagen H (2014) In vivo study of a biodegradable orthopedic screw (MgYREZr-alloy) in a rabbit model for up to 12 months. J Biomater Appl 28:667–675
9. Huehnerschulte TA, Reifenrath J, Rechenberg BV, Dziuba D, Seitz J, Bormann D, Windhagen H, Meyer-Lindenberg A (2012) In vivo assessment of the host reactions to the biodegradation of the two novel magnesium alloys ZEK100 and AX30 in an animal model. Biomed Eng Online 11:14
10. Sealy MP, Guo YB, Liu JF, Li C (2016) Pulsed laser cutting of magnesium-calcium for biodegradable stents. Procedia CIRP 42:67–72
11. Charpentier E, Barna A, Guillevin L, Juliard J (2015) Fully bioresorbable drug-eluting coronary scaffolds: a review. Arch Cardiovasc Dis 108:385–397
12. Iqbal J, Onuma Y, Ormiston J, Abizaid A, Waksman R, Serruys P (2014) Bioresorbable scaffolds: rationale, current status, challenges, and future. Eur Heart J 35:765–776
13. Di Mario C, Griffiths H, Goktekin O, Peeters N, Verbist J, Bosier M, Deloose K, Heublein B, Rohde R, Kasese V, Ilsley C, Erbel R (2004) Drug-Eluting bioabsorbable magnesium stent. J Interv Cardiol 17:391–395
14. Peeters P, Bosiers M, Verbist J, Deloose K, Heublein B (2005) Preliminary results after application of absorbable metal stents in patients with critical limb ischemia. J Endovasc Ther 12:1–5
15. Chalisgaonkar R (2020) Insight in applications, manufacturing and corrosion behaviour of magnesium and its alloys—a review. Mater Today Proc 26:1060–1071
16. Waksman R, Erbel R, Di Mario C, Bartunek J, de Bruyne B, Eberli FR, Erne P, Haude M, Horrigan M, Ilsley C, Böse D, Bonnier H, Koolen J, Lüscher TF, Weissman NJ (2009) Early- and long-term intravascular ultrasound and angiographic findings after bioabsorbable magnesium stent implantation in human coronary arteries. JACC Cardiovasc Interv 2:312–320
17. Hermawan H, Dubé D, Mantovani D (2010) Degradable metallic biomaterials: design and development of Fe-Mn alloys for stents. J Biomed Mater Res 1–11 Part A 93A
18. Wong HM, Yeung KWK, Lam KO, Tam V, Chu PK, Luk KDK, Cheung KMC (2010) A biodegradable polymer-based coating to control the performance of magnesium alloy orthopedic implants. Biomaterials 31:2084–2096
19. Kuah KX, Salehi M, Ong WK, Seet HL, Nai MLS, Wijesinghe S, Blackwood DJ (2022) Insights into the influence of oxide inclusions on corrosion performance of additive manufactured magnesium alloys. NPJ Mater Degradation 36:1–10
20. Liu J, Yin B, Song F, Liu B, Peng B, Wen P, Tian Y, Zheng Y, Ma X, Wang C (2022) Improving corrosion resistance of additively manufactured WE43 magnesium alloy by high temperature oxidation for biodegradable applications. J Magnesium Alloys, 1–14
21. Lin X, Tan L, Zhang Q (2013) The in vitro degradation process and biocompatibility of a ZK60 magnesium alloy with a forsterite-containing micro-arc oxidation coating. Acta Biomater 9:8631–8642
22. Gu XN, Li N, Zhou WR (2011) Corrosion resistance and surface biocompatibility of a microarc oxidationcoating on a Mg–Ca alloy. Acta Biomater 7:1880–1889
23. Trinidad J, Arruebarrena G, Marco I, Hurtado I, Argandoña E (2013) Effectivity of fluoride treatment on hydrogen and corrosion product generation in temporal implants for different magnesium alloys. Proc IMechE. Part H: J Eng Med 227(12):1301–1311
24. Luffy SA, Chou D, Waterman J, Wearden PD, Kumta PN, Gilbert TW (2014) Evaluation of magnesium-yttrium alloy as an extraluminal tracheal stent. J Biomed Mater Res A 102:611–620
25. Jang Y, Owuor D, Waterman JT, White L, Boyce C, Sankar J, Gilbert TW, Yun Y (2014) Effect of mucin and bicarbonate ion on corrosion behavior of AZ31 magnesium alloy for airway stents. Materials 7:5866–5882

26. Zhang S, Zheng Y, Zhang L, Bi Y, Li J, Liu J, Guo H, Li Y (2016) In vitro and in vivo corrosion and histocompatibility of pure Mg and a Mg-6Zn alloy as urinary implants in rat model. Mater Sci Eng C 68:414–422
27. Li SJ, Li XK, Hou WT (2018) Fabrication of open cellular (porous) titanium alloy implants: osseointegration, vascularization and preliminary human trials. Sci China Mater 61(4):525–536
28. Fojt J, Joska L, Malek J (2013) Corrosion behavior of porous Ti-39Nb alloy for biomedical applications. Corros Sci 2013(71):78–83
29. He XC, Li Y, Bi YJ (2020) Finite element analysis of temperature and residual stress profiles of porous cubic Ti-6Al-4V titanium alloy by electron beam melting. J Mater Sci Technol 44:191–200
30. Lee JTY, Leng Y, Chow KL (2011) Cell culture medium as an alternative to conventional simulated body fluid. Acta Biomater 7(6):2615–2622
31. Garcia-Ramirez MJ, Lopez-Sesenes R, Rosales-Cadena I (2018) Corrosion behaviour of Ti–Ni–Al alloys in a simulated human body solution. J Market Res 7(3):223–230
32. Yehia HM, El-Tantawy A, Ghayad IM (2020) Effect of zirconia content and sintering temperature on the density, microstructure, corrosion, and biocompatibility of the Ti-12Mo matrix for dental applications. J Market Res 9(4):8820–8833
33. Buciumeanu M, Bagheri A, Shamsaei N (2018) Tribocorrosion behavior of additive manufactured Ti-6Al-4V biomedical alloy. Tribol Int 119:381–388
34. Seo DI, Lee JB (2020) Influence of heat treatment parameters on the corrosion resistance of additively manufactured Ti–6Al–4V alloy. J Electrochem Soc 167:1–18
35. Ettefagh AH, Zeng C, Guo S, Raush J (2019) Corrosion behavior of additively manufactured Ti-6Al-4V parts and the effect of post annealing. Addit Manuf 28:252–258
36. Olsson CO, Landolt D (2003) Passive films on stainless steels—chemistry, structure and growth. Electrochim Acta 48:1093–1104
37. Sander G, Thomas S, Cruz V, Jurg M, Birbilis N, Gao S, Brameld M, Hutchinson C (2017) On the corrosion and metastable pitting characteristics of 316L stainless steel produced by selective laser melting. J Electrochem Soc 164:C250–C257
38. Murr LE, Martinez E, Hernandez J, Collins S, Amato KN, Gaytan SM, Shindo PW (2012) Microstructures and properties of 17–4 PH stainless steel fabricated by selective laser melting. J Market Res 1:167–177
39. Mazumder J, Choi J, Nagarathnam K, Koch J, Hetzner H (1997) The direct metal deposition of H13 tool steel for 3-D components. Jom 49:55–60
40. Schaller RF, Taylor JM, Rodelas J, Schindelholz EJ (2017) Corrosion properties of powder bed fusion additively manufactured 17–4 PH stainless steel. Corrosion 73:796–807
41. Sun Y, Moroz A, Alrbaey K (2014) Sliding wear characteristics and corrosion behaviour of selective laser melted 316L stainless steel. J Mater Eng Perform 23:518–526
42. Laleh M, Hughes AE, Xu W, Cizek P, Tan MY (2020) Unanticipated drastic decline in pitting corrosion resistance of additively manufactured 316L stainless steel after high-temperature post-processing. Corros Sci 165:108412
43. Trelewicz JR, Halada GP, Donaldson OK, Manogharan G (2016) Microstructure and corrosion resistance of laser additively manufactured 316L stainless steel. Jom 68:850–859
44. Arifvianto B, Mahardika M, Dewo P, Iswanto P, Salim U (2011) Effect of surface mechanical attrition treatment (SMAT) on microhardness, surface roughness and wettability of AISI 316L. Mater Chem Phys 125:418–426
45. Roland T, Retraint D, Lu K, Lu L (2006) Fatigue life improvement through surface nanostructuring of stainless steel by means of surface mechanical attrition treatment. Scripta Mater 54:1949–1954
46. Jirandehi AP, Mehdizadeh M, Khonsari M (2020) Temperature-induced buckling of ductile metals during cyclic loading and the subsequent early fracture. Int J Mech Sci 176:105525
47. Van Boven G, Chen W, Rogge R (2007) The role of residual stress in neutral pH stress corrosion cracking of pipeline steels. Part I Pitting Cracking Occurrence Acta Materialia 55:29–42
48. Ornek C (2018) Additive manufacturing–a general corrosion perspective. Corros Eng Sci Technol 53:531–535

49. Buchbinder D, Meiners W, Pirch N, Wissenbach K, Schrage J (2014) Investigation on reducing distortion by preheating during manufacture of aluminum components using selective laser melting. J Laser Appl 26:012004
50. Zaeh MF, Branner G (2010) Investigations on residual stresses and deformations in selective laser melting. Prod Eng Res Devel 4:35–45
51. Zuo Y, Wang H, Xiong J (2002) The aspect ratio of surface grooves and metastable pitting of stainless steel. Corros Sci 44:25–35

Chapter 9
Emerging Functionally Graded Materials for Bio-implant Applications—Design and Manufacturing

Rakesh Kumar and Anupam Agrawal

1 Introduction

Human body architecture has several joints and connections contributing to its efficient functioning. Any damaged part must be replaced with an artificial or synthetic look-a-like part called a "Bio-Implant" [1]. As per the report published in 2018 [2] on bio-implant market analysis, its global market size was USD 65 Billion at a CAGR of 5.90%, which has tremendously increased in the latest report of 2022 [3] to USD 117.3 Billion and expected to raise upto USD 126.7 Billion by 2032 at a whooping CAGR of 10.00% during this time. This tremendous surge in implant market size exhibits the high demand for implant and implant surgeries caused due to accidents, sports injuries, severe health issues, etc. This demand for bio-implants has opened up a gateway for many research, start-up, and biomedical industries related to innovative designing, fabrication techniques, and development of advanced materials with enhanced mechanical, structural, and biological properties (Fig. 1).

With the increasing scientific and technological advancements, the quality and capability of these artificial implants are also increasing regularly. There are two crucial factors for the development of bio-implants, (a) the proper selection of biomaterial and (b) the proper selection of fabrication method [4, 5]. An ideal implant material should be durable, easily moldable, and, more importantly, biocompatible, allowing easy tissue growth. So, the process of tissue engineering starts with proper biomaterial selection, followed by the fabrication of implants. Recently, AM processes have somehow solved the fabrication issues with their unparalleled degrees of freedom (design, material, hierarchical structure, etc.) to fabricate any complex 3D

R. Kumar · A. Agrawal (✉)
Advanced Manufacturing Technology Lab, Department of Mechanical Engineering, Indian Institute of Technology Ropar, Rupnagar, Punjab 140001, India
e-mail: anupam@iitrpr.ac.in

A. Mahajan et al. (eds.), *Additive Manufacturing of Bio-implants*, Biomedical Materials for Multi-functional Applications, https://doi.org/10.1007/978-981-99-6972-2_9

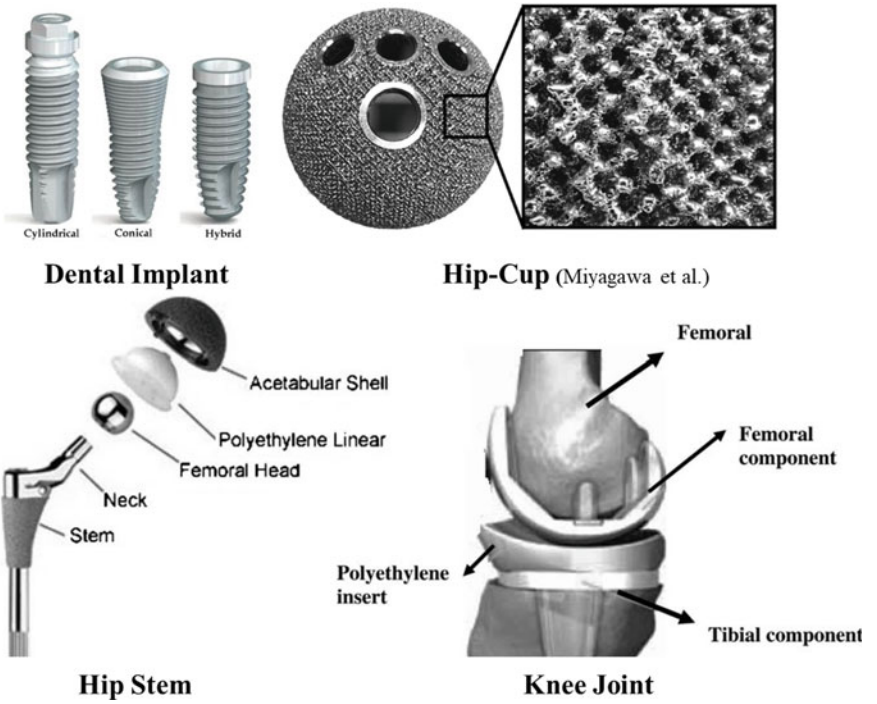

Fig. 1 Examples of a few commercial implants [6]

geometry using just a CAD model [7, 8]. The concept of design for additive manufacturing (DfAM) is becoming revolutionary in modifying and obtaining optimized designs with better functionality.

The existing mono-material-based implants are somehow inefficient because of their mechanical properties and bioactivity behavior, and they sometimes cause toxicity due to the release of toxic particles/debris during use. Stress shielding occurs due to the more significant mismatch in mechanical properties in the case of metallic and high-load-bearing ceramic or polymeric material, which further causes the deterioration of existing bone and surrounding tissues. The main concern with an implant is its response to the tissue and its proper functioning. Recent advancements in biocompatible materials and design that mimic the actual bone architecture have shown minimization in these negative responses during its functionality [9]. Different materials (generally used for orthopedic implants, i.e., titanium, stainless steel, CoCr, etc.) have higher modulus and stiffness than natural bones. This significant deviation alters the stress distribution in normal physiological conditions after implantation thus contributing to damage to surrounding body parts [10]. To address the issues of mechanical properties of artificial implants, an innovative material needs to be designed that can have functional properties according to the requirement. Looking into the problems raised due to more significant differences in mechanical behavior

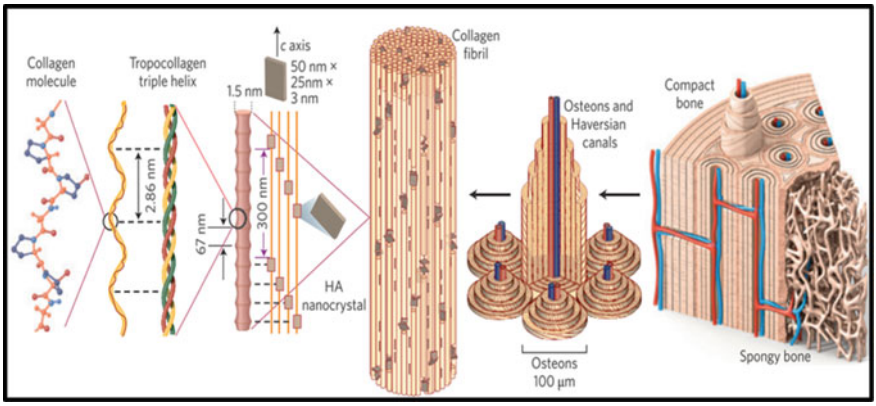

Fig. 2 Hierarchical graded structure of bone [13]

and the need for functional properties, functionally graded materials (FGMs) emerge as the best viable solution to both issues. FGMs are specially designed materials with gradient tailoring properties [11]. Japanese researchers initially developed FGMs in 1984 as a thermal barrier in spacecraft to counter excessive temperature differences in an aircraft during its flight time. The tailored design and mechanical behavior within a bulk system can be obtained by distributing the material and porosity in a gradient manner. Thus, the actual bone structure (Fig. 2) can be mimicked with the combined mechanical behavior of cortical and cancellous/spongy bone. The implants with graded material or unit cell-based cellular structure can also be the best alternative design to minimize stress-shielding issues [12].

2 Biomaterials

Different materials, from polymers and ceramics to metals, have found their applications as bio-implant materials for replacing different body parts, depending upon their material characteristics and bioactivity [14–16]. Various lightweight polymers such as Polylactic acid (PLA) and Polycaprolactone (PCL) are used as tissue replacements to treat wounds and as a scaffold to support other organs. Ceramics are primarily used for dental implants and as a scaffold to support high-load-bearing body parts. Similarly, metals are used primarily to replace high-load-bearing implants and manufacture biomedical devices for surgeries. State-of-the-art literature suggests many metal-matrix composites emerge as a better alternative to metallic biomaterials with enhanced mechanical and bioactivity behavior (Table 1).

Table 1 List of widely popular biomaterials that can be used to design and fabricate FGMs with their extensive properties and appropriate applications

Material and alloy	Mechanical property	Biological property	Applications
Titanium (Ti)	E- 100–110 GPa ρ- 4.5 g/cc	Biocompatible	Femur, Hip Cup, Dental Implants
Ti6Al4V alloy	E—100–115 GPa ρ—4.4 g/cc	Biocompatible	Femur, Hip Cup, Dental Implants
Iron (Fe)	E—210 GPa ρ—7.87 g/cc	Biodegradable	Implant Fixation and Medical Devices
SS 316L	E—190 GPa ρ—8.0 g/cc	Biocompatible	Implant Fixation and Medical Devices, Hip Cup, Maxillofacial Implant
CoCr	E—240 GPa ρ—8.5 g/cc	Biocompatible	Stent, Medical Devices
Magnesium (Mg)	E—45 GPa ρ—1.74 g/cc	Biodegradable	Scaffolds, bone-supporting implant
Tantalum (Ta)	E—180-185 GPa ρ—16.65 g/cc	Bioactive	High-load bearing Implants
Polylactic Acid (PLA)	E—3–3.5 GPa ρ—1.24 g/cc	Biodegradable	Cardiovascular Stents
Polycaprolactone (PCL)	E—3.2–3.7 GPa ρ—1.14 g/cc	Biodegradable	Scaffolds
Hydroxyapatite (HAp)	E—80–100 GPa ρ—3.16 g/cc	Biocompatible	Dental, Scaffolds
Calcium Phosphate (CaP)	E—80–100 GPa ρ—3.14 g/cc	Biocompatible	Dental, Scaffolds

3 Classification of FGMs

FGM is a new class of non-homogenous composite with a graded pattern of material, porosity, and microstructure to attain tailored properties depending upon the requirement. This material constituent/properties tailoring may be gradual or stepwise within the domain [17]. The FGMs have found their acceptability in numerous industrial applications, such as providing a thermal barrier in thermal power plants, lightweight and heat resistance in aerospace applications, automobile, and packaging. The FGMs are classified into three main categories depending on their applications and needs, as shown in Figure 3.

An FGM with gradient material or chemical composition is designed and fabricated by the varying composition of the material in a particular direction to obtain the desired variation in mechanical, thermal, or physical properties. Similarly, microstructure also plays a vital role in determining mechanical behavior at the macro level. Hence, the microstructure-based gradient can be obtained by varying

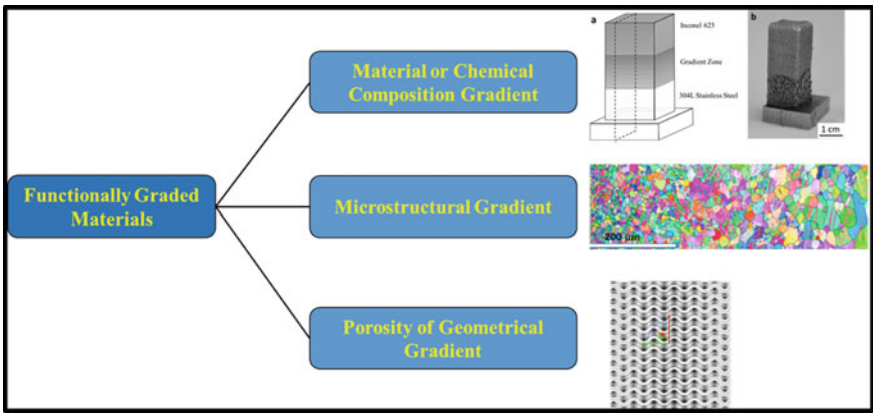

Fig. 3 Classification of FGMs

the localized processing and post-processing condition to achieve desired properties in specific regions of any material. In bulk materials, the density of the material significantly affects mechanical behavior. Thus, by varying the density in a bulk material by inducing porosity in a gradient manner, porosity or geometrically gradient FGMs can be designed [18].

4 Design of Functionally Graded Porous Scaffolds

The scaffolds are basic structures that support or fill the gap between the two damaged bone parts. The scaffold design should mimic the actual bone architecture to allow the actual functioning of the part, such as the circulation of body fluid and blood plasma through it. Porous structures in biomedical Implants attract extensive interest from researchers as they can reduce the modulus mismatch and facilitate long stable life employing full bone ingrowth. Thus Functionally Graded (FG) porous scaffolds are introduced, which can minimize the stress-shielding effects in the implant area [19]. Different unit cell-based, TPMS, fractal geometry, etc., based repetitive structure-based architectures are used to design scaffolds with varying porosity distribution, changing the density along particular directions [20] (as shown in Fig. 4). While developing such a porous scaffold, the essential thing that needs to be considered is that the pores should be interconnected throughout the scaffold, providing enough space for cell culture and transportation of body fluids that carry the requisite protein and minerals needed for cell growth. One of the significant objectives for providing porosity in the scaffold is to allow an effective proliferation of cells or tissue with respect to time and heal the damaged part. The porous scaffolds and bone parts can also be mimicked by imaging, CAD designing, and reconstructing the damaged body parts [21].

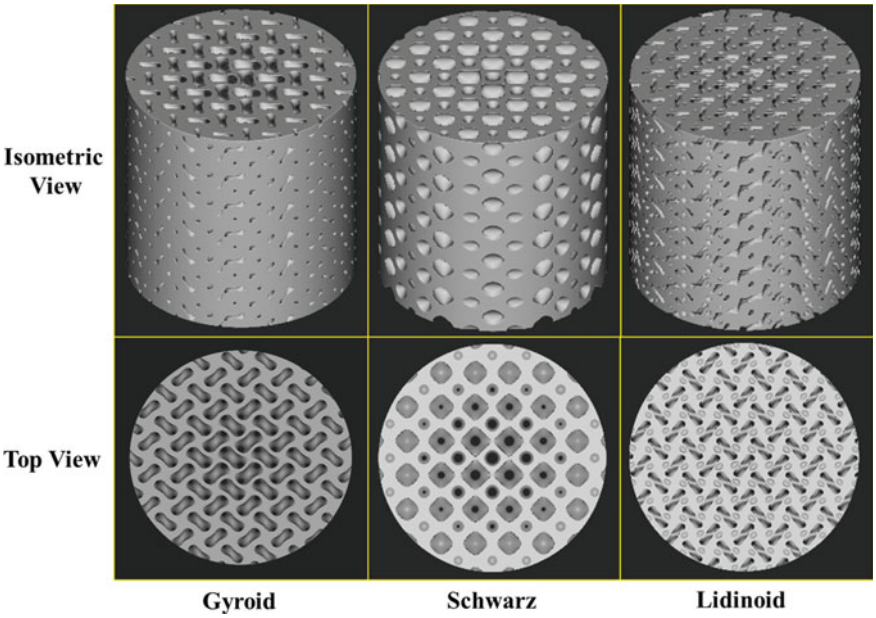

Fig. 4 Various unit cells based on functionally graded porous scaffold architecture having interconnected pores with radially varying density

5 Fabrication of FGMs

Material with functionally graded coating and layering are being made using plasma spraying, thermal spraying, Chemical vapor deposition (CVD), etc. The bulk FGMs with tailorable material properties are conventionally fabricated using centrifugal casting [17, 22]. However, the limitation of the process is that it can only manufacture shell or cylindrical FGM parts. The development of layered manufacturing processes has been considered a breakthrough for effectively fabricating bulk FGMs. Layer-based manufacturing processes allow the addition of new layer material at the requisite position with a suitable combination of material and process parameters. All the existing additive manufacturing processes can easily fabricate porosity-based graded material structures with the input of required CAD geometry. However, material-based graded FGMs can be manufactured using Direct Energy Deposition (DED) (Fig. 5), Laser Engineered Net Shaping (LENS), and Selective Laser Melting/Sintering (SLM/SLS) processes. Polymer-based graded implants and scaffolds can be manufactured using extrusion-based free-form technique (fused deposition modeling) and Stereolithography (SLA) techniques. Polymer-based implants are relatively cheaper but have less lifespan because of their high degradation rate under physiological medium.

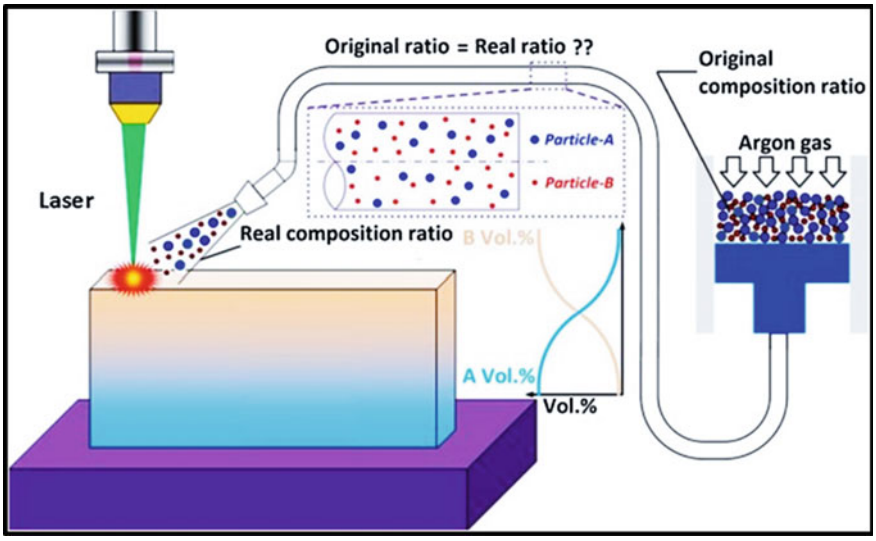

Fig. 5 Schematic illustration of the fabrication of FGM by LMD process [23]

6 Properties of a Bio-Implant Material

A bio-implant should have different properties so that it can be readily acceptable, i.e.,

- Physical and Mechanical properties;
- Chemical and Elemental properties;
- Surface properties;
- Biological characteristics.

6.1 Physical and Mechanical Properties

An implant should have good mechanical properties as per its applications with different loading conditions. Depending upon loading conditions, implants are classified into two categories, i.e., high-load-bearing implants (e.g., hip-cup, femur replacement, knee implant, etc.) and low-load-bearing implants (e.g., dental implant, maxillofacial implant, etc.). High load-bearing bones possess different structural and mechanical characteristics along their cross section; hence, an implant must have tailored material, porosity, and mechanical characteristics to replace such body parts. This tailoring may not only mimic the actual bone architecture and structural behavior; instead, using suitable material can somehow resolve the stress-shielding issue between the implant and existing surrounding bone and tissues. Usually, cortical

bone and cancellous bone have a modulus of 3.9–12 GPa and 0.1–2 GPa, respectively. The light metallic biomaterial, i.e., magnesium, has 45 GPa, larger than the natural cortical bone. That's why stress shielding occurs when a pure metallic implant has been placed inside a human body due to a significant mismatch in mechanical behavior. Hence, live tissue and bone start deteriorating to cause bone loss. The stress-shielding causes loss in bone density and aseptic loosening, increasing the chances of periprosthetic fracture [24].

6.2 Chemical and Elemental Properties

The chemical composition, specifically polymer-based implants, is significant as their monomers should not be toxic; thus, it does not affect the usual functioning. The chemicals/elements that allow appetite formation under physiological conditions are always considered to be suitable to be used as implant materials. The Ca:P ratio is another important factor determining whether the material is good enough to allow cell culture and bone repair [25]. The Ca:P ratio should be 1.6 for adequate cell culture conditions, specifically in phosphate-based materials.

6.3 Surface Properties

Surface morphology, wear, friction, hardness, etc., are various properties that define an implant's surface characteristics. The surface hardness and composition evenly contribute to wear characteristics. Tribological tests are performed to estimate the type of wear, wear rate, and contact properties. The surface of an implant should have enough roughness and pores so tissues can adhere properly and proliferate over it. The surface should resist corrosion so that it doesn't get degraded easily. Hence, different laser and heat treatments can be performed over the metallic implants to enhance corrosion resistance.

7 Biocompatibility

Bioceramics are the vital mineral component of hard tissue body parts such as bones, and their reinforcement with biocompatible metallic material enhances the bioactivity of the composite [26]. Hence, material-based FGMs consisting of metal and bioceramic can be more profound with tissue growth, allowing other biological activity. Similarly, porosity-based FGMs can mimic the natural bone architecture. They thus will provide sufficient interconnected pore and pore density to allow cell/tissue to

adhere and proliferate over time. Few biodegradable polymers and metal-ceramic-based FGMs can be used to self-heal and grow new tissue and replace the damaged parts over time.

Tailoring the mechanical behavior of the implant's constituent can improve the implant's overall properties by effectively reducing the stress-shielding with enhanced bioactivity properties. Hence, FGM-based implants can be advantageous for biomedical surgeries and industries.

References

1. Van Eck CF, Chen AF, Klatt BA et al (2009) The classification of implants: class I, II, III. J Long Term Eff Med Implants 19:185–193. https://doi.org/10.1615/JLongTermEffMedImplants.v19.i3.30
2. Global Bio-implant Market Size, Share | Industry Report, 2019-2026
3. Bio-implants Market Size, Share, Outlook & Trends—2023 | FMI
4. Saini M (2015) Implant biomaterials: a comprehensive review. World J Clin Cases 3:52. https://doi.org/10.12998/wjcc.v3.i1.52
5. Stephen JDG, Kumar GL, Vinesh R, Vikram G (2017) Bio implant materials: requirements, types -and properties– a review, 18–26
6. Geetha M, Singh AK, Asokamani R, Gogia AK (2009) Ti based biomaterials, the ultimate choice for orthopaedic implants—a review. Prog Mater Sci 54:397–425. https://doi.org/10.1016/j.pmatsci.2008.06.004
7. Dilberoglu UM, Gharehpapagh B, Yaman U, Dolen M (2017) The role of additive manufacturing in the era of industry 4.0. Procedia Manuf 11:545–554. https://doi.org/10.1016/j.promfg.2017.07.148
8. Ho CMB, Ng SH, Yoon YJ (2015) A review on 3D printed bioimplants. Int J Precis Eng Manuf 16:1035–1046. https://doi.org/10.1007/s12541-015-0134-x
9. Onuki Y, Bhardwaj U, Papadimitrakopoulos F, Burgess DJ (2008) A review of the biocompatibility of implantable devices: current challenges to overcome foreign body response. J Diabetes Sci Technol 2:1003–1015. https://doi.org/10.1177/193229680800200610
10. Staiger MP, Pietak AM, Huadmai J, Dias G (2006) Magnesium and its alloys as orthopedic biomaterials: a review. Biomaterials 27:1728–1734. https://doi.org/10.1016/j.biomaterials.2005.10.003
11. Miyamoto Y, Kaysser WA, Rabin BH, et al (1999) Functionally graded materials design, processing and applications. Springer Science+ Business Media New York
12. Limmahakhun S, Oloyede A, Sitthiseripratip K et al (2017) Stiffness and strength tailoring of cobalt chromium graded cellular structures for stress-shielding reduction. Mater Des 114:633–641. https://doi.org/10.1016/j.matdes.2016.11.090
13. Wegst UGK, Bai H, Saiz E et al (2014) (2014) Bioinspired structural materials. Nat Mater 141(14):23–36. https://doi.org/10.1038/nmat4089
14. Bergström JS, Hayman D (2016) An overview of mechanical properties and material modeling of polylactide (PLA) for medical applications. Ann Biomed Eng 44:330–340. https://doi.org/10.1007/s10439-015-1455-8
15. Oh S, Oh N, Appleford M, Ong JL (2006) Bioceramics for tissue engineering applications—a review. Am J Biochem Biotechnol 2:49–56. https://doi.org/10.3844/ajbbsp.2006.49.56
16. Hermawan H (2012) Biodegradable metals: state of the art. Biodegradable Metals. Springer, New York, pp 13–22
17. El-Galy IM, Saleh BI (2019) Ahmed MH (2019) Functionally graded materials classifications and development trends from industrial point of view. SN Appl Sci 111(1):1–23. https://doi.org/10.1007/S42452-019-1413-4

18. Shi H, Zhou P, Li J et al (2021) Functional gradient metallic biomaterials: techniques, current scenery, and future prospects in the biomedical field. Front Bioeng Biotechnol 8:1510. https://doi.org/10.3389/FBIOE.2020.616845/BIBTEX
19. Parthasarathy J, Starly B, Raman S (2011) A design for the additive manufacture of functionally graded porous structures with tailored mechanical properties for biomedical applications. J Manuf Process 13:160–170. https://doi.org/10.1016/j.jmapro.2011.01.004
20. Liu F, Mao Z, Zhang P et al (2018) Functionally graded porous scaffolds in multiple patterns: new design method, physical and mechanical properties. Mater Des 160:849–860. https://doi.org/10.1016/J.MATDES.2018.09.053
21. Sun W, Starly B, Nam J, Darling A (2005) Bio-CAD modeling and its applications in computer-aided tissue engineering. CAD Comput Aided Des 37:1097–1114. https://doi.org/10.1016/j.cad.2005.02.002
22. Naebe M, Shirvanimoghaddam K (2016) Functionally graded materials: a review of fabrication and properties. Appl Mater Today 5:223–245. https://doi.org/10.1016/j.apmt.2016.10.001
23. Li W, Karnati S, Zhang Y, Liou F (2018) Investigating and eliminating powder separation in pre-mixed powder supply for laser metal deposition process. J Mater Process Technol 254:294–301. https://doi.org/10.1016/J.JMATPROTEC.2017.11.045
24. Raffa ML, Nguyen V, Hernigou P et al (2021) Stress shielding at the bone-implant interface: influence of surface roughness and of the bone-implant contact ratio. J Orthop Res 39:1174–1183. https://doi.org/10.1002/jor.24840
25. Hou X, Zhang L, Zhou Z et al (2022) Calcium phosphate-based biomaterials for bone repair. J Funct Biomater 13:187. https://doi.org/10.3390/jfb13040187
26. Watari F, Yokoyama A, Omori M et al (2004) Biocompatibility of materials and development to functionally graded implant for bio-medical application. Compos Sci Technol 64:893–908. https://doi.org/10.1016/j.compscitech.2003.09.005

Chapter 10
Biomechanical Evaluation of Load Transfer and Stability in a Corrugated Hip Stem: A Comparative Analysis

Vivek Gupta, Gurpreet Singh, and Arnab Chanda

1 Introduction

Total hip replacement (THR) has become increasingly common in orthopedics over the past two decades. Typically, THR is performed on individuals over the age of 50 with a body mass index (BMI) above 25 [1–3]. According to research data, it is projected that the annual number of total hip arthroplasty procedures will increase significantly, reaching 498,000 replacements by 2020 (a 34% increase), 652,000 replacements by 2025 (a 75% increase), 850,000 replacements by 2030 (a 129% increase), and 1,429,000 replacements by 2040 (a 284% increase) [4, 5]. Total hip and total knee arthroplasty trends are comparable, with women and people aged 45–64 and 65–84 having a somewhat higher frequency [4, 5]. An estimated 300,000 hip replacement procedures are performed annually in the United States alone [6]. The need for hip replacement arises from various conditions such as osteoarthritis, rheumatoid arthritis, post-traumatic arthritis, and osteonecrosis [3, 7]. Despite the significant challenge of managing postsurgical pain, the success rates of THR across different ethnicities are relatively low, particularly due to medical implant failures within the first 18 months [8]. A THR implant's typical lifespan is anticipated to be around 10–15 years, necessitating many hip replacement surgeries over the course of a patient's lifetime, particularly in younger individuals [7, 9].

A healthy hip joint has a ball and socket mechanism in which the femoral head rotates within the acetabulum (socket). Figure 1 illustrates the different components of the hip joint anatomy [10]. The proximal section of the femur is replaced with

V. Gupta · G. Singh · A. Chanda (✉)
Centre for Biomedical Engineering, Indian Institute of Technology (IIT) Delhi, New Delhi 110016, India
e-mail: arnab.chanda@cbme.iitd.ac.in

A. Chanda
Department of Biomedical Engineering, All India Institute of Medical Sciences (AIIMS) Delhi, New Delhi 110029, India

A. Mahajan et al. (eds.), *Additive Manufacturing of Bio-implants*, Biomedical Materials for Multi-functional Applications, https://doi.org/10.1007/978-981-99-6972-2_10

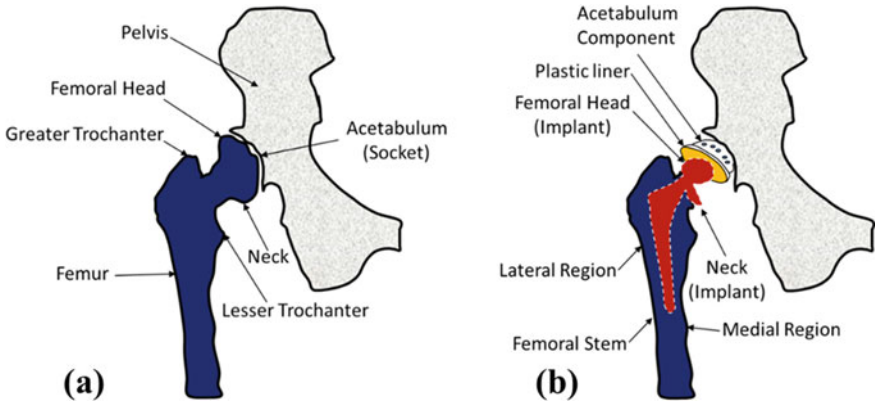

Fig. 1 Schematic of **a** Healthy hip joint anatomy and **b** Femoral THR implantation. Reproduce with permission [10]

an implant consisting of a femoral stem and a modular head during a standard hip replacement procedure. A hemispherical cup is attached to the pelvic bone socket on the acetabular side (Fig. 1) [11, 12]. Several common issues arise with the femoral stem, including stress shielding (where the implant absorbs stress instead of the natural bone), instability or micro-motion between the implant and the femur, and bone resorption, resulting in discomfort and pain [13, 14]. Surgical studies over the years have shown that the micro-motion between the implant stem and the surrounding femoral cavity should be less than 40 μm to reduce wear, facilitate primary bone emancipation, and avoid fibrous tissue formation [15]. However, none of the existing hip implants have been able to achieve such minimal micro-motions at the interface (i.e., great stability), which is a primary factor contributing to the failure of hip replacement surgeries [16].

Hip replacement surgeries employ a variety of hip implants, including tiny and lengthy implants, implants with massive head diameters, and implants with big neck diameters. It has been observed that small implants stimulate bone growth [17, 18], but their positioning during revision procedures poses a challenge [19]. Implants with bigger head and neck diameters transmit a lower load to the femoral component [20]. Implants with non-flat neck designs produce significant stresses on the femur and contribute to wear [21]. Moreover, the current procedure for replacing existing hip implants during revision surgeries is complex and requires multiple excruciating femoral drilling procedures for implant removal and replacement [22, 23]. There is a need for patient-specific implant matching to address stability and revision surgery issues [24], given the substantial variation in hip joint anatomy between patients. However, this is not a viable solution due to the high cost and complexity of designing and implementing patient-specific hip implants. Instead, there is a need for the development of new and innovative implants that can overcome the challenges associated with existing hip implants and enhance the implant–femur interface's stability and loading. Shrivastava et al. [25] conducted a tribological study on metal-on-plastic

implants with various motion patterns during the gait cycle, emphasizing variations in values throughout the cycle. Burn et al. [26] conducted a patient-specific study comprising 13,961 hip replacement patients, taking into account variables such as age, sex, and BMI. The results provided hip replacement estimates based on various patient configurations.

In this work, we have developed and evaluated a novel design for a hip implant that offers ease of installation and replacement, with the potential to minimize interfacial micro-motion, alleviate stress shielding, and enhance the dynamic stability of total hip replacements (THR). Our design incorporates perforations in the shaft region, facilitating implant insertion, removing, and providing an increased surface area for optimized load transfer. To ensure biocompatibility, corrosion resistance, structural compliance, and high strength, we selected a titanium alloy (Ti6Al4V) as the implant material. A virtual operation was performed to mimic the placement of our implant design into a femur bone. Utilizing finite element modeling (FEM), a 3kN force was applied, and the effects on the implant and femur were examined. The subsequent sections of this study comprise a detailed description of the design and testing methodology, the presentation and analysis of the results, followed by a comprehensive discussion, and, ultimately, the conclusion.

2 Materials and Methods

2.1 Geometrical Modeling

The development of the innovative implant design took into account various biomechanical factors. Rhinoceros® (Robert McNeel & Associates, Seattle, USA), an open-source 3D modeling software, was utilized for the design process. Figure 2 provides a perspective, front, and side views of the novel implant design. The implant dimensions were determined based on ASTM standards [27], with a maximum length of 127 mm and a thickness of 10 mm. The femoral head, with a diameter of 13.6 mm, will contact the acetabular cup at the implant's proximal end. The neck part, having a diameter of 17 mm, comes next. The middle region of the implant shaft features eight grooves extending from the medial to the lateral region. These grooves increase the contact area between the implant and the surrounding bone, redistributing loads along the shaft instead of concentrating them on the femoral head (thereby reducing stress shielding). Furthermore, the grooves were engineered such that the entire implant could be readily put and removed during revision surgery, obviating the need for additional femoral drilling. The groove angle was optimized to make sure that the grooves span the whole width of the implant, allowing for optimum implant placement and removal guidance. A long stem shape was adopted to confirm the optimal placement of the implant within the femur cavity.

The geometrical representation of the femur was obtained from Sawbones (Pacific Research Laboratories, Inc., WA, USA) [28]. The cancellous (internal) and cortical

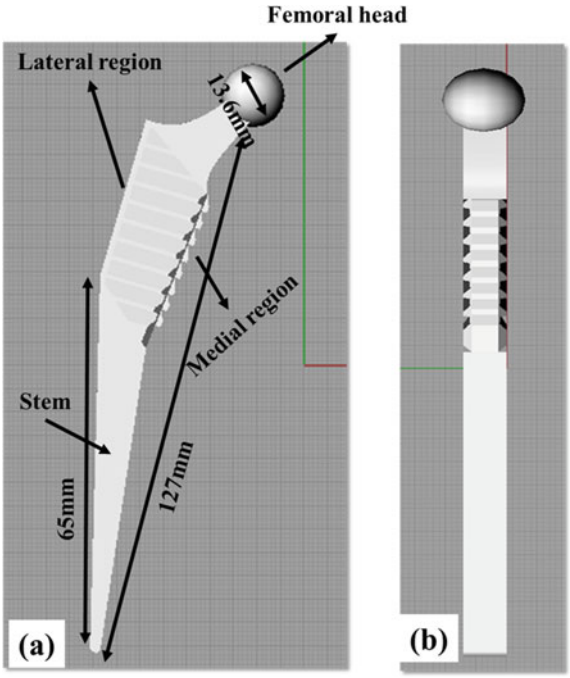

Fig. 2 The geometry of novel corrugated implant hip implant: **a** Front view, **b** Side view. Reproduce with permission [10]

(external) bone sections were included in the femur model, which captured realistic aspects of the proximal region, greater trochanter, lesser trochanter, shaft, and distal regions. Additionally, the surface roughness characteristics of the bone were preserved. The femur CAD model was converted into the stereolithographic file format (STL) and put into the Rhinoceros® open-source program to assist further analysis. Figure 3a depicts the femur model used in this study.

A virtual total hip replacement (THR) surgery was conducted on the femur model, involving two sequential steps. In the first step, the femoral head section was cut at a specific angle of 50°, adhering to the THR standards set by the ASTM [29] (Fig. 3b). Following that, the innovative implant was put into the modified femur by first positioning the grooves parallel to the plane of the femoral incision and then advancing perpendicularly to the direction of the grooves. At the final position of the implant, the femoral cut surface and the implant neck were brought into close proximity. To establish the relationship between the innovative implant and the femur models in the next stages, the overlapping piece was removed from the femur, essentially simulating the construction of a cavity to permit the implant's implantation and then reconstructed.

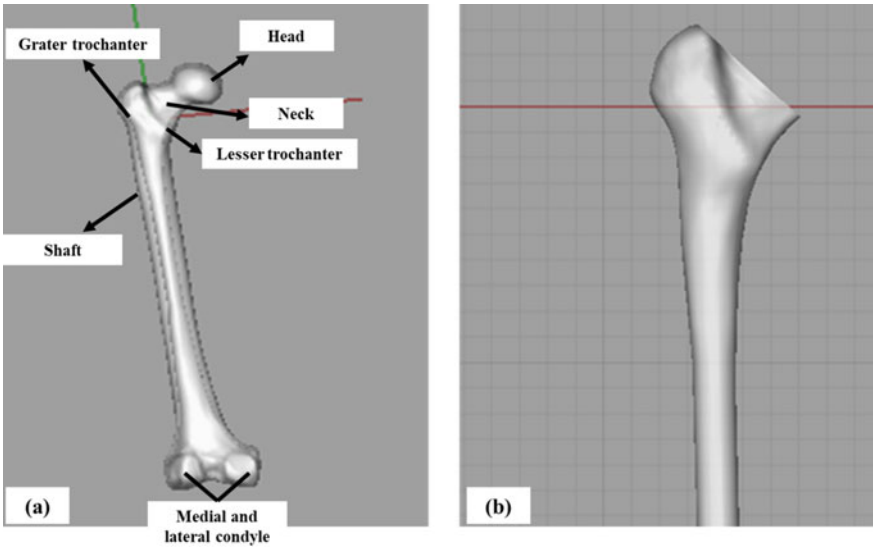

Fig. 3 **a** Femur model, **b** Modified femur without the femoral head. Reproduce with permission [10]

2.2 Finite Element (FE) Modeling

The femur and new implant models were loaded into FEA ICEM CFD 15.0 (FEA Inc., PA, USA), and volumetric meshes with 20-noded Solid 186 tetrahedral elements were generated. This element type was chosen because it can handle significant deflections, nonlinearities at contacts, and large strain deformations [30–33]. The volumetric meshes were loaded into mechanical APDL Product Launcher 15.0 (ANSYS Inc., PA, USA) for further analysis. The model was rotated 10 degrees laterally in the frontal plane and 10 degrees dorsally in the sagittal plane [10, 34] to mimic a normal femoral position and offer realistic normal loads. Normal loads were given to the femoral head in line with ASTM hip implant testing standards, and the distal part of the femur was restricted in all degrees of freedom (i.e., its solid connection to the lower extremity was imitated) [35]. The hip stem material properties (Ti6Al4V) and cortical and cancellous bone sections were taken from the literature [36] and are in accordance with ASTM standards [29].

A comprehensive analysis was performed to determine the appropriate mesh density that would ensure computational accuracy for the subsequent analyses. The convergence of the mesh was assessed by examining the percentage variation of von Mises stresses as the number of elements increased, with a focus on variations of $\leq 5\%$ [25, 30, 32, 37–42]. Four meshes were generated, ranging from coarse to fine, with the total number of elements being 24,760, 49,780, 110,784, and 169,120. Figure 4 illustrates four of these meshes, along with the applied loads and constraints on the model.

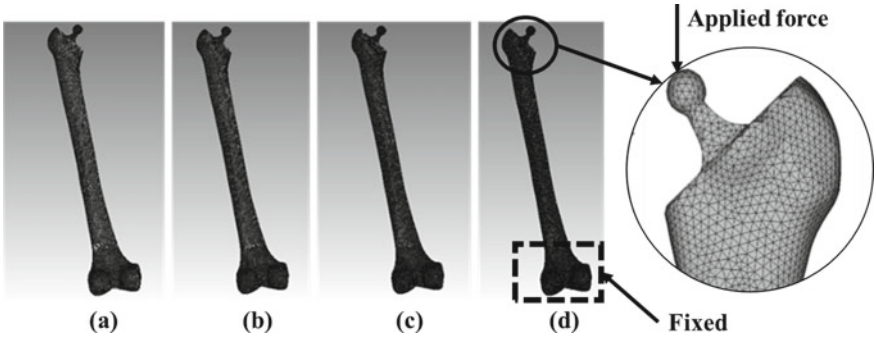

Fig. 4 View of a meshed FE model with loads and constraints and the four meshes (with different numbers of elements) used in the mesh convergence study. **a** 24,760 elements, **b** 49,780 elements, **c** 110,784 elements, and **d** 169,120 elements

A contact pair was formed between the implant's surface and the inside surface of the simulated femoral cavity produced during surgery simulation [30, 32, 37, 40]. Two types of contact conditions were studied: bonded, which represented an exceptionally snug fit between the implant and the femur, and frictional, which represented a typical fit between the implant and the femur. The contacts were defined as flexible using the augmented Lagrangian approach with a normal penalty stiffness factor of 1 and a penetration tolerance factor of 0.1. The initial penetration and surface offset of the contact surface were assumed to be zero. An automated correction for gap closure and penetration reduction was used for accurate contact representation. The frictional coefficient of 0.3, based on literature [43], was utilized for the analyses. Forces of 1.5kN, 3kN, and 6kN were applied to simulate the peak loads experienced by the femoral head during various gait activities such as walking, running, and jumping [35]. The maximum von Mises stress created in the new implant was measured to conduct the mesh convergence investigation. The previously estimated optimal density mesh was subjected to the produced displacements and stresses in the femur–implant system.

3 Results and Discussion

3.1 Mesh Convergence Results

The maximum von Mises stress experienced by the novel implant under different mesh densities was compared under loadings of 1.5 kN, 3 kN, and 6 kN (Fig. 5). A substantial variation in the peak von Mises stress was observed when transitioning from 24,760 to 169,120 elements, indicating the influence of mesh sizing on the results. However, the variation was significantly reduced between 110,784 and 169,120 elements, falling within a range of ± 70 MPa. This range corresponds to

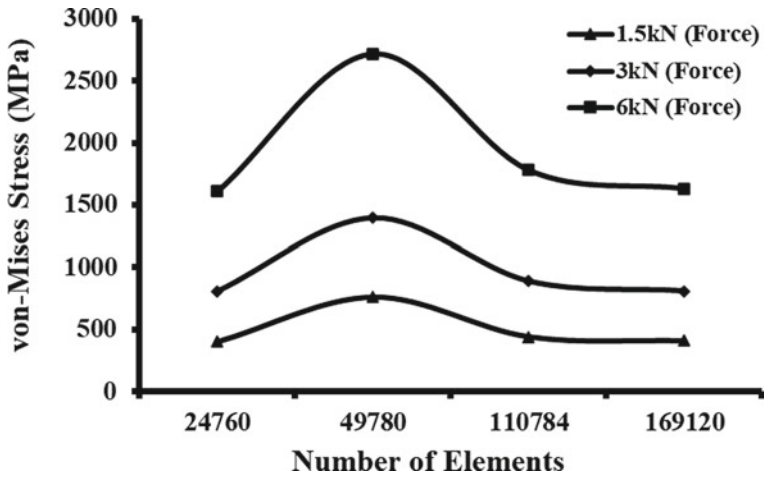

Fig. 5 Peak von Mises stress versus number of mesh elements for different loadings

approximately ± 5% of the results [25]. Consequently, the mesh comprising 110,784 elements was deemed the most accurate and computationally efficient for subsequent analyses.

3.2 Impact of Intact Analysis

In orthopedics, accurate stress measurement is critical for understanding varied activities. This research aimed to look into the distribution of stress and strain in the femur during mid-stance. Two loading scenarios were considered: the hip joint reaction force and the hip joint reaction force. The intact femur, representing the femur without any hip replacement, served as the baseline model for predicting the performance of other models. The intact model faithfully replicated the properties and structure of a real femur bone, as depicted in Fig. 6. In the intact model, the total stress applied to the femur was measured at 777 Pa, with the cancellous part experiencing a stress of 91 Pa (Fig. 6). The proximal region exhibited the highest stress, while the epiphysis demonstrated lower stress levels. The distal part of the bone experienced minimal to no stress.

3.3 Impact of Bonded Interface Implant Bone Model

The bonded model closely resembles the actual model post-hip replacement, as illustrated in Fig. 6. In this model, the implant was inserted, the proximal region of the femur was removed, and the implant was placed perpendicular to the bone.

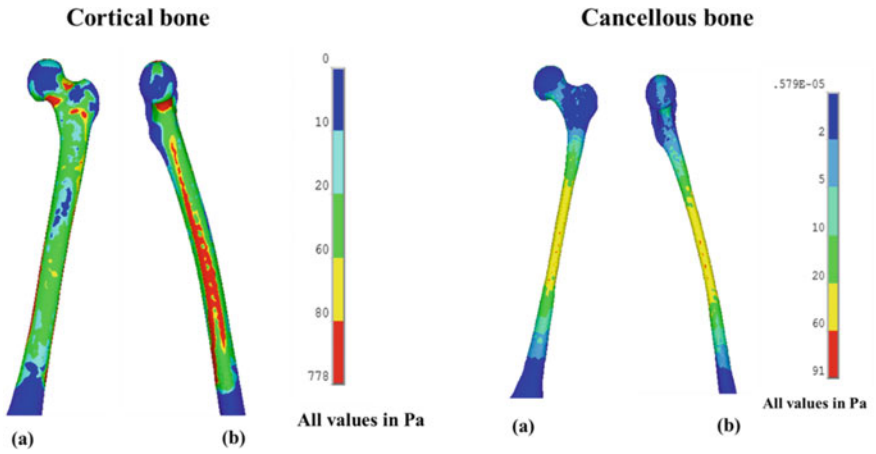

Fig. 6 Von Mises stress distribution in the **a** anterior and **b** medial aspects of the cortical and cancellous bone

The von Mises stress contour plots for the cortical, cancellous, and implant models are presented in Fig. 7. The bonded model compares and evaluates the similarities between the realistic data and the intact model. As depicted in Fig. 7, the bonded model exhibits similar properties to the intact model. The maximum stress observed in the bonded model is 744.423 Pa.

cancellous bone, and implant.

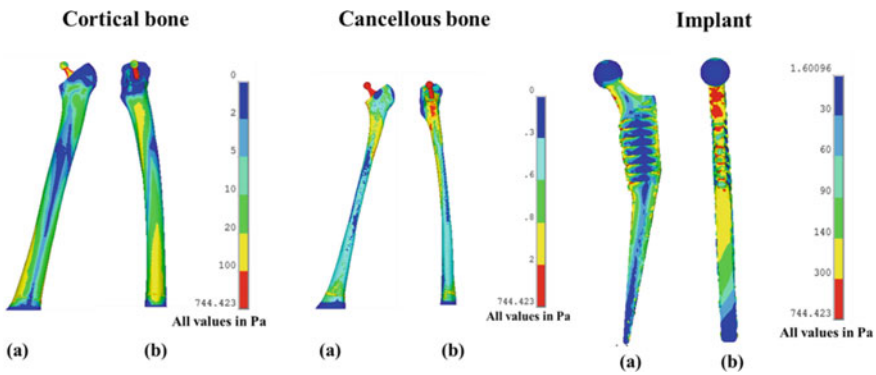

Fig. 7 Von Mises stress distribution in the **a** anterior and **b** medial aspects of the cortical,

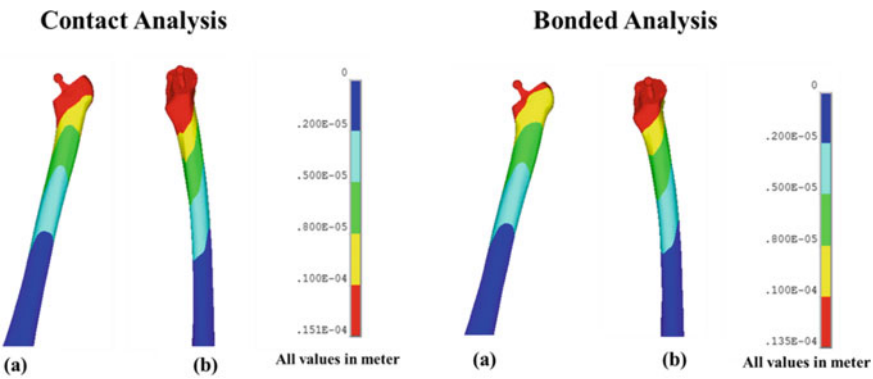

Fig. 8 Displacement vector sum distribution in the **a** anterior and **b** medial aspects of the contact and bonded analysis

3.4 Displacement Analysis of Implant Bone Model

In both the analysis (contact and bonded model), the total maximum displacement vector sum is as shown in Fig. 8, and the value of the maximum displacement vector sum in the bonded analysis was 15.1 μm, and in the contact analysis, it was 13.1 μm. In both analyses, we give the boundary conditions (zero displacements in the distal region in the bone) and apply force vertically downwardly. The effect, as shown in Fig. 8, the maximum displacement is in the proximal region, where the hip stem and femoral bone are attached together. As the displacement between the femoral bone and hip stem is minimum, the pain of the patient will also be reduced.

4 Conclusions

This study produced a unique Ti6Al4V hip implant design that can overcome the obstacles associated with current hip implant-based failures. According to ASTM standards, implant dimensions were chosen to have big head and neck diameters for minimum stress shielding at the implant and a long stem for convenience of implant positioning. A novel corrugated design was implemented to guide and remove the implant during initial and revised surgeries. Computational modeling was used to surgically attach this implant to a femur (with both cortical and cancellous parts). Detailed mesh convergence research was performed to choose a computationally accurate finite element (FE) mesh. The effect of the new implant's tight and frictional fit with the femur was investigated. The characterization of interfacial micro-motion and generated stresses was used to quantify stability and loading. For bonded fitting modes (i.e., tight and frictional), micro-motions as small as 13 m were recorded, which promotes bone development and minimizes wear. Overall stresses created at

the implant and the femur were lower than those experienced by a healthy hip joint and were within elastic limits. While the stress and displacement distributions did not change considerably across the contact and bonded fit and frictional evaluations, the frictional analysis produced more realistic quantitative findings than the tight fit study. To date, no such strong design and numerical testing framework for femoral hip prosthesis has been developed, which could lead to improved long-term surgical standards and results.

Funding No funding was received for this work.

Conflict of Interest The authors declare no conflict of interest with respect to the research, authorship, and/or publication of this article.

References

1. Evans JT, Evans JP, Walker RW, Blom AW, Whitehouse MR, Sayers A (2019) How long does a hip replacement last? A systematic review and meta-analysis of case series and national registry reports with more than 15 years of follow-up. Lancet (London, England) 2019. https://doi.org/10.1016/S0140-6736(18)31665-9
2. Fitzpatrick R, Shortall E, Sculpher M, Murray D, Morris R, Lodge M, et al (1998) Primary total hip replacement surgery: a systematic review of outcomes and modelling of cost-effectiveness associated with different prostheses. Health Technol Assess (Rockv).https://doi.org/10.3310/hta2200
3. Total Hip Replacement—OrthoInfo—AAOS n.d. https://orthoinfo.aaos.org/en/treatment/total-hip-replacement/. Accessed August 11, 2021
4. Increased Rate of Total Joint Replacements Predicted From 2020 to 2040—Rheumatology Advisor n.d. https://www.rheumatologyadvisor.com/home/topics/osteoarthritis/increased-rate-of-total-joint-replacements-predicted-from-2020-to-2040/. Accessed August 11, 2021
5. Singh JA, Yu S, Chen L, Cleveland JD (2019) Rates of total joint replacement in the United States: future projections to 2020–2040 using the national inpatient sample. J Rheumatol 46:1134–1140. https://doi.org/10.3899/JRHEUM.170990
6. Kremers HM, Larson DR, Crowson CS, Kremers WK, Washington RE, Steiner CA et al (2014) Prevalence of total hip and knee replacement in the United States. J Bone Jt Surg Am. https://doi.org/10.2106/JBJS.N.01141
7. Total Hip Arthroplasty for Femoral Neck Fracture: What Are the Contemporary Reasons for Failure? | Elsevier Enhanced Reader n.d. https://reader.elsevier.com/reader/sd/pii/S0883540321001340?token=2FEF05FC8DFDBD0E2CC7A5EC993CCBBA02AA32963D8E8A5E15039683B3CA925427B2912C7C576219C3AA366F3BCEA052&originRegion=eu-west-1&originCreation=20210914103326. Accessed September 14, 2021
8. Losina E, Barrett J, Mahomed NN, Baron JA, Katz JN (2004) Early failures of total hip replacement: effect of surgeon volume. Arthritis Rheum.https://doi.org/10.1002/art.20148
9. Corbett KL, Losina E, Nti AA, Prokopetz JJZ, Katz JN (2010) Population-based rates of revision of primary total hip arthroplasty: a systematic review. PLoS ONE. https://doi.org/10.1371/journal.pone.0013520
10. Gupta V, Chanda A (2022) Finite element analysis of a hybrid corrugated hip implant for stability and loading during gait phases. Biomed Phys Eng Express 8:035028. https://doi.org/10.1088/2057-1976/AC669C

11. Heap M, Munglani R, Klinck J, Males A (1993) Elderly patients' preferences concerning life-support treatment. Anaesthesia 48:1027–1033. https://doi.org/10.1111/(ISSN)1365-2044
12. Fischer HBJ, Simanski CJP, Kehlet H, Bonnet F, Camu F, McCloy HRF et al (2005) A procedure-specific systematic review and consensus recommendations for analgesia after total hip replacement. Anaesthesia 60:1189–1202. https://doi.org/10.1111/J.1365-2044.2005.04382.X
13. Gallo J, Gibon E, Goodman SB (2017) Implants for joint replacement of the hip and knee. Mater Dev Bone Disord.https://doi.org/10.1016/B978-0-12-802792-9.00004-5
14. Ray GS, Ekelund P, Nemes S, Rolfson O, Mohaddes M (2019) Changes in health-related quality of life are associated with patient satisfaction following total hip replacement: an analysis of 69,083 patients in the Swedish Hip Arthroplasty Register 91:48–52. http://www.TandfonlineCom/Action/AuthorSubmission?JournalCode=iort20&page=instructions. https://doi.org/10.1080/17453674.2019.1685284.
15. Baharuddin MY, Salleh SH, Hamedi M, Zulkifly AH, Lee MH, Mohd Noor A et al (2014) Primary stability recognition of the newly designed cementless femoral stem using digital signal processing. Biomed Res Int. https://doi.org/10.1155/2014/478248
16. Piazza SJ, Delp SL (2001) Three-dimensional dynamic simulation of total knee replacement motion during a step-up task. J Biomech Eng. https://doi.org/10.1115/1.1406950
17. Patient-specific finite element analysis of femurs with cemented hip implants | Elsevier Enhanced Reader n.d. https://reader.elsevier.com/reader/sd/pii/S0268003318305382?token=7E9B21631325FA0328606F860B557AA7034660740388C648EC34F3714555BFDBFC87A2F1123613AAE1C288976C0FA231&originRegion=eu-west-1&originCreation=20210914105324. Accessed September 14, 2021
18. Finite element wear prediction using adaptive meshing at the modular taper interface of hip implants | Elsevier Enhanced Reader n.d. https://reader.elsevier.com/reader/sd/pii/S1751616117304666?token=FE2654E1B1D3162FD1CCF752C45DA405195887A1AD4945011CE240DC3DC4C88163CA8ED8AD90ADCD36309BACE3CACB1F&originRegion=eu-west-1&originCreation=20210914105229. Accessed September 14, 2021
19. Loppini M, Grappiolo G (2018) Uncemented short stems in primary total hip arthroplasty: the state of the art. EFORT Open Rev. https://doi.org/10.1302/2058-5241.3.170052
20. Latham B, Goswami T (2004) Effect of geometric parameters in the design of hip implants paper IV. Mater Des. https://doi.org/10.1016/j.matdes.2004.01.012
21. Ridzwan MIZ, Shuib S, Hassan AY, Shokri AA, Mohammad Ibrahim MN (2007) Problem of stress shielding and improvement to the hip implant designs: a review. J Med Sci. https://doi.org/10.3923/jms.2007.460.467
22. Bozic KJ, Rubash HE (2004) The painful total hip replacement. Clin Orthop Relat Res. https://doi.org/10.1097/00003086-200403000-00004
23. Kyriakopoulos G, Poultsides L, Christofilopoulos P (2018) Total hip arthroplasty through an anterior approach. 3:574–83. https://doi.org/10.1302/2058-5241.3.180023
24. Jun Y, Choi K (2010) Design of patient-specific hip implants based on the 3D geometry of the human femur. Adv Eng Softw.https://doi.org/10.1016/j.advengsoft.2009.10.016
25. A predictive framework of the tribological impact of physical activities on metal-on-plastic hip implants | Elsevier Enhanced Reader n.d. https://reader.elsevier.com/reader/sd/pii/S2352573820300421?token=88A508B4AFBB35FBC31A7FDDF85CE4E00838C13EB6FE3C076F59BB159D25A9F82CFE5C56D59B8F3DC2E99D3333DDA541&originRegion=eu-west-1&originCreation=20210914105637. Accessed September 14, 2021
26. Burn E, Edwards CJ, Murray DW, Silman A, Cooper C, Arden NK et al (2019) Lifetime risk of knee and hip replacement following a diagnosis of RA: Findings from a cohort of 13 961 patients from England. Rheumatol (United Kingdom) 58:1950–1954. https://doi.org/10.1093/rheumatology/kez143
27. Values T, Hip T, Materials P (2005) Standard specification for total hip joint prosthesis and hip endoprosthesis bearing surfaces made of metallic, ceramic, and polymeric. Components. https://doi.org/10.1520/F2033-05.2

28. Dickinson AS, Taylor AC, Ozturk H, Browne M (2011) Experimental validation of a finite element model of the proximal femur using digital image correlation and a composite bone model. J Biomech Eng. https://doi.org/10.1115/1.4003129
29. (ASTM) AS for T and M. Standard Specification for Femoral Prostheses — Metallic Implants 1. ASTM Int 2004. https://doi.org/10.1520/F2068-09.2.
30. Gupta S, Gupta V, Chanda A (2022) Biomechanical modeling of novel high expansion auxetic skin grafts. Int j Numer Method Biomed Eng 38:e3586. https://doi.org/10.1002/cnm.3586
31. Gupta V, Singh G, Gupta S, Chanda A (2023) Expansion potential of auxetic prosthetic skin grafts: a review. Eng Res Express 5. https://doi.org/10.1088/2631-8695/accfe5
32. Gupta V, Singh G, Chanda A (2022) Development and testing of skin grafts models with varying slit orientations. Mater Today Proc 62:3462–3467. https://doi.org/10.1016/j.matpr.2022.04.282
33. Wang E, Nelson T, Rauch R (2004) Back to elements—Tetrahedra vs . Hexahedra. CAD-FEM GmbH, Munich, Ger
34. Sieniawski J, Ziaja W, Kubiak K, Motyk M (2013) Microstructure and mechanical properties of high strength two-phase titanium alloys. Titan Alloy Adv Prop Control, https://doi.org/10.5772/56197
35. Bergmann G, Bender A, Dymke J, Duda G, Damm P (2016) Standardized loads acting in hip implants. PLoS ONE. https://doi.org/10.1371/journal.pone.0155612
36. Rawal BR, Ribeiro R, Malhotra R, Bhatnagar N (2012) Design and manufacturing of femoral stems for the Indian population. J Manuf Process. https://doi.org/10.1016/j.jmapro.2011.12.004
37. Gupta V, Chanda A (2022) Expansion potential of skin grafts with novel I-shaped auxetic incisions. Biomed Phys Eng Express 8:100071. https://doi.org/10.1088/2057-1976/ac3b72
38. Gupta V, Chanda A (2022) Expansion potential of skin grafts with alternating slit based auxetic incisions. Forces Mech 7:100092. https://doi.org/10.1016/j.finmec.2022.100092
39. Chanda A, Chatterjee S, Gupta V (2020) Soft composite based hyperelastic model for anisotropic tissue characterization. J Compos Mater 54:4525–4534. https://doi.org/10.1177/0021998320935560
40. Gupta V, Gupta S, Chanda A (2022) Expansion potential of skin grafts with novel rotating triangle shaped auxetic incisions. Emerg Mater Res 11:1–9. https://doi.org/10.1680/jemmr.22.00026
41. Gupta V, Chanda A (2022) Biomechanics of skin grafts: effect of pattern size, spacing and orientation. Eng Res Express 4:015006. https://doi.org/10.1088/2631-8695/ac48cb
42. Singh G, Gupta V, Chanda A (2020) Mechanical characterization of rotating triangle shaped auxetic skin graft simulants. Facta Univ Ser Mech Eng 1–16. https://doi.org/10.22190/FUME220226038S
43. Mattei L, Di Puccio F, Piccigallo B, Ciulli E (2011) Lubrication and wear modelling of artificial hip joints: a review. Tribol Int. https://doi.org/10.1016/j.triboint.2010.06.010

Chapter 11
Applications of 3D Printing in Medical, Engineering, Agricultural, and Other Sectors

Shaik Himam Saheb

1 Introduction

In general, there are five steps in the 3D printing process. First, using any computer-aided design (CAD) software (like Proe Catia, SolidWorks, etc.), a 3D model is produced. The surface geometry of the model is then written into. STL format that a 3D printing machine can able to understand. The model is then divided into several layers so that the 3D printer may be fed printing instructions. The product is then extruded layer by layer in a 3D printer using Additive Manufacturing (AM) technology. Finally, post-processing is done to improve the 3D printed object's print quality. Figure 1 shows the stages in 3D printing process.

2 Traditional Manufacturing vs Digital Manufacturing

Traditional manufacturing and digital manufacturing are two distinct approaches to production processes. Here's a comparison between the two methods.

2.1 Traditional Manufacturing

Traditional manufacturing refers to the conventional methods of manufacturing that have been in use for centuries. It involves physical processes and manual labor to produce goods. Some examples of traditional manufacturing techniques

S. H. Saheb (✉)
Department of Mechatronics Engineering, Faculty of Science and Technology, The ICFAI Foundation for Higher Education, Hyderabad, Telangana, India
e-mail: himam.mech@gmail.com

A. Mahajan et al. (eds.), *Additive Manufacturing of Bio-implants*, Biomedical Materials for Multi-functional Applications, https://doi.org/10.1007/978-981-99-6972-2_11

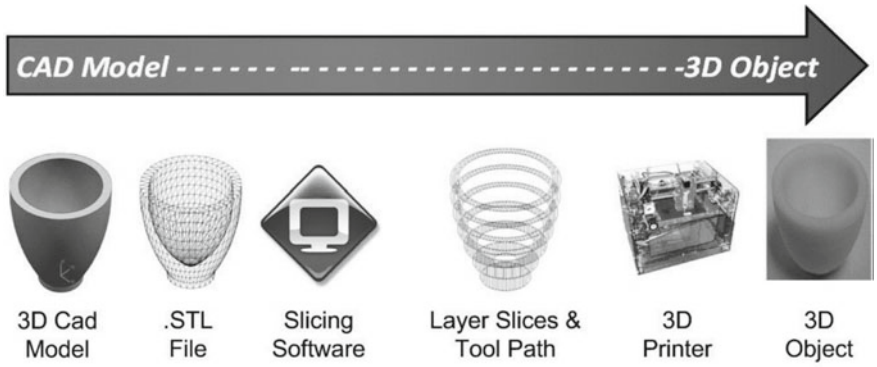

Fig. 1 Stages in 3D printing

are carpentry, machining, welding, forging, forming, sheet metal operations, etc. Here are some key characteristics of traditional manufacturing.

Tools and Machinery: Traditional manufacturing relies on various tools and machinery such as lathe machines, drills, molds, and assembly lines to produce goods. These tools are operated manually or with the help of human labor.

Prototyping: Traditional manufacturing often requires the creation of physical prototypes before full-scale production. This can involve additional time and cost to develop and refine prototypes.

Mass Production: These methods are well suited for mass production of standardized goods. The assembly line approach allows for efficient production and economies of scale.

Longer Lead Times: These processes typically have longer lead times due to the need for tooling, setup, and manual labor. Changes in production require reconfiguration of equipment, which can be time-consuming.

Higher Cost: Traditional manufacturing processes often require a significant investment in machinery, labor, and facilities. This can result in higher production costs, especially for smaller batch sizes. Based on the required accuracy and precision, the cost of product varies as the customer needs a more accurate product then there are high possibilities of an increase in the production cost and vice versa.

2.2 Digital Manufacturing

Digital manufacturing is a big umbrella under this there are several techniques which use digital tools for manufacturing, additive manufacturing or 3D printing is a small branch under digital manufacturing, which is a relatively new approach that utilizes digital design and fabrication technologies. Here are some key characteristics of digital manufacturing, the various branches of digital manufacturing are shown in Fig. 2

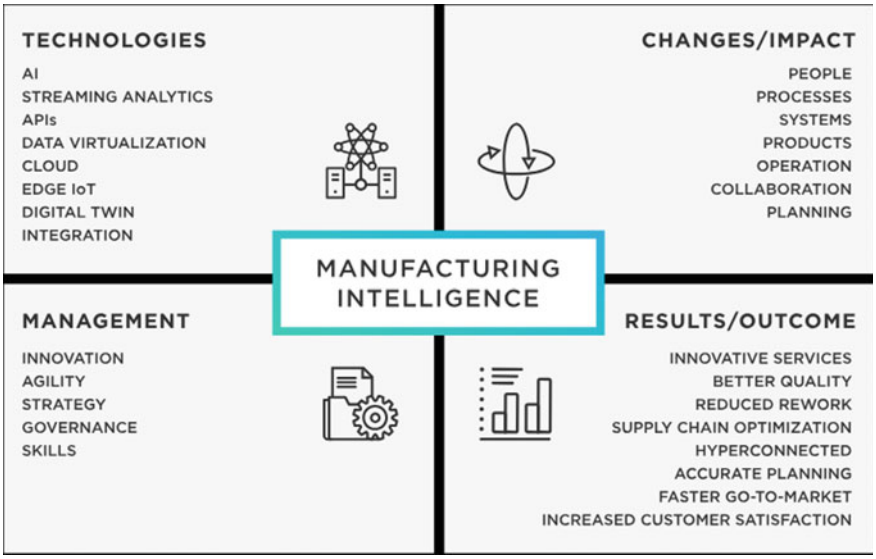

Fig. 2 Capabilities of digital manufacturing

Digital Design: Digital manufacturing relies on CAD/any other geometric modeling software tool to create virtual 3D models of products. These models can be easily modified and shared digitally. Some of the digital fabrication techniques like computer numerical control and direct numerical control use G and M codes to control and to give instructions to machines in the form of digits.

Layer-by-Layer Fabrication: In digital manufacturing, objects are created layer by layer by adding material rather than subtracting it. This allows for complex geometries and customization, whereas some processes involve step-by-step material removal.

Rapid Prototyping: Digital manufacturing enables rapid prototyping as 3D printers can directly produce physical prototypes from digital designs. This speeds up the design iteration process.

On-Demand Production: With digital manufacturing, products can be produced on-demand, eliminating the need for large inventories. This enables greater flexibility and reduces storage costs.

Lower Cost for Small Batch Sizes: Digital manufacturing is particularly cost-effective for smaller batch sizes since it doesn't require costly tooling or setup changes. This makes it ideal for customization and niche markets.

Reduced Waste: Digital manufacturing can be more sustainable compared to traditional manufacturing because it generates less waste material. It only uses the exact amount of material needed to build an object.

It's worth noting that traditional manufacturing and digital manufacturing are not equally exclusive. In some cases, they can complement each other within a production

ecosystem, with traditional manufacturing methods being used for certain processes and digital manufacturing used for specific applications or customization.

2.3 Digital Fabrication

Digital fabrication refers to the process of using computer-controlled machinery and tools to create physical objects from digital designs. Digital fabrication typically involves the following steps, the possible capabilities are explained in detail by Hernandez et al. [1]

Design: The object or product is first designed with the help of CAD software. The design can range from simple 2D shapes to complex 3D models.

Digital Modeling: The CAD software creates a digital representation of the object, specifying its dimensions, geometry, and other relevant properties.

Slicing: The digital model is divided into thin horizontal layers, creating a virtual representation of how the object will be built layer by layer.

Machine Setup: The design is transferred to computer-assisted machines, such as 3D printers, laser cutters, CNC machines, or robotic arms. These machines are equipped with appropriate tools and materials.

Fabrication: The machine executes the instructions from the digital design, following the specified tool paths and building the object layer by layer. The process can involve additive techniques (building up layers) or subtractive techniques (removing material).

Digital fabrication enables precise and customizable manufacturing with various materials, like plastics, metals and non-metals, and composites. The technology has gained popularity due to its ability to produce complex shapes, reduce lead times, and provide cost-effective solutions for small-scale production and a variety of applications.

3 Additive Manufacturing

AM technology, also referred to as 3D printing where the manufacturing of objects done by layer-by-layer material addition, the detailed process of additive manufacturing is described.

Design: The design is saved as a digital file in a specific format (such as STL or OBJ) which is read by the 3D printer.

Slicing: The digital design is processed by slicing software that divides it into a series of thin horizontal layers. Each layer is typically a fraction of a millimeter thick, depending on the capabilities of the 3D printer. After slicing the printing of the object starts.

Material Deposition: The printer nozzle or extruder moves along the X, Y, and Z axes, depositing material in a precise pattern according to the sliced design. The material can be in the form of filament, powder, liquid resin, or even metal.

Layer-by-Layer Building: The printer starts from the bottom layer and builds upward, adding one layer at a time. Each layer fuses or solidifies with the previous layer, creating a cohesive structure. After this step, the post-processing of the end product is processed.

Design Flexibility: Complex geometries and intricate internal structures can be created without the constraints of traditional manufacturing processes.

Customization: Each object can be easily customized or personalized without incurring additional costs or time-consuming processes.

Rapid Prototyping: Additive manufacturing allows for the quick production of prototypes, enabling faster design iterations and reducing development cycles.

Reduced Waste: The process is more material-efficient as it only uses the necessary amount of material to build the object, minimizing waste.

Additive manufacturing is widely used in various industries, including aerospace, automotive, health care, consumer products, and education. It continues to advance, with ongoing research and development focusing on new materials, improved printing techniques, and larger scale production capabilities. There are different types of 3D Printing processes as discussed by different researchers. Some of the major additive manufacturing processes are given below:

3.1 Fused Deposition Modeling (FDM)

It involves creating 3D objects by depositing layer by layer of molten thermoplastic material in a predetermined pattern. The basic steps of FDM 3D printing are as follows:

FDM 3D printing has several advantages, including.

- A wide range of material options: PLA, ABS, PETG, TPU, and other materials can be used in FDM printers, offering different properties like strength, flexibility, and temperature resistance.
- Cost-effectiveness: FDM printers are relatively affordable, making them accessible to a broad audience.
- Simplicity: FDM printing is straightforward and user-friendly, making it an excellent choice for beginners and hobbyists.
- Strong and functional parts: FDM-printed objects can be structurally robust and suitable for various functional applications.

However, FDM also has some limitations, such as limited printing resolution compared to other 3D printing techniques like stereolithography or selective laser sintering and the need for support structures for overhangs and complex geometries.

3.2 Stereolithography and Digital Light Processing

These technologies use liquid resin that is cured layer by using a UV light source. The resin hardens when exposed to the light, creating the desired object. SLA was one of the earliest 3D printing technologies developed by Charles Hull. In SLA, a liquid photopolymer resin is used as the raw material. This resin is sensitive to light, particularly ultraviolet (UV) light. The SLA 3D printer has a platform that can move vertically. It starts the printing process by lowering the platform to just below the surface of the liquid resin. A UV laser or a digital light projector (DLP) then exposes specific areas of the liquid resin with the desired cross section of the 3D model. The UV light causes the resin to solidify and become a thin layer. SLA gives high-resolution and fine prints, making it suitable for applications that require precision and smooth surface finishes. SLA is used in industries such as automotive, aerospace, jewelry, and health care for producing prototypes, custom parts, and investment casting patterns.

Digital light processing is another 3D printing technology that also utilizes photopolymer resins, similar to SLA. It was developed in the mid-1980s, with Texas Instruments pioneering the digital micromirror device (DMD) technology that became crucial for DLP 3D printing. Unlike SLA, where a laser selectively cures the resin, DLP uses a digital projector to flash an entire layer of the 3D model onto the resin at once. The DLP projector contains an array of micromirrors, each representing a pixel of the projected image. These micromirrors tilt to either allow light to pass (solidifying the resin) or block the light (leaving the resin in its liquid state), depending on the digital model's layer information. DLP is generally faster than SLA since an entire layer is cured in one exposure. However, it may have a slightly lower resolution due to the fixed pixel size of the projector. DLP is also used in various industries for producing prototypes, dental models, jewelry, and other objects that require relatively high detail and smooth surfaces. Both SLA and DLP offer advantages such as high precision, intricate details, and excellent surface quality compared to FDM (Fused Deposition Modeling). However, the choice between SLA and DLP depends on specific project requirements, desired resolution, speed, and budget considerations.

3.3 Selective Laser Sintering (SLS)

In this process, a laser selectively fuses powdered material, typically polymers or metals, layer by layer. The unfused powder acts as support for the printed object. However, SLS utilizes a different approach and material compared to these other technologies. The main features of SLS are as follows:

Powder-based Technology: SLS employs a powder-based approach. Instead of using filament or liquid resin, SLS 3D printers use a powdered material as the raw

material. Common materials include nylon (polyamide), thermoplastic elastomers, and even metal powders for metal 3D printing.

Sintering Process: The SLS process involves selectively sintering the powdered material with the help of a high-powered laser. The laser scans and fuses the powder particles together, layer by layer, based on the 3D model data.

Heated Build Chamber: SLS 3D printers have a heated build chamber to maintain a controlled temperature during the printing process. This prevents the printed layers from warping and helps in achieving better mechanical properties.

No Need for Support Structures: SLS does not require support structures to hold up overhangs or complex geometries. The unsintered powder surrounding each printed object acts as a natural support during the printing process. SLS can use versatility in materials.

Industrial and Functional Applications: SLS is commonly used in industrial settings for manufacturing functional prototypes, end-use parts, tooling, and components with high mechanical and thermal properties.

Selective laser sintering is known for its ability to produce parts with good strength, durability, and intricate geometries, making it a valuable technology in industries like aerospace, automotive, health care, and consumer goods. However, it requires specialized equipment and is typically more expensive than FDM or SLA 3D printing. One of the advantages of EBM is its faster printing speed compared to SLM, as the electron beam can scan larger areas more quickly. EBM is also performed in an inert gas atmosphere to prevent oxidation during the melting process and ensure the material's integrity. EBM is often utilized in industries where high-quality, geometrically complex metal parts are required, particularly in the aerospace and medical fields.

Both SLM and EBM are well suited for manufacturing end-use metal parts with high mechanical properties, excellent surface finish, and intricate geometries. However, the choice between the two technologies depends on specific requirements, material preferences, and budget considerations. These additive manufacturing methods have significantly contributed to advancements in various industries, revolutionizing how complex metal parts are designed and produced.

4 Advancements of 3D Printing: 4D Printing

It is an emerging technology that builds upon the principles of 3D printing but adds the dimension of time. It refers to the procedure of creating objects that can self-transform or change their shape, structure, or functionality over time in retort to external stimuli, like heat, water, light, or other environmental factors. The fourth dimension in 4D printing is time, representing the object's ability to morph or adapt after the initial printing. an overview of how 4D printing works is shown in Fig. 3.

Design: Similar to 3D printing, the procedure begins with a digital model creation or design of the object using CAD software. However, in 4D printing, additional parameters are specified to indicate how the object should transform or behave over time.

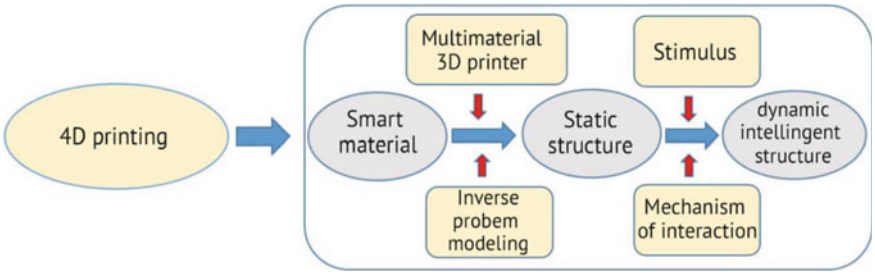

Fig. 3 Working Principle of 4D Printing

Material Selection: Special materials known as "smart materials" or "programmable materials" are used in 4D printing. These materials possess specific properties that allow them to respond to external stimuli and change their shape or behavior accordingly. Common examples include shape-memory polymers, hydrogels, or composites with embedded responsive components.

Printing and Activation: The object is 3D printed using the selected smart materials. The printing process may involve multiple layers or components that are strategically designed to interact with each other and trigger the desired transformation. Once the printing is complete, the object is typically in a dormant or temporary state.

Stimulus and Transformation: When exposed to the appropriate environmental stimulus, such as heat, water, light, or a specific trigger, the smart materials within the 4D printed object respond and initiate the transformation. This can involve changes in shape, folding, expansion, contraction, or other desired actions. The transformation occurs as a result of the material's inherent properties or the arrangement of responsive components within the object.

The potential applications of 4D printing are diverse and still being explored as follows:

Biomedical Applications: 4D printed objects can have applications in medicine and healthcare, such as self-assembling implants, drug delivery systems, tissue engineering scaffolds, or devices that adapt to a patient's specific anatomy.

Architecture and Construction: 4D printing can enable the creation of structures that can change their shape or adapt to different conditions, such as self-assembling buildings or structures that respond to environmental changes.

Robotics and Manufacturing: 4D printing can be used to produce adaptive or shape-shifting components for robots, machinery, or devices that need to change their functionality based on the surrounding conditions.

Aerospace and Defence: The technology could be utilized in the creation of adaptive components for aerospace applications, such as morphing wings or structures that adjust their shape during flight.

Consumer Products: 4D printing has the potential to revolutionize the design and functionality of consumer products, including clothing, footwear, furniture, or toys that can self-transform or adapt to user preferences.

4D printing is still an active area of research and development, with ongoing efforts to refine the materials, printing processes, and design techniques. As technology advances, it is expected to open up new possibilities for dynamic and responsive objects, enabling innovative solutions across various industries.

5 Applications of 3D Printing

3D printing has found applications in various fields which helps to solve traditional engineering problems. Many researchers explained various applications of the additive manufacturing process in [2–4].

Manufacturing: 3D printing is ever more used for small production, custom manufacturing, and on-demand production of parts and products. The cost-effectiveness rate is high when compared with traditional manufacturing in case of mass production.

Quick Prototyping: 3D printing allows for the quick production of prototypes, enabling faster design iterations and reducing the time and cost associated with traditional prototyping methods.

Consumer Products and DIY: 3D printing has opened up avenues for personal creativity, allowing individuals to design and print their own objects, toys, accessories, and household items.

Aeronautical Engineering: 3D printing has several applications in the aeronautical fields, the number of small intricate parts is replaced with single intricate structure or part, which reduces the wear and vibrations.

5.1 3D Printing Applications in Medical Field

3D printing has made significant contributions to the medical field, revolutionizing the way healthcare professionals approach patient care, surgical planning, medical training, and the production of custom medical devices [5, 6]. Here are some key applications of 3D printing in the medical field. The human anatomy and the possible 3D printing parts are shown in Fig. 4

- *Patient-Specific Anatomical Models*: 3D printing enables the creation of highly accurate patient-specific anatomical models based on medical imaging data, such as CT or MRI scans. These models help surgeons visualize complex structures, plan surgical procedures, and improve patient outcomes by practicing on an accurate replica before the actual surgery. They can be used for preoperative planning, education, and enhancing communication between healthcare teams and patients.
- *Custom Implants and Prosthetics*: 3D printing allows for the production of patient-specific implants and prosthetics tailored to individual anatomies. By utilizing 3D

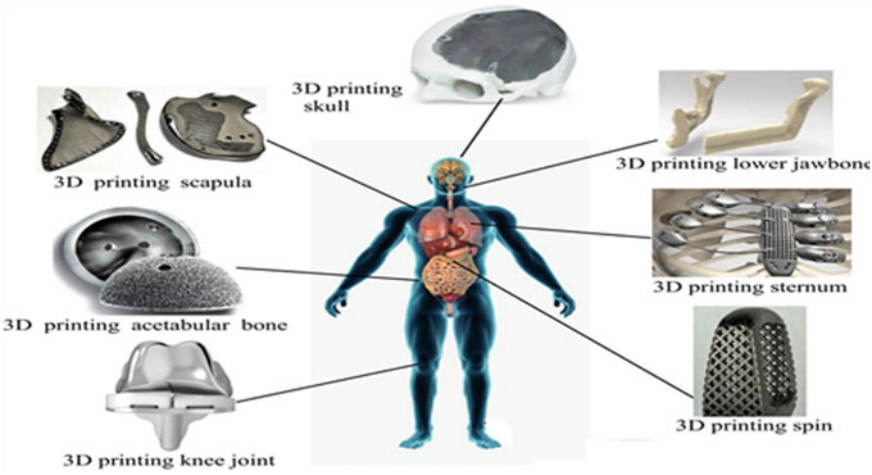

Fig. 4 The 3D printing applications around the human anatomy

scans of patients, implants or prosthetics can be precisely designed and manufactured to fit unique anatomical structures, leading to improved comfort and functionality. This technology has been particularly beneficial in craniofacial reconstruction, orthopedics, and dental applications.

- *Surgical Guides and Instrumentation*: 3D printing enables the creation of surgical guides and instrumentation that assist surgeons during complex procedures. Customized guides can be designed based on patient-specific anatomy to ensure precise placement of surgical tools or implants. These guides enhance surgical accuracy, reduce surgical time, and minimize risks [7].
- *Medical Education and Training*: 3D printing provides valuable tools for medical education and training. Medical schools and training institutions can produce anatomical models, surgical simulators, and educational aids to enhance the learning experience. These models allow students and trainees to gain hands-on experience, practice surgical techniques, and improve their understanding of complex anatomical structures.
- *Pharmaceutical Applications*: 3D printing has also been applied to the fabrication of personalized medications, such as customized drug dosage forms or multi-drug combinations in a single pill. This technology has the potential to improve medication adherence, dosage accuracy, and patient outcomes.

The use of 3D printing in the medical field continues to evolve, driven by advancements in materials, printing techniques, and regulatory frameworks. It has the potential to revolutionize patient care, enable personalized medicine, and shape the future of health care.

5.2 3D Printing in Medical Field During COVID

During the COVID-19 pandemic, 3D printing played a critical role in supporting the medical field in various ways. The technology was harnessed to address urgent needs for personal protective equipment (PPE), medical devices, and other supplies. Here are some specific applications of 3D printing in the medical field during the COVID-19 pandemic the detailed explanation of the application are as follows:

- *Face Shields and Masks*: 3D printing was used to rapidly produce face shields and mask components, which are crucial for protecting healthcare workers from exposure to the virus. By utilizing 3D printing, manufacturers and individuals were able to quickly respond to the shortage of PPE and provide additional protective gear to healthcare facilities.
- *Ventilator Parts and Accessories*: As the demand for ventilators surged during the pandemic, 3D printing was utilized to manufacture critical components and accessories for ventilators. This included valves, adapters, splitters, and other essential parts. 3D printing helped to bridge the supply gap and provide life-saving equipment to patients in need.
- *Nasopharyngeal Swabs*: 3D printing was instrumental in the production of nasopharyngeal swabs, which are used for COVID-19 testing. The technology allowed for the rapid production of swabs when there was a shortage of traditional swabs. 3D printed swabs were designed and validated to meet medical standards, enabling increased testing capacity.
- *Isolation Wards and Temporary Structures*: 3D printing was employed to fabricate components for temporary isolation wards and structures. This included partitions, modular walls, and other elements needed to quickly set up temporary medical facilities to accommodate the increased number of patients.
- *Education and Training Tools*: 3D printing served as a valuable tool for medical education and training during the pandemic. It enabled the production of anatomical models, simulators, and training aids that allowed healthcare professionals to enhance their skills and knowledge while adhering to social distancing measures.

It's worth noting that, while 3D printing played a crucial role in addressing immediate needs during the COVID-19 pandemic, the manufactured components and equipment still needed to meet specific safety and regulatory standards. Extensive collaboration and validation processes were undertaken to ensure the quality and efficacy of 3D printed medical devices and supplies. The collaborative efforts between 3D printing experts, medical professionals, regulatory authorities, and manufacturers demonstrated the versatility and agility of the technology in responding to urgent healthcare challenges. The experiences and knowledge gained during the pandemic will likely inform and shape future applications of 3D printing in the medical field.

5.3 Dental Applications of 3D Printing

3D printing has made significant advancements in dental applications, revolutionizing various aspects of dentistry, including diagnostics, treatment planning, prosthetics, and orthodontics. Here are some key areas where 3D printing has been utilized in dental applications:

Dental Models: 3D printing allows for the production of accurate and highly detailed dental models. These models are used in diagnostics, treatment planning, and the creation of various dental appliances. With 3D printing, dental professionals can quickly create physical models of patients' teeth and oral structures, facilitating better visualization, analysis, and communication.

Surgical Guides: 3D printing enables the creation of precise surgical guides for dental implant placement and other oral surgeries. By utilizing preoperative scans and 3D printing technology, custom surgical guides can be fabricated, providing dentists with precise guidance during procedures, improving accuracy, and reducing surgery time.

Prosthetics and Restorations: 3D printing has transformed the fabrication of dental prosthetics and restorations, such as crowns, bridges, and dentures. With digital scanning and CAD/CAM technology, dental professionals can design and manufacture highly accurate and customized dental restorations. 3D printers can produce these restorations using materials that closely mimic the natural appearance and properties of teeth, resulting in improved aesthetics and functionality.

Clear Aligners and Orthodontic Appliances: 3D printing has revolutionized orthodontics by enabling the production of clear aligners, such as Invisalign, and other orthodontic appliances. Through digital scans and 3D printing technology, custom aligners and retainers can be fabricated, offering patients a more comfortable and discreet alternative to traditional braces. 3D printing also allows for the creation of orthodontic models and appliances used in treatment planning.

Dental Surgical Instruments and Guides: 3D printing has facilitated the production of custom surgical instruments and guides used in dental procedures. Dentists can design and manufacture specialized instruments tailored to specific patient cases or unique anatomical structures. This customization enhances precision, efficiency, and patient outcomes during surgical interventions.

Dental Education and Training: 3D printing has become a valuable tool in dental education and training. Dental schools and training programs utilize 3D printed models, simulators, and replicas of dental structures for hands-on learning. This technology enables students and professionals to practice procedures, improve their skills, and gain a better understanding of dental anatomy and treatment techniques.

The integration of 3D printing in dentistry has resulted in improved accuracy, customization, and efficiency in various dental procedures. It has transformed the way dental professionals diagnose, plan treatments, and fabricate dental appliances, enhancing patient care and outcomes. As the technology continues to advance, 3D printing is expected to further expand its role in dentistry, enabling more innovative solutions and personalized treatments.

5.4 3D Printing Applications in Prosthesis

3D printing has had a profound impact on the field of prosthetics, offering numerous applications and benefits. Here are some key ways in which 3D printing has been used in the production of prostheses:

Customization: 3D printing allows for the creation of highly personalized and custom-fitted prosthetic devices. By utilizing 3D scanning technology, the exact shape and dimensions of the residual limb can be captured and used to design a prosthetic that perfectly fits the individual's anatomy. This customization enhances comfort, function, and overall satisfaction with the prosthesis.

Complex Geometries: 3D printing enables the fabrication of prosthetic components with intricate and complex geometries. This includes the creation of organic shapes, lattice structures, and internal cavities that can optimize the weight, strength, and flexibility of the prosthesis. By tailoring the design to meet specific functional requirements, 3D printing allows for the production of prostheses that closely mimic the natural movements of the limb.

Lightweight and Comfortable Design: 3D printing enables the production of prosthetic devices that are lightweight, yet durable and robust. Traditional manufacturing methods often involve the use of materials that can be heavy and uncomfortable for the user. However, 3D printing allows for the use of lightweight materials, such as carbon fiber-reinforced polymers, which significantly improve comfort and ease of use.

Cosmetic Covers and Aesthetics: 3D printing allows for the creation of cosmetic covers and aesthetic enhancements for prosthetic devices. Using various materials and design techniques, 3D printed covers can closely resemble the appearance of natural limbs or be customized with unique patterns and designs. These covers not only enhance the aesthetic appeal of the prosthesis but also promote self-confidence and acceptance.

Assistive Devices and Accessories: 3D printing has facilitated the production of assistive devices and accessories that complement prosthetic limbs. These can include tools, attachments, or adaptive equipment specifically designed for prosthetic users to enhance their functional capabilities and improve daily activities.

The use of 3D printing in prosthetics has significantly advanced the field, allowing for greater customization, improved functionality, and increased accessibility of prosthetic devices. It has empowered individuals with limb loss to have prosthetic solutions tailored to their unique needs, enabling better mobility and quality of life. However, it's important to note that while 3D printing offers numerous benefits, it should be integrated with the expertise and guidance of prosthetists and healthcare professionals to ensure proper fit, function, and ongoing care of the prosthetic device.

5.5 3D Printing Applications in Agriculture Industries

Equipment and Tools: 3D printing allows for the rapid production of custom equipment and tools tailored to specific agricultural needs. Farmers and agricultural professionals can design and fabricate specialized parts, components, and prototypes on demand, reducing downtime and costs associated with traditional manufacturing methods. This includes creating replacement parts for machinery, customized irrigation components, sensor mounts, and more.

Precision Farming: 3D printing can contribute to precision farming techniques by enabling the production of custom sensor housings, drone parts, or other devices for data collection and analysis. This facilitates the implementation of precision agriculture practices, such as soil and crop monitoring, pest management, and efficient resource utilization [8, 9].

Farming Structures and Greenhouses: 3D printing can be used to construct farming structures, such as greenhouses, hydroponic systems, and vertical farming modules. The technology offers the flexibility to create intricate designs and optimize structures for specific growing conditions. 3D printed components can be lightweight, durable, and tailored to the unique requirements of indoor farming environments.

Agricultural Prototypes and Research: Researchers and agricultural scientists can leverage 3D printing to fabricate prototypes for experimental purposes and innovative agricultural technologies. This accelerates the development and testing of new ideas, allowing for faster iterations and refinement of agricultural techniques.

Plant Tissue Culture and Biotechnology: 3D printing techniques, combined with biofabrication, hold promise in plant tissue culture and biotechnology applications. It enables the creation of complex scaffolds, microfluidic systems, or bioreactors for the growth and manipulation of plant tissues, cells, and microorganisms. This technology may have implications for plant breeding, tissue engineering, and plant-based pharmaceutical production.

Customized Farming Solutions: 3D printing can facilitate the creation of custom-designed solutions for specific farming challenges. For example, farmers can develop innovative irrigation systems, livestock management devices, or animal housing structures that are tailored to their unique needs, optimizing efficiency and animal welfare.

It's important to note that 3D printing in agriculture is still an evolving field, and there are challenges to be addressed, such as scalability, material availability, and cost-effectiveness. However, as technology advances and becomes more accessible, it holds the potential to transform agricultural practices, improve productivity, and contribute to sustainable and innovative farming methods.

5.6 3D Printing Applications in the Architecture Field

3D printing has emerged as a valuable tool in the field of architecture, providing architects and designers with new possibilities for design, prototyping, and construction [10]. Here are some key applications of 3D printing in the architecture field:

Conceptual Design and Visualization: 3D printing allows architects to create physical models of their designs, aiding in visualizing and communicating their concepts more effectively. These models provide tangible representations of architectural spaces, allowing clients, stakeholders, and design teams to better understand the proposed designs in three dimensions.

Prototyping and Iterative Design: 3D printing enables architects to quickly produce scaled-down prototypes of building components, allowing for iterative design processes. It facilitates the exploration of different design variations and the evaluation of structural, aesthetic, and functional aspects before committing to full-scale construction.

Complex Geometries and Customization: 3D printing offers architects the freedom to design and fabricate complex geometries that would be challenging or costly to achieve with traditional construction methods. It enables the creation of unique, intricate, and customized architectural elements, such as façade components, ornamental features, and interior fixtures.

Rapid Production of Building Components: 3D printing can be employed to produce building components, such as wall panels, partitions, and façade elements, with faster production times and reduced costs compared to traditional manufacturing methods. This can help streamline the construction process, improve efficiency, and facilitate customization.

Sustainable Construction: 3D printing in architecture has the potential to contribute to sustainable construction practices. By using precise material deposition, 3D printing minimizes waste and optimizes material usage. It also allows for the integration of sustainable materials, such as recycled plastics or bio-based materials, in the printing process, promoting environmental consciousness in building construction.

Construction in Challenging Environments: 3D printing offers advantages in construction projects in remote or challenging environments. It provides the capability to construct structures on-site, reducing transportation costs and logistical challenges associated with conventional construction methods. This makes 3D printing a viable solution for emergency shelters, disaster relief, or off-grid construction.

5.7 3D Printing Applications in Aerospace Industries

3D printing, also known as additive manufacturing, has had a significant impact on the aerospace industry. It has revolutionized the way aerospace components are designed,

prototyped, and manufactured. Here are some key applications of 3D printing in the aerospace field [11].

Lightweight and Complex Components: 3D printing allows for the creation of lightweight structures with complex geometries that were previously challenging or impossible to achieve using traditional manufacturing methods. By building components layer by layer, 3D printing enables the production of intricate designs, optimized for strength-to-weight ratios. This helps reduce the overall weight of aircraft, leading to fuel efficiency and improved performance.

Rapid Prototyping and Design Iteration: 3D printing allows aerospace engineers to quickly produce prototypes of complex parts and test them for fit, function, and performance. This accelerates the design iteration process, enabling engineers to refine designs and make necessary adjustments more efficiently. Rapid prototyping also supports faster innovation and shorter development cycles for new aerospace technologies.

Customized and Low-Volume Production: Aerospace applications often require customized components tailored to specific aircraft or mission requirements. 3D printing provides the flexibility to produce low-volume, highly customized parts without the need for expensive tooling or molds. This reduces manufacturing lead times and costs associated with producing unique or small-batch components.

Engine Components and Turbine Parts: 3D printing has been used to manufacture complex engine components and turbine parts. These components require high precision and withstand extreme temperatures and stresses. By utilizing advanced metal printing techniques, such as Direct Metal Laser Sintering (DMLS) or Electron Beam Melting (EBM), aerospace manufacturers can produce durable, heat-resistant parts with intricate internal structures and optimized cooling channels.

Repair and Maintenance: 3D printing has proven valuable in the repair and maintenance of aerospace equipment. It allows for the on-demand production of replacement parts, reducing the need for extensive inventory and long lead times for sourcing specialized components. This is particularly beneficial for older aircraft models or discontinued parts that may be challenging to obtain through traditional supply chains.

Space Exploration: 3D printing is being explored for its potential use in space exploration and colonization. It offers the ability to manufacture tools, spare parts, and even habitats using local resources, such as lunar or Martian regolith. This reduces the need for extensive payload during space missions and opens up possibilities for long-duration space travel and establishing sustainable colonies.

The 3D printing technologies continue to advance, the aerospace industry is expected to leverage its capabilities for more critical components and larger scale production. However, challenges related to certification, material performance, and scaling production still need to be addressed to fully integrate 3D printing into aerospace manufacturing workflows. Nonetheless, the technology's potential to drive innovation, reduce costs, and enhance performance makes it an exciting prospect for the future of aerospace.

5.8 3D Printing Applications in Film Industry

While the use of 3D printing in the film industry is not as widespread as in some other fields, it has still found valuable applications, primarily in the production of props, costumes, and visual effects. Here are some ways in which 3D printing has been utilized in the film industry:

Prop Design and Production: 3D printing allows filmmakers to create highly detailed and intricate props efficiently. Whether it's futuristic weapons, creature masks, or unique objects, 3D printing provides a cost-effective and time-saving method for producing custom props. It enables filmmakers to achieve complex designs that would be challenging or expensive to create through traditional manufacturing methods [12].

Costume Design and Accessories: 3D printing has been employed in costume design to create intricate and elaborate pieces. It allows for the fabrication of customized accessories, jewelry, armor, and other elements that can enhance the visual appeal and authenticity of characters. 3D printing offers designers the flexibility to experiment with various designs and materials, pushing the boundaries of creativity in costume design.

Special Effects and Prosthetics: 3D printing has been used to create special effects and prosthetics for films. By utilizing 3D scans of actors, prosthetic limbs, facial masks, or creature features can be custom-designed and manufactured with precise fit and intricate details. This technology enables the production of realistic and visually compelling special effects that enhance storytelling and character development.

Miniatures and Set Design: 3D printing has been utilized in the creation of miniatures and set design for films. It allows for the production of highly detailed models of buildings, landscapes, vehicles, or other elements required for the film's visual effects or practical effects. 3D printing provides a cost-effective and time-efficient method for producing intricate and accurate miniatures, helping filmmakers bring their vision to life.

Pre-visualization and Prototyping: 3D printing supports the previsualization process in filmmaking. It allows filmmakers to create physical prototypes of sets, props, or characters, enabling them to visualize and refine their designs before committing to full-scale production. This helps streamline the creative process, saves time, and allows for more accurate planning and budgeting.

While 3D printing in the film industry offers exciting possibilities, it's important to note that it is often used in conjunction with traditional manufacturing techniques and craftsmanship. The integration of 3D printing into film production workflows requires collaboration between designers, technicians, and artists to ensure the seamless integration of digital fabrication techniques with traditional filmmaking processes. As the technology continues to advance, 3D printing is likely to play an increasingly significant role in the film industry, providing filmmakers with more creative freedom, efficiency, and cost-effectiveness in the production of props, costumes, visual effects, and set design.

6 Conclusions

3D Printing technologies have many promising applications in the present engineering world and there lot many more applications in the coming future. These techniques have reduced the time to conceptualize the ideas, build, and test the prototypes. The applications of 3D printing have proven to be transformative across numerous industries and engineering fields. The technology has revolutionized manufacturing and design processes, enabling new levels of customization, efficiency, and cost-effectiveness. Key areas of application include prototype manufacturing and model development, precision equipment manufacturing and production, and architecture. Additive manufacturing usage in supply chains democratizes production and empowers individuals and businesses to create complex and intricate objects with relative ease. As the technology evolves continuously, can anticipate future advancements, increased adoption, and the materialization of even more innovative applications in the future. 3D printing is emerging into 4D printing with various advanced applications, the major drawback with these technologies is cost, as these technologies are not cost effective for mass production.

References

1. Wong KV, Hernandez A (2012) A review of additive manufacturing. Int Scholarly Res Notices
2. Shahrubudin N, Lee TC, Ramlan RJPM (2019) An overview on 3D printing technology: technological, materials, and applications. Procedia Manuf 35:1286–1296
3. Goh GD, Sing SL, Yeong WY (2021) A review on machine learning in 3D printing: applications, potential, and challenges. Artif Intell Rev 54(1):63–94
4. Chunhua S, Guangqing S (2020) Application and development of 3D printing in medical field. Modern Mech Eng 10(03):25–33
5. Dodziuk H (2016) Applications of 3D printing in healthcare. Kardiochirurgia i Torakochirurgia Polska/Polish. J Thoracic Cardiovascular Surgery 13(3):283–293
6. Ventola CL (2014) Medical applications for 3D printing: current and projected uses. Pharmacy and Therapeutics 39(10):704
7. Durfee WK, Iaizzo PA (2019) Medical applications of 3D printing. In: Engineering in medicine, pp 527–543. Academic Press
8. Crisostomo JLB, Dizon JRC (2021) 3D printing applications in agriculture, food processing, and environmental protection and monitoring. Adv Sustain Sci Eng Technol 3(2):372312
9. Baiano A (2022) 3D printed foods: a comprehensive review on technologies, nutritional value, safety, consumer attitude, regulatory framework, and economic and sustainability issues. Food Rev Intl 38(5):986–1016
10. Bilal M (2017) A review of internet of things architecture, technologies and analysis smartphone-based attacks against 3D printers. arXiv preprint arXiv:1708.04560
11. Balaji D, Ranga J, Bhuvaneswari V, Arulmurugan B, Rajeshkumar L, Manimohan MP, Masi C (2022) Additive manufacturing for aerospace from inception to certification. J Nanomaterials
12. Junk S, Kuen C (2016) Review of open source and freeware CAD systems for use with 3D-printing. Procedia CIRP 50:430–435